INVESTIGATING HIV/TB CO-INFECTION WITHIN HUMANIZED MICE

INVESTIGATING IMMUNE RESPONSES AND PATHOLOGY DURING HIV/TB CO-INFECTION WITHIN HUMANIZED MICE

By JACK (XIAOZHI) YANG, BHSc. (Hons)

A Thesis Submitted to the School of Graduate Studies in Partial Fulfilment of the Requirements for the Degree Master of Sciences

McMaster University MASTER OF SCIENCES (2022) Hamilton, Ontario (Infection & Immunity)

TITLE: Investigating Immune Responses And Pathology During HIV/*Mtb* Co-Infection Within Humanized Mice AUTHOR: Jack (Xiaozhi) Yang, BHSc. (Hons) (McMaster University) SUPERVISOR: Dr. Amy Gillgrass NUMBER OF PAGES: xxiii, 185

Lay Abstract:

There are over 2 billion individuals infected with TB and 37.7 million people living with HIV (PLWH) worldwide. When someone is co-infected with both diseases, the risk of death is greatly increased. Research in co-infection and developing effective TB vaccination for PLWH are urgent global issues. Animal studies are currently limited because studying HIV requires human immune cells. Our lab has established humanized mice (hu-mice) that develop many different human immune cells and are useful for HIV/*Mtb* co-infection research. When hu-mice were co-infected, they showed more dying lung tissue, immune cell loss, and bacteria in the lungs. Hu-mice were also used to study human immune responses to a novel TB vaccine delivered to the lungs. Trends of higher immune responses towards TB were observed in the lung and spleen of immunized hu-mice. Overall, this project shows the utility of hu-mice as pre-clinical models of HIV/*Mtb* co-infection and *Mtb* vaccine studies.

Abstract:

There are an estimated 2 billion individuals infected with *Mtb*, and 37.7 million people living with HIV (PLWH) worldwide. HIV/*Mtb* co-infection increases the risk of developing active tuberculosis by over 20-fold, and 210,000 of 1.5 million deaths from TB were among co-infected PLWH in 2020. Therefore, development of effective TB vaccination, particularly within the vulnerable PLWH population, is an urgent global issue. With limited *in vivo* models to study co-infection, humanized NRG (huNRG) mice and humanized DRAG-A2 mice (a next-generation of huNRG mice expressing HLA class I and II transgenes with improved human immune reconstitution, huDRAG-A2) are promising tools for HIV and TB reserach as they develop robust human immune cell populations and recapitulate many aspects of HIV or TB clinical disease. HIV/*Mtb* co-infection was investigated using huNRG and hu-DRAG-A2 mice in separate experiments where intravaginal (with DMPA pre-treatment) or intraperitoneal HIV-1 infection was administered, respectively, and intranasal infection of *Mtb* was administered 3.5 weeks later. Both huNRG and huDRAG-A2 mice recapitulated hallmark features of HIV/*Mtb* co-infection such as severe granuloma pathology, hCD4+ T cell depletion in lung and spleen tissue, and human like lung pathology such as *Mtb*-infected foamy macrophages in the granuloma. Co-infected huDRAG-A2 mice also displayed significantly higher bacterial burden in the lungs, increased extrapulmonary dissemination into spleen and liver, and significantly lower hCD4+ T cells in the peripheral blood post-*Mtb* infection when compared to the *Mtb*-only infected group. To investigate TB vaccine immunogenicity, huNRG and huDRAG-A2 mice were immunized with a novel trivalent vaccine,

AdCh68MV. Upon intranasal immunization, both models showed trends of developing higher *Mtb* antigen-specific hCD4+ T cell responses in the lung and spleen. Overall, this project sets the initial stages of a pre-clinical HIV/*Mtb* co-infection model in huNRG and huDRAG-A2 mice appropriate for immune investigations, therapeutic and vaccination development.

Acknowledgements:

I am beyond grateful to have had the opportunities to meet and bond with all the individuals throughout my graduate studies and to perform and experience the cutting edge research that I have been a part of. There are many individuals whom I would like to acknowledge that has played a great part in my thesis project and academic career in graduate school:

I would first like to thank Dr. Amy Gillgrass. She has been the most kind, caring, supportive, empathetic, and altruistic supervisor that I could ever ask for and I cannot thank her enough for that. Through thick and thin, with anything going on in or outside of the lab, she would always try to make time for me and support me. Her passion for science carries through the entire lab and seeing her devotion to science played a large part in motivating me through my graduate studies. Dr. Amy Gillgrass was initially my professor in an undergraduate immunology course, became my employer when I worked for her during my summer research position, and became my undergraduate and graduate thesis supervisor. But throughout all of these roles, she has always been a true mentor and someone who continues to inspire me to work harder. I hope that our paths would cross again in the future one day and that we could work closely again. Thank you Amy!

I would also like to thank Dr. Ali Ashkar and Dr. Zhou Xing who are my thesis committee members, as well as Dr. Charu Kaushic who is an incredible advisor. They have all played a crucial role in helping me progress through my thesis with their invaluable contributions in discussion points, ideas, and expertise that helped shape and develop my project. Their continuous support has helped me flourish in the lab and has also helped the Gillgrass lab as a whole in setting goals and becoming fully established as a new and expanding lab.

My lab mates in the Gillgrass lab is like a second family. I would like to thank Madeleine (Maddie) Lepard for all her help and support in the lab. Completing this project would not have been possible without her. Maddie and I shared many novel scientific discoveries in the lab. Being the first members in the Gillgrass lab, we've truly been through many challenges with troubleshooting, but also excitement and elation with successful experiments that generated extraordinary results. Lab work wouldn't be the same without Alexis Chacon, who never fails to turn any dull or boring moment into fun. I'd like to thank Alexis for not only her help in experiments and around the lab, but also her constant enthusiasm and charisma during those long-hour (and sleepless) days and nights. Thank you Maddie and Alexis for all the incredible times we've had in the lab (and yes, including our lab-ventures)! I'd also like to also thank Carmina Isidoro and the newest lab member Margaret Choi for their help in all the tasks around the lab, they may seem small but they are definitely very much appreciated.

I would also like to thank Dr. Sam Afkhami, whom I consider a big brother around the lab as he has helped me so much throughout my project. From data analysis to perfecting experimental techniques to managing stress during high-stake experiments, I have learned so much from him. Especially during the latter half of my graduate studies, his unconditional support and entertaining banter was also a huge part of what got me through the many tough experiments and long hours in the lab. Thank you Sam, many of my experiments would not have been possible without all your help and guidance!

I would like to thank Dr. Aisha Nazli and Anna Zganiacz for their invaluable technical help and training throughout my graduate studies. Their help, support, and advice in working with HIV and TB was what helped me start and complete many of my experiments. Thank you Aisha for all your help, especially with those tricky HIV assays! Thank you Anna for everything you do for us in the level 3 facility and guiding us through many of the challenges with TB work in level 3!

Dr. Fatemeh (Leila) Vahedi, Tom Mu, and Cheryl Kipling all played a large role in helping me establish the humanized mouse models in our lab. Thank you Leila for your technical support during our initial stages in developing humanizing mice. Thank you Tom and Cheryl for all of your technical help and advice in HLA typing.

I would also like to thank many of the Kaushic lab members: Christina, Amanda, Tushar, Ingrid, Nuzhat, Sydney, and Andrew. These incredible friends have all contributed in their own ways (especially outside of lab meetings) that made my experiences in and around the lab so much more fun, exciting, and enjoyable.

Working in the containment level 3 facility is no walk in the park and I would like to thank all the other level 3 facility users (especially Mike D'Agostino and Ali Zhang) for always trying their best in helping around the facility.

I would like to acknowledge and thank all of my friends, fellow graduate students, and fellow scientists. Whether it's letting me borrow reagents and materials, those long talks about life and future career goals, or all of the little things that I may need help with during my day-to-day lab work is very much appreciated as they have all played a part in helping me get to where I am today.

Finally, I would like to thank my family. My aunts, uncles, and cousins who are nearby and overseas have always been extremely caring and supportive of my academic endeavours.

Thank you all so much! I would also like to thank my grandparents, especially my grandmother who has cared for me throughout my entire childhood and would always pray for my success and offer words of encouragement – thank you so much Ahma! I'd like to also acknowledge my little brother Jerry. He is also a source of unconditional support, and I have learned, grown, and matured so much from being his older brother. Thank you little bro! And of course my parents – they are the reasons why I am able to have all of these extraordinary opportunities; to be a part of scientific discoveries, and to be able to meet and interact with so many of the incredible individuals mentioned above. Mom and Dad, both of you have sacrificed so much for me to be where I am today and I will forever be grateful. Thank you so much Mom and Dad from the bottom of my heart!

Table of Contents:

List of Figures:

List of Supplementary Figures:

List of Tables:

List of Supplementary Tables:

List of Symbols and Abbreviations:

ACK ····· Ammonium-Chloride-Potassium lysing buffer
Ad ····· Adenovirus
AFB ····· Acid fast bacilli
Ag ····· Antigen
AIDS ····· Acquired immune deficiency syndrome
APC ····· Antigen presenting cell
ART ····· Antiretroviral therapy
ATB ····· Active tuberculosis disease
BAF ····· Bronchoalveolar lavage fluid
BAL ····· Bronchoalveolar lavage
BCG ····· Bacillus Calmette-Guérin
BLT ····· Bone marrow-liver-thymus
bNAbs ····· Broadly neutralizing antibodies
bp ····· Base pairs
BRG ····· $Rag1^{null}Il2rg^{null}$
BSA ····· Bovine serum albumin
cART ····· Combination antiretroviral therapy
CBMC ····· Cord blood mononuclear cells
CCR ····· C-C chemokine receptor
CD ····· Cluster of differentiation
CFCB ····· Culture filtrate and crude BCG
CFU ····· Colony forming units
cGy ····· Centigray
Ch ····· Chimpanzee
CO2 ····· Carbon dioxide
COVID-19 ····· Coronavirus disease 2019
CRISPR ····· Clustered regularly interspaced short palindromic repeats
cRPMI ····· Supplemented complete RPMI culture media
CT ····· Computed tomography
Ct ····· Cycle threshold
CXCR ····· C-X-C chemokine receptor
DC ····· Dendritic cell
DKO ····· Double knock-out
DMPA ····· Depot-medroxyprogesterone acetate
DNA ····· Deoxyribonucleic acid
DRAG ····· NRG mice expressing HLA Class II (DRB1*04:01)
EDTA ····· Ethylenediaminetetraacetic acid
Env ····· Envelope
Fc ····· Fragment crystallizable
FDA ····· United States Food and Drug Administration
FRT ····· female reproductive tract
GALT ····· Gut-associated lymphoid tissue

gp ····· glycoprotein
GvHD ····· Graft-versus-host disease
h ····· Human
H&E ····· Hematoxylin and Eosin
HAART ····· Highly active antiretroviral therapy
hCD ····· human cluster of differentiation
HEPES ····· Hydroxyethyl piperazineethanesulfonic acid
HiREB ····· Hamilton Integrated Research Ethics Board
HIV ····· Human immunodeficiency virus
HLA ····· Human leukocyte antigen
HSC ····· Hematopoietic stem cells
Hu ····· Human
Hu-mice ····· Humanized mice
Hu-mouse ····· Humanized mouse
huDRAG-A2 ····· humanized DRAG-A2 mice (using the HSC-method)
huDRAGA ····· humanized DRAGA mice (using the HSC-method)
huNRG ····· humanized NRG mice (using the HSC-method)
huNSG ····· humanized NSG mice (using the HSC-method)
huNSG-BLT ····· Humanized NSG mice (using the BLT-method)
huNSG-hIL15 ····· humanized NSG-hIL15 (using the HSC-method)
IDO ····· Indoleamine 2,3-dioxygenase
IFN ····· Interferon
IGRA ····· Interferon gamma release assay
IH ····· Intrahepatic
IHC ····· Immunohistochemistry
IL ····· Interleukin
IM ····· Intramuscular
IN ····· Intranasal
IP ····· Intraperitoneal
IRIS ····· Immune reconstitution inflammatory syndrome
IU ····· Infectious unit
IV ····· Intravenous
kg ····· Kilograms
KI ····· Knock-in
KO ····· Knock-out
LTBI ····· Latent tuberculosis infection
MDR ····· Multi-drug resistant
mg ····· Milligrams
MHC ····· Major histocompatibility complex
MHC ····· Major histocompatibility complex
MIBI ····· Multiplexed Ion Beam Imager
mL ····· Milliliter
Mm ····· *Mycobacterium Marinum*
MPA ····· Medroxyprogesterone acetate

Mtb ····· *Mycobacterium tuberculosis*
ng ····· Nanogram
NHP ····· Non-human primates
NK ····· Natural killer
NNRTI ····· Non-nucleoside reverse transcriptase inhibitors
NOD ····· Non-obese diabetic
NOG ····· NOD.Cg-Prkdc^{scid}Il2rg^{tm1Sug}
NRG ····· NOD.Cg-Rag1^{tm1MoM}Il2rg^{tm1Wjl}
NRG-A2 ····· NRG mice expressing HLA class I (A*02:01)
NRTI ····· Nucleoside reverse transcriptase inhibitors
NSG ····· NOD.Cg-Prkdc^{scid}Il2rg^{tm1Wjl}
OADC ····· Oleic acid-albumin-dextrose-catalase
PBMC ····· Peripheral blood mononuclear cells
PBS ····· Phosphate buffered saline
PCR ····· Polymerase chain reaction
PD-L ····· Programmed death ligand
PET ····· Positron emission tomography
PFU ····· Plaque forming unit
pH ····· Potential of hydrogen
PLWH ····· Persons living with HIV
PMA ····· Phorbol myristate acetate
PrEP ····· Pre-exposure prophylaxis
PRR ····· Patter-recognition receptor
qPCR ····· Quantitative polymerase chain reaction
Rag ····· Recombination-activating gene
RBC ····· Red blood cell
RIF ····· Rifampicin
RNA ····· Ribonucleic acid
RPMI ····· Roswell Park Memorial Institute culture media
RT-qPCR ····· Reverse transcription quantitative polymerase chain reaction
SARS ····· Severe acute respiratory syndrome
SCID ····· Severe combined immunodeficiency
SEM ····· Standard Error of Mean
SHIV ····· Simian human immunodeficiency virus
SIRP ····· Signal regulatory protein
SIV ····· Simian immunodeficiency virus
TB ····· Pulmonary tuberculosis
TBE ····· Tris Borate EDTA buffer
TCID50 ····· Median Tissue Culture Infectious Dose
TDF ····· Tenofovir disoproxil fumarate
Tg ····· Trangenic
TG ····· Trivalent pooled whole proteins (Ag85A, TB10.4, RpfB)
TGF ····· Tumour growth factor
Th ····· T helper

TLR ····· Toll-like receptor
TNF ····· Tumour necrosis factor
Treg ····· T regulatory cell
TST ····· Tuberculin skin test
U ····· Units
UCB ····· Umbilical cord blood
V(D)J ····· Variability, diversity, and joining
VV ····· Viral-vectored
WHO ····· World Health Organization
XDR ····· Extensively-drug resistant
α ····· Alpha
γ ····· Gamma
µg ····· Microgram
µL ····· Microliter
µm ····· Micrometer/micron
µM ····· Micromolar
^{o}C ····· Degrees Celsius

Declaration of Academic Achievement:

I declare that this thesis dissertation has been composed by myself and based on original research. This thesis document was written entirely by myself, with editing and feedback from Dr. Amy Gillgrass (thesis supervisor). I confirm that the work submitted is an accurate representation of the experiments and findings that I have contributed to during my time as a M.Sc. candidate. As indicated below, the work and research conducted is my own and in collaboration with others:

Jack (Xiaozhi) Yang:
HLA-typing, mouse genotyping, mouse breeding, animal monitoring, cord blood processing, CFU plating, humanizing mice, experimental planning, HIV-1 preparation and infections, *Mtb* preparation and infection, mouse immunization, sample collection and processing, *in vitro* cell cultures, flow cytometry, RT-qPCR, histology imaging, data generation and analysis

Madeleine Lepard:
HLA-typing, Mouse breeding, animal monitoring, cord blood processing, CFU plating, humanizing mice, HIV-1 infections, sample collection and processing, histology processing, flow cytometry, RT-qPCR, data analysis

Dr. Amy Gillgrass:
Experimental designs and planning, protocol specific training, CFU plating, tissue processing, data analysis

Dr. Sam Afkhami:
Experimental planning, *Mtb* infection, mouse immunization, sample collection and processing, data analysis

Alexis Chacon:
Mouse breeding, sample collection and processing, *in vitro* cell cultures, flow cytometry

Dr. Aisha Nazli:
Troubleshooting assays and RT-qPCR, HIV-1 preparation

Anna Zganiacz:
BCG preparation and CFU plating

Chapter 1. Introduction

Chapter 1.1. Tuberculosis

1.1.1. TB Epidemiology and Significance

Mycobacterium tuberculosis (*Mtb*) is a non-motile, obligate aerobe, acid-fast bacillus that causes the disease pulmonary tuberculosis (TB). An estimated 2 billion people (around 1/4 of the current global human population) are infected with the *Mtb* bacteria and in 2020 over 4000 individuals died from the infection every day [1,2]. Although the majority of these infections do not display clinical symptoms, and thus are considered latent TB infection (LTBI), TB is still a major global concern for several reasons. Over 95% of TB cases and deaths occur in developing countries; these areas are also facing many other health, nutrition, and information provision challenges which exacerbate the TB endemic [2]. For instance, the financial burden of accessing healthcare (hospitalization, transportation, treatment, etc.) is greater for those with lower incomes [3]. Public awareness and information dissemination regarding TB is still lacking within those with lower social economic status and this reduces the effectiveness of the efforts in prevention and control of the disease [4–6].

Another serious concern regarding TB is the increase in multi-drug resistant (MDR) *Mtb* and extensively-drug resistant (XDR) *Mtb*. The decades of anti-*Mtb* drug use is becoming increasingly ineffective as strains of *Mtb* bacteria are now resistant to at least one or more of these drugs [7]. This issue is worsened by the non-compliance from patients prescribed mono-drug therapies. With the increase in drug-resistant *Mtb*, global treatment success is

greatly reduced (around 56% success rate) leading to increased patient mortality from TB [8]. Only one third of those with drug-resistant TB accessed treatment in 2020 illustrating that MDR-*Mtb* and XDR-*Mtb* is a global public health crisis [9]. Despite the fact that individuals with LTBI do not show clinical symptoms, there is still a concerningly large pool of bacterial reservoir within the human population. Those with LTBI can have up to a 10% lifetime risk of developing active tuberculosis (ATB) which can cause lung necrosis and death if untreated [10]. The overall reported incidence of TB is declining at a very slow rate, and in many countries MDR- and XDR- *Mtb* cases are on the rise [2]. However, it is notable that some studies showing the capability of *Mtb* self-clearance (meaning that individuals fully clear infection and do not sustain lifetime infection) may offer evidence that the 2 billion latently infected individuals could be an overestimation [11–13]. Regardless, it is clear that TB is an urgent global issue that warrants further research in not only treatment and cure, but also vaccination and disease prevention.

1.1.2. Mycobacterium Tuberculosis Transmission and Host-pathogen Interactions

Mtb is transmitted through the air via respiration when an individual with the disease expels airborne bacteria in droplets or aerosolized bacterial particles which are inhaled through close contact by another host [14]. The inhaled dose of *Mtb* is dependent on the proximity of contact, respiratory rate, and exposure duration [15,16]. Although higher inhaled doses

of infectious particles may increase the likelihood of more severe disease, the minimum infectious dose in the human lung can be as low as fewer than 10 bacteria [17]. After gaining access into the lower respiratory tract, *Mtb* infects resident alveolar macrophages and other phagocytes such as dendritic cells (DCs). Upon infection of alveolar macrophages and DCs, *Mtb* is able to evade the killing mechanisms of these phagocytes by preventing the fusion and acidification of phagosomes and lysosomes to form phagolysosomes [18–20]. As a result, *Mtb* is able to survive and replicate within the phagosomes which can lead to cell death via necrosis rather than apoptosis. Apoptosis would contain the infection and allow for antigen processing, while necrosis allows *Mtb* to further disseminate and infect other cells [21]. Toll-like receptors (TLR) and other pattern-recognition receptor (PRR) pathways of these macrophages and DCs are activated by *Mtb* ligands to produce proinflammatory cytokines and chemokines that recruit more phagocytes [22]. Specifically, neutrophils and monocytes first arrive to phagocytose the remaining *Mtb* and again produces more cytokines and chemokines [23]. In this cycle of phagocyte recruitment, *Mtb* gains access to more host cells to infect, replicate, and establish a larger bacterial reservoir. These antigen presenting cells (APCs) also travel to surrounding lymph nodes to present *Mtb* antigen to lymphocytes in an effort to activate adaptive immunity [24]. NK cells and T lymphocytes such as CD4+ T cells and CD8+ T cells are then recruited to the site of infection and contributes to the formation of granulomas which is the hallmark lung pathology of TB [25–27]. For instance, DCs can prime T cell differentiation into T helper 1 (Th1), T helper 17 (Th17), and cytotoxic effector T cell subsets [28,29]. Studies have suggested that the involvement of adaptive immunity is often delayed during TB infection,

and as a result provides *Mtb* more time to replicate and establish a substantial bacterial reservoir prior to lymphocytes arriving to help contain the infection [30,31]. However, once the full immune granuloma structure is formed with CD4+ T cells helping the activation of macrophages, the granulomas are very effective in containing, but not eliminating the infection [32]. CD4+ T cells secrete many important cytokines such as interferon (IFN)-γ, tumour necrosis factor (TNF)-α and interleukin (IL)-2, which are necessary for cell-mediated immunity activation and anti-mycobacterial responses [33]. During this process, *Mtb* can also evade adaptive immunity mechanisms such as preventing the recognition of infected macrophages by inhibiting major histocompatibility complex (MHC) class II antigen presentation [34]. This would hinder CD4+ T cell-mediated immunity to *Mtb* as macrophages also greatly rely on CD4+ T cell activation for microbicidal functions such as nitric oxide production [35,36].

Due to variability in individual immune cell responses and host-pathogen interactions in humans, the granuloma is an organized aggregation of different immune cells forming a complex, variable, and heterogenous structure. Separate granulomas can have unique micro-environments each independently influenced by the quality of the localized immune response, the number of bacteria, and the extent/status of tissue pathology or disease [35,37]. In general, TB granulomas are organized in a spherical structure where *Mtb* populate most abundantly near the centre and are immediately surrounded by macrophages that are at various stages of activation [38]. These macrophages are surrounded by NK cells, neutrophils, and lymphocytes such as T cells and B cells [39]. As the lung granuloma

matures, fibroblasts and other highly differentiated macrophages such as foamy cells/macrophages, multinucleated giant cells, and epithelioid cells can also be found within the structure [40,41]. During this stage, the structure can also form an outer fibrous cuff that encompasses the macrophage layer and many lymphocytes can be excluded or walled-off from the granuloma center and accumulate around the outside the fibrous cuff [41]. In more severe stages of granulomas which are more frequent in ATB, the granuloma centre will have an increasing accumulation of necrotic macrophages and foamy macrophages that develop after up-taking excess lipids from the dead cells [42,43]. Further apoptosis and necrosis of cells accumulate in the core and this cycle leads to the buildup of lipids forming a central necrotic core termed the caseum [44]. Eventually severe cavitation develops from the dissolution of the caseum, and the granuloma structure fails to contain *Mtb* bacilli leading to release of infectious *Mtb* into extrapulmonary tissue [42,45].

The formation of granulomas is the result of both the host cell-mediated immunity and pathogen immune evasion creating a host-pathogen equilibrium. Recruited cells that are meant to control infection are also supplying *Mtb* with more host cells to infect. This balance is mostly maintained until a disruption occurs such as through introduction of immunosuppressive therapies [46,47] or factors like HIV-1 infection [48]. When the scale is tipped towards *Mtb* replication or away from host immunity, the granuloma may no longer be able to contain the infection leading to bacterial dissemination and the development of ATB. Although *in vitro* studies and animal models have offered good insight into host-pathogen interaction within the granuloma, there are more complex

mechanisms (especially considering different granuloma microenvironments) within both immunocompetent and immunocompromised individuals that require further investigation.

1.1.3. Clinical Presentation

Exposure to *Mtb* can present with three different outcomes. Some individuals are able to fully eliminate *Mtb* upon exposure which is likely due to enhanced innate immune responses [12]. The majority are unable to fully eradicate the pathogen with solely their innate immunity and subsequently sustain *Mtb* infection. As described in chapter 1.1.2. the adaptive immunity generated to contain infection and prevent dissemination is often not sterilizing immunity, and thus the host remains latently infected which is defined clinically as LTBI. Individuals who are latently infected (especially those with weakened immunity) are at risk of developing clinical ATB [14,49]. Finally, within some individuals, infection with *Mtb* can directly result in ATB likely due to an inability to mount a sufficient innate and/or adaptive immune response to control the initial exposure and *Mtb* replication. Clinical diagnosis of LTBI can be challenging as no symptoms are displayed and can present on a clinical spectrum varied across individuals. Once cellular immunity has been established during LTBI, the tuberculin skin test (TST) and the interferon gamma release assay (IGRA) can be used to confirm the status of latent infection [14]. TSTs subjectively measure non-specific tuberculin antigen reactivity on the skin, while IGRAs measure IFN-γ released from *Mtb*-specific T cells after peripheral blood mononuclear cells are stimulated

by *Mtb*-specific antigens. Although the TST is overall more cost effective and is advantageous in low-resource settings, IGRAs report to have higher specificity than TST for detecting tuberculosis infection [50–52]. IGRAs results are also not influenced by subjectivity of interpretation and are not confounded by previous exposure to Bacillus Calmette-Guérin (BCG) vaccination or non-tuberculous mycobacterial infections [50]. However, the relatively low and inconsistently reported sensitivity of both tests ranging from 70%-90% means that a negative result cannot completely rule out latent infection [50]. Some individuals especially young children may have low reactivity to TST [52].

Both of the aforementioned diagnostic tests have poor predictive value of ATB, and thus upon confirmation of *Mtb* infection with a positive screening test, a patient can undergo several other diagnostic tests including imaging (using chest X-rays or PET-CT scans), microscopy of sputum smears [53], *Mtb* culture-based tests [54], and molecular detection methods [55–57]. Imaging tests are normally used for ATB screening and will require further culture or molecular diagnosis upon a positive result [58]. These diagnostics for ATB are well-established for adults but diagnostics for young children still remain challenging due to their relatively inconsistent and unreliable results which can often present as negative due to paucibacillary TB (having low numbers of bacilli). Nucleic acid amplification assays such as the Xpert *MTB*/RIF has been developed to not only detect *Mtb* but also identify MDR-*Mtb* and it is currently recommended by the World Health Organization (WHO) as the frontline diagnostic testing for both children and adults suspected to have ATB [56,57]. When diagnostic results are still ambiguous, they are often paired with exposure history and other signs and symptoms for diagnosis of disease [14].

Common symptoms of ATB can include coughing with sputum and/or blood, chest pains, weight loss, fever, and night sweats [59]. It is important to note that these clear classifications of LTBI and ATB are used for simplicity in the clinical setting. In reality, TB disease presents on a wide spectrum of clinical presentations where LTBI patients can present with different testing results, and ATB patients may also be classified as having subclinical disease only being periodically contagious.

1.1.4. Human Pathology

To fully understand the complexity of human pathology, specifically lung pathology during TB infection, it can be useful to differentiate primary TB and secondary TB infection as pathology may differ in these separate cases. Primary TB infection is the first exposure to *Mtb* and includes early infection where *Mtb* is either eliminated, contained (such as in LTBI), or directly progressed to ATB. In the first 2 cases, macrophages and other cell mediated immunity have developed responses against *Mtb*. Secondary TB (also termed post-primary TB) is defined as either a secondary exposure to *Mtb* (second infection) or reactivation of TB during later stages of LTBI after *Mtb*-specific immune responses are established. Individuals who are exposed to *Mtb* as adults normally display pathology consistent with “secondary TB” where they can contain infection as LTBI and potentially have re-activation which is then classified as secondary TB/post-primary TB [60,61].

For over a century, histopathology analysis of human patient samples was used to study TB infection [62]. In the 1950s, antibiotics discovery led to beliefs that TB could soon be eradicated and along with advancements in molecular biology and genetics in the 20th century, research had shifted way from TB morphologic pathology assessments and studies [62]. As a result, fewer post-mortem human patient samples are available to study chronic disease, especially secondary TB. Currently, more advanced imaging techniques including molecular imaging and histology techniques such as immunohistochemistry can help overcome the diminished research in previous decades due to lack of human tissue samples [63].

Whole lung histopathology and bacilli location in human LTBI was mostly based on autopsy samples of patients who died of other causes. These samples may not be fully representative of LTBI and thus many animal models attempt to recapitulate LTBI *in vivo* for histopathology investigation. From early human pathology studies, LTBI lesions were described as remaining scars from granulomas lesions healing [64]. Due to the heterogeneous nature and spectral presentation of granuloma and lesion formation within the lungs, evolution of granulomas are difficult to elucidate and this data has been mostly extrapolated from animal studies. However, human lung pathology can be generally characterized by significant inflammation evident from vasodilatation, edema, extensive fibrous protein and cell collection in cavities, and lymphocyte infiltration [64]. Classical human granuloma formation consists of macrophage aggregates that transform into multinucleated giant cells which are characteristic of a classical granuloma or tubercle [44]. Caseous necrotic lesions within the lungs are characterized by solid central regions with

very few bacilli and develop into hardened tissue or calcification [64]. The caseum within caseous necrotic lesions can also soften with the presence of large bacterial loads where development of ATB may follow [64]. From these characterizations in human disease, some important characteristics for animal models to recapitulate are the following features: the development of caseous necrosis within the granuloma surrounded by a collagen/fibrous rim, intracellular and extracellular populations of bacilli, and cavity formation within lesions resulting from the liquefying of the caseum.

More recent studies have used advanced imaging technique of multiplexed ion beam imaging (MIBI) on human archived tissues and biopsies to obtain further insight on granuloma immunoregulation, structural composition, and microenvironments. As expected, TB granulomas were composed of mainly T cells and myeloid cells [65]. Macrophages expressing human CD68 and CD11b are concentrated mostly within the central area of the granuloma with some spread throughout the periphery [66]. Human T cells, in particular CD8+ T cells, are in the periphery surrounding the core of the of macrophages. Cell density of CD68+ macrophages and CD8+ T cells were also found to be higher in granulomas with more *Mtb* compared to granulomas with fewer *Mtb* [66]. The core of the granulomas appear to be more immunosuppressive with myeloid cells expressing immunoregulatory molecules programmed death ligand 1 (PD-L1) and Indoleamine 2,3-dioxygenase 1 (IDO1) co-localizing with tumour growth factor β (TGF-β) [65]. This is consistent with a findings that anti-inflammatory TGF-β or IL-10 production suppresses inflammation and induces peripheral regulatory T cell (Treg) activity [67].

Overall, this supports previous understanding of the immune down-regulatory environments within the granuloma to promote *Mtb* survival [68,69]. Non-immune cells such as endothelial cells, fibroblasts, and epithelial cells were found to be most abundant in lung lesions. Out of the total immune cells enumerated and averaged from different lesions, approximately 2.5% were neutrophils while other lower abundance cell populations such as 1% of Tregs, 0.6% of mast cells, 0.2% of CD209+ DCs, and 0.1% of γδ T cells were also identified [65]. CD4+ and CD8+ T cells were present at around 17% and 12% in diagnostic biopsy tissue, respectively. However, significantly lower percentages of both CD4+ and CD8+ T cells were found in post-mortem specimen when compared to biopsy tissue [65]. Since post-mortem specimen tissue were from patients with fatal TB, this can indicate potential depletion of CD4+ and CD8+ T cells within the granulomas of more severe TB disease. It is of note that once again, these studies have highlighted the heterogeneity and complexity of granulomas where different subpopulations proportions of lymphocytes, myeloid cells, and non-immune cells can be present within different granulomas. Many of these complexities including the evolution of granulomas or whole lung histopathology of primary TB infection cannot be ethically investigated without the aid of animal models.

1.1.5. Animal Models for Investigating TB

Mtb is naturally a human-specific pathogen, and although it is able to infect most mammals, these animals do not easily transmit the infection. Regardless, a multitude of animal models have provided great insight to the basic understanding of TB pathology, pathogenesis, vaccination, antimicrobial drug treatments, and recapitulating different aspects of human TB disease. Small animals used for TB studies ranked in order of frequency in literature include mice, guinea pigs, and zebrafish [70]. Large animals that are useful for TB studies include rabbits, cattle, and non-human primates (NHPs). In small animals, the zebrafish has advantages in investigating *Mtb* pathogenesis as the transparency of the organism during the larval stage allows easy accessibility for imaging techniques [71]. The zebrafish model requires infection with *Mycobacterium marinum* (*Mm*) (a mycobacterium genetically related to *Mtb*) and can develop granuloma-like structures that form necrotic and caseous, but non-fibrotic granulomas [72,73]. However, the use of *Mm* can be a limitation due to inherent differences when compared to *Mtb* infection. For instance, neutrophils do not interact with *Mm* upon infection [74], whereas in human *Mtb* infection, neutrophils play a prominent role in initial/early infection [23]. Standard inbred mice have contributed greatly to TB literature and is reviewed in detail elsewhere [75,76]. In brief, insight on macrophage responses in early infection, T cell recruitment and functionality, and granuloma formation has largely resulted from *Mtb* studies within inbred mice [75]. More recent studies using transgenic and knockout (KO) mouse models have improved upon the inbred mice and have provided deeper understanding of more complex immune responses and pathology. For example, the FeJ mutant on the C3HeB mouse background allows for low-dose *Mtb* infection and develops severely organized necrotic granuloma lesions with caseation,

which is largely absent in other strains of mice [77]. IFN-γ-KO mice [78], TNF receptor-KO mice [79], and CD4-KO mice have all contributed to the defining the role of IFN-γ, TNF-α, and CD4+ T cells in controlling *Mtb* infection [80]. Guinea pigs have shown great ability in recapitulating many aspects of human TB disease. In particular, caseating necrotic granuloma lesions with calcification was identified [81,82]. Extrapulmonary dissemination of *Mtb* into tissues such as the spleen, liver, and pancreas was also established in the model [82].

Rabbits which are larger animals have some resistance in *Mtb* infection and as a result may be useful in studying LTBI or paucibacillary TB [83]. Rabbit models are more susceptible to *Mycobacterium Bovis* or they require higher doses of *Mtb*, and consequently they are able to develop cavitation within granuloma lesions in addition to caseation and necrosis [83,84]. NHP models of tuberculosis (mostly using macaque species) may serve as one of the most representative model of human TB disease. Macaques are even able to model human LTBI in displaying similar diagnostic testing results such as IGRA and TST, and develop clinical symptoms displayed in ATB [85,86]. Most granuloma features are recapitulated within NHPs including immune cell infiltration, necrosis and caseation, calcification, and cavitation [86]. Host-pathogen interactions involving the variety of immune cells such as macrophages, neutrophils, T cells, epithelioid macrophages, and multinucleated giant cells were also elucidated from the NHP models [85,87]. The main disadvantage of these large animal models is the feasibility considering cost, maintenance,

and ethics which can pose a significant barrier to widespread use of the model and swiftly advancing research in the field.

1.1.6. Available Treatments and Development of Vaccinations

TB is a treatable and curable disease. However, the course of antibiotic treatment is lengthy and requires high adherence to the regimen. Due to these compliance issues within patients prescribed the treatment, this greatly contributes to the development of MDR- and XDR-*Mtb* strains.

Standard treatment for those with LTBI is a 6 to 9 month course of daily isoniazid and/or rifampicin (the 2 of the most effective first-line anti-TB drugs), or other multi-drug regimens [88]. If isoniazid or rifampicin mono-resistant *Mtb* is suspected, a more intensive treatment regimen consisting of the 4 drugs (isoniazid, rifampicin, pyrazinamide, and ethambutol) can be prescribed [89]. With improved diagnostic testing, MDR-*Mtb* and XDR-*Mtb* can also be detected with a more advanced Xpert *MTB*/RIF test (introduced in chapter 1.1.3) termed Xpert *MTB*/RIF Ultra and Xpert *MTB*/XDR [90,91]. MDR-TB is defined as resistance of *Mtb* to at least isoniazid and rifampicin while XDR-TB is defined as additional resistance to any fluoroquinolones and second line injectable drugs and can causes more severe disease. Both MDR-TB and XDR-TB require more intensive, longer duration, and increased combination of first and second-line drugs for treatment [92]. Many studies including clinical trials are currently investigating the efficacy of both novel and

combination of drugs in shorter and injection-free treatment regimens [92]. However, the evolution of more drug resistant strains may still be inevitable. Therefore, the prevention of disease through vaccination may be more effective in not only reducing clinical burden, but also preventing the progressive development of *Mtb* drug resistance. As such, vaccination should be a major area of consideration in prevention and elimination of TB globally.

Currently, Bacillus Calmette-Guerin (BCG) which is a live-attenuated form of *Mycobacterium bovis*, is the only clinically approved TB vaccine that is widely used to prevent *Mtb* and other mycobacterial infections. Although the BCG vaccine has demonstrated efficacy against the severe, disseminated childhood forms of TB, it fails to confer protection against the pulmonary TB in adults or secondary TB [93]. Ideally, an effective TB vaccine will prevent initial *Mtb* infection which means IGRA tests would remain negative for vaccinated individuals. There are 3 main platforms of prophylactic vaccines being developed: recombinant BCG strains, protein subunit and adjuvanted formulations, and viral-vectored (VV) platforms [94].

Recombinant BCG vaccines aim to fully replace the existing BCG vaccine. Currently, VPM1002 is the only recombinant BCG vaccine in clinical trials [95,96]. The VPM1002 strain is modified to improve accessibility of immunogenic antigens and prevent inhibition of phagolysosome maturation. As a result, infected cells undergo rapid phagosome acidification and subsequent phagolysosome fusion causing the release of antigens and

bacterial DNA into the cytosol triggering autophagy and apoptosis as antigen delivery [97]. Protein subunit and adjuvanted vaccines are designed to express immune-dominant *Mtb* antigens with strong adjuvants. Many more subunit-adjuvanted vaccines are undergoing clinical trials such as the M72/AS01$_E$ vaccine. M72/AS01$_E$ is derived from 2 immunogenic *Mtb* antigens (*Mtb*39A and *Mtb*32A) which induces lymphocyte proliferation and IFN-γ production [98]. This vaccine is particularly promising as it demonstrated safety and elicited robust short-term and some levels of long-term (3 years) humoral and cell-mediated responses within persons living with HIV on ART [99,100]. MVA85A was a promising viral-vectored vaccine recently in Phase IIb clinical trials. This VV platform used modified Vaccinia Ankara virus that expresses antigen 85A (Ag85A), an immunodominant *Mtb* protein. Despite demonstrating efficacy in guinea pigs and rhesus macaques, no protective efficacy against *Mtb* infection was noted in humans in their last major clinical trial [101]. Adenoviral-vectored vaccines are a subset of VV vaccines and also demonstrate great promise in protective efficacy. A successful phase one clinical trial of human type 5 adenovirus expressing Ag85A (AdHu5Ag85A) demonstrated safety and immunogenicity as primary and booster vaccinations against *Mtb* infection [102,103]. AdHu5Ag85A was also administered in a humanized mouse model showing protection against TB and improved pathogen-specific T cell responses [104]. The development of a novel chimpanzee based AdCh68Ag85A expressing the same antigen showed enhanced immunogenicity and efficacy, especially following respiratory mucosal (intranasal) administration when compared to their human adeno-vector counterpart [105,106].

Overall, targeting *Mtb* is a challenging task and based on both previous and current vaccines, several factors should be considered to optimize delivery, immunogenicity, and protective efficacy. Firstly, since *Mtb* infects the lower respiratory tract as a mucosal pathogen, respiratory mucosal administration of the TB vaccine may confer better protection when compared to parenteral administration [107]. Route of immunization can affect the location of which antigen-specific T cells reside [108], and thus intranasal or aerosolization delivery of vaccines may allow for more memory T cells to home within lung tissue which is the site of infection. Secondly, pre-existing immunity should be considered when developing a vaccine platform. BCG may not confer as much protective efficacy in adults due to having more time and opportunity for prior mycobacteria exposure within the environment [109]. In a similar manner, humans are also frequently exposed to adenoviruses and may develop pre-existing anti-human adenovirus antibodies and immunity [110]. Based on this knowledge, non-human adenoviruses can be considered when designing an adenoviral-vectored TB vaccine. Finally, identifying the optimal immunogenic antigen for the vaccine should be consider especially given the complex life cycle of *Mtb*. The *Mtb* genome can express multiple functionally redundant proteins which means that a monovalent vaccine may not be as effective once *Mtb* escapes the immune pressure [111,112]. *Mtb* can also express different antigens given the stage of its life cycle [113,114]. Therefore, it may be optimal for a vaccine to select for more than one antigen by simultaneously targeting acute, dormancy, and persistence antigens to ensure that immunity will be primed against a wider array/spectrum of antigens capable of targeting *Mtb* irrespective of the stage of its life cycle.

Chapter 1.2. Human Immunodeficiency Virus

1.2.1. HIV-1/AIDS Epidemiology and Significance

Human immunodeficiency virus 1 (HIV-1), is a retrovirus that causes acquired immune deficiency syndrome (AIDS) within persons living with HIV (PLWH). HIV/AIDS maintains a significant disease burden worldwide, with approximately 37.7 million PLWH as of 2020 [115]. HIV infection is most prevalent in many regions of sub-Saharan Africa, where women are disproportionally affected. Countries with the highest HIV burden per capita are South Africa, Swaziland, Lesotho, and Botswana [116]. Approximately half (53%) of the PLWH are women, and this proportion is even higher (63%) in sub-Saharan Africa [115]. Alarmingly, six in seven new HIV infections in sub-Saharan Africa within adolescents aged 15–19 years are among girls. In addition to social factors such as lack of care, accessibility, and education, many biological factors also contribute to the disproportional disease burden within women [117]. For instance, women have lower viral set points than men meaning that disease progression and pathologies are elicited despite having lower viral loads [118]. Women can also have increased risk of co-morbidities than men and display more inflammation which can play a role in target cell recruitment [119].

Within the past decade, there has been steady decline in new HIV infections [115]. This decline may be attributed to factors such as protected sex which reduces HIV transmission [120], lower prevalence of sexually transmitted infections which reduces risk of acquiring HIV infection [121], and most importantly the use of antiretroviral therapy (ART) greatly reducing transmissibility [122]. Despite the effectiveness of ART in reducing viral load and disease burden within PLWH, adherence is essential in ensuring effectiveness which is difficult to achieve in a substantial proportion of patients [123]. Furthermore, there is currently still no treatment or cure to eradicate HIV, leaving PLWH vulnerable to opportunistic infections including *Mtb* and severe acute respiratory syndrome coronavirus 2 (SARS-CoV-2) resulting in increased risk of infection and displaying significantly worse disease outcomes [124,125].

1.2.2. HIV-1 Transmission, Infection, and Host-pathogen Interaction

HIV-1 is a single-stranded RNA retrovirus with a genome composed of two identical copies of RNA surrounded by capsid protein and a lipid membrane layer [126]. HIV-1 is mainly transmitted through mucosal tissue, blood, or damaged skin contacting infected body fluids (most commonly through the vaginal, rectal, or oral mucosa) [127]. Plasma viral load is a major factor determining the risk of sexual transmission, where transmission risk can be increased by 2-4 times for every log-fold increase in plasma viral load [128]. Additionally, hormonal contraceptives can also lead to increased risk of HIV infection caused by the thinning of the vaginal epithelium, disrupting vaginal barrier function, altering vaginal

microbiota, and increasing numbers of target cells to the site of infection [129–131]. Hours after mucosal exposure to HIV-1, the virus can enter the body through breaks within the epithelial barrier and gain access to target cells [132]. The primary target receptor for HIV-1 is human CD4, which is expressed on the surface of CD4+ T cells, monocytes, macrophages, and dendritic cells. To initiate membrane fusion and release of viral core for infection, HIV envelope (Env) glycoprotein gp120 binds to CD4 and a co-receptor [133,134]. HIV requires co-receptors CCR5 and CXCR4 to gain entry into the host cell. Different HIV-1 variants may require one or both of the co-receptors and are classified as R5 (requires chemokine receptor CCR5), X4 (requires chemokine receptor CXCR4), and R5X4 (uses both receptors) [135]. CCR5 is expressed at high levels in memory T cells, macrophages and dendritic cells, while CXCR4 is expressed on memory and naïve T cells [135]. Although all cells expressing CD4 and accompanying a co-receptor are susceptible to HIV-1 infection, activated T cells are the predominant targets [135]. Upon entry into the mucosa, resting CD4+ T cells are infected and the initial virus population of HIV (termed founder population) expands locally. This expansion of virus allows for viral dissemination into the draining lymph node and blood stream with the help of APCs such as macrophages and DCs. During this time, DCs secrete pro-inflammatory cytokines and chemokines such as IFN-γ and TNF-α as an anti-viral response, but this also further recruits more target cells such as activated CD4+ T cells and macrophages to the site of infection [135]. Upon activating adaptive immune responses, the large influx of CD8+ T cells are critical in controlling infection with the expansion and activation of HIV-specific cytotoxic T cells [136]. Even though this response is insufficient to clear the infection and prevent systemic

dissemination, the degree of response is a determining factor in disease progression [137]. However, during chronic infection, the CD8+ T cells can become exhausted and dysfunctional leading to poorer control of HIV if therapeutics are not administered [138,139].

Within infected cells, the HIV RNA is reverse transcribed into pro-viral DNA which is then integrated into the host genome. Using the host's cell machinery, the HIV genome is transcribed, viral proteins are assembled, and more mature virions are released. As a retrovirus, HIV is able to establish latent infection within $CD4^+$ T cells, monocytes, and macrophages, and the infected host cells can proliferate with the integrated HIV genome [140,141]. The pro-viral integration along with HIV mutants' immune escape from CD8+ T cell killing results in an establishment of pro-viral reservoirs within infected cells. Interestingly this reservoir of infected cells can be established as early as 3 days post-infection [142]. ART is able to control viral load and prevent HIV infection of new cells, but it is unable to eliminate latent infection and viral reservoir. As a result, HIV remains uncurable, with the possibility of viral rebound once ART is interrupted or stopped [143,144].

1.2.3. Clinical Presentation and Available Therapies

HIV-1 infection can be diagnosed with rapid tests or higher sensitivity assays that detect anti-HIV antibodies or p24 antigen [145,146]. During the initial stage of infection (0 to 3 weeks), target cells are infected by HIV and a viral reservoir is established while adaptive immunity is recruited. Between 3 weeks to 2 months of acute infection, some patients may be symptomatic presenting with fever, lymphadenopathy, rash, and muscle aches, but most are asymptomatic. During this time, plasma viral load can be detected by measuring HIV RNA copies which normally peaks to around $1x10^6$ – $1x10^7$ copies per mL, meanwhile CD4+ T cell counts transiently but rapidly decrease [135]. After cellular immunity develops, HIV viral load dramatically decreases to a "viral set-point" which can widely range from $1x10^3$ to $1x10^6$ copies of HIV RNA per mL of blood while CD4+ T cell counts rebound close to normal levels [147,148]. Those with higher viral set points may progress more rapidly to AIDS and death when compared to those with lower viral set points [147,149,150]. After the viral set point is established, the chronic phase of infection begins where without treatment/therapy CD4+ T cells continually decline until progression to AIDS leading to death or the development of an opportunistic infection that leads to death [135].

The development of drugs and therapeutics have greatly reduced HIV transmission and improved the quality of life and patient outcome for PLWH. HIV entry inhibitors such as maraviroc prevent HIV from entering the cell by competitively binding to the CCR5 co-receptor. Nucleoside reverse transcriptase inhibitors (NRTIs) tenofovir and emtricitabine block reverse transcriptase through incorporation into HIV DNA and terminates HIV DNA

synthesis. Non-nucleoside reverse transcriptase inhibitors (NNRTIs) such as rilpivirine inhibits reverse transcriptase by binding near the active site to change enzyme conformation. Integrase inhibitors daltegravir and dolutegravir prevents insertion of HIV proviral DNA into the host genome [135,151]. As of 2022 there are over 45 FDA approved ART drugs and combination treatments. Combination treatment generally consist of two NRTIs along with a third drug from one of the other classes (integrase inhibitor, protease inhibitor, or NNRTI) [152]. These therapy regimens can greatly reduce viral burden to virtually undetectable levels of HIV RNA copies within plasma within weeks [153]; the immune system (in particular CD4+ T cells) recovers most of its lost functions, and the development of AIDS is prevented.

For individuals known to be at high risk of becoming infected with HIV, pre-exposure prophylaxis (PrEP) with antiretroviral drugs such as oral tenofovir disoproxil fumarate (TDF) and emtricitabine can provide effective protection [154]. Post-exposure prophylaxis using TDF and emtricitabine as soon as possible after known HIV exposure (ideally within 72 hours) also show efficacy in reducing risk of infection [155].

1.2.4. Animal Models for HIV Research

Small animals including standard inbred mice, rats, and hamsters are not susceptible to HIV-1 infection and fail to sustain HIV viral load within blood plasma [156]. Since human

CD4 along with human CCR5 and/or CXCR4 receptors are necessary for HIV-1 infection, transgenic small animals such as transgenic mice and rats with immune cells expressing these human receptors have been developed. Even though the transgenic expression of human CD4 and CCR5 receptors in mice allow for HIV entry and infection of mouse immune cells, systemic infection could not be sustained *in vivo* [157]. Human CD4 and CCR5 expressing cells in transgenic rats could also sustain HIV infection, but systemic infection was inconsistent with very low plasma viral load at up to 7 weeks post-infection [158].

Due to the lack of success in the use of small animals for HIV studies, a large portion of *in vivo* HIV research is from NHP models. The most commonly used species of NHPs for investigating HIV/AIDS are the rhesus macaque, pig-tailed macaque, and cynomolgus macaque [159]. These macaques species can be infected with simian immunodeficiency virus (SIV) or the chimeric simian human immunodeficiency virus (SHIV) via vagina, rectal, or oral routes. SIV is a retrovirus very closely related to HIV and is believed to be the lineage origin of HIV [160]. Rhesus macaques models can recapitulate human vaginal and rectal transmission using low dose SIV infection where small populations of early founder virus were observed and establish productive infection similar to human transmission [161,162]. In vaginal challenge models, the varying menstrual cycles causing differences in vaginal epithelium thickness can affect the efficiency of virus transmission and thus causing inconsistency in infection. Pre-treatment of the animals with depot-

medroxyprogesterone acetate (DMPA) can induce thinning of the vaginal epithelium allowing for increased susceptibility for SIV infection within all animals [163].

NHP studies in SIV/AIDS pathogenesis has also contributed greatly to shape our understanding of HIV and influence research objectives. For instance, the discovery that disease progression is not only determined by plasma viral load, but also viral replication in lymph nodes and different CD4+ T cell subsets during chronic immune activation during chronic infection has directed research focus towards CD4+ central memory cells and lymphoid tissue involvement in disease progression [164,165]. Studies in NHPs have also shown that HIV disease progression is attributed to intestinal microbial imbalance providing insight that probiotics can improve responses to ART in SIV-infected macaques [166]. Finally, the establishment of ART models in SIV-infected macaques showed ART regimens being very effective in suppressing virus replication similar to studies in humans [167,168]. This can allow future investigations on the efficacy of other therapeutics within ART-treated HIV-infected individuals.

Non-human primate models have also been greatly involved in HIV vaccine studies and contributed to vaccine design. The *nef* gene of HIV has a multitude of supporting functions for HIV infection and replication [169]. Infecting NHPs with *nef* gene-deleted SIV demonstrated protection against naïve SIV infection [170]. This prompted further development of live-attenuated SIV as vaccine models within NHPs and the observation

that live-attenuated SIV may induce sufficient activated effector memory T cells in lymph nodes to suppress early SIV replication at these high replication lymphoid sites [171].

Although NHPs have greatly contributed to the knowledge and understanding of HIV/AIDS as well as the development of therapeutics and vaccines, there are still major limitations with their use. NHPs present with practical challenges such as cost and labour in maintenance, reaching sufficient sample size for statistical power, and the inherent difference between SIV/SHIV and HIV. Therefore, *in vivo* models for HIV research still requires small animal models that can recapitulate HIV infection such as humanized mice in order to further advance research progress.

Chapter 1.3. HIV/*Mtb* Co-Infection

1.3.1. Epidemiology and Significance

As described in Chapters 1.1 and 1.2., pulmonary TB and HIV/AIDS alone causes significant burden on individuals living with the disease. Coincidentally, the predominant immune cells that are infected by HIV (CD4+ T cells, and macrophages), are also involved in maintaining structure and control of TB granulomas to prevent growth and spread of *Mtb* within the lungs [49,172]. This is believed to contribute to individuals with LTBI co-infected with HIV having an increased risk of ATB reactivation by over 20-fold [173]. Furthermore, despite undergoing long-term ART, the risk of TB disease in PLWH can still remain 4 to 7 fold higher than persons without HIV [174,175]. HIV/*Mtb* co-infection also

increases patient mortality as *Mtb* infection is the leading cause of death within PLWH, and out of the 1.5 million deaths from TB in 2020, over 210,000 deaths were among co-infected PLWH [176]. HIV and TB incidences also present with significant geographical overlap, where sub-Saharan Africa and some parts of Latin America and Southeast Asia face the highest HIV prevalence in new and relapsed cases of TB [177]. Since both diseases are associated with stigma, there is a notable social barrier that dissuades individuals from seeking appropriate testing and treatment [178,179]. The consequences of non-treatment is even more severe for co-infected individuals as disease progression of HIV to AIDS is accelerated [180].

Clinically in co-infected individuals, HIV infection is often discovered upon an initial ATB diagnosis and subsequent HIV test. It is recommended that therapeutics such as ART begin either as soon as initiation of TB drug treatment or within 8 weeks of beginning TB treatment depending on the patient's CD4+ T cell counts [181]. Treatment for TB is already an intensive process that can take months to sometimes years depending on the drug-resistance and drug-susceptibility status of the *Mtb* and patient responses to treatment [182]. In combination with the necessary lifetime adherence to ART for effective viral suppression, non-compliance also becomes a much greater issue to not only the individual, but also public health in terms of controlling MDR and XDR pathogens [183]. As a result, incidence of MDR- and XDR-*Mtb* is higher within PLWH [184] causing higher risk for drug-resistance despite obtaining treatment [185].

HIV/*Mtb* co-infection can also complicate both diagnostics and therapies [176,184,186,187]. For instance, diagnostic sensitivity of IGRAs for detecting *Mtb* infection in PLWH may be impaired due to the reduced counts of IFN-producing CD4+ T cells [188]. As a result, the use of IGRA for effective diagnosis for PLWH is still debated and thus can limit the available testing in populations where HIV-infection is prevalent [189]. Therapies in the context of co-infection are also complicated as *Mtb* infection in PLWH presents as an opportunistic infection, and upon initiating ART, a phenomenon termed immune reconstitution inflammatory syndrome (IRIS) can occur [190,191]. IRIS develops from the rapid recovery of immune responses after ART which can lead to excessive immune activation, and more specifically, TB-associated IRIS (TB-IRIS) which can present in two forms. Paradoxical TB-IRIS occurs when TB treatment is initially effective, but upon starting ART, the disease progression ensues and unexpectedly becomes worse with treatment [191,192]. The second form called "Unmasking" IRIS is generally associated with ART-triggered inflammatory responses causing a previously subclinical TB infection to become clinically detectable [191,192]. Unmasking-IRIS is still poorly defined and understood, and thus requires further research to help patients deal with these treatment complications [193]. Although it is evident that effects of HIV and *Mtb* infections provide reciprocal advantages that work to exacerbate each other's pathogenesis, the exact host-pathogen immune interactions and mechanisms are not well elucidated *in vivo* [194,195]. Therefore, it is clear that in order to develop effective vaccines, therapeutics, and cure, further investigation into HIV/*Mtb* co-infection is a necessary and urgent topic for research.

1.3.2. Human Pathology and Animal Models Informing Current Knowledge

Clinical studies with human samples have clearly illustrated worse disease outcome for individuals co-infected with HIV-1 and *Mtb* when compared to those with single infections. Based on current literature, various human studies have contributed to a foundation of understanding immune responses, pathogenesis, and host-pathogen interaction during co-infection. However, the pathology, disease pathogenesis, and mechanistic pathways *in vivo* that leads to more severe disease outcomes for co-infected individuals are still largely unclear and require further investigation.

In human lung epithelial cell samples, HIV infections disrupt barrier integrity and function which may affect initial *Mtb* transmission and protection against *Mtb* infection [196]. Additionally, HIV infected human alveolar macrophages from bronchoalveolar lavage (BAL) samples were associated with reduced macrophage apoptosis from *Mtb* infection compared to singly-*Mtb* infected macrophages [197,198]. As described in Chapter 1.1.2., apoptosis is an important mechanism in the control of *Mtb* infection, thus HIV may be altering innate immunity to favour *Mtb* replication leading to the increased risk of developing ATB. *Mtb* infection may also be increasing the expression of both CCR5 and CXCR4 co-receptors on CD4+ T cells while also increasing HIV replication within co-infected macrophages [199–201]. In addition to CD4+ T cell depletion from HIV-1

infection, mycobacteria-specific T cell responses in PLWH may also be impaired [202,203]. CD4+ T cells collected from bronchoalveolar lavage fluid (BAF) of BCG vaccinated PLWH showed significantly fewer IFN-γ and TNF-α producing CD4+ T cells than HIV-negative individuals [204]. The pro-inflammatory responses observed in different stages of HIV infection are also a factor for co-infection, but this area is complex and poorly understood, especially in human tissues. For instance, some pro-inflammatory responses that alter microbicidal and antigen-presenting function of APCs are protective against *Mtb*, while other inflammatory responses such as type I IFN production that is driven by HIV may promote *Mtb* proliferation [205–207].

With regards to granuloma pathology, it is commonly hypothesized that HIV-1 infection disrupts TB granuloma formation, organization, and structure by killing CD4+ T cells, and altering normal T cell and macrophage functions. As a result, the fine balance of the TB granuloma is disturbed to favour *Mtb* growth and cell death leading to uncontained granulomas and extrapulmonary bacterial dissemination. The conclusions that led to these hypotheses are based on *in vitro* studies such as those mentioned above, or are mostly derived from human peripheral sampling such as collected peripheral blood mononuclear cells (PBMCs) and BAF. As described in Chapter 1.1.4., granulomas are complex and heterogenous. Human sample data may only be capturing incomplete parts of the heterogeneous variations in cell composition, microenvironment and immune responses within and around granulomas of co-infected individuals. Therefore, examination of *in vivo*

granulomas is the most accurate and informative to investigate co-infection human pathology.

In the current literature, there is still no consensus on whether co-infection affects certain features of the granuloma, for example, the caseating necrosis within granuloma formation. Some studies in human lung pleura [208,209] and lymph nodes [210,211] show no differences in granulomatous caseation between co-infected and singly-infected individuals, while one study showed increased necrotic granulomas within the lungs of co-infected individuals [212]. Thus, it is unclear whether HIV-1 co-infection affects the likelihood of caseous granulomas development. On the other hand, the reduction in peripheral human CD4+ T cell counts within co-infected individuals is likely associated with both poorer granuloma formation and higher *Mtb* bacterial load. Those with higher peripheral human CD4+ T cells developed well-formed granulomas within biopsied lymph nodes, while those with lower counts had a combination of well-formed and poorly-formed granulomas, and those with the lowest counts had mostly necrosis with an abundance of macrophages [211,213]. Other immunological and pathological features such as immune cell composition, *Mtb* bacterial load, and cytokine milieu within the human TB granuloma still warrants significant further investigation and clarification for consensus within the literature [48].

The advantages of animal models include the abilities to control the timing, dose, and strain of infection and sampling or necropsy at predetermined time points. Currently limited *in*

vivo animal models are capable of investigating co-infection, and this limitation is therefore is one of the main challenges in advancing co-infection research. The most commonly used large animal models are NHP models. In particular, rhesus macaques infected with SIV can develop AIDS-like disease progression upon BCG or *Mtb* co-infection [214,215]. Disease progression was also accompanied with depletion and suppression of antigen-specific CD4+ T cells in co-infected animals, especially pulmonary CD4+ T cells [214–217]. However, the importance of CD8+ T cells were also illustrated in macaques when higher effector CD8+ T cells functionality reduced TB pathology and reactivation [215]. LTBI re-activation also can be well-modelled with cynomolgus macaques and rhesus macaques co-infected with SIV and *Mtb* [218–220]. This has led to the development of macaque models of SIV/*Mtb* co-infection with ART to investigate viral replication, immune cell functions, and different cases of ART treatment initiation *in vivo*. It is notable that despite the effectiveness of ART controlling SIV viral load and restoring CD4+ T cells in macaques, it still does not fully prevent TB reactivation [221]. Furthermore, a similar macaque model demonstrated that the timing of ART initiation may also play a role in disease control and severity. Earlier initiation of ART reduced *Mtb* granuloma pathology, lung bacterial load, extrapulmonary dissemination, and increased survival rate when compared to later or no ART initiation [222]. These findings corroborate the results observed in human clinical studies and thus offer further *in vivo* insight to the host-pathogen interactions during therapies for HIV/*Mtb* co-infection [223,224].

There are very limited conventional small animal models available that demonstrate potential in co-infection studies and this includes the use of chimeric HIV (termed

EchoHIV) within conventional mice [225,226]. HIV-transgenic mice have been used to investigate the effect of *Mtb* infection on HIV gene expression and found that HIV viral gene expression was activated by *Mtb*, but suppressed upon administration of anti-TB chemotherapy.

Overall, there are limitations to large animal models to investigating HIV/*Mtb* co-infection such as cost and ethical concerns along with the use of SIV and BCG as surrogates to represent HIV and *Mtb* [227]. Meanwhile all aforementioned small animals including those in Chapters 1.1.5. and 1.2.4., develop neither human immune cells nor immune cells that are functionally similar enough to humans to fully recapitulate both HIV and TB infections. Therefore, it is critical for better and more representative small animal models to be developed to further the progress in research for HIV/*Mtb* co-infection. Humanized mouse models (which are small animals that also develop human immune cells and functions) have steadily improved its ability to recapitulate the human immune system and is populating the research landscape of HIV and TB. The use of humanized mouse models may become the most dominant model in HIV, TB, and co-infection studies and will be discussed in Chapter 1.4.

1.3.4. Outstanding Questions for Co-infection Investigation

PLWH are vulnerable to opportunistic infections due to an altered immune repertoire from HIV-1 infections, and while this is improved with initiation of ART, immune response and functionality is not fully recovered. Therefore, the effects of primary HIV-1 infection on *in vivo* immune responses to interventions such as ART or vaccination are complex. The development of TB-IRIS as discussed in Chapter 1.3.2. and other unknown potential complication within PLWH undergoing TB treatment or receiving TB vaccination require further *in vivo* investigation. There are many hypotheses that attempt to explain the worse disease outcomes of individuals co-infected with HIV-1 and *Mtb*. Although these hypotheses seem plausible given our current knowledge of HIV and TB, they still remain largely unproven in the context of co-infection as mechanistic studies are exceptionally challenging in humans. Due to the difficulty in studying representative co-infected granulomas in humans (specifically non-necropsy lung granuloma), many questions surrounding the effects of co-infection on granulomas still exist.

A systematic review and meta-analysis on existing literature of human granulomas in co-infection identified several features of the granuloma formation that are still unclear with limited consensus in literature [48]. In the context of granuloma compositional changes, it is still unclear whether HIV-1 significantly changes the number of granulomas developing within the lungs as there is great variability between studies. The effect of HIV-1 on the cellular composition within granulomas is also unconfirmed. For instance, results from non-lung granulomas showed different results regarding the presence of CD4+ and CD8+ T cells where some reported reduction in cellularity, while other reported differences only

in some co-infected participants [48]. The presence of pathological macrophages within granulomas such as epithelioid macrophages and giant cells were described to be more frequent but highly variable within PLWH. This variability indicates that the effects of HIV-1 on the presence of these cell types in granulomas are inconclusive [48]. Lastly, although it is believed that *Mtb* dissemination can be exacerbated due to HIV-1 impairing granuloma formation, Diedrich et al. concluded that evidence to support this hypothesis is also limited and conflicting. Therefore, major questions still remain including how/if HIV-1 changes overall granuloma formation and structure, whether immune cell presence such as CD4+ T cells is altered by co-infection, and if HIV-1 presence correlates with *Mtb* bacterial load within the granuloma. In the context of granuloma functional changes, cytokine expression in co-infected granulomas was also highly inconclusive and conflicting [48]. In particular, TNF-α production was observed to be higher in some co-infected individuals, but lower in others. Meanwhile no difference in expression of type I IFNs was observed in another study. From these reports, altered cytokine responses may not be directly caused by the presence of HIV-1 within the granulomas, as there may be an indirect correlation between peripheral CD4+ T cells counts and granuloma cytokine expression [48]. Therefore, cytokine expression and whether peripheral CD4+ T cell depletion is associated with any functionality or composition changes within the granuloma still remain question to be addressed.

As evidenced in Chapter 1.3.3., animal models are required to address these outstanding questions within the granuloma (especially lung granuloma). Due to a lack of available

animal models for HIV/*Mtb* co-infection research, it is critical that small animals such as humanized mice that well-recapitulate human immune functionality are developed to further research in understanding both pathogenesis, and vaccines and therapeutics.

Chapter 1.4. Humanized Mice

1.4.1. Application and Utility of Humanized Mice

Through Chapters 1.1 to 1.3, it is evident that a small animal model capable of sustaining HIV and TB infection while recapitulating human immune responses is greatly needed to advance HIV, TB, and co-infection research. Humanized mice (hu-mice) are immunocompromised mice that are engrafted with human tissues and/or immune cells and subsequently develop substantial and functional populations of human immune cells.

The rapid development of successive versions of hu-Mouse models over the past 30 years has proven to be an essential tool for investigating and advancing the knowledge of multiple facets of infectious disease research [228–233]. Hu-mice can not only accurately reproduce many aspects of human infections, but are also a smaller, more cost-effective, and more widely available *in vivo* model for infectious disease studies.

Hu-mice develop susceptible and permissive human cells (such as human CD4+ T cells and macrophages) representing the natural targets of HIV infection *in vivo*; as such,

reagents and therapeutic strategies currently designed for humans can directly be applied to Hu-Mouse models. These mice have proven to be an effective tool in studying various aspects of HIV pathogenesis during active infection, as well as potential therapeutic strategies, and hold great potential in advancing research within the field.

1.4.2. Development of Humanized Mouse Models

The development of several background strains of immunodeficient mice were critical in developing methods to successfully engraft human cells into mice. Humanizing mice requires xenogeneic transplantation of either human cells and/or tissue, and to prevent rejection of the engraftment, highly immunodeficient mouse recipients are necessary. The breakthrough utilization of the *Prkdc*^{scid} (SCID) mutation in CB17 mice in 1988 gave rise to the first successful engraftment of human peripheral blood lymphocytes [234]; since this discovery, these mice have been used in a broad variety of basic and pre-clinical studies. The *Prkdc* gene [235] encodes for essential DNA damage repair mechanisms as well as V(D)J recombination for the development of mature T and B lymphocytes [236]. The absence of viable mouse T and B lymphocytes result in severe immunodeficiency and allow for engraftments to be sustained [237]. However, despite the lack of T and B cell function, high natural killer (NK) cell and innate immune activity is still present in these mice [237]. Thus, the incomplete immune depletion of the SCID model still posed challenges for reconstitution of both human myeloid and lymphoid cell lineages [234,238].

The next advancement in improving hu-mouse models was crossing the non-obese diabetic (NOD) mouse strain with SCID mice. NOD mice have signal regulatory protein-α (SIRPα) with more homology to human SIRPα than inbred strains such as C57BL/6 and BALB/c mice [239].

The stronger affinity of SIRPα for human CD47 results in a stronger "don't eat me" signal from human immune cells to the NOD-murine macrophages upon binding, thus preventing phagocytosis of the engrafted human stem cells [240]. Additionally, NOD mice have a mutation in the *Idd3* gene, which is involved in IL-2 signaling [241]. This results in reduced IL-2 production and therefore impairs murine helper T cell, cytotoxic T lymphocyte, and natural killer (NK) cell activity and again improves engraftment of human stem cells [241]. The last major breakthrough in addition to the NOD-SCID background is the targeting and mutating of the IL-2 receptor γ-chain locus (*Il2rg*) [242]. This mutation further impairs murine immunocompetency, as the common γ-chain is an integral component of high-affinity receptors and is required for the binding and signaling of a wide variety of pro-inflammatory cytokines [242]. These mutations in the *Il2rg* gene further enhance the model by completely eliminating mouse NK cell activity [243].

Using these immunocompromising mutations or other mutations or knockouts (KOs) to achieve similar murine immunodepleting effects, many useful immunodeficient murine backgrounds have been created. Some of the most commonly used backgrounds in literature include the *Il2rg* KO NOD.Cg-Prkdc^{scid}Il2rg^{tm1Wjl}(NSG) mice [244,245],

NOD.Cg-Rag1^{tm1MoM}Il2rg^{tm1Wjl} (NRG) mice, NOD.Cg-Prkdc^{scid}Il2rg^{tm1Sug} (NOG) mice [246], and Rag1^{null}Il2rg^{null} or Rag2^{null}Il2rg^{null} (DKO or BRG) mice [245,247]. Other backgrounds are discussed extensively elsewhere [228,231], as this project will be focusing on the NSG and NRG background strains for reasons discussed in Chapter 1.4.3.

After choosing the immunodeficient background mice, there are two main methods of engraftment. First is the administration of human CD34+ hematopoietic stem cells (HSCs) upon sublethal doses of irradiation [248]. HSCs may be obtained from umbilical cord blood, bone marrow, fetal liver or mobilized whole blood and engrafted via intravenous injection in adult mice, or intrahepatic injection in newborn pups [249]. This method will now be referred to as the "HSC-method" of engraftment. The second method involves the engraftment of human fetal liver and thymus tissue by surgically implanting the tissues into adult immunodeficient mice under a renal-capsule. Human CD34+ HSCs derived from the bone marrow or liver of the same fetal donor is then engrafted via intravenous injection [250–252]. This method will now be referred to as the "BLT-method" of engraftment. The addition of human thymus tissue using the BLT-method allows for the generated T cells to be educated in the context of human leukocyte antigen (HLA) within the human thymus instead of mouse major histocompatibility complex (MHC) [253]. Both the HSC-method and BLT-method of engraftment are able to successfully generate hu-mice that reconstitute with human monocytes, dendritic cells, T cells, and B cells in peripheral blood and tissues. The BLT-method generates higher overall levels of human lymphoid populations, but have lower reconstitution from the myeloid lineage [250–254]. More specifically, the BLT-

method also yielded higher percentages and counts of CD3+ T cells in the spleen [253] and had better GALT development [255]. On the other hand, the HSC-method demonstrated better human B cell and certain myeloid cell development such as myeloid dendritic cells [253].

1.4.3. Current and Next-generation Models

Several aforementioned immunodeficient background strains such as the NSG, NRG, NOG, and BRG used for engraftment can be considered the current-generation of hu-mouse models [245,247]. These current-generation models have all been widely used in the literature for infectious diseases research [231,256–258]. Between these strains, the HSC-methods of engraftment in NSG and NRG models develop higher levels of human T cells following HSC engraftment in the blood and secondary lymphoid organs compared to the BRG model due to their NOD background [259]. Compared to NSG mice, which has a complete KO of the IL-2 receptor, NOG mice express a truncated form of the IL-2 receptor that only eliminates downstream cell signaling [260]. Human immune cell repopulation in NOG mice is comparable to NSG mice within the spleen and thymus, but are lower in bone marrow using the HSC-method of engraftment [245]. Within the current generation of hu-mice, humanized NSG (huNSG) and humanized NRG (huNRG) may offer slight advantages in human immune cell repopulation compared to other models and thus will be highlighted in this project. Although no significant differences were found in engraftment levels between huNSG and huNRG [261], NSG mice have poorer tolerability to radiation

(where only radiation below 400cGy was tolerated [244]) due to the SCID mutation leading to defective DNA repair activity [262]. Conversely, NRG mice can tolerate higher doses of radiation of up to 650cGy since the targeted mutations at the recombination-activating gene 1 (Rag1) and Rag2 loci to eliminate murine lymphoid populations does not affect DNA repair mechanisms [261]. As a result, NRG mice have fewer complications with the doses of sublethal irradiation during the HSC engraftment process.

The BLT-method of engraftment can also be used for NSG mice, termed humanized NSG-BLT model (huNSG-BLT). The huNSG-BLT mice offer some advantages over HSC-methods as described in Chapter 1.4.2. However, there are several major challenges with using the huNSG-BLT model such as issues with ethically obtaining human fetal tissue, consistently performing technically challenging surgical procedures, and the development of graft-versus-host disease (GvHD) post-engraftment (which can limit the experimental timeline for a study) [263,264]. Therefore, the development of a more practical and reliable humanized mouse model using the HSC-method would be ideal for longer term *in vivo* pathogenesis investigations for HIV/*Mtb* co-infection.

Next-generation hu-mice are developed to further improve upon current-generations where there are low myeloid populations (such as macrophages and DCs) and lack of isotype-switched antibodies from the absence of mature B cells. Next-generation hu-mice use the immunodeficient mice of current generation models with additional knock-in (KI) or transgenic modifications to support HSC-engraftment and repopulation of human immune

cells and functionality. A variety of next-generation KI and transgenic hu-mice have been developed and are discussed elsewhere [228,231,265–267]. To choose the appropriate hu-mouse model will depend on the study of interest. For instance, hu-mice that specifically express the human IL-15 transgene are able to develop high levels of IL-15 to support the development of human NK cell populations. In particular, the humanized NSG-hIL15 (huNSG-hIL15) model [268] and a similar humanized SRG-hIL15 model [269] showed improved development and functional maturation of circulating and tissue-resident human NK cells. Although the development of *in vivo* NK cells allow these models to be used for cancer studies, the model also has potential for use in infectious diseases studies such as HIV that involve investigation of NK cells.

Humanized DRAGA mice (HuDRAGA) present as a good candidate for HIV/*Mtb* investigation [270]. DRAGA mice are on the NRG background and express transgenic HLA class I and II molecules (specifically, HLA-A*02:01 and HLA-DRB1*04:01, respectively) [270,271]. When engrafted with HLA-matched HSCs, humanized DRAGA (huDRAGA) mice demonstrated development of fully functional and robust levels of human CD4+ and CD8+ T cells, Treg cells, and T follicular helper cells [270,271]. Human isotype-switched antibody production was also observed, indicating development of mature and functional human B cells. Additionally, human CD4+ T cells, which are targets of HIV, repopulated the female reproductive tract (FRT) of huDRAGA mice allowing for intravaginal HIV infection [272]. The reconstitution improvements in the lymphoid population is largely due to the ability for the human T cells to undergo partially HLA-

matched thymic education and development. As a result, T cells become HLA-restricted while developing antigen-specific responses to pathogens [273,274]. Overall, these findings illustrate the improvements of the huDRAGA model over current generation models to more closely recapitulate many aspects of the human immune system and functionality [270,275]. Therefore, within the context of investigating HIV/*Mtb* co-infection host-pathogen interactions and immune responses to therapies and vaccinations, huDRAGA mice present as a promising small animal model for widespread use to advance research in the field.

1.4.4. The Use of Humanized Mice for HIV Studies

As discussed in chapter 1.2.4., NHP models have dominated the HIV/SIV research landscape due to the lack of small animal models that are susceptible to HIV infection. Although NHPs have contributed greatly to the foundational knowledge and understanding of HIV, these large animals are impractical for widespread use and can be limited in powering efficacy and safety studies for pre-clinical drug/therapeutics testing [276]. In the past couple of decades, HIV studies using hu-mice are populating the literature especially within vaccine development and therapeutics testing [277,278].

Hu-mice are permissive to vaginal and rectal infection of both the R5- and X4-tropic variants of HIV [251,279–285], and overall, both cellular and humoral immune responses

to HIV were also observed *in vivo* [251]. Hu-mice also well-recapitulate human disease upon HIV infection where infection persistence leading to viremia, human CD4+ T cell depletion, and viral infection of lymphoid tissues were all observed [284,286–289]. Furthermore, HIV-1 viral load was also detected in the FRT, gut mucosa, kidney, spleen, lung, liver, and brain post-infection [271,272,290]. Interestingly, a T cell-deficient hu-mouse model repopulated with mainly human macrophages was still capable of sustaining HIV infection. This discovery directly contributed to the knowledge that human macrophages can be and are infected by HIV-1 [291–293]. Due to the ability for hu-mice to well-recapitulate so many aspects of HIV infection and pathogenesis, the use of hu-mice have tapped into a multitude of fields in HIV pre-clinical studies including therapy, prevention, viral latency and cure.

In therapeutics and prevention, various different hu-mouse models have been used for novel ART and PrEP testing regimens. Testing of ART drugs including combination ART (cART) [294–297], highly active ART (HAART) [298,299], and long-acting ART [300,301] have all demonstrated substantial HIV replication suppression with CD4+ T cell recovery *in vivo* [297]. Similar to humans, upon the termination of ART, HIV viral rebound accompanied by CD4+ T cell loss was observed in these studies. Administration of PrEP protects against HIV-1 challenge [302] and in some cases, irrespective of the route of exposure (i.e. mucosal, rectal, and intravenous) [303]. Pharmacokinetic trends of PrEP in hu-mice also reflect those seen in human studies, highlighting its potential use for pre-clinical PrEP studies [304]. Persistence of HIV-1 reservoirs in the presence of ART *in vivo* can also be investigated in

hu-mice, where latent HIV-1 reservoirs remained stable independent of the length of cART administration [305]. These observations can provide more insight into rebounding viremia after ART termination and serve as potential *in vivo* HIV latency models [306].

Other novel HIV therapies and cure strategies have also been extensively tested in hu-mice. These therapies include adoptive transfer of modified CD4+ T cells [307], broadly neutralizing antibodies (bNAbs) against HIV-1 [308–310], latency-reversing agents [311], and gene therapies including CRISPR-Cas9 [312,313]. These therapeutics have also demonstrated effective control of HIV-1 infection in the hu-mice, and have even shown the possibility of eliminating the HIV viral reservoir [311,313].

1.4.5. The Use of Humanized Mice for TB and Co-infection Studies

With recent advancements in hu-mouse models to better recapitulate human immune responses, hu-mice have been much more popularized within literature. However, due to the widely used and well-established standard inbred mouse and NHP models for TB (outlined in chapter 1.1.5.), there are still relatively fewer hu-mouse models investigating single *Mtb*-infection.

Initially, studies using BCG infection demonstrated the potential of the huNSG-BLT model, and the huNSG models using the HSC-method of engraftment to be used for *Mtb* infection [314,315]. These mice demonstrated granuloma-like structures within the lungs upon BCG

infection. Notably, mice that were humanized hosted much more severe lesions and pathology compared to their non-humanized counterparts illustrating the importance of human immune cells within the hu-mice in order to fully recapitulate mycobacteria infection [315]. Although BCG induced immune human macrophage and T cell responses, the formation of granulomas were significantly less severe than *Mtb* infection such as the development of a necrotic core [315]. Subsequent studies using huNSG-BLT mice in *Mtb* infection demonstrated features that well recapitulate human pathology such as granuloma formation within the lung and liver. Specifically, the formation of cellular cuffing with immune cell organization surrounding central necrosis of lung granulomas was observed along with extrapulmonary dissemination [316]. These studies consolidated hu-mice as good models for *Mtb* studies and have led to TB therapeutic investigations such as the testing of vaccination and treatments. For instance, huNRG mice were used to evaluate the protective efficacy of the human adenoviral-vectored vaccine AdHu5Ag85A [104]. This study demonstrate that both protective efficacy against *Mtb* infection and *Mtb*-specific immunogenicity elicited by the vaccine upon respiratory mucosal administration [104]. Other studies have also used huNSG mice and transgenic hu-mice to evaluate TB combination antibiotics treatments [317], vaccination [318], and infection response pathways [319].

In the context of HIV/*Mtb* co-infection, there are currently two major published papers that have used hu-mice. Both demonstrate the ability for hu-mice to recapitulate many aspects of human pathology and offer further insight on disease progression and host-pathogen

interactions. The first co-infection study used the huNSG-BLT model establishing primary HIV-1 infection followed by subsequent low-dose *Mtb* (H37Rv strain) infection [320]. The study found an increasing trend of lung pathology in co-infected huNSG-BLT mice when compared to TB-only mice, and illustrated pathological features such as TB pneumonia and bronchial occlusion. This study also provided insight on HIV localization during co-infection within the lungs where HIV-1 may be exclusively localized around granuloma lesions [320]. The huNSG-BLT model has also been used in one other HIV/*Mtb* co-infection study where paucibacillary TB was successfully modelled in *Mtb*-infected huNSG-BLT mice after TB treatment, and subsequent post-drug TB relapse was observed after HIV-1 infection [321]. Overall, these huNSG-BLT models have shown great promise as an *in vivo* small animal model for HIV/*Mtb* co-infection. However, as discussed in Chapter 1.4.3., the BLT-method of engraftment can pose several challenges including ethical and resource limitations of obtaining fetal tissue samples which restricts widespread use of the model to rapidly advance *in vivo* HIV/*Mtb* co-infection research. Therefore, one of the purposes of this project is to validate both current and next-generation of hu-mice using the more feasible HSC-method of engraftment for advancing HIV/*Mtb* co-infection research.

Chapter 1.5 Rationale and Project Overview

Currently, there are limited small animal models that are appropriate to investigate HIV-1 infections and better recapitulate human lung TB pathology *in vivo*. This leads to even

fewer options for *in vivo* HIV/*Mtb* co-infection research. Due to the high morbidity and mortality of co-infection and many unanswered questions to be addressed regarding disease interactions, small animal models of HIV/*Mtb* co-infection are required to further advance research. We aim to establish functional current- and next-generation hu-mouse models for HIV/*Mtb* co-infection that well-recapitulate host-pathogen responses and serve as pre-clinical models for understanding immune interactions, as well as vaccine and therapeutics testing. The huNRG model will serve as the current-generation model used in this project. In the literature, transgenic modifications to immunodeficient mice have allowed for increased immune cell engraftment and functionality, depending on the modification. The huNSG-hIL15, which produce human IL-15 required for human NK cell development allows for the addition of robust NK cell levels to the immune cell repertoire. In the context of infectious diseases, this is a promising model to establish in hopes of developing an *in vivo* system to investigate the role of NK cells in HIV infection. Therefore, this project will establish and compare the huNSG-hIL15 to the huNRG model. Transgenic models that express human HLA molecules can be engrafted with partially matched-HSCs which allow HLA-matching during T cell development to improve the repopulation of lymphoid lineages. In particular, the huDRAGA expresses both HLA class I and II (HLA-A*02:01, and HLA-DRB1*04:01, respectively) [270]. HuDRAGA mice have not only demonstrated better T cell engraftment, but also improved B cell functionality where isotype-switched antibodies were observed. This project will establish a similar model by crossing NRG mice expressing HLA class I (A*02:01) and NRG mice expressing HLA class II (DRB1*04:01), termed NRG-A2 and DRAG mice respectively. From here on, this model will be termed

DRAG-A2 and becomes the humanized DRAG-A2 (huDRAG-A2) upon HSC engraftment. HuDRAG-A2 mice will be considered the next-generation hu-mouse model used in this project. The improved immune functionality described in HLA transgenic mice make these ideal models to investigate HIV, *Mtb*, and HIV/*Mtb* co-infection. Upon establishing the huNRG and huDRAG-A2 models, HIV-1 and *Mtb* infections will be established individually to confirm that both models are capable of sustaining and recapitulating key features of human infection. (Note: the results from these single-infection studies will not be presented in this thesis as they have been submitted for publication and are currently under review: *Viruses*; April 28, 2022; Manuscript ID: viruses-1725813; Jack X. Yang*, Madeleine Lepard*; *co-first authors. These results are also presented in the MSc. thesis by Lepard M.). Both models will then be used to establish HIV/*Mtb* co-infection *in vivo* where the primary outcome will be the comparison between the pathogenesis of co-infection and single-*Mtb* infection. Lung granuloma pathology/histopathology will be another major outcome as granuloma development, formation, and composition are areas with multiple questions unaddressed due to the limited *in vivo* models and literature. Finally, effective vaccination against TB is an urgent global issue as 1.5 million people a year die from the disease. Despite over 37.7 million individuals living HIV globally who are the populations most at risk of dying from TB, PLWH are rarely included in clinical trials for TB vaccines. Due to the action of HIV on the immune cells that are key to TB defense, many worry that vaccines tested in HIV-negative individuals may not be efficacious in PLWH. Dr. Zhou Xing (McMaster University, Hamilton, ON) has developed a novel multivalent adeno-vectored respiratory mucosal TB vaccine (AdCh68MV). This vaccine is

unique in features such as the route of respiratory mucosal administration and the ability to stimulate immune cells to target multiple stages of the *Mtb* life cycle (discussed in Chapter 1.1.6.). These features may allow the vaccine to better induce protective immune responses in humanized mice against *Mtb* and even overcome HIV-mediated immune suppression in PLWH. Here we will test the immunogenicity of this novel vaccine in the current- and next-generation huNRG and huDRAG-A2 mice as one of the first steps to establishing a TB-vaccination platform and strategy for persons without HIV and PLWH.

Chapter 1.6 Project Aims, Objectives, and Hypotheses

Aim 1 – Develop and compare current- and next-generation humanized mouse models with human immune cells capable of sustaining both HIV and TB infections.

Hypothesis: We hypothesize that the huNRG, huNSG-hIL15, and huDRAG-A2 models will successfully develop human immune cell populations essential for investigating HIV and TB infection. We also hypothesize that the huDRAG-A2 mice will develop higher levels and more functional human lymphoid populations than huNRG mice, while huNSG-hIL15 mice will reconstitute with higher levels of NK cells than huNRG mice.

Aim 2 – Establish HIV/*Mtb* co-infection in huNRG and huDRAG-A2 mice and investigate host-pathogen responses, immune function, and histopathology within blood and tissues *in vivo*.

Hypothesis: We hypothesize that both huNRG and huDRAG-A2 mice can sustain infection with HIV and TB alone and serve as viable models to investigate co-infection that recapitulate many aspects of human disease. Furthermore, when infected with HIV and subsequently *Mtb*, human CD4+ T cells and macrophages will be depleted resulting in poor control of *Mtb* bacteria within tissues of co-infected mice when compared to *Mtb*-only infected mice. We also hypothesize that co-infected mice of both models will develop more necrotic and disorganized lung granulomas when compared to *Mtb*-only infected mice.

Aim 3 – Elucidate the immunogenicity of adeno-vectored TB vaccines in generating *Mtb*-specific immune responses within huNRG and huDRAG-A2 mice.

Hypothesis: We hypothesize that the trivalent AdCh68MV vaccinated huNRG and huDRAG-A2 mice will generate significant *Mtb*-specific human T cell responses within the lung and spleen. We also hypothesize that the huDRAG-A2 mice will develop elevated *Mtb*-specific T cell responses when compared to huNRG mice, due to increases in immune functionality.

CHAPTER 2. METHODS

Chapter 2.1. Aim 1: Develop and compare current- and next-generation humanized mouse models with human immune cells capable of sustaining both HIV and TB infections.

2.1.1. Breeding and generation of NRG, NSG-hIL15, and DRAG-A2 mice

NRG mice (NOD.Cg-*Rag1*^{tm1Mom} *IL2rg*^{tm1Wjl}) and NSG-hIL15 mice (NOD.Cg-*Prkdc*^{scid} *Il2rg*^{tm1Wjl} Tg(IL15)1Sz/SzJ), were obtained from The Jackson Laboratory (JAX, strain#: 007799, and strain#: 030890, respectively). To generate DRAG-A2 mice that express both homozygous HLA-A*02:01 and HLA-DRB1*04:01, homozygous NRG-A2 mice (NRG mice expressing homozygous HLA-A*02:01) and DRAG mice (NRG mice expressing homozygous HLA-DRB1*04:01) were crossed mated. The homozygous NRG-A2 mice were obtained as a generous gift from Dr. Ali Ashkar and Dr. Yonghong Wan (McMaster University, Hamilton, ON). These NRG-A2 mice were generated by back-crossing the HLA-A*02:01 transgene from the NSG-A2 strain (JAX, strain#: 009617) onto the NRG background. Only heterozygous DRAG mice could be obtained from The Jackson Laboratory (JAX, strain#: 017914), and therefore, homozygous DRAG mice had to be first generated prior to crossing the DRAG with NRG-A2 to generate DRAG-A2 mice. Heterozygous DRAG mice were mated, and only their progeny (first generation) that were genotyped to be positive for the HLA-DRB1*04:01 allele were then mated with NRG mice

(not expressing HLA-DRB1*04:01 transgene). The second generation (litters of the first generation) are again genotyped for the HLA-DRB1*04:01 transgene. If 100% of the second generation (n>10) expresses HLA-DRB1*04:01, their parents (first generation) DRAG parent can be confirmed to be homozygous. If any mouse from that litter fails to express HLA-DRB1*04:01, then their DRAG parent is confirmed to be heterozygous.

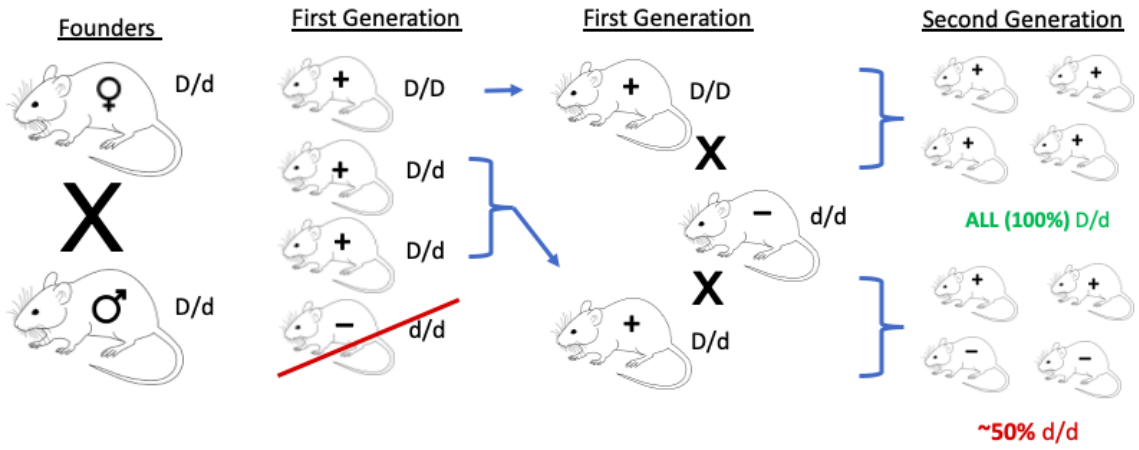

Figure 1. Method used for establishing the homozygous DRAG colony.
Heterozygote founders produce first generation of "parents" that are crossed with NRG mice. Second generation litters with 100% positive genotyping for the HLA-DRB1*04:01 allele confirms their parents are homozygotes. D/D = Homozygous and D/d = heterozygous for HLA-DRB1*04:01 allele; d/d = does not express HLA-DRB1*04:01 allele; "+" = positive genotype test for the HLA-DRB1*04:01 allele; "–" = negative genotype test for the HLA-DRB1*04:01 allele.

2.1.2. Genotyping of NSG-hIL15, and DRAG mice

DRAG mice required genotyping as part of the method to establish homozygous expression of the transgenic HLA-DRB1*04:01 allele. NSG-hIL15 mice required genotyping to ensure the expression of transgenic IL-15 allele. Both DRAG and NSG-hIL15 mice were

ear tagged and a small sample of ear tissue was obtained. Ear tissue was used in the DNeasy Blood & Tissue Kit (QIAGEN, cat# 69506) to extract purified DNA.

DRAG:

Polymerase chain reaction (PCR) genotyping was performed using the Platinum II Hot-Start PCR Master Mix (Invitrogen, cat# 14000011) mixed with primers specific for the allele of interest: HLA-DRB1*04:01 allele (forward primer: 5'-GTT TCT TGG AGC AGG TTA AAC-3'; reverse primer: 5'-CTG CAC TGT GAA GCT CTC AC-3'), internal control primers (forward internal control: 5'-CAA ATG TTG CTT GTC TGG TG-3'; reverse internal control: 5'- GTC AGT CGA GTG CAC AGT TT-3'), and sample DNA. PCR samples were loaded on 1.5% agarose gel (Invitrogen, cat#16500-500) with EZ VISION loading dye (VWR, cat# 97064-190) at a 1:5 to 1:10 DNA/loading dye ratio and ran with gel electrophoresis at 100 volts. Results positive for HLA-DRB1*04:01 will appear as double bands where both the internal control band (~270bp) and the transgene band (~320bp) could be observed under UV-illumination. Samples without the transgene will only show the single internal control band.

NSG-hIL15:

Real time quantitative PCR (qPCR) was performed using the Platinum II Hot-Start PCR Master Mix with primers specific for the Tg(IL15)1Sz allele (forward primer: 5'-GGT GGC CTG ACC TAA GGA AG-3'; reverse primer: 5'-GTG CCA TCG AGA CTT CCA CT-3'), internal control primers (forward internal control: 5'-CAC GTG GGC TCC AGC

ATT-3'; reverse internal control: 5'-TCA CCA GTC ATT TCT GCC TTT G-3'), transgenic probe (5'- /56-FAM/TGC CAT AGC /ZEN/ AGG TAA TAC CAG CTT/3IABkFQ-3'), the internal control probe (5'- /5SUN/CCA ATG GTC /ZEN/ GGG CAC TGC TCA A/3IABkFQ/ -3'), and sample DNA. Samples were run on the StepOnePlus Real Time PCR System (Applied biosystems) and results were analysed on the StepOne Software (version 2.3).

Detailed reagent volumes, qPCR cycling, and machine settings will be outlined below as this method is adapted from The Jackson Laboratory for the first time in the Gillgrass Lab (https://www.jax.org/Protocol?stockNumber=030890&protocolID=31472).

Optimized qPCR reagent mix (per tube):

- Platinum II Hot-Start PCR Master Mix = 10 µL
- Forward primer (100 µM) = 0.8 µL
- Reverse primer (100 µM) = 0.8 µL
- Internal forward primer (100 µM) = 0.8 µL
- Internal reverse primer (100 µM) = 0.8 µL
- Transgenic probe (10 µM) = 0.3 µL
- Internal control probe (10 µM) = 0.3 µL
- DNase-free water (H_2O) = 2.2 µL
- DNA = 4 µL

Optimized qPCR Cycling:

1. Pre-PCR read*: 25ºC, 30 seconds
2. Holding stage: 94ºC, 2 minutes
3. Cycling stage*: (40 cycles)
    a. 98ºC, 5 seconds
    b. 60ºC, 20 seconds
4. Post-PCR read*: 25ºC, 30 seconds

*Select "Data Collection ON" option during these steps.

Other Program settings (StepOne Software v2.3):

- Experiment type: Genotyping

- Reagents: TaqMan
- Ramp Speed: Fast
- Plate Setup:
    - Allele 1/Allele 2 Reporter: FAM/VIC
    - Dye for Passive reference: NONE
- Reaction set up and materials list: Default, no changes made

2.1.3. Obtaining CD34+ Hematopoietic Stem Cells for Engraftment

CD34+ hematopoietic stem cells isolation:

Human umbilical cord blood (UCB) was collected with consent after delivery (HiREB 13-813; Department of Obstetrics and Gynecology, McMaster Children's Hospital, Hamilton, ON). All samples were processed within 48 hours to remove red blood cells from nucleated cells using an erythrocyte aggregation agent (HetaSep, StemCell Technologies, cat: 07906). Subsequently, enrichment of human CD34+ hematopoietic stem cells (HSCs) was performed by depleting CD2, CD3, CD14, CD16, CD19, CD24, CD56, CD66b cells and glycophorin A red blood cells using an antibody negative selection kit (RosetteSep, StemCell Technologies, cat: 15066). This was followed by separation using density gradient centrifugation (Lymphoprep, StemCell Technologies, cat: 07851). The final enriched samples were cryopreserved in a commercially available medium (CryoStor, StemCell Technologies, cat: 07930) and stored in liquid nitrogen. CD34+ HSC processing was adapted from Kwant-Mitchell et al. [322,323]. Additionally, 1mL of each UCB sample were aliquoted to be processed to isolate for cord blood mononuclear cells (CBMCs) using only the Lymphoprep density gradient centrifugation and cryopreserved for future

autologous NK cell expansion. Approximately 100uL of the final processed CBMC and CD34+ HSC was aliquoted for flow cytometry analysis. 500-750µL of UCB samples were also collected after the erythrocyte aggregation step and stored in -20ºC for HLA typing.

HLA tissue typing of UCB samples:

DNA was extracted from the 500-750µL of aliquoted UCB samples using the Qiagen Blood & Cell Culture DNA Midi Kit (QIAGEN, cat#: 13343). All final DNA samples were ideally concentrated between the range of 25-200ng/µL with an A260/A280 purity ideally between 1.65-1.80. Samples were screened for both HLA-DRB1*04:01 (DRAG allele) and HLA-A*02:01 (A2 allele). Samples were first screened for the DRAG allele using the MicroSSP Allele Specific HLA- typing class II DNA typing trays - DRB1*04:01 (OneLambda, cat#: SSPR2-104). Only upon testing positive for the DRAG allele, samples are then screened for the A2 allele using the MicroSSP Allele Specific HLA-typing class I DNA typing trays - OneLambda, cat#: SSPR1-A2). Tissue typing trays were run with the PCR protocol recommended by the manufacturer.

In detail, the PCR amplification cycles follows the program below for testing both HLA alleles:

1. 96ºC for 2 min 10 sec
2. 63ºC for 1 min
3. 96ºC for 10 sec
4. 63ºC for 1 min
5. Repeat step 3-4 for 9 cycles
6. 96ºC for 10 sec
7. 59ºC for 50 sec
8. 72ºC for 30 sec

9. Repeat steps 6-8 for 20 cycles
10. Hold at 4ºC

After PCR, gel electrophoresis was performed using 2.5% agarose gel (ThermoFisher Scientific, cat#: 16500500) in 1x Tris Borate EDTA buffer (1x TBE) (ThermoFisher Scientific, cat#: AM9863). Agarose Gel was prepared with the addition of 1µL/mL GelRed Nucleic Acid Gel Stain (Biotium, cat#: 41003) instead of the recommended 0.5 µg/ml ethidium bromide. The unique gel dock used for electrophoresis is the Micro SSP Gel System (One Lambda, cat#: MGS108), available on: https://www.onelambda.com. The final photographed image is analyzed with the HLA Fusion software (version 4.2.0) which is available for paid download from https://www.onelambda.com.

HLA fusion analysis:

The HLA Fusion software provides multiple possibilities of allele pairs **(Figure 2)**. Therefore, likely HLA allele pairings for the analyzed sample were determined based on common alleles from databases and by ruling out rare alleles (1 in $1x10^6$–$1x10^7$). For example, from the DRB1*04:01 typing results possible allele pairs may show as strings of possible combinations **(Figure 2)**. Positive samples should have the allele of interest (DRB1*04:01) in at least one of the two alleles within a pair indicating heterozygous expression. In the context of this project, UCB samples can be used for engraftment if they are have either homozygous or heterozygous expression of the allele of interest [324].

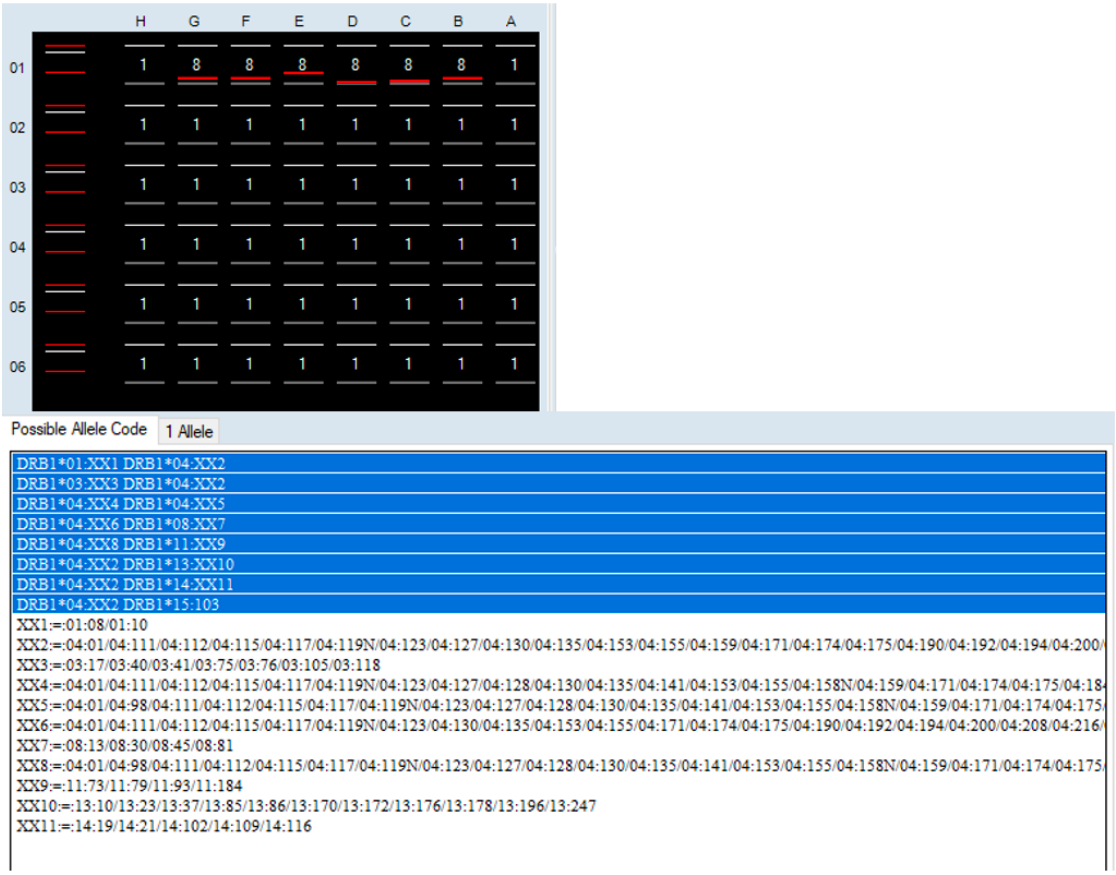

Figure 2. Possible allele combinations from a HLA-DRB1*04:01 positive sample.
Potential allele pairs are highlighted in blue. HLA isotype specificity are denoted by XX1, XX2, etc. and are applied to the allele pairs to determine the HLA isotypes within the allele pairs. For instance, the left allele in the first allele pair can potentially be DRB1*01:08 or DRB1*01:10, while the right allele can potentially be DRB1*04:01, or DRB1*04:111, or DRB1*04:112, etc. The long sting of potential alleles are ordered in the most to least common alleles (from left to right). The ambiguity of alleles should be clarified with the online database by ruling out rare alleles **(Figure 3)**. Upon confirming that an allele is rare there is no need to check additional alleles further down the string. In this case, when checking the XX2 line, DRB1*04:01 is the allele of interest, and the next possible allele is DRB1*04:111 which according to the HLA database only has a 0.16% population frequency in the Chilean population, and thus can be considered a rare allele. Therefore, there is no need to check alleles further down the line. Any allele with the XX2 notation can be confirmed as DRB1*04:01. Every allele pair in blue has at least one XX2 (DRB1*04:01) which means considering all possibilities, the samples is heterozygous for DRB1*04:01. Since samples that are either heterozygous or homozygous can be used for engraftment, this sample is considered to be positive for DRB1*04:01 (DRAG allele).

To determine the frequency/rarity of HLA alleles, online HLA database search tools were used (http://www.allelefrequencies.net) [325,326]. This is not always necessary for

determining sample HLA allotype, since presence of just one allele (heterozygous expression) is required for the sample for engraftment. However, if the fusion software provides allele possibilities that do not contain the alleles of interest within the pair, it is important to rule out these pairings as rare/unlikely before confirming the sample as positive. An example is demonstrated in (**Figure 3)**.

30	DRB1*03:24	USA NMDP European Caucasian	0.0000012	1,242,890	See	
31	DRB1*03:28	USA NMDP European Caucasian	0.0000044	1,242,890	See	
32	DRB1*03:34	USA NMDP European Caucasian	0.0000004	1,242,890	See	
33	DRB1*03:37	USA NMDP European Caucasian	0.0000020	1,242,890	See	
34	DRB1*03:39	USA NMDP European Caucasian	0.0000012	1,242,890	See	
35	DRB1*03:48	USA NMDP European Caucasian	0.0000004	1,242,890	See	
36	DRB1*03:49	USA NMDP European Caucasian	0.0000004	1,242,890	See	
37	DRB1*03:60	USA NMDP European Caucasian	0.0000004	1,242,890	See	
38	DRB1*04:01	USA NMDP European Caucasian	0.0878	1,242,890	See	
39	DRB1*04:02	USA NMDP European Caucasian	0.0106	1,242,890	See	
40	DRB1*04:03	USA NMDP European Caucasian	0.0079	1,242,890	See	
41	DRB1*04:04	USA NMDP European Caucasian	0.0388	1,242,890	See	
42	DRB1*04:05	USA NMDP European Caucasian	0.0067	1,242,890	See	
43	DRB1*04:06	USA NMDP European Caucasian	0.0004	1,242,890	See	
44	DRB1*04:07	USA NMDP European Caucasian	0.0112	1,242,890	See	
45	DRB1*04:08	USA NMDP European Caucasian	0.0039	1,242,890	See	

Figure 3. Allele frequency results after searching for specific alleles reported by the HLA Fusion Software on the online database.

As an example for analysis, if a sample reports to have the allele possibilities of DRB1*03:24 and DRB1*03:60, this pair can be ruled out as a rare allele pair possibility within the Caucasian population since their allele frequencies are extremely close to zero (these alleles have a population frequency of 0.00024% and 0.00008%, respectively, meaning 0.00024% and 0.00008% of individuals in the sample size of 1,242,890 would that express these alleles, respectively). However, if an allele pair is reported to be DRB1*03:24, and DRB1*04:02, this pair would could not be definitively ruled out as there is still 2.1% (higher proportion) of individuals with the DRB1*04:08 allele. For reference, DRB1*04:01 has 16.8% of individuals with this allele in the European Caucasian population. Population frequency or the "% of individuals that have the allele" can be calculated with the following formula: % = [1 – (1 – allele frequency)^2] x 100%. All reported information is available on: http://www.allelefrequencies.net

2.1.4. Generating huNRG, huNSG-hIL15, and huDRAG-A2

Generating huNRG and huNSG-hIL15 mice:

UCB derived human CD34+ HSCs that tested negative for both HLA-DRB1*04:01 and HLA-A*02:01 alleles were selected for engrafting NRG and NSG-hIL15 mice. Newborn pups (24-72 hours old) were irradiated with 3 cGy irradiation dose at three hours before engraftment and immediately prior to engraftment. Irradiated pups engrafted with approximately $1x10^5$ – $1x10^6$ CD34+ HSCs in 30 uL of phosphate buffered saline (PBS) via intrahepatic (IH) injection (Supplementary Table 1). Pups were then returned to their mother and monitored for post-irradiation complication and survival. Mice were weaned at approximately 4 weeks old and were monitored regularly for radiation poisoning and GvHD.

Generating huDRAG-A2 mice:

UCB derived human CD34+ HSCs that were tested positive for both the HLA-DRB1*04:01 and HLA-A*02:01 alleles were used for engraftment of DRAG-A2 mice. Adult DRAG-A2 mice (6-10 weeks old) were irradiated with 550 cGy immediately prior to tail intravenous (IV) injection of $5x10^5$ – $1x10^6$ CD34+ HSCs in 200 uL of PBS (Supplementary Table 1). All mice were monitored regularly for radiation poisoning or GvHD post-engraftment.

2.1.5. Flow cytometry analysis of hu-mice reconstitution and HSC sample quality

Hu-mice human immune cell reconstitution:

HuNRG and huDRAG-A2 mice were checked for human immune cell reconstitution at 12, 16 and/or 20 weeks post-engraftment using flow cytometry. If hCD45+ leukocyte populations were low but detectable (between 2-10%, or between 10,000 to 50,000 hCD45+ leukocytes), mice were also checked past 20 weeks post-engraftment as human hCD45+ populations may still increase. HuNSG-hIL15 mice were checked for human immune cell reconstitution at 8, 12, 14, and 16 weeks post engraftment. Approximately 50 uL of blood was collected from the facial vein of all animals. Red blood cells (RBCs) were lysed with two rounds of ACK lysis buffer treatment (Quality Biological, cat# 10128-802). Subsequently, human and mouse Fc block were added to samples, and cells were then stained for 30 minutes in an antibody mix containing hCD45-Pacific Blue, mCD45-AlexaFluor 700, hCD3e-Qdot 605, hCD4-PerCP-Cy5.5, hCD8a-PE-Cy7, hCD14-AlexaFluor 647, and hCD19-PE. Cells were also stained with fixable viability dye (eFluor 780) prior to fixation. For huNSG-hIL15 samples, cells were stained with an antibody mix containing hCD45-Pacific Blue, mCD45-AlexaFluor 700, hCD3e-Qdot 605, hCD4-PerCP-Cy5.5, hCD8a-PE-Cy7, hCD14-AlexaFluor 647, hCD19-PE, hCD16-FITC, hCD56-PE-CF594, and NKp46-BV786. Cells were then ran on the CytoFlex LX flow cytometer and data was analysed using FlowJo software (version 10.8).

Chapter 2.2. Aim 2: Establish HIV/*Mtb* co-infection within huNRG and huDRAG-A2 mice and investigate host-pathogen responses, immune dysfunction, and histopathology within blood and tissues *in vivo*.

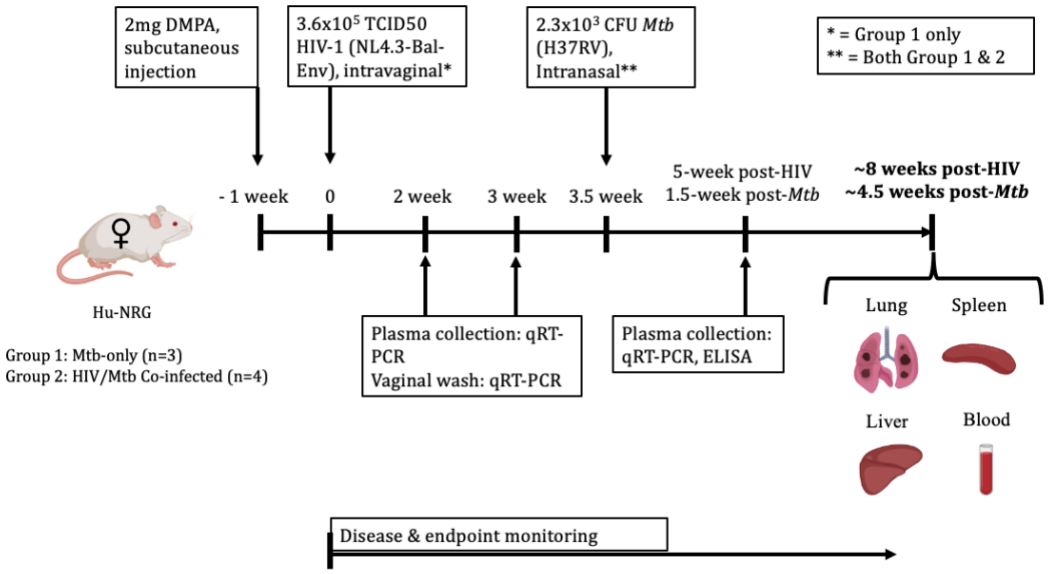

Figure 4. Experimental plan to establish HIV/*Mtb* co-infection within huNRG mice.

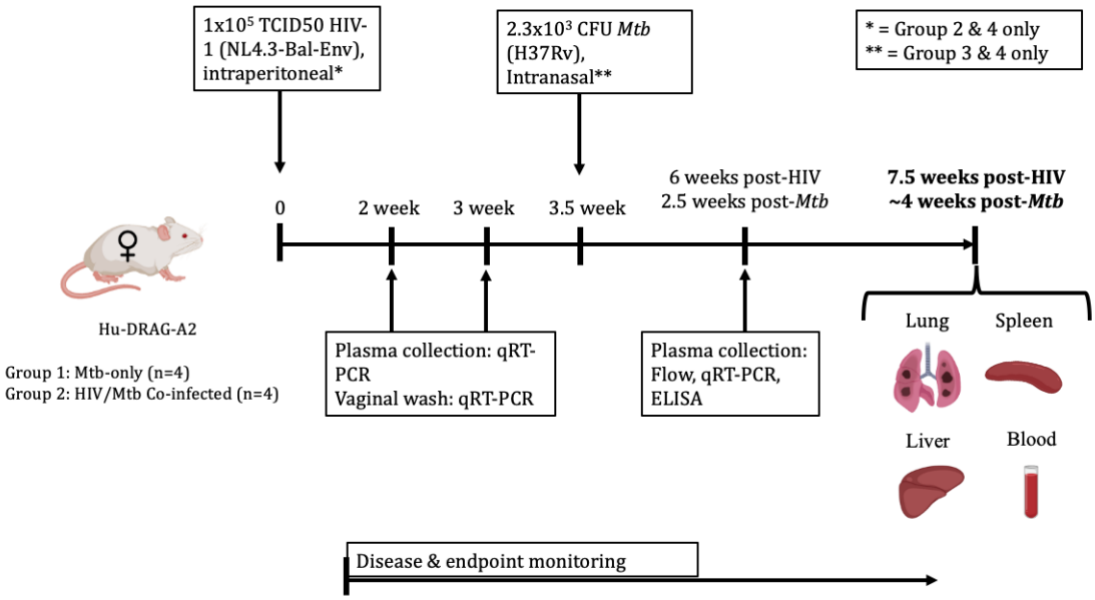

Figure 5. Experimental plan to establish HIV/*Mtb* co-infection within huDRAG-A2 mice.

2.2.1. Primary HIV-1 infection of huNRG and huDRAG-A2 mice:

Intravaginal HIV-1 infection of huNRG mice:

To ensure consistent HIV-1 infection, diestrus (the progesterone-high phase of the murine estrous cycle) was induced within all huNRG mice by administering 2mg Depot-medroxyprogesterone acetate (DMPA) subcutaneously (McMaster Hospital Pharmacy, DIN# 00585092). DMPA administration can improve susceptibility to HIV-1 upon intravaginal challenge, and by inducing diestrus in all animals, this eliminates the variability in estrous cycles between each animal which can affect susceptibility to HIV-1 [131]. 5 days post-DMPA administration, vaginal washes using 2 x 30 µL sterile PBS was performed to confirm diestrus microscopically within all huNRG mice. Sample containing

mostly leukocytes with little to no cornified epithelial cells indicates the hu-mice are in the diestrus phase [131]. 1 week after the DMPA treatment, huNRG mice in the HIV/*Mtb* co-infected group (n=4) received $3.6x10^5$ TCID50 NL4.3-Bal-Env HIV-1 **(Figure 4).** The NL4.3-Bal-Env (R5-tropic) HIV-1 was obtained as a generous gift from Dr. Charu Kaushic (McMaster University, Hamilton, ON). HuNRG mice were first anesthetized with approximately 72 mg/kg ketamine and 4.8 mg/kg xylazine diluted in sterile saline via intraperitoneal (IP) injection. The vagina was swabbed gently to remove mucous and $3.6x10^5$ TCID50 (approximately $7.5x10^5$ IU) of NL4.3-Bal-Env HIV-1 was pipetted into the vaginal canal in a 25 µL volume. All huNRG mice were placed in a supine position to ensure liquid remains in the vaginal canal for 30 to 60 minutes as they recover from anesthesia. All hu-mice were regularly monitored for severe health reactions to the infection and GvHD. Plasma viral load was assessed at 2 and 3 weeks post-HIV infection to confirm successful HIV infection.

Intraperitoneal HIV-1 infection of huDRAG-A2 mice:

This method of HIV-1 infection avoids the use of DMPA. HuDRAG-A2 mice in the HIV/*Mtb* co-infected group (n=4) received $1x10^5$ TCID50 NL4.3-Bal-Env HIV-1 **(Figure 5).** HuDRAG-A2 mice were first anesthetized with gaseous isoflurane and $1x10^5$ TCID50 (approximately $1.75x10^5$ IU) of NL4.3-Bal-Env HIV-1 was administered into the peritoneum in a 100 µL volume. All hu-mice were regularly monitored for severe health

reactions to the infection and GvHD. Plasma viral load was assessed at 2 and 3 weeks post-HIV infection to confirm successful HIV infection.

2.2.2. *Mtb* infection of huNRG and huDRAG-A2 mice:

HuNRG (*Mtb*-only n=3, co-infected n=4) and huDRAG-A2 mice (*Mtb*-only n=4, co-infected n=3) were infected with *Mtb* at 3.5 weeks post-HIV infection in the McMaster University containment level 3 facility. Mice were first anesthetized with gaseous isoflurane until an unconscious plane of 1 breath every 2 seconds was reached. Both the *Mtb*-only and HIV/*Mtb* co-infected groups were infected intranasally with a planned low-dose $1x10^3$ CFU/mouse (actual dose = $2.3x10^3$ CFU/mouse) of H37Rv *Mtb* in a 25 µL volume. The H37Rv strain of *Mtb* was obtained as a generous gift from Dr. Zhou Xing (McMaster University, Hamilton, ON). The infection dose along with the stock of *Mtb* used for infection was titred and plated to determine the actual dose of *Mtb* infection. 2.5 to 3 weeks after plating, the actual infection CFU titre of *Mtb* was confirmed.

2.2.3. Quantification of plasma and vaginal wash viral load:

Vaginal wash and blood plasma samples were collected in HIV-1 infected huNRG mice at 2 and 3 weeks post-infection, and only plasma was collected at 5 weeks post-infection. Plasma samples were collected at 2, 3, and 6 weeks post-infection in HIV-1 infected

huDRAG-A2 mice. Whole blood was collected via facial bleed into EDTA-coated blood tubes (VWR, cat# CABD365974L). Both vaginal wash and whole blood was centrifuged before collecting the vaginal wash supernatant and plasma, respectively and stored in -80°C. RNA was extracted from 50 µL of plasma and/or vaginal wash using the QIAamp MinElute Virus Spin Kit (QIAGEN, cat# 57704). Quantification of viral load was performed using an established in-house reverse transcription qPCR (RT-qPCR) protocol. RT-qPCR reactions were set up with the SensiFAST Probe Hi-ROX One-Step Kit (FroggaBio, BIO-77005) mixed with HIV-1 specific primers (forward primer: 5′- GCC TCA ATA AAG CTT GCC TTG A-3’; reverse primer 5′- GGC GCC ACT GCT AGA GAT TTT -3’), and probes (reporter probe: 5′- /6-FAM/ AAG TAG TGT GTG CCC GTC TGT TRT KTG ACT/TAMRA/ -3’). Samples were run on the StepOnePlus Real Time PCR System (Applied biosystems) with no-template controls, no-reverse transcriptase controls, positive control RNA from infected plasma, and negative control RNA from uninfected vaginal wash and plasma. Results are generated on the StepOne Software (version 2.3). Final analysis of HIV-1 viral load is based on HIV RNA copies per mL derived from standard curve extrapolation of Ct values quantified by the Mount Sinai Department of Microbiology (Toronto, Ontario).

2.2.4. Quantification of immune cells and pathology within plasma and tissue:

Flow Cytometry:

At experimental endpoint for huNRG mice (8 weeks post-HIV, 4.5 weeks post *Mtb* infection), and for huDRAG-A2 mice (7.5 weeks post-HIV, 4 weeks post *Mtb* infection) blood and the accessory (post-caval) lobe of lungs were collected for flow cytometry analysis. Blood was also collected at 6 weeks post HIV-infection (2.5 weeks post *Mtb* infection) in huDRAG-A2 mice for flow cytometry analysis. Blood was processed as described in Chapter 2.1.5. Lungs were cut into small pieces and digested by collagenase type I (Fisher Scientific, cat#: 17100017) (150U/mL) for 45 minutes to 1 hour to release cells. Lungs were strained through 100µm pore size filters (VWR, cat#: 352360), and RBCs were lysed with ACK lysing buffer and cells were again passed through 100µm filters prior to flow cytometry staining as described in Chapter 2.1.5. Peripheral blood cells were stained with hCD45-Pacific Blue, mCD45-AlexaFluor 700, hCD3e-Qdot 605, hCD4-PerCP-Cy5.5, hCD8a-PE-Cy7, hCD14-AlexaFluor 647, and hCD19-PE. Lung cells were stained with hCD45-Pacific Blue, hCD3e-Qdot605, hCD4-PerCP-Cy5.5, hCD8a-PE-Cy7, hCD14-BV785, hCD169-PE and hCD206-APC. Samples were run on the CytoFlex LX flow cytometer and data was analysed using FlowJo software (version 10.8).

Immunohistochemistry:

At experimental endpoint, the left lung and one-half spleen were also collected and fixed in 10% formalin for 1 week, and subsequently transferred to 70% ethanol. Histology protocols were performed by the McMaster Histology Core Facility. Briefly, tissue sections were deparaffinized and boiled in Tris/EDTA (pH=9) for 20 minutes. Tissue sections were then blocked with 5% bovine serum albumin (BSA), and incubated with 1:50 mouse anti-

human CD4 monoclonal antibodies (clone 4B12, Leica Biosystems, cat#: PA0371) or mouse anti-human CD68 monoclonal antibodies (clone PG-M1, Dako, cat#: GA61361-2) for 1 hour at room temperature. Sections were visualized with the Bond Polymer Refine Red Detection kit (Leica BioSystems, cat# DS9390) on an automated Leica Bond RX autostainer (Leica Biosystems).

2.2.5. Quantification of *Mtb* bacterial load and pathology within tissues:

Mtb bacterial plate culturing:

The right lobe of the lung and one-half spleen were mechanically homogenized in 2mL of 10% glycerol (Fisher Scientific, cat# FLBP2291) and 0.1% Tween 80 (Fisher Scientific, cat# T164500) in PBS. 10-fold serial dilutions of homogenates were plated on agar plates containing 10% Middlebrook oleic acid-albumin-dextrose-catalase (OADC) enrichment (Fisher Scientific, cat# B11886), 0.5% glycerol, 5 µg/mL ampicillin (Sigma, cat#: A5354) and 50 µg/mL cycloheximide (Sigma, cat#: C7698). Titer plates were incubated for 2.5-3 weeks at 37°C. *Mtb* colonies were counted to quantify the bacterial load in respective tissues.

Histology and histopathology:

Upon tissue fixation and histology protocols as described in Chapter 2.2.4.. The left lung and one-half spleen was also stained with Hematoxylin and Eosin (H&E), acid-fast bacilli

(AFB) staining to visualise granuloma structures and *Mtb* bacilli within tissues. Granulomatous tissue within lung H&E sections were quantified using the ImageJ software developed by NIH (https://imagej.nih.gov/ij/download.html) and represented as area percentage of granulomatous tissue out of total lung tissue.

Chapter 2.3. **Aim 3:** Elucidate the immunogenicity of adeno-vectored TB vaccines in generating *Mtb*-specific immune responses within huNRG and huDRAG-A2 mice.

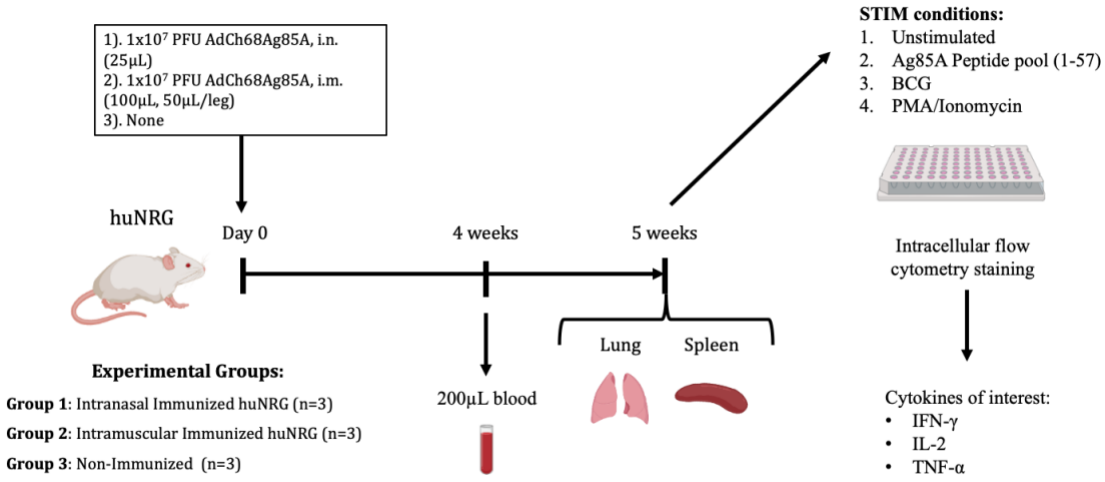

Figure 6. Experimental plan for pilot study testing T cell responses to AdCh68Ag85A vaccination within huNRG mice.

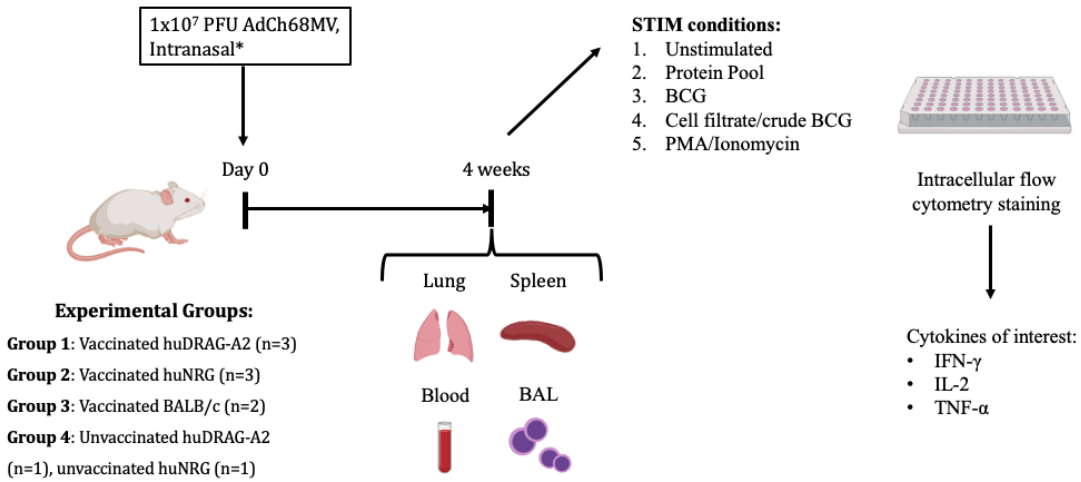

Figure 7. Experimental plan to investigate antigen-specific T cell responses within huNRG and huDRAG-A2 mice vaccinated with AdCh68MV as the primary vaccine.

2.3.1 Administration of TB vaccines

Respiratory mucosa route of administration:

Hu-mice and BALB/c mice were vaccinated with either $1x10^7$ PFU monovalent AdCh68Ag85A vaccine, or $1x10^7$ PFU of multivalent AdCh68Ag85A:rpfB:TB10.4 (AdCh68MV) via intranasal infection in a 25 µL volume. Mice were first anesthetized with gaseous isoflurane until an unconscious plane of 1 breath every 2 seconds was reached. 25 µL of the vaccine volume was pipetted on the nares of animals while the mouth of the animals was held closed to ensure the volume is mostly aspirated into the respiratory tract. Upon fully aspirating the vaccine, the mouth of the animals were still held closed for 10 to 20 more seconds to ensure that the vaccine was aspirated into the lower respiratory tract. It is important at this stage to closely monitor the breathing pattern and depth of respiration

of the animal. If breathing was irregular and each breath seemed shallow or laboured, the grip on the mouth was released to allow for more air into the lungs. All animals were monitored regularly for severe immune responses or reactions to the vaccine along with development of GvHD.

Parenteral route of administration:

HuNRG were vaccinated with $1x10^7$ PFU monovalent AdCh68Ag85A via intramuscular (IM) injections in a total 100µL volume. Mice were first anesthetized with gaseous isoflurane and the hind legs of huNRG were sterilized with 70% EtOH. 50µL of the vaccine volume was injected into the most muscular part of each inner hind leg. Successful IM injection will lead to some restrictions in hind leg movement. All animals were monitored regularly for severe immune responses or reactions to the vaccine along with development of GvHD

2.3.2. Isolation of mononuclear cells from blood, lung, spleen, and bronchoalveolar lavage (BAL)

Supplemented complete RPMI 1640 media (cRPMI) (RPMI 1640 media with 10% FBS, 1% L-Glutamine, 1% HEPES, 1% sodium pyruvate, 1% non-essential amino acids, 0.1% β-mercaptoethanol, and 100 U/ml of Penicillin) was prepared for collected samples. Streptomycin was not added to any growth media as it can inhibit the growth of BCG bacteria. At experimental endpoint, peripheral blood from the facial vein was collected into

EDTA-coated blood tubes. Exhaustive bronchoalveolar lavage (BAL) was performed by lavage of the lungs with a total of 1.35 mL of cRPMI (250 µL, 200 µL, 300 µL, 300 µL, 300 µL) using a polyethylene cannula inserted into the trachea. BAL fluid was passed through a 40µm cell pore size filter (VWR, cat# 352340) to reduce debris and ensure single-cell suspension. Whole lavaged lung and whole spleen was collected into tubes with cRPMI. Blood and lungs were processed as described in chapters 2.1.5. and 2.2.4., respectively. Spleens were crushed through a 100 µm pore size filter, treated with ACK lysis buffer, and passed through a 40 µm filter.

2.3.3. Antigen stimulation and quantification of mononuclear cells

BAL, lung, and spleen cells were plated on U-bottom 96-well plates at a concentration of approximately 1 million cells/mL, 5 million cells/mL and 10 million cells/mL respectively. PBMCs were directly plated and distributed evenly across controls without cell counting. To control for baseline stimulation, all samples were stimulated *ex vivo* with an unstimulated control condition in cRPMI supplemented with co-stimulatory 1 µg/ml of monoclonal anti-human CD28 (clone
CD28.2; ThermoFisher, cat#: 16-0289-81) and anti-human CD49d antibodies (clone 9F10; ThermoFisher, cat#: 16-0499-81) [327]. All other stimulation conditions were also supplemented with both co-stimulatory antibodies. To optimize and determine the most ideal stimulation conditions, samples were stimulated with different sources of *Mtb*

antigens (Table 1). Additionally, the supplementation of costimulatory antibodies was also modified in the culture filtrate/crude BCG condition where instead of the aforementioned clones of hCD28 and hCD49d antibodies, the clones described in Yushi et al. 2017 were used at 1.75µL/well [104]. Upon treating samples with respective stimulation conditions, cells were incubated in 37ºC, at 5% CO_2 for the durations outlined in Table 1. Five hours before completion of stimulation, 1:400 GolgiPlug (BD Biosciences, cat#: 555028) was added to all wells to trap cytokines within the cells.

Table 1. Antigen stimulation conditions used in each experiment.
Monovalent refers to the experiment using monovalent AdCh68Ag85A vaccine; Trivalent refers to the experiment using trivalent AdCh68MV vaccine.

Experiment	Stimulation Condition	Concentration/ quantity per well	Tissue & Stimulation Duration	Source
Monovalent	Ag85A peptide pool (1-57)	2.8µL/1x10^6 cells	All: 24 hours	Dr. Zhou Xing (McMaster University)
Trivalent	Whole protein pool: Ag85A (1µg/µL) TB10.4 (0.8µg/µL) RpfB (1µg/µL)	Ag85A = 5µg/well TB10.4 = 5µg/well RpfB = 5µg/well	BAL: 6 hours Lung and spleen: 24 hours	Dr. Zhou Xing (McMaster University)
Trivalent	Culture filtrate and Crude BCG	Culture filtrate = 2µL/well Crude BCG = 1µL/well	All: 24 hours	Dr. Zhou Xing (McMaster University)
Monovalent and Trivalent	Live BCG (Pasteur strain)	MOI of 6	All: 24 hours	Dr. Zhou Xing (McMaster University)
Monovalent and Trivalent	PMA/Ionomycin	2µL/mL	All: 6 hours	ThermoFisher, cat#: 00-4970-93
Trivalent	Culture filtrate and Crude BCG (supplemented with	Culture filtrate = 2µL/well	Spleen: 24 hours	Dr. Zhou Xing (McMaster University)

	costimulatory antibodies used by Yao et al. 2017)	Crude BCG = 1µL/well		

Intracellular Flow cytometry:

To detect *Mtb* antigen-specific cytokine-producing human CD4+ and CD8+ T cells, intracellular staining for pro-inflammatory cytokines (IFN-γ, IL-2, and TNF-α) was performed. Cells were surface stained with hCD45-Pacific Blue, hCD3e-Qdot605, hCD4-PerCP-Cy5.5, and hCD8-PE-Cy7. Stained cells were then fixed and permeabilized with BD CytoFix/CytoPerm (BD Biosciences, cat#: 555028) and stained for intracellular cytokines with anti-human IFN-γ-PE, IL-2-APC, and TNF-α-FITC antibodies. Samples were then ran on the CytoFlex LX flow cytometer and data was analysed using FlowJo software (version 10.8).

Statistical analysis statement:

Groups were compared using unpaired parametric T tests. Data were considered significant if p-values were < 0.05. Significant differences are noted as $*p < 0.05$, $**p < 0.01$, $***p < 0.001$. Data are expressed as mean +/- SEM for all groups.

CHAPTER 3. RESULTS

Chapter 3.1. Aim 1: Develop and compare current- and next-generation humanized mouse models with human immune cells capable of sustaining both HIV and TB infections

*Note: The data presented here will be that which was not in the thesis of Madeleine Lepard who was co-first author with Jack X. Yang in the initial establishment of the huNRG and huDRAG-A2 models and single HIV and TB infection within the hu-mouse models.

3.1.1. HLA-typing analysis of HSC-samples results summary

Engrafting DRAG-A2 mice to generate huDRAG-A2 mice require HLA-matched HSCs, specifically, both HLA-DRB1*04:01 and HLA-A*02:01 must be tested to ensure the HSC samples express both alleles. Out of the total 71 tested samples, 11 were positive for the HLA class II allele (HLA-DRB1*04:01) yielding approximately 15.5% as positive. Out of the 23 total samples tested for the HLA class I allele (HLA-A*02:01), 11 were positive which yields approximately 47.8% as positive (Table 2). The 11 HLA-DRB1*04:01 were then tested for expression of HLA-A*02:01, where 5 were positive. Therefore, 5 of the total 71 tested samples were double positive for both alleles of interest yielding approximately 7%. Samples that were only positive for HLA-DRB1*04:01, or HLA-A*02:01 were used to engraft DRAG and NRG-A2 mice, respectively. Samples that were negative for both alleles were used to engraft NRG and NSG-hIL15 mice.

Table 2. HLA-typing results for UBC samples obtained from McMaster's Children's Hospital labour and delivery unit.

Samples are first HLA-typed for the DRB1*04:01 isotype. Positive samples are subsequently tested for the A*02:01 isotype. Some samples that were negative for the DRB1*04:01 isotype were also tested for HLA-A*02:01 to obtain samples that were single-positive HLA-A*02:01.

HLA Isotype	Positive Result	Negative Result	Total Samples Tested
HLA-DRB1*04:01	**11**	**60**	**71**
HLA-A*02:01	**11**	**12**	**23**

3.1.2. Next-generation huDRAG-A2 mice develop significantly higher immune cell populations compared to huNRG mice

Data is generated in conjunction with Madeleine Lepard and is currently submitted in a publication under peer-review: (Viruses; April 28, 2022; Manuscript ID: viruses-1725813: Jack X Yang*, Madeleine Lepard*; *co-first author) ~ This publication under review will hereafter be referred to and cited as: (Lepard and Yang, 2022; *Viruses* - in review)

In brief, huDRAG-A2 and huNRG mice were engrafted as newborns between 24-72 hours via intrahepatic injection. At 12 weeks post-engraftment, huDRAG-A2 mice reconstituted with significantly higher counts of human CD45+ (hCD45+) lymphocytes, human CD3+ (hCD3+) T cells, human CD4+ (hCD4+) T cells, and human CD14+ (hCD14+) monocytes/macrophages in peripheral blood (Lepard and Yang, 2022; *Viruses* - in review). Despite the huDRAG-A2 developing higher levels of immune cells, the huNRG still develop robust levels of lymphoid cells. This data sets up both huNRG and huDRAG-A2 models for HIV and TB studies.

3.1.3. HuDRAG-A2 mice develop Th17 cells upon T cell stimulation

As a pilot study, one huDRAG-A2 mouse was used to investigate CD4+ T cell subset development within tissues. Upon stimulation of isolated lung and spleen cells with PMA/Ionomycin, huDRAG-A2 mice developed a substantial population of IL-17 producing hCD4+ T cells. This shows that the huDRAG-A2 mouse was capable of generating a population of functional Th17 cells (Figure 8).

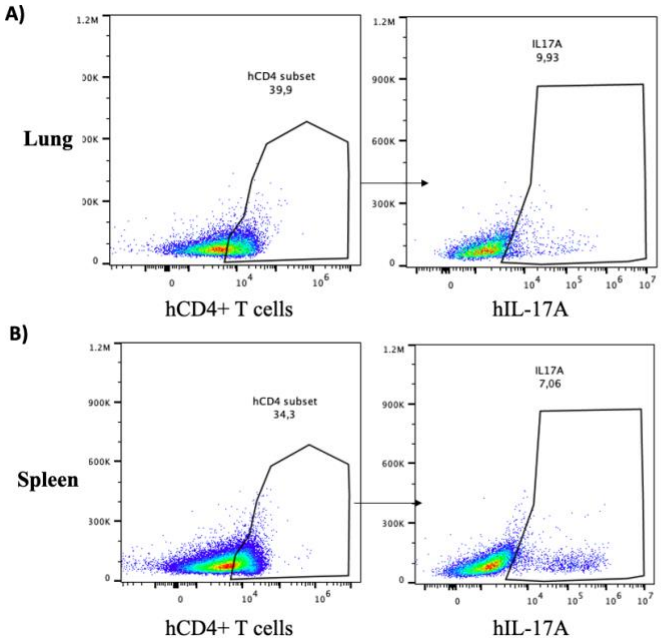

C)

Tissue	Percent of hCD4+ T cells producing hIL-17	Cells/Organ producing hIL-17
Lung	9.93%	22,177
Spleen	7.06%	71,553

Figure 8. HuDRAG-A2 mice develop functional human Th17 cells within the lung and spleen upon PMA stimulation.

Flow cytometry plot gating **(A)** lung and **(B)** spleen hIL-17 producing hCD4+ T cell populations. **(B)** Percent and total counts of hIL-17 producing hCD4+ T cells in the whole lung and spleen organs. Plots are generated with FlowJo Software.

3.1.3. Establishing huNSG-hIL15 genotyping

We wanted to develop a humanized mouse model that also reconstituted with robust levels of NK cells since current-generation hu-mice such as huNRG mice develop scarce levels of NK cells due to a lack of human IL-15, a cytokine key to NK cell development, proliferation and survival [268,328]. NSG-hIL15 was obtained from The Jackson Laboratory, and to confirm that the NSG-hIL15 mice to be used for engraftment expresses transgenic IL-15, a qPCR method of detection was established. The StepOne Software can provide an "allelic discrimination plot" which will indicate if the qPCR confirmed that samples expressed both IL-15 and internal control or only the internal control which would indicate positive and negative results, respectively (Figure 9). An amplification plot for a positive result for the IL-15 allele would show two amplification curves, with the higher curve plateauing at just above $1x10^5$ ΔRn indicating the transgene, while the internal control curve plateaus between $1x10^4$ and $1x10^5$ (Figure 10A). Negative controls were also run under the same qPCR conditions and yielded only the internal control curves (Figure 10B-D). DNA samples from NRG-A2 and DRAG mice were also tested to ensure that their transgenes would not be detected. Samples form NRG, NRG-A2 and DRAG all test negative with only the internal control curve, and thus can all be used as negative controls for the qPCR.

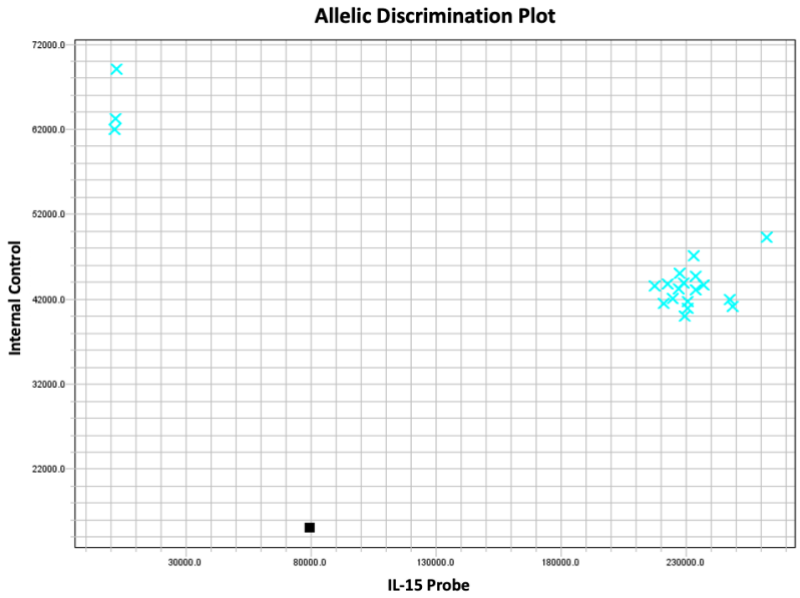

Figure 9. Quantitative PCR discriminates samples expressing transgenic IL-15 allele from controls. Samples that express transgenic IL-15 are amplified on both the x- and y-axis while control samples are only amplified on the y-axis for the internal control. Chart was generated on the StepOne Software.

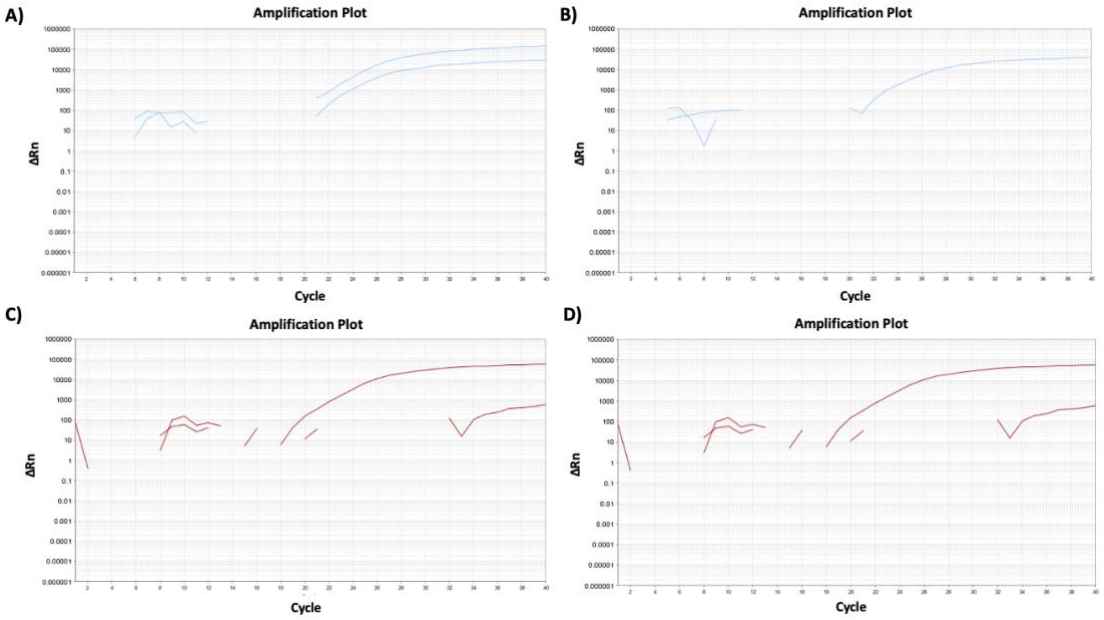

Figure 10. Examples of amplification plots generated for qPCR tests.
Amplification plot for **(A)** NSG-hIL15, **(B)** NRG, **(C)** NRG-A2, and **(D)** DRAG mice. IL-15 transgene peaks at 100,000 ΔRn; internal control peaks between 10,000 and 10,000 ΔRn. Detection of amplification at approximately 20 cycles indicates presence of target DNA. Chart was generated on the StepOne Software.

3.1.4. Developing the huNSG-hIL15 mice and comparing immune cell reconstitution to huNRG

To perform initial characterization of the this model, NSG-hIL15 mice (n=8) and NRG mice (n=2) were engrafted with the same sample of unmatched-HSCs. While NRG mice are not perfect controls for a transgenic model on the NSG background, NRG mice were the best controls available to use had at the time and huNRG mice have shown similar low engraftments of NK cells as huNSG mice [261]. At 16 weeks post engraftment, huNSG-hIL15 mice appear to reconstitute with higher trends of hCD45+ leukocytes and hCD4+ T cells in peripheral blood compared to huNRG mice (Figure 11). From 8 to 16 weeks post-engraftment, hu-NSGIL-15 consistently demonstrated significantly higher percentages of hCD56+hCD3- NK cells in the blood (Figure 12A). Absolute NK cell counts were only significantly higher at 16 weeks post-engraftment (Figure 12B).

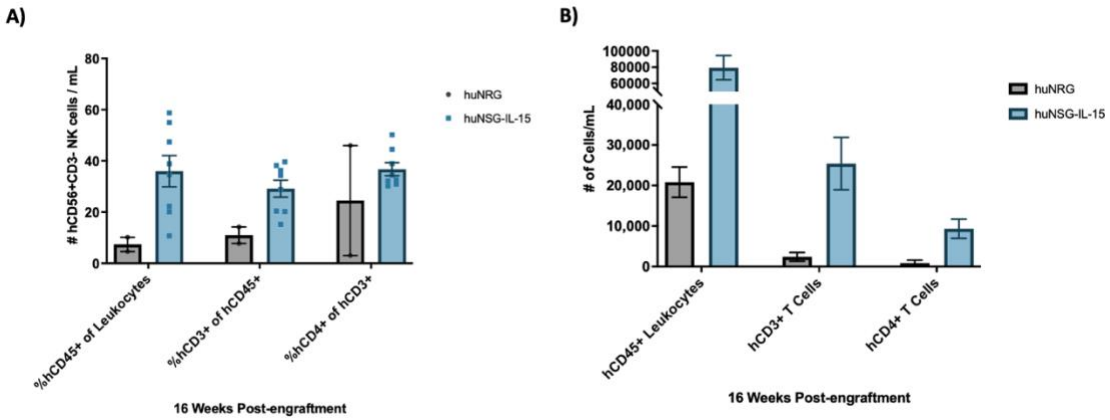

Figure 11. Human T cell reconstitution in peripheral blood of huNRG and huNSG-hIL15 mice at 16 weeks post-engraftment.
(A) Percent of hCD45+ leukocyte population, hCD3+ of hCD45+ leukocytes, and hCD4+ of hCD3+ T Cells. **(B)** Number of hCD45+ leukocytes, hCD3+ T cells, and hCD4+ T cells per mL of blood. No statistical significance between huNRG (n=2) and huNSG-hIL15 (n=8). Data are expressed as mean +/- SEM.

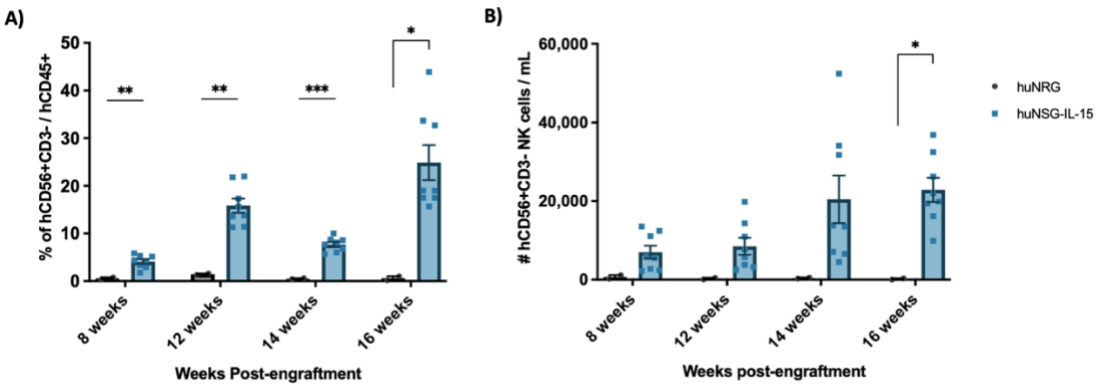

Figure 12. Human NK cell (hCD56+hCD3-) reconstitution in peripheral blood of huNRG and huNSG-hIL15 mice post-engraftment.
(A) Percent of hCD56+hCD3- NK cells out of hCD45+ leukocyte population at 8, 12, 14, and 16 weeks post-engraftment. **(B)** Number of hCD56+hCD3- NK cells per mL of blood post-engraftment. Data are expressed as mean +/- SEM. Data are expressed as mean +/- SEM, huNRG (n=2) and huNSG-hIL15 (n=8), p value = * <0.05, ** <0.01, *** <0.001.

Chapter 3.2. Aim 2: Establish HIV/*Mtb* co-infection in huNRG and huDRAG-A2 mice and investigate *in vivo* host-pathogen responses, immune function, and histopathology

3.2.1. Establishing HIV-1 and *Mtb* single-infection in huNRG and huDRAG-A2 mice

This data is generated in conjunction with Madeleine Lepard, and the corresponding data is reported in Lepard and Yang, 2022; *Viruses* - in review, and the Master's thesis by Madeleine Lepard.

In brief, huNRG and huDRAG-A2 mice were infected with HIV-1 alone (Figure 13) and *Mtb* alone (Figure 14). Both huNRG and huDRAG-A2 mice were able to sustain single HIV-1 infection and *Mtb* infection. Hallmark features of HIV and TB such as CD4+ T cell

depletion and development of organized granulomas was observed in both models (Lepard and Yang, 2022; *Viruses* - in review). These results demonstrate that both huNRG and huDRAG-A2 models can be used to study HIV/*Mtb* co-infection.

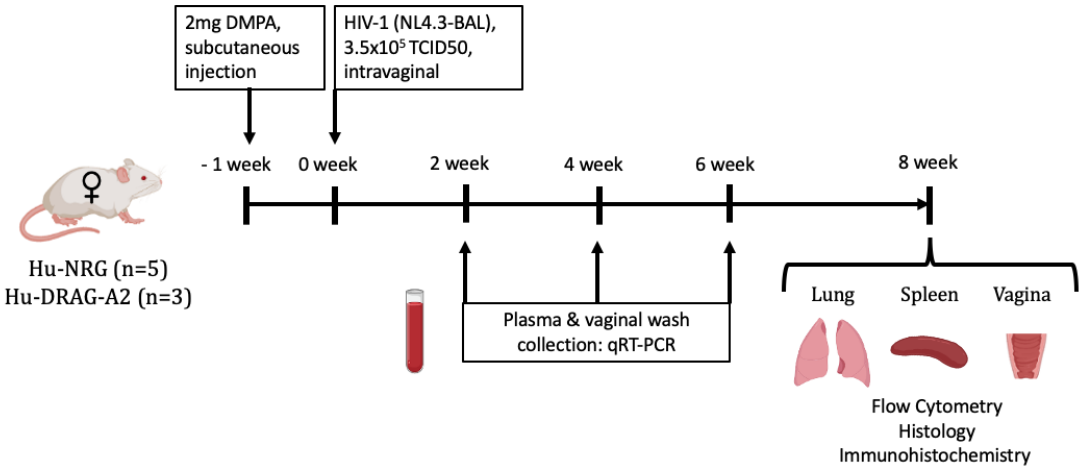

Figure 13. Experimental plan to establish HIV infection within huNRG and huDRAG-A2 mice. All animals used in the experiment were female.

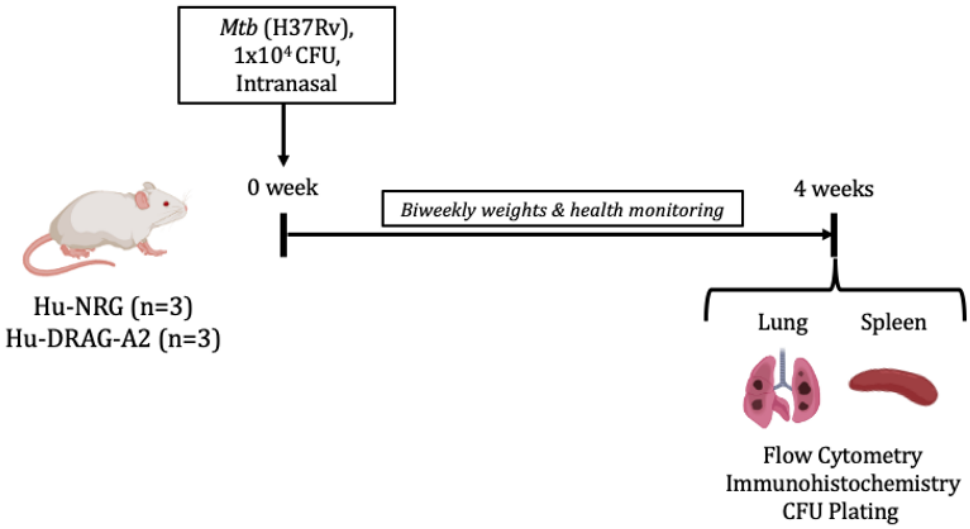

Figure 14. Experimental plan to establish TB infection within huNRG and huDRAG-A2 mice. HuNRG male n=3, huDRAG-A2 female n=2, huDRAG-A2 male n=1.

Aim 2: Establishing and investigating HIV/*Mtb* co-infection in huNRG mice

3.2.2. Confirmation of primary HIV-1 infection of huNRG mice prior to *Mtb* infection

To establish HIV/*Mtb* co-infection within huNRG mice, primary HIV-1 infection was first established prior to *Mtb* infection (Figure 4, Supplementary Table 2). One week after DMPA administration, huNRG mice in the co-infected group were infected with $3.6x10^6$ TCID50 NL4.3-Bal-Env HIV-1 intravaginally and tested for plasma and vaginal wash viral load using RT-qPCR 2 weeks post-infection. 3 of 4 huNRG mice were well-infected with HIV-1 with high viral load within plasma (Table 3). One huNRG (indicated by the *asterisk) was unable to be confirmed as well-infected with HIV as the plasma viral load was near the detection threshold of the StepOnePlus Real Time PCR System (~1500 RNA copies/mL). After co-infection with *Mtb*, this huNRG mouse will be referred to as co-infected (HIV low).

Table 3. HIV-1 Viral load in plasma and vaginal wash of huNRG mice at 2 weeks post-infection.
Accurate detection threshold is at approximately 10,000 RNA copies/mL. *Successful HIV-1 infection cannot be confirmed as viral load was below accurate detection threshold.

Mouse ID	Plasma Viral Load (RNA Copies/mL)	Vaginal Wash Viral Load (RNA Copies/mL)
HTB-NRG1	86,195	59,480
HTB-NRG2*	5,444	6,363
HTB-NRG3	10,624	147,351
HTB-NRG4	31,579	51,741

3.2.3. HIV/*Mtb* co-infection do not show significant differences in bacterial burden within tissue, but may show more severe pathology in the lung and spleen of huNRG mice.

HIV-infected huNRG mice (n=4) and *Mtb*-only mice (n=3) were co-infected with $2.3x10^3$ CFU of H37Rv *Mtb* (planned dose: $1x10^3$) 3.5 weeks post-HIV infection. This timepoint generally allows for HIV-1 to successfully establish and disseminate into the plasma, but not develop chronic HIV. At experimental endpoint (4.5 weeks post-*Mtb* infection, or 8 weeks post-HIV infection), lung, spleen, and liver were collected to assess bacterial burden, and histopathology. Only 2 of the 3 *Mtb*-only huNRG mice survived until endpoint (non-*Mtb* related death). All huNRG mice showed very high bacterial burden in the lungs ranging from 8 to 9 log of CFU of *Mtb* (Figure 15). Substantial extrapulmonary bacterial dissemination was observed where high CFUs were also detected in the liver at around 6 to 8 logs, but no differences were observed between groups (Figure 15). Similarly, high *Mtb* dissemination was observed in spleen tissue, however there may be a trend of higher CFU within the co-infected huNRGs. The co-infected (HIV low) huNRG mouse was separated from group analysis, but still demonstrated consistently high CFU levels across all tissues (Figure 15). Overall, both *Mtb*-only and co-infected huNRG mice show high bacterial load in the lung, as well as dissemination to the spleen and liver.

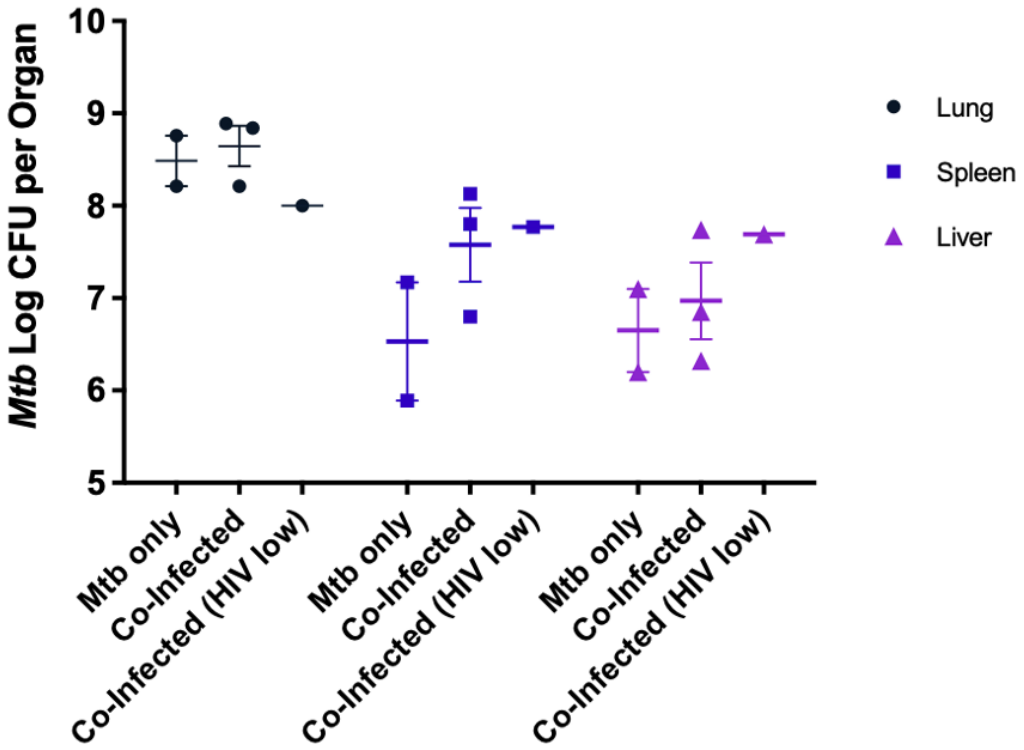

Figure 15. Tissue *Mtb* colony forming units (CFU) of *Mtb*-only, co-infected, and co-infected with low HIV huNRG mice 4.5 weeks post-*Mtb* infection.
Mtb-only huNRG (n=2), co-infected high HIV viral load huNRG (n=3), and co-infected low HIV viral load huNRG (n=1). Data are expressed as mean +/- SEM.

Histopathology of the lungs was also quantified using ImageJ software by calculating the percentage of total granulomatous tissue within 3 total lung sections. Co-infected huNRG mice may be displaying a trend of more severe lung granuloma legions, and interestingly, the co-infected (HIV low) huNRG mouse was show the greatest area of granulomatous lesions (Figure 16A). When examining individual granulomas, co-infected huNRG mice appear to develop more severe uncontained granulomas with a caseating necrotic core (representative of 2 out of 3 confirmed co-infected huNRG mice, 1 out of 3 confirmed co-infected huNRG mouse had severe karyorrhexis but limited caseation) (Figure 17A, B).

The co-infected huNRG granulomas also show *Mtb* bacteria disseminating from the granuloma structure, while the *Mtb*-only infected granulomas show better containment of *Mtb* within the structural borders of the granuloma (Figure 17C, D).

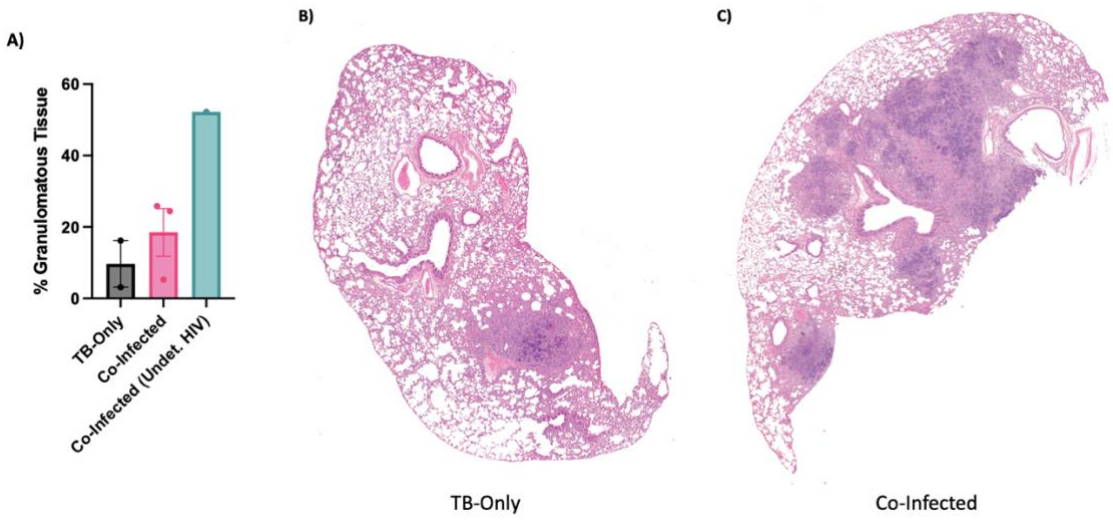

Figure 16. Quantification of granulomatous lung tissue in singly *Mtb*-infected and HIV/*Mtb* co-infected huNRG mice 4.5 weeks post-*Mtb* infection.
(A) Percent of lung granulomatous tissue; percentage reported as the total area of granulomatous tissue out of total lung tissue (3 sections of lungs were measured for each sample); quantification performed using ImageJ software. H&E stain of whole lung sections of **(B)** *Mtb*-only huNRG (lung is representative of n=2 of 2 *Mtb*-only infected huNRG mice) and **(C)** co-infected huNRG mice (lung is representative of n=2 of 3 confirmed co-infected huNRG mice) . Data are expressed as mean +/- SEM.

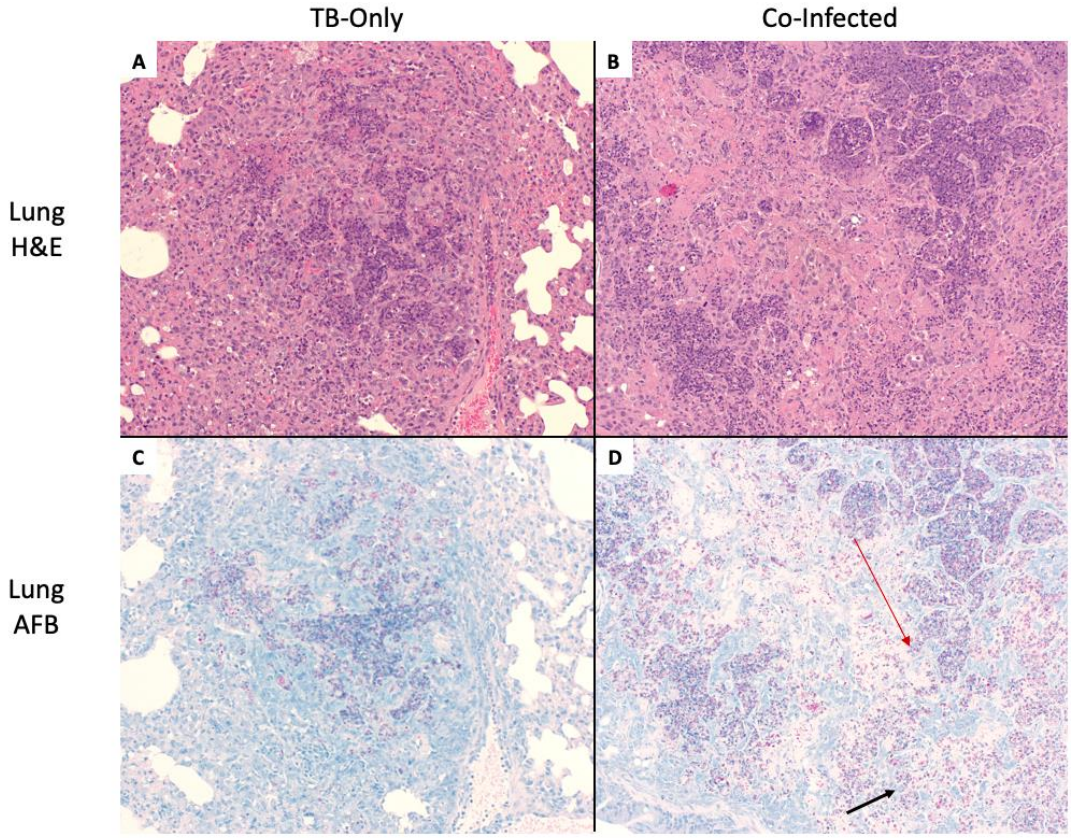

Figure 17. Visualization of lung granuloma formation, structure, and *Mtb* localization in singly *Mtb*-infected and HIV/*Mtb* co-infected huNRG mice 4.5 weeks post-*Mtb* infection.
H&E stain (10x) of lung granuloma in **(A)** *Mtb*-only huNRG and **(B)** co-infected huNRG mice. Acid fast bacilli stain (10x) of lung granuloma in **(C)** *Mtb*-only huNRG (*Mtb*-containment in granuloma is representative of n=2 *Mtb*-only infected huNRG) and **(D)** co-infected huNRG mice (*Mtb*-containment in granuloma is representative of n=3 confirmed co-infected huNRG mice). *Mtb* bacilli are stained red. Red arrow indicates direction of dissemination; black arrow indicates bacteria disseminated outside of granuloma.

3.2.4. HIV/*Mtb* co-infected huNRG mice show depleted hCD4+ T cells and hCD68+ macrophages within lung tissue but not in spleen.

Immunohistochemistry staining of hCD4+ and hCD68+ in the *Mtb*-only infected huNRG lung showed the granuloma surrounded by hCD4+ T cells with hCD68+ macrophages scattered around and throughout the granuloma structure (representative in 1 of 2 TB-only huNRG mouse; 1 of 2 TB-only huNRG mouse had very low reconstitution of human

immune cells) (Figure 18A, C). In contrast, the co-infected lung had little to no hCD4+ T cells or hCD68+ macrophages illustrating severe depletion of these immune cells likely due to HIV (representative of all confirmed co-infected huNRG mice) (Figure 18B, D). When examining the spleen, the *Mtb*-only infected huNRG did not show notable pathology where the only notable feature are likely white pulp regions that are populated with hCD68+ macrophages that appear to be surrounded by hCD4+ T cells (Figures 19A, C and 20A, C). In the co-infected huNRG mice, splenic granulomas were identified where a well-organized circular structure was formed (representative in 2 of 3 confirmed co-infected huNRG mice) (Figure 19B). The illustrated granuloma had a very prominent necrotic core with severe karyorrhexis (the destructive fragmentation of nuclei) and a high concentration of *Mtb* bacilli (Figure 19B, D).

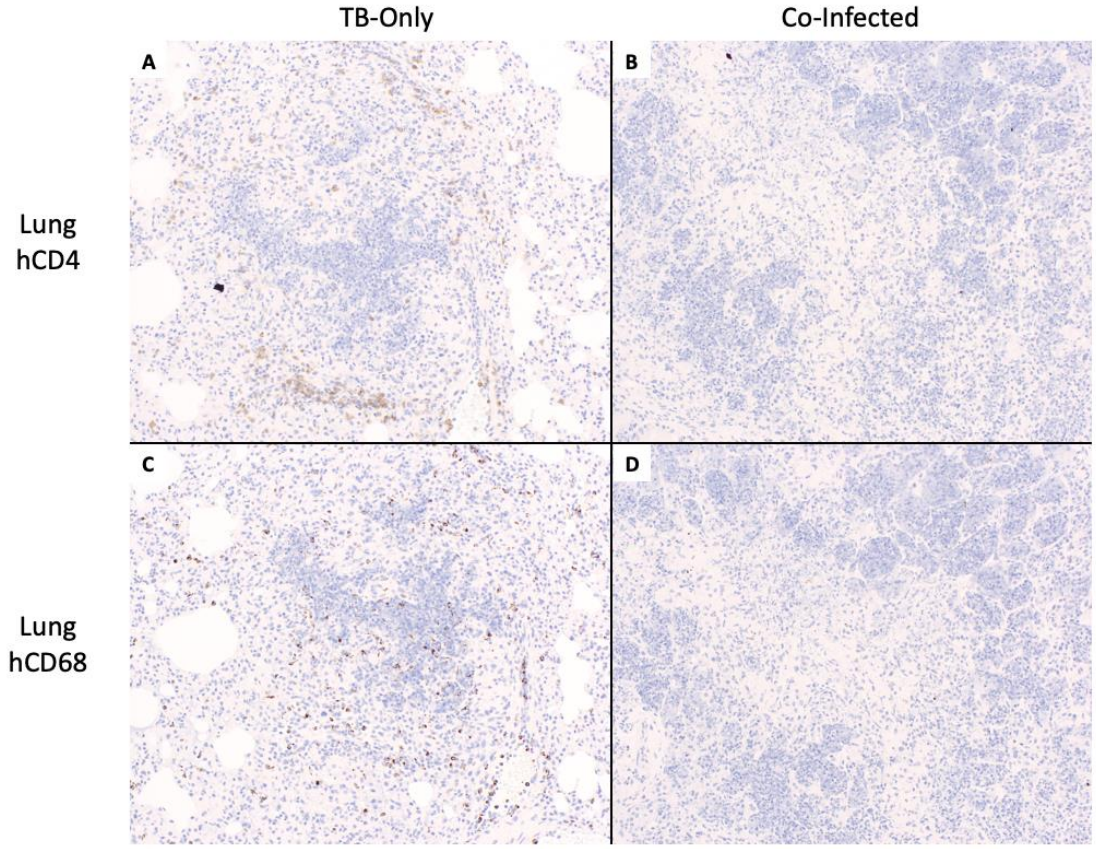

Figure 18. Visualization of human CD4+ T cells and human CD68+ macrophages in the lung granulomas of singly *Mtb*-infected and HIV/*Mtb* co-infected huNRG mice 4.5 weeks post-*Mtb* infection.

IHC of hCD4 (10x) of lung granuloma in **(A)** *Mtb*-only huNRG and **(B)** co-infected huNRG mice; hCD4 stained brown. IHC of hCD68 (10x) of lung granuloma in **(C)** *Mtb*-only huNRG and **(D)** co-infected huNRG mice; hCD68 stained brown. Representative of TB-only (n=1 of 2) and confirmed co-infected (n=3).

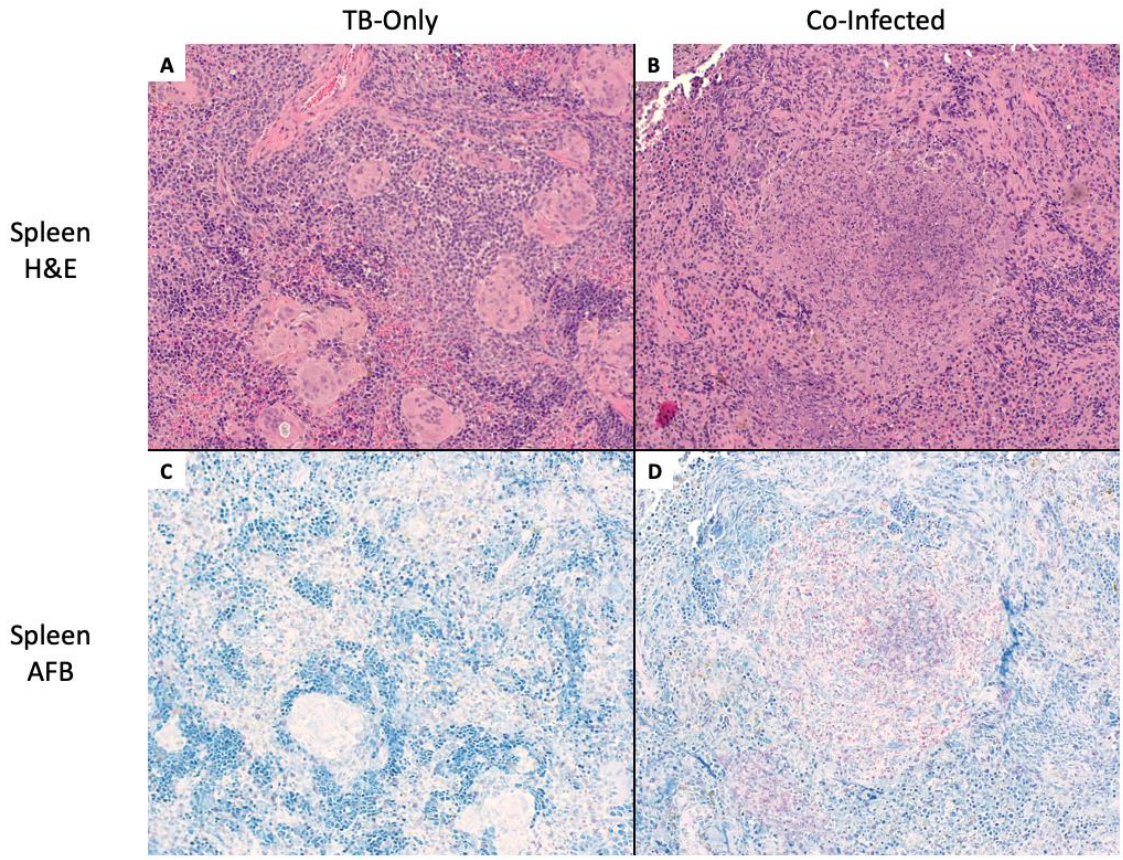

Figure 19. Visualization spleen pathology of singly *Mtb*-infected and HIV/*Mtb* co-infected huNRG mice 4.5 weeks post-*Mtb* infection.
H&E stain (10x) of **(A)** spleen in *Mtb*-only huNRG and **(B)** spleen granuloma in co-infected huNRG mice. Acid fast bacilli stain (10x) of **(C)** spleen in *Mtb*-only huNRG and **(D)** spleen granuloma in co-infected huNRG mice. *Mtb* bacilli are stained red. Representative of TB-only (n=2) and confirmed co-infected (n=2 of 3).

In contrast with the co-infected lung, the spleen still had an abundance of both hCD4+ T cells and hCD68+ macrophages both surrounding the granuloma structure (Figure 20B, D). The depletion of hCD4+ T cells and hCD68+ macrophages mostly within the lungs may indicate an effect or mechanism is predominantly occurring within the lungs during co-infection. Peripheral blood was also assessed using flow cytometry to quantify immune cell changes. It is notable that one of the huNRG mice in the *Mtb*-only group reconstituted with

very low levels of human immune cell populations, and as a result may be an outlier within the data (indicated as the red point in the data; TB-N1 in supplementary table 2) (Figure 21, Supplementary table 2). As a result, it is difficult to make concrete comparisons between the groups. However, if the outlier was removed, there may be a potential trend of lower hCD4+ and hCD8+ T cells and hCD14+ monocytes counts in the co-infected group. Meanwhile the co-infected (HIV low) huNRG mouse show the highest counts of T cells and monocytes in peripheral blood.

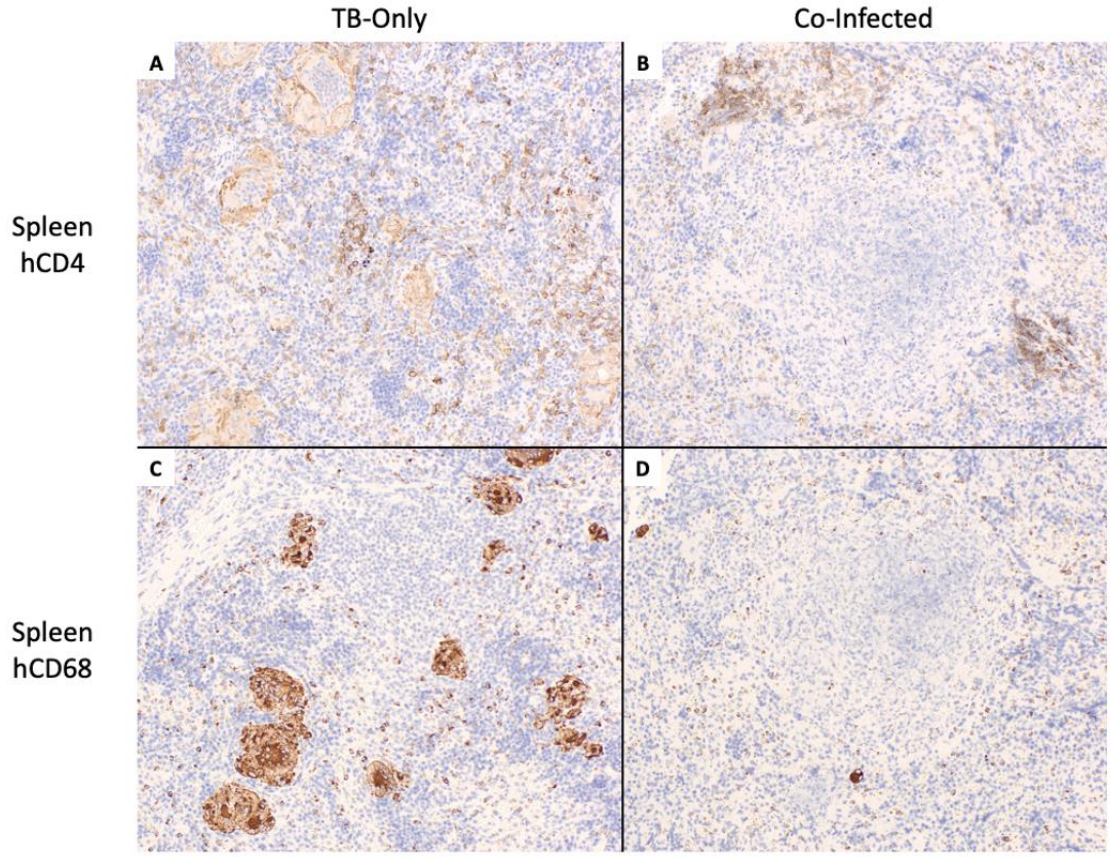

Figure 20. Visualization of spleen hCD4+ T cells and hCD68+ macrophages in the spleen of singly *Mtb*-infected and HIV/*Mtb* co-infected huNRG mice 4.5 weeks post-*Mtb* infection.

IHC of hCD4 (10x) of **(A)** spleen in *Mtb*-only huNRG and **(B)** spleen granuloma in co-infected huNRG mice; hCD4 stained brown. IHC of hCD68 (10x) of **(C)** spleen in *Mtb*-only huNRG and **(D)** spleen granuloma in co-infected huNRG mice; hCD68 stained brown. Immune cell presence is representative of TB-only (n=2) and confirmed co-infected (n=3).

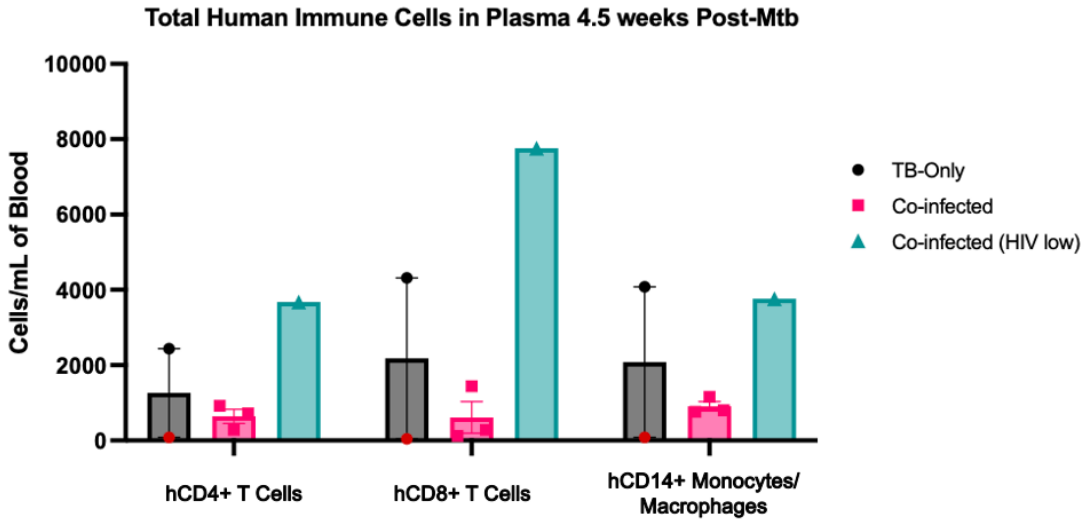

Figure 21. Flow cytometry of peripheral blood of TB-only huNRG and co-infected huNRG mice 4.5 weeks post-*Mtb* infection.
Data are expressed as mean +/- SEM. *Mtb* only huNRG (n=2), co-infected low HIV viral load huNRG (n=1), co-infected high HIV viral load huNRG (n=3). Data are expressed as mean +/- SEM. The red point in the TB-only group corresponds with a poorly engrafted mouse.

3.2.5. HIV/*Mtb* co-infected HuNRG mice recapitulate human immune cell TB pathology within the lung and spleen and offer further insight on lung pathology.

Within the core of the co-infected huNRG granuloma, severe necrosis can be identified with the presence of karyorrhexis (Figure 22A). In areas near the co-infected granuloma, foamy macrophages are identified which are indicative of pathological immune cell differentiation and morphology in TB disease (Figure 22B). The co-infected spleen also harboured multinucleated giant cells, which again indicates more severe pathology during

later stages of disease progression as observed in humans (Figure 22C). Co-infected huNRG also developed foamy macrophages within the airways/alveolar airspace accompanied by hyaline in the airspace (Figure 23A). Unlike the foamy macrophages around granulomas, these airway foamy macrophages are not infected by *Mtb* as bacilli were not identified to be localized within the cytoplasm of the foamy macrophages in AFB staining (Figure 23B). These features were observed also observed less consistently in *Mtb*-only infected huNRG mice.

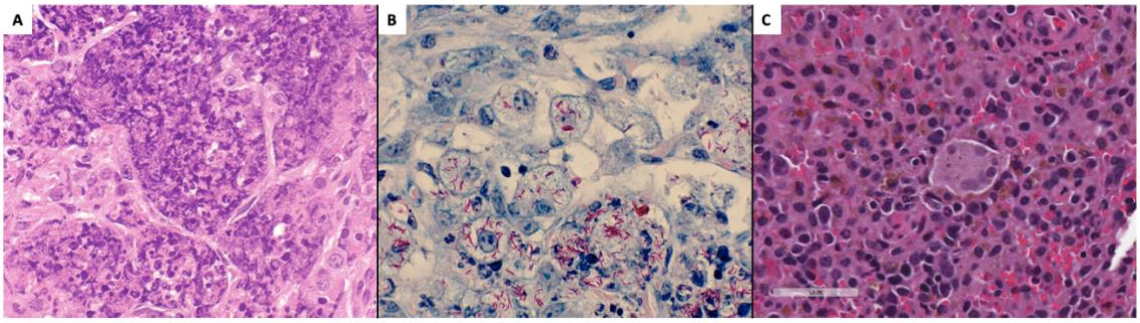

Figure 22. Co-infected huNRG mice show severe TB pathology and recapitulate features observed in severe human disease 4.5 weeks post-*Mtb* infection.
(A) H&E stain of severe nuclei fragmentation of cell aggregates in co-infected huNRG (20x). **(B)** Acid fast bacilli staining showing *Mtb* localized within foamy macrophages around lung granuloma tissue of co-infected huNRG mice (63x); *Mtb* bacilli are stained red. **(C)** Multinucleated giant cell within the spleen tissue of huNRG mice. All figures are representative of n=3 confirmed co-infected huNRG mice.

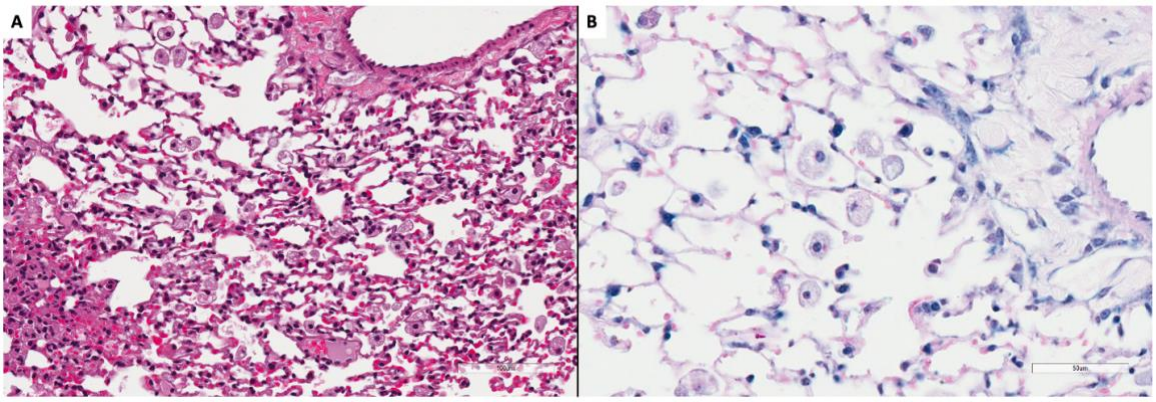

Figure 23. Airway foamy macrophages identified in co-infected huNRG lungs near granulomatous lesion 4.5 weeks post-*Mtb* infection.
(A) H&E stain of lung airspace near granuloma showing foamy macrophages and hyaline in the airway of lungs (20x). **(B)** Acid fast bacilli staining showing no *Mtb* localization within airway foamy macrophages of co-infected huNRG mice (40x); *Mtb* bacilli stained red. Representative of n=3 confirmed co-infected huNRG mice.

3.2.6. Low-dose intranasally infected *Mtb*-only huNRG mice did not show significant pathology at 3 weeks post-infection

One *Mtb*-only infected huNRG mouse developed a tumour that reached endpoint size at 3 weeks post-*Mtb* infection and did not reach experimental endpoint. This was likely not due to *Mtb* pathogenesis as there were no other physical signs of TB-related illness. Based on other experiments or during maintenance (prior to experiments) spontaneous tumour development is expected with huNRG mice. To make the most out of the infected huNRG mouse, lung and spleen tissue was collected for histology and CFU plating to characterize bacterial load and pathogenesis at an acute timepoint given the low dose of *Mtb*. Very low bacterial CFU load was found in the lungs ($5.8x10^3$ total CFU) and spleen ($6x10^2$ total CFU). Histological acid fast bacilli (AFB) staining revealed similar findings where no AFB was identifiable within the lung and spleen sections (Figure 24B). Furthermore, H&E staining presented with no identifiable granulomatous tissue or severe pathology other than minor presentation of hyaline indicative of potential pneumonia within the lung (Figure 24A, C). Therefore, it is evident that with a low dose intranasal infection ($2.3x10^3$ CFU/mouse) of H37Rv *Mtb*, 3 week post-*Mtb* infection is likely insufficient time to observe any significant pathology within huNRG mice.

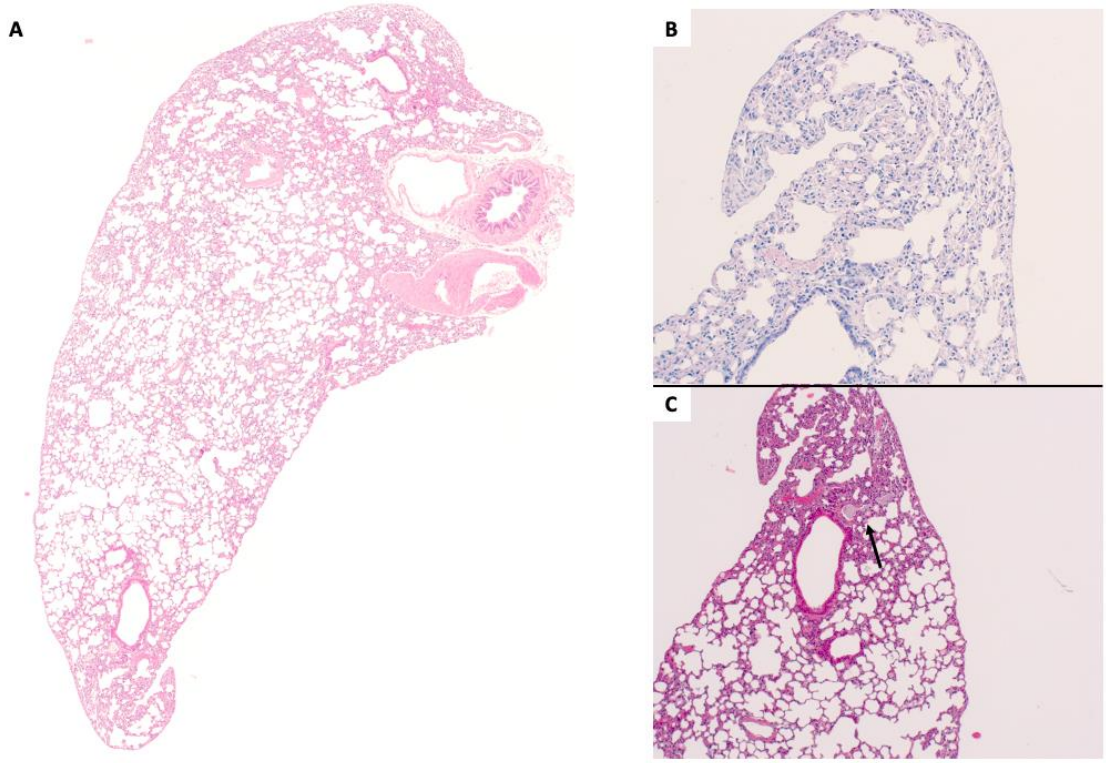

Figure 24. Visualization of histopathology in huNRG lung 3 weeks after low-dose *Mtb* infection. **(A)** Scan of whole lung section (H&E stain). **(B)** Acid fast bacilli stain show absence of *Mtb* bacilli (10x). **(C)** H&E stain of lung air space (5x); arrow indicates presence of hyaline within air space. HuNRG n=1.

Aim 2: Establishing and investigating HIV/*Mtb* co-infection in huDRAG-A2 mice

3.2.7. Confirmation of primary HIV-1 infection in huDRAG-A2 mice prior to *Mtb* infection

To establish HIV/*Mtb* co-infection within huDRAG-A2 mice, primary HIV-1 infection was first established followed by subsequent *Mtb* infection (Figure 5, Supplementary Table 3). HuDRAG-A2 mice in the co-infected group were infected with $1x10^5$ TCID50 NL4.3-Bal-Env HIV-1 via intraperitoneal injection to avoid the use of DMPA. To confirm successful

HIV infection, plasma was taken at 2 weeks post-HIV infection and viral load was quantified using RT-qPCR. 3 of 4 huDRAG-A2 mice were well infected with HIV-1 with 1 of 4 unconfirmed (indicated by the *asterisk) as viral load was near the accurate threshold of the RT-qPCR assay (Table 4). After co-infection with *Mtb*, this huDRAG-A2 mouse will be referred to as co-infected (HIV low) huDRAG-A2.

Table 4. HIV-1 Viral load in plasma of huDRAG-A2 mice at 2 weeks post-infection.
Accurate detection threshold is at approximately 10,000 RNA copies/mL. *Successful HIV-1 infection cannot be confirmed as viral load was below accurate detection threshold.

Mouse ID	Plasma Viral Load (RNA Copies/mL)
HTB-D1*	3,909
HTB-D2	38,288
HTB-D3	158,933

3.2.8. HIV/*Mtb* co-infection in huDRAG-A2 mice significantly increases *Mtb* bacterial load within lungs and bacterial dissemination into spleen and liver tissue.

To determine the effect of co-infection on the growth and dissemination of *Mtb* in huDRAG-A2 mice, CFU was measured in the lung, spleen, and liver. Co-infected huDRAG-A2 mice developed significantly higher bacterial burden ($p<0.05$) within the lungs at 4 weeks post-*Mtb* infection. Co-infected huDRAG-A2 mice also developed significantly higher bacterial load within both the spleen and liver ($p<0.05$), which indicates more severe extrapulmonary bacterial dissemination (Figure 25). Re-plating of one lung

sample in the TB-only group is currently in progress as the CFU was so low that titres were not observed on the dilutions plated (the lowest TB only mouse- was assumed at 1 colony on lowest dilution plated, thus the actual CFU will be equal to or lower than reported in Figure 25).

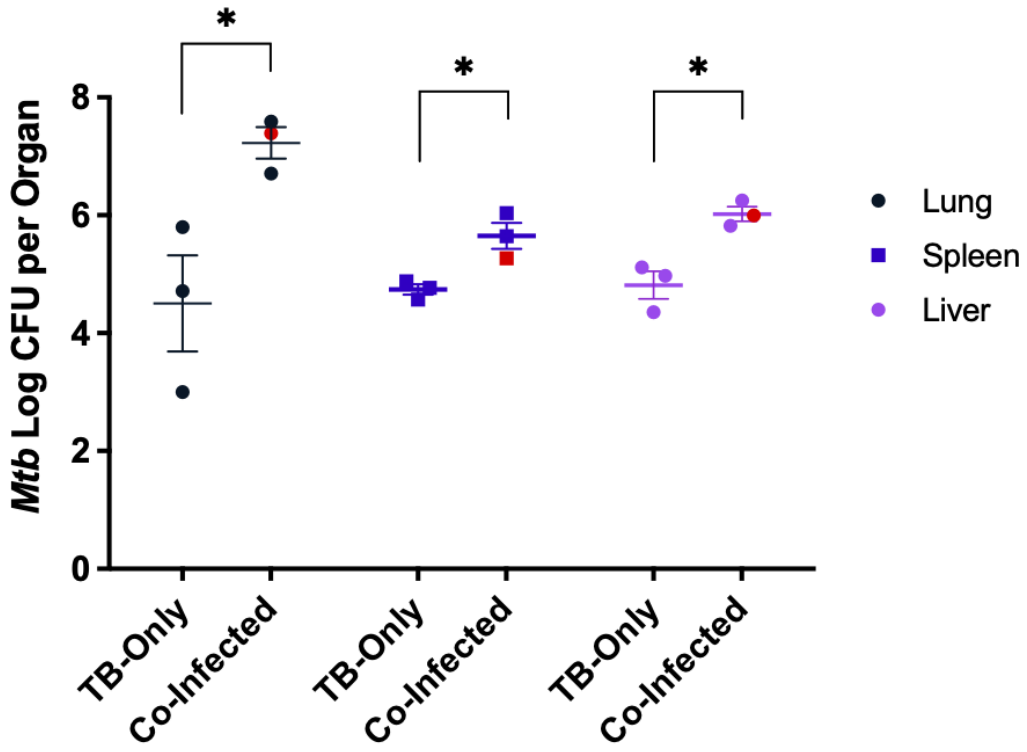

Figure 25. *Mtb* bacterial load in tissues of *Mtb*-only, co-infected huDRAG-A2 mice 4 weeks post-*Mtb* infection.
Mtb-only huDRAG-A2 (n=3), co-infected huDRAG-A2 (n=3*) *N number includes the co-infected huDRAG-A2 mouse with low HIV viral load pre-*Mtb* infection. Red point indicates co-infected (HIV low) huDRAG-A2. Data are expressed as mean +/- SEM. p value = * <0.05.

3.2.9. HIV/*Mtb* co-infection may exacerbate TB pathology in huDRAG-A2 mice.

Lung and spleen tissues were microscopically examined for histopathology. Lungs of co-infected huDRAG-A2 mice showed more severe pathology compared to TB-only infected mice from visual examination. Figure 26 shows the largest granulomas that developed from the lungs of each group. Quantification of the percent of granulomatous area out of total lung sections showed a trend of greater overall percent of granulomatous tissue formation within the co-infected group (Figure 26A). At 10x magnification, foamy macrophages can be observed in both the TB-only granuloma and co-infected granuloma (Figure 27A, B). Within the center of the co-infected granuloma, more caseation and cavitation were also present. AFB staining revealed that in both TB-only and co-infected granulomas, the foamy macrophages were infected with *Mtb* as evidenced by the red rod shaped bacilli localized in the cytoplasm of the foamy macrophages (Figure 27C, D).

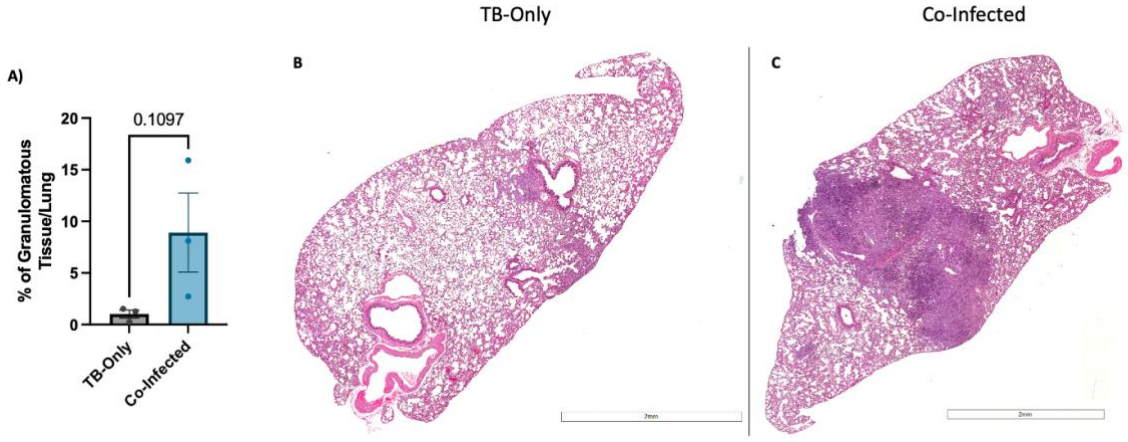

Figure 26. Quantification of granulomatous lung tissue in singly *Mtb*-infected and HIV/*Mtb* co-infected huDRAG-A2 mice 4 weeks post-*Mtb* infection.

(A) Percent of lung granulomatous tissue; percentage reported as the total area of granulomatous tissue out of total lung tissue (3 sections of lungs were measured for each sample); quantification performed using ImageJ software. H&E stain of whole lung sections of **(B)** *Mtb*-only huDRAG-A2 and **(C)** co-infected huDRAG-A2 mice. Whole lungs are selected based on largest granulomas observed in each group.

Representative of TB-only huDRAG-A2 (n=3) and co-infected huDRAG-A2 (n=3*) *Including the co-infected (HIV low) huDRAG-A2. Data are expressed as mean +/- SEM.

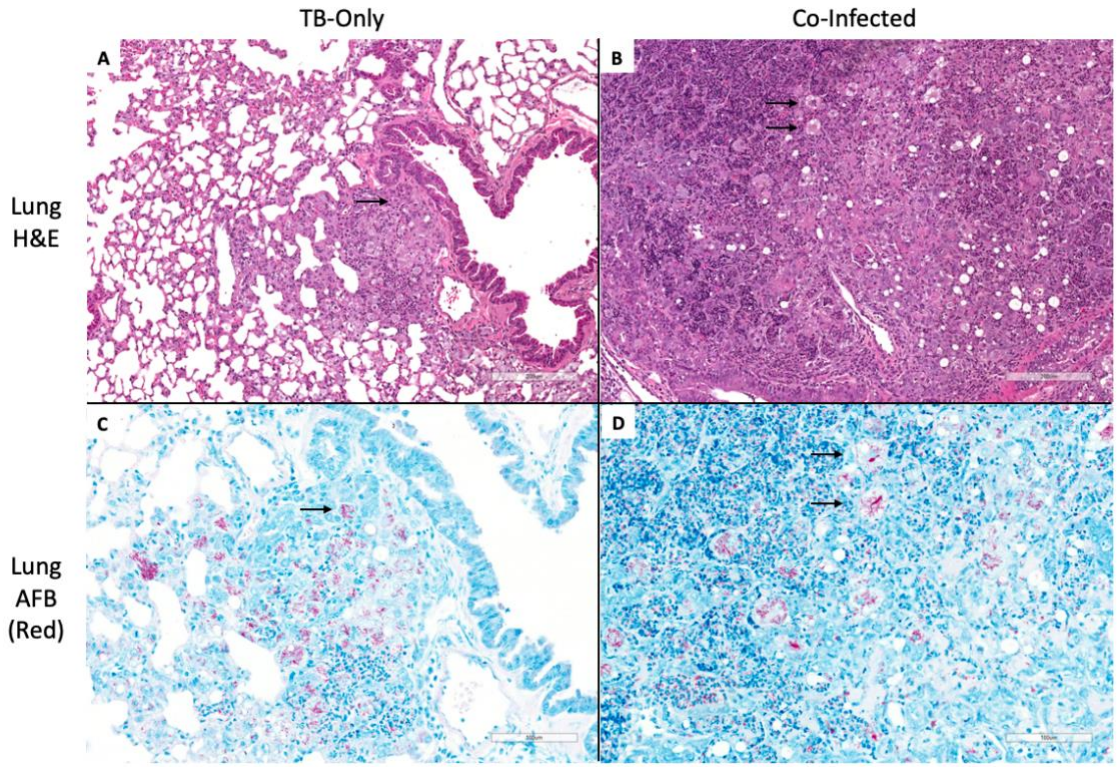

Figure 27. Visualization of lung granuloma formation, structure, and *Mtb* localization in singly *Mtb*-infected and HIV/*Mtb* co-infected huDRAG-A2 mice 4 weeks post-*Mtb* infection.
H&E stain (10x) of lung granuloma in **(A)** *Mtb*-only huDRAG-A2 and **(B)** co-infected huDRAG-A2 mice; black arrow indicates foamy macrophages. Acid fast bacilli stain (20x) of lung granuloma in **(C)** *Mtb*-only huDRAG-A2 and **(D)** co-infected huDRAG-A2 mice; black arrow indicates foamy macrophages infected with *Mtb* bacteria. *Mtb* bacilli are stained red. Representative of TB-only huDRAG-A2 (n=3) and co-infected huDRAG-A2 (n=3*) *Including the co-infected (HIV low) huDRAG-A2.

3.2.10. HIV/*Mtb* co-infection reduces hCD4+ T cells within blood and tissues of huDRAG-A2 mice.

To investigate changes in immune cell frequencies, immunohistochemistry was used to visualize cellularity with the lung and spleen and flow cytometry was used to quantify

immune cells in peripheral blood and lung. Within TB-only granulomas, an abundance of hCD4+ T cells and hCD68+ macrophages can be seen around the granuloma structure and throughout the lung tissue. In contrast, both hCD4+ T cells and hCD68+ macrophages were depleted in co-infected granulomas and were scarce throughout the lungs (Figure 28B, D). No notable granuloma lesions or pathology were observed in the spleens of either group. However, both hCD4+ T cell and hCD68+ macrophage frequencies were again reduced in the co-infected spleen (Figure 29).

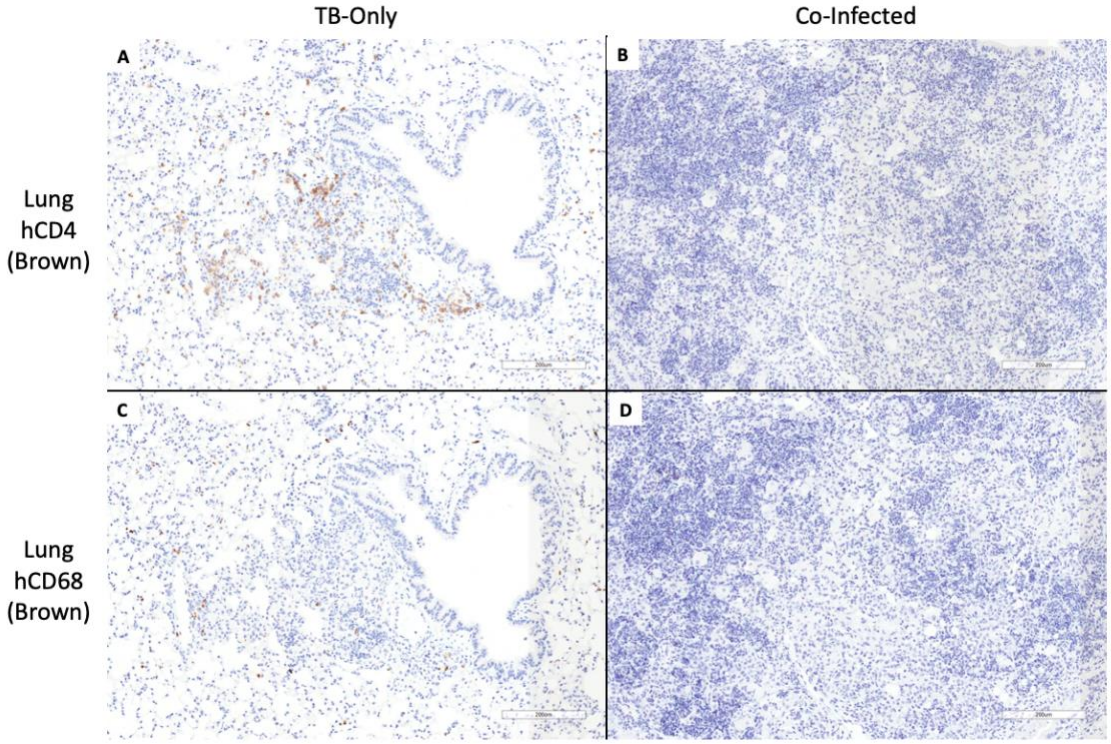

Figure 28. Visualization of human CD4+ T cells and human CD68+ macrophages in the lung granulomas of singly *Mtb*-infected and HIV/*Mtb* co-infected huDRAG-A2 mice 4 weeks post-*Mtb* infection.

IHC of hCD4 (10x) of lung granuloma in **(A)** *Mtb*-only huDRAG-A2 and **(B)** co-infected huDRAG-A2 mice; hCD4 stained brown. IHC of hCD68 (10x) of lung granuloma in **(C)** *Mtb*-only huDRAG-A2 and **(D)** co-infected huDRAG-A2 mice; hCD68 stained brown. Representative of TB-only huDRAG-A2 (n=3) and confirmed co-infected huDRAG-A2 (n=2).

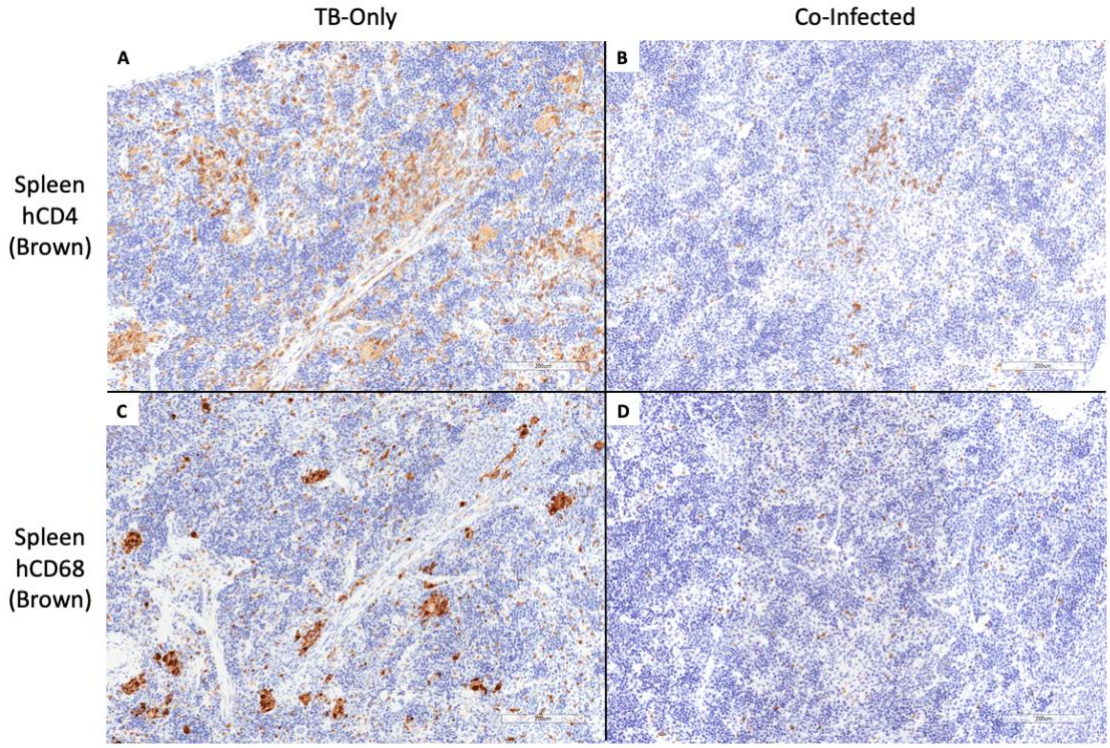

Figure 29. Visualization of spleen hCD4+ T cells and hCD68+ macrophages in the spleen of singly *Mtb*-infected and HIV/*Mtb* co-infected huDRAG-A2 mice 4 weeks post-*Mtb* infection.
IHC of hCD4 (10x) of **(A)** spleen in *Mtb*-only huDRAG-A2 and **(B)** spleen granuloma in co-infected huDRAG-A2 mice; hCD4 stained brown. IHC of hCD68 (10x) of **(C)** spleen in *Mtb*-only huDRAG-A2 and **(D)** spleen granuloma in co-infected huDRAG-A2 mice; hCD68 stained brown. Representative of TB-only huDRAG-A2 (n=3) and confirmed co-infected huDRAG-A2 (n=2).

At 2.5 weeks post-*Mtb* infection, HIV/*Mtb* co-infected huDRAG-A2 mice had significantly lower proportions of hCD4+ T cells and higher proportion of hCD8+ T cells in the blood compared to TB-only infected huDRAG-A2 mice (Figure 30A). No significant differences were observed in cell counts per mL of blood between the groups when the co-infected (HIV low) huDRAG-A2 mouse was included (indicated in blue) (Figure 30B). At 4 weeks post-*Mtb* infection (experimental endpoint), no significant differences were observed in

cell counts per mL of blood (Figure 31). Within the lungs, no notable differences in hCD14+hCD169+hCD209+ alveolar macrophages were observed, but hCD14+hCD169-hCD209+ interstitial macrophages may show a trend of depletion in co-infected mice if the co-infected (HIV low) huDRAG-A2 mouse is considered an outlier (Figure 32B). However, co-infection did significantly reduce the percentage of hCD4+ T cells in the lung compared to TB-only infected huDRAG-A2 (Figure 32A). Flow cytometry data corroborates observations in histology illustrating significant depletion of hCD4+ T cells within the lung tissue of co-infected huDRAG-A2 mice. Total remaining immune cells at 2.5 weeks and 4 weeks post-*Mtb* infection were compared to pre-experiment levels where a trend of reduced human immune cells may be observed in the co-infected group (Supplementary figure 2). However, one *Mtb*-only infected huDRAG-A2 mouse had an abnormally high pre-experiment reconstitution level which skewed the calculated percentage and thus may be misleading.

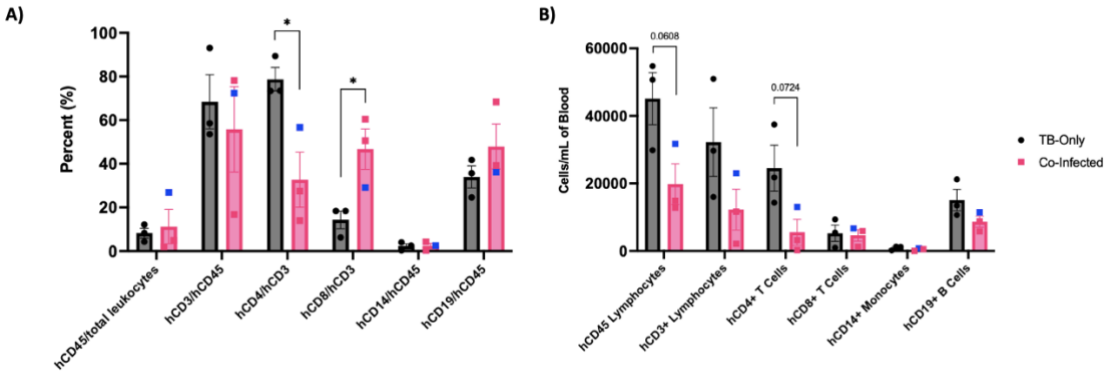

Figure 30. Flow cytometry on peripheral blood of singly-*Mtb* infected and co-infected huDRAG-A2 mice 2.5 weeks post-*Mtb* infection.
(A) Percent of human immune cells within the blood and **(B)** number of immune cells per mL of blood in huDRAG-A2 mice. TB-Only (N = 3) and Co-infected (N=3). Data are expressed as mean +/- SEM, p value

= * <0.05. Blue data points represent co-infected huDRAGA2 mouse with low HIV viral load pre-*Mtb* infection.

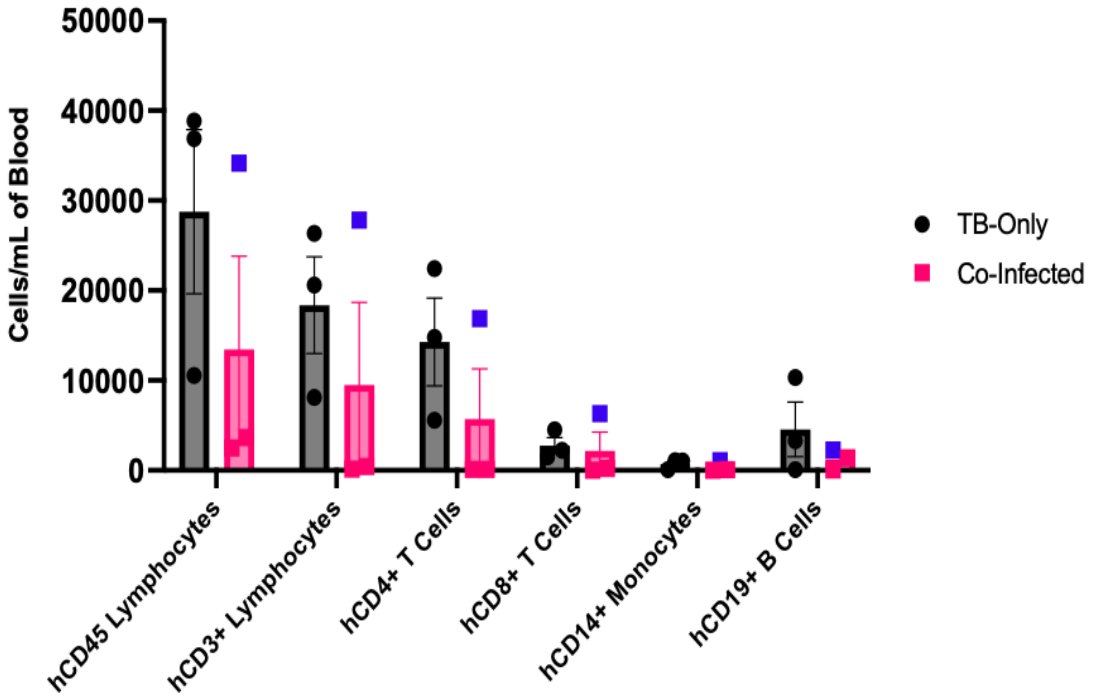

Figure 31. Flow cytometry of huDRAG-A2 peripheral blood at 4 weeks post-*Mtb* infection endpoint. Number of immune cells per mL of blood in huDRAG-A2 mice. TB-Only (N = 3) and Co-infected (N=3). Data are expressed as mean +/- SEM. Blue data points represent co-infected huDRAGA2 mouse with low HIV viral load pre-*Mtb* infection.

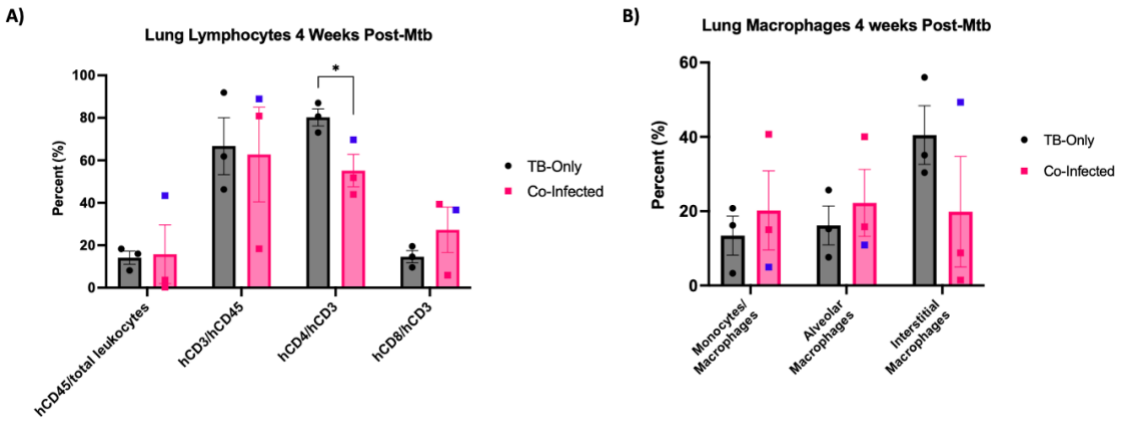

Figure 32. At 4 weeks post-*Mtb* infection, HIV/*Mtb* co-infected huDRAG-A2 mice have significantly lower proportions of hCD4+ T cells in the lung compared to TB-only infected huDRAG-A2.
(A) Percent of human lymphocytes and **(B)** percent of human macrophages within huDRAG-A2 lung. TB-Only (N = 3) and Co-infected (N=3). Alveolar macrophages are defined by hCD14+hCD169+hCD209+ markers, interstitial macrophages are defined by hCD14+hCD169-hCD209+ markers. Data are expressed as mean +/- SEM, p value = * <0.05. Blue data points represent co-infected huDRAGA2 mouse with low HIV viral load pre-*Mtb* infection.

3.2.11. HuDRAG-A2 mice develop TB granulomas that provide insight into the progression of TB lung pathology.

Further histopathology analysis at 20x magnification showed an abundance of foamy macrophages within a severe granuloma lesion in HIV/*Mtb* co-infected HuDRAG-A2 lungs (Figure 33A). These foamy macrophages appear to range in sizes where larger cells have more lipid-filled pockets. Circular cavities can also be seen adjacent to foamy macrophage with some cavities still appearing to contain the nucleus of a cell (Figure 33A). In a lower magnification (10x), a large line of foamy macrophages and cavity pockets can be seen near the center of the granuloma, and this may be the beginning stages of the formation of a large cavitation within the granuloma (Figure 33B).

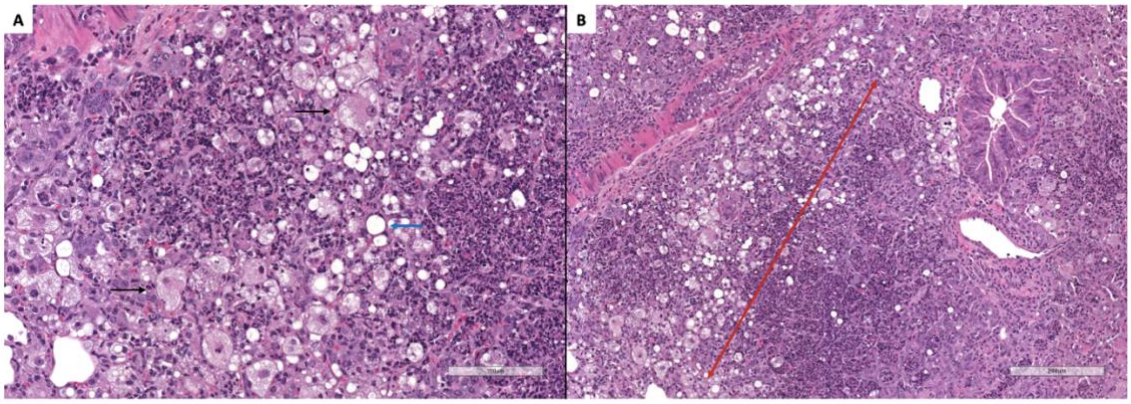

Figure 33. Foamy macrophages and necrosis-associated cavities within HIV/*Mtb* co-infected huDRAG-A2 lung granuloma core 4 weeks post-*Mtb* infection.
(A) H&E stain of lung granuloma core illustrating foamy macrophages within the core of a severely necrotic granuloma (20x); black arrows indicates foamy macrophages, blue arrow indicates cavity left behind from lipid dissolution. **(B)** Abundance of adjacent foamy macrophages and cavities forming a line (10x); red double-arrow is next to the line of small cavities and foamy macrophage and indicates the potential region of tissue cavitation if disease progression continues. Representative of co-infected huDRAG-A2 (n=2*) *Including the co-infected (HIV low) huDRAG-A2.

AFB staining of co-infected granuloma at 8x magnification illustrates that there are high concentrations of *Mtb* bacilli localized within the foamy macrophages (Figure 34A), but *Mtb* bacilli are in abundance through the entirety of the granuloma as illustrated by a higher magnification (20x) in an area with fewer foamy macrophages (Figure 34B). The heterogeneity of granuloma structures was also observed in both co-infected and *Mtb*-only infected huDRAG-A2 mice. In particular, granulomas that may represent the different stages of granuloma formation/development are illustrated by Figure 35. For consistency, all lung granulomas represented in Figure 35 are of *Mtb*-only infected huDRAG-A2 mice. With the combination of H&E and AFB staining, earlier stages of granuloma formation appear to well-contain the *Mtb* bacilli, while later stages of granulomas fail to contain the bacilli resulting in dissemination out of the structure. Immune cells such as hCD4+ T cells and hCD68+ macrophages also appear more centralized to the granuloma structure in early-mid stages and in late-stages become more scattered throughout the lung and appear less involved in the granuloma structure (Figure 35).

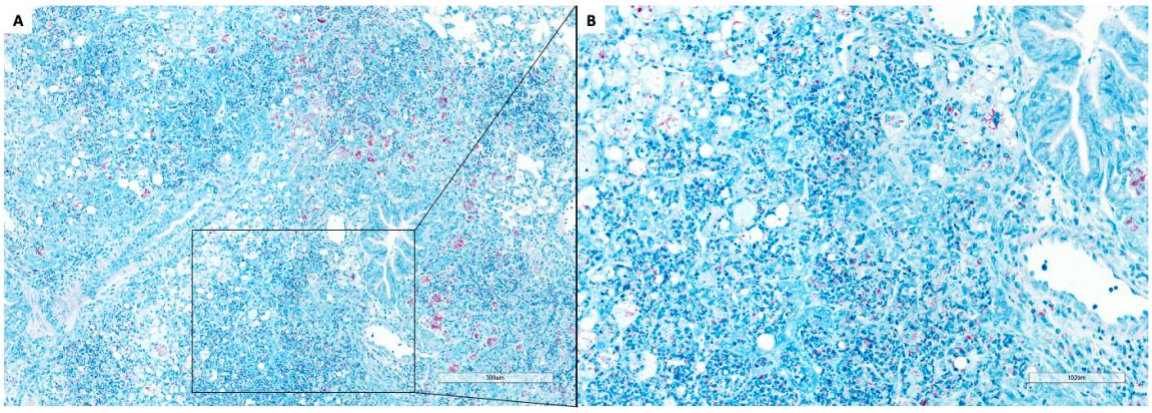

Figure 34. Foamy macrophages within granulomas harbour high loads of *Mtb* bacteria and necrosis-associated cavities within HIV/*Mtb* co-infected huDRAG-A2 lung granuloma core 4 weeks post-*Mtb* infection.

(A) Acid fast bacilli stain of co-infected lung granuloma core illustrating high concentration of *Mtb* localized within foamy macrophages (8x); black box and lines indicate the area that was magnified. **(B)** 20x magnification of necrotic core area without foamy macrophages illustrating the presence of *Mtb* scattered in lower concentration. *Mtb* bacilli stained red. Representative of co-infected huDRAG-A2 (n=3*) *Including the co-infected (HIV low) huDRAG-A2.

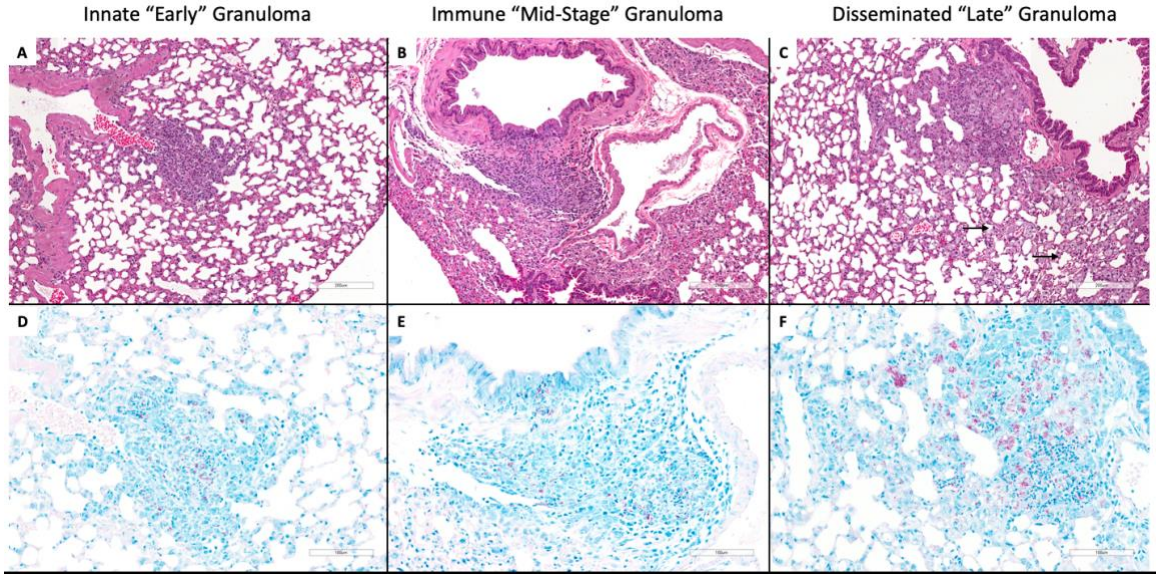

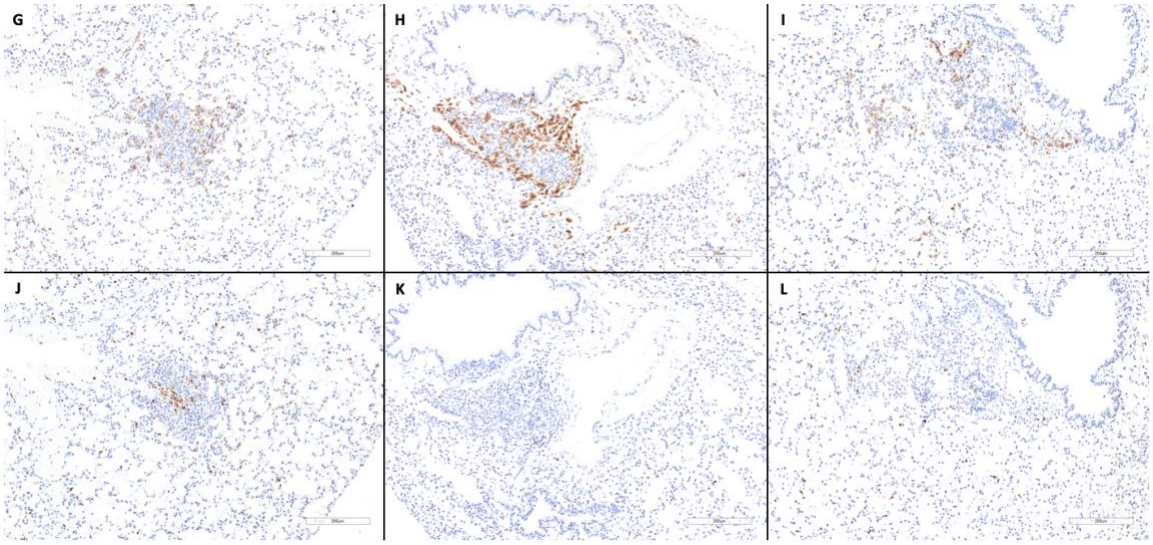

Figure 35. Lung Granuloma heterogeneity in singly *Mtb*-infected huDRAG-A2 mice illustrates potential developmental stages of *Mtb* lung granuloma 4 weeks post-*Mtb* infection.
(A-C) H&E (10x) of lung granulomas; black arrows indicate foamy macrophages within the airway surrounding granuloma. **(D-F)** Acid fast bacilli stain (20x) of lung granulomas; *Mtb* bacilli stained red. IHC of **(G-I)** hCD4 and **(J-L)** hCD68 of lung granulomas (of lung granulomas); hCD4 and hCD68 stained brown.

Chapter 3.3. Aim 3: Elucidate the immunogenicity of adeno-vectored TB vaccines in generating *Mtb*-specific immune responses within huNRG and huDRAG-A2 mice

3.3.1. Pilot study investigating the immunogenicity of mucosal and parenteral administration of TB vaccine (AdCh68Ag85A) in huNRG mice.

A pilot experiment was conducted to investigate T cell responses in AdCh68Ag85A-vaccinated huNRG mice and to establish methods for future immunogenicity studies. HuNRG mice were vaccinated with $1x10^7$ PFU chimpanzee adeno-vectored AdCh68Ag85A using the respiratory mucosal route via intranasal administration (n=3), and parenteral route via intramuscular injection (n=3). Tissues were collected for *in vitro* T cell stimulation with Ag85A peptide pool (1-57), BCG, or PMA/Ionomycin as a positive

control for 24 hours to assess cytokine production (IFN-γ, IL-2, and TNF-α) (Figure 6). One huNRG mouse did not wake up during intranasal infection, and since one main objective of the study was to investigate antigen-specific responses after respiratory mucosal vaccination, one huNRG from the unvaccinated control group was moved to the intranasal immunization group. At 4 weeks post-vaccination, 1 huNRG mouse from both vaccinated groups neared weight loss endpoint (likely from GvHD) and was sacrificed. Peripheral blood was collected from all the mice at 4 weeks post-vaccination and stimulated with Ag85A peptide pool (1-57). However, flow cytometry analysis revealed that the volume of survival blood (200µL) collected from huNRG mice did not contain enough human immune cells to yield any informative data on vaccine specific immune responses. Therefore, at the planned experimental endpoint of 5 weeks post-vaccination, only whole lung and spleen tissues were collected from huNRG mice (n=2) in all groups.

Due to the final sample size of 2 within all groups, statistical significance could not be assessed for this experiment. Graphical analysis of lung and spleen tissue under every stimulation condition showed that the Ag85A peptide pool (1-57) stimulation in particular did not demonstrate any trends or differences between groups (data not shown). The PMA/Ionomycin condition served as a positive control stimulation condition since it non-specifically activates T cells for cytokine production [329,330]. Although no trends were observed between groups with PMA stimulation, T cells within huNRG lung and spleen were able to produce all three pro-inflammatory cytokines (IFN-γ, IL-2, and TNF-α) upon activation, indicating that they were polyfunctional (Figure 36).

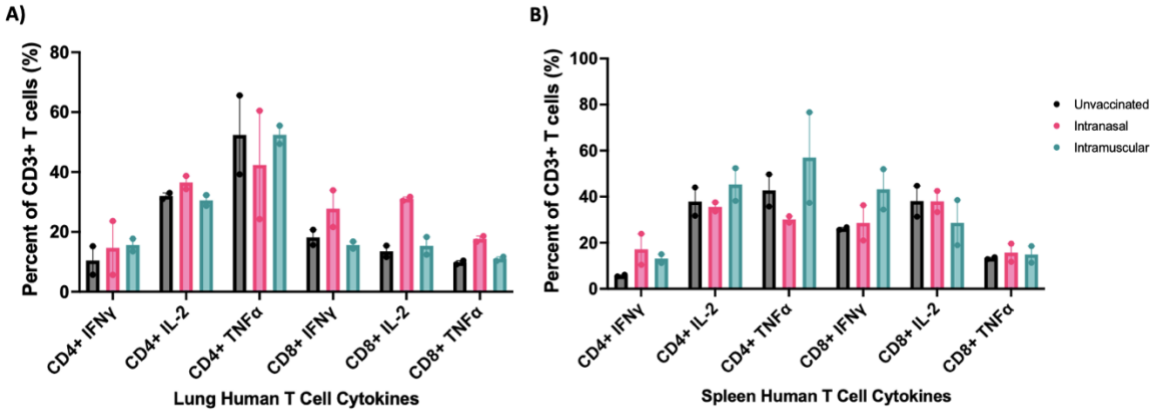

Figure 36. Percent of human CD4+ and CD8+ T cells producing pro-inflammatory cytokines in huNRG 5 weeks post-vaccination after PMA/Ionomycin stimulation.
24 hours PMA/Ionomycin stimulation of huNRG **(A)** lung and **(B)** spleen. Data are expressed as mean +/- SEM. (n=2).

Upon 24 hour stimulation of huNRG lung and spleen cells in the BCG stimulation condition, both the intranasal and intramuscular vaccinated mice may show a higher trend in frequencies of IL-2 producing hCD4+ T cells 5 weeks post-vaccination (Figure 37A, B). Since this was a pilot study, these observations will need to be confirmed with more huNRG mice to increase samples size as the TB specific immune responses were overall quite low (< 5%). However, this experiment was able to set the foundation (in establishing methods, materials, and protocols) for the next study to investigate a more immunogenic TB vaccine (AdCh68MV).

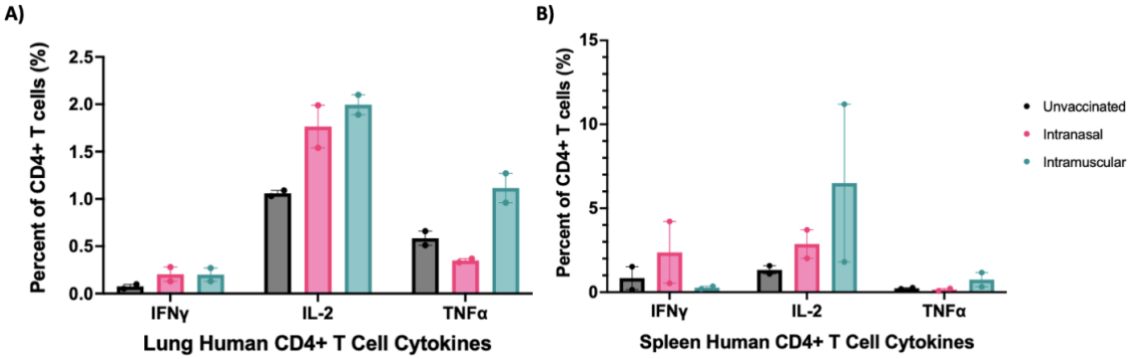

Figure 37. Antigen-specific cytokine production by human CD4+ T cell 5 weeks post-vaccination after BCG stimulation.
Percent of human CD4+ T cells producing pro-inflammatory cytokines after 24-hour stimulation with BCG within huNRG **(A)** lung and **(B)** spleen. Data are expressed as mean +/- SEM.

3.3.2. Investigating the immunogenicity of novel trivalent TB vaccine (AdCh68MV) via mucosal delivery in generating *Mtb*-specific immune responses within huNRG and huDRAG-A2 mice.

The AdCh68MV vaccine (also known as AdCh68Ag85A:rpfB:TB10.4) is a chimpanzee adenovirus 68-vectored TB vaccine constructed to express three different *Mtb* antigens (Ag85A, rpfB, and TB10.4). To investigate the immunogenicity of AdCh68MV, both huNRG (n=3) and huDRAG-A2 (n=3) mice were vaccinated with $1x10^7$ PFU via intranasal administration and will be compared to an unvaccinated control from each model (**Figure 7**). 4 weeks post-infection, animals were sacrificed and BAL, lung, and spleen cells were stimulated with 5 different conditions (Unstimulated, whole protein pool, BCG, cell filtrate and crude BCG, and PMA/Ionomycin) for 24 hours, with the exception of PMA which was only stimulated for 6 hours. Multiple stimulation conditions were tested to determine the ideal *Mtb*-antigen stimulation for hu-mouse models.

Number of cells per lung or spleen that produced cytokines in the unstimulated condition were subtracted from every antigen-stimulation condition in order to remove cells that non-specifically produced cytokines (data represented as frequencies/percent of cytokine producing cells did not have cytokine producing cells in the unstimulated condition removed from stimulated conditions). Based on graphical observation, it was evident that the cell filtrate and crude BCG (hereafter termed CFCB) stimulation is likely the best of the three antigen stimulation conditions. CFCB was the only condition that was able to activate substantial and consistent levels of hCD4+ and hCD8+ T cells producing IFN-γ and TNF-α cytokines in both lung and spleen (Figure 38, Supplementary figure 4). None of the stimulation conditions were able to generate appreciable antigen-specific IL-2 production from either hCD4+ and hCD8+ T cells within the lung and spleen (Figure 38). Therefore, results hereafter are reported without IL-2 to reduce the skewing of graphs by 0 or very low values.

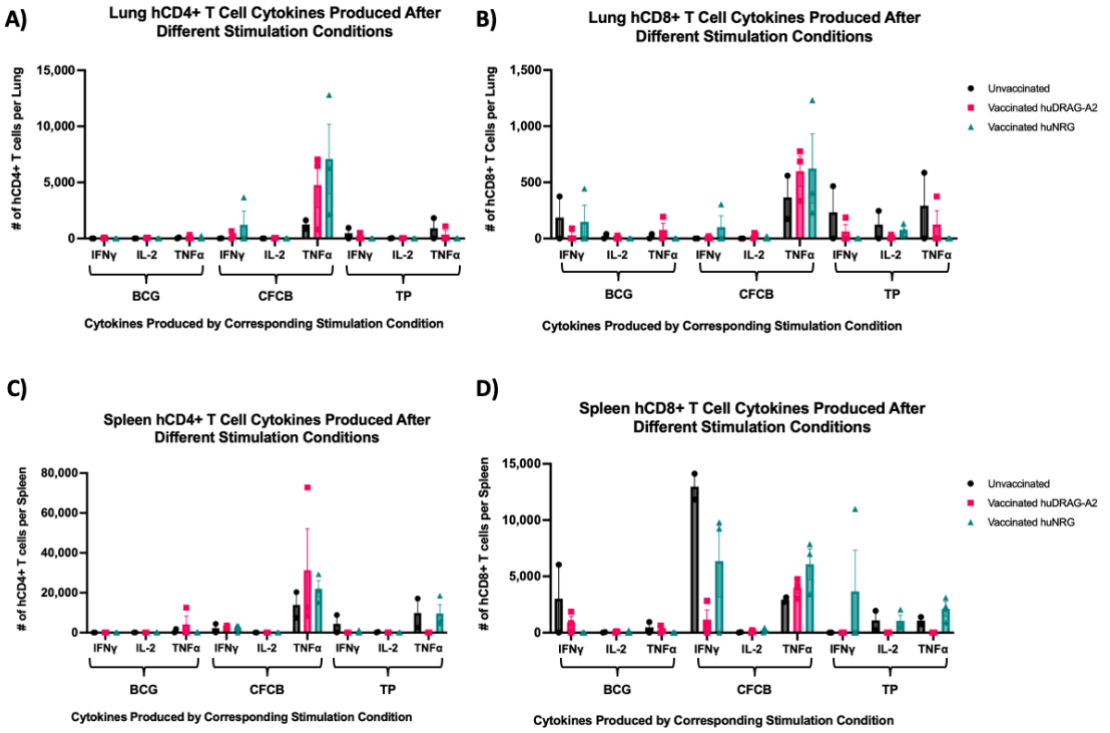

Figure 38. Human CD4+ and CD8+ T cell cytokine production under different stimulations conditions.

Total number of hCD4+ T cells producing pro-inflammatory cytokines after stimulation in **(A)** whole lung and **(C)** spleen for 24 hours. Total number of cytokine producing hCD8+ T cells in **(B)** whole lung and **(D)** spleen. BCG = Bacillus Calmette–Guérin; CFCB = Culture filtrate and crude BCG; TP = Trivalent Protein Pool (Ag85A, rpfB, and TB10.4 whole protein). Number of cells producing cytokines in the unstimulated condition were subtracted from each stimulation condition (to remove non-specifically stimulated cells in each condition). Unvaccinated group (huNRG n=1, huDRAG-A2 n=1); vaccinated huDRAG-A2 group n=3; vaccinated huNRG group n=3. Data are expressed as mean +/- SEM.

Since in Figure 38 the AdCh68MV vaccinated huNRG and huDRAG-A2 mice both developed hCD4+ T cells in the lungs that responded to specific *Mtb* antigens with CFCB stimulation, we will further examine the results from the CFCB stimulation condition. In particular, lung hCD4+ T cells in vaccinated huNRG and huDRAG-A2 mice showed higher trends in frequency and total numbers of cells producing TNF-α compared to the unvaccinated group (Figure 39A, B). *Mtb* antigen-specific responses were also observed (to a lower degree) in hCD8+ T cells. It is notable that the high percentages of IFN-

producing hCD8+ T cells in the unvaccinated group (Figure 39C) are non-representative and misleading as they are based on a very low number of cells (Figure 39B). Overall, despite insufficient sample size to reach statistical significance to compare between vaccinated and unvaccinated groups, huNRG and huDRAG-A2 mice both show the ability to generate hCD4+ and hCD8+ T cells in the lungs that produce *Mtb* antigen-specific inflammatory cytokine responses.

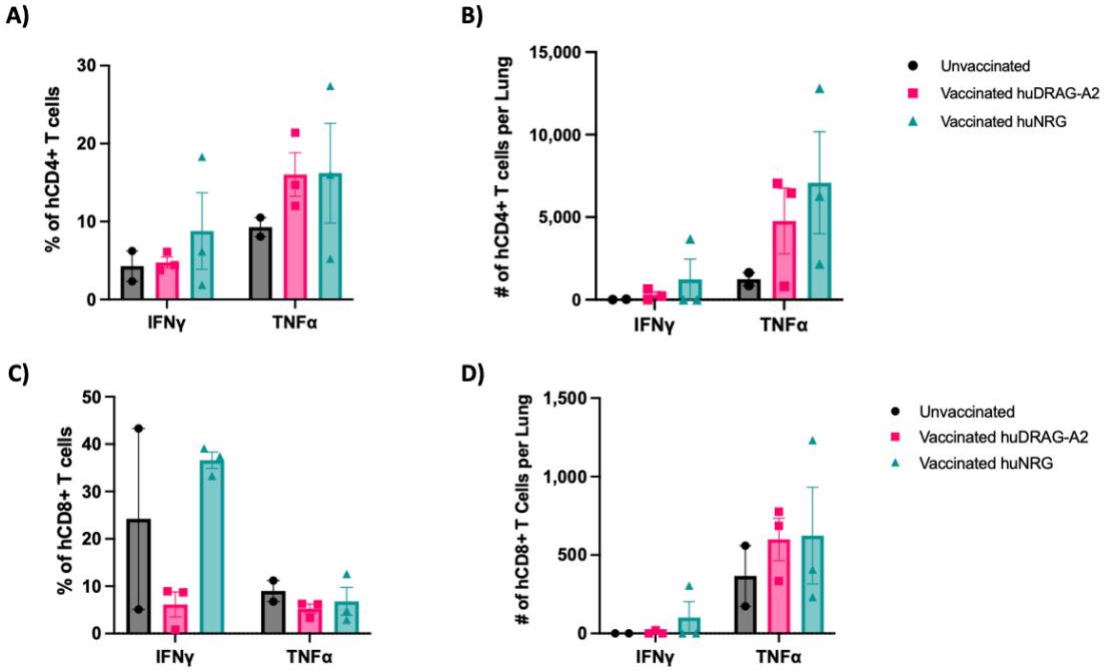

Figure 39. Antigen-specific lung hCD4+ and hCD8+ T cell cytokine production after culture filtrate and crude BCG stimulation 4 weeks post-vaccination.

Percent of lung **(A)** hCD4+ T cells and **(C)** hCD8+ T cells that produce pro-inflammatory cytokines after culture filtrate and crude BCG stimulation for 24 hours. Total number of cytokine producing **(B)** hCD4+ T cells and **(D)** hCD8+ T cells in whole lung where the number of cells producing cytokines in the unstimulated condition were subtracted from CFCB stimulated cells (to remove non-specifically stimulated cells in each condition). Unvaccinated group (huNRG n=1, huDRAG-A2 n=1); vaccinated huDRAG-A2 group n=3; vaccinated huNRG group n=3. Data are expressed as mean +/- SEM. Note: percent of cytokine producing cells in unstimulated conditions were not subtracted from percent of cytokines produced by stimulated conditions.

Within the spleen of AdCh68MV vaccinated huNRG and huDRAG-A2 mice, similar observations were made where vaccinated hu-mice generated *Mtb* antigen-specific hCD4+ T cells after CFCB stimulation (Figure 40). Vaccinated HuDRAG-A2 mice may also be showing a higher trend of antigen-specific TNF-α producing hCD4+ T cell frequencies compared to vaccinated huNRG mice (Figure 40A). On the other hand, vaccinated huNRG mice may show a higher trend of total counts of antigen-specific TNF-α producing hCD8+ T cells (Figure 40D). Again, despite insufficient sample size to reach statistical significance for comparisons between vaccinated and unvaccinated groups, both huNRG and huDRAG-A2 mice show the ability to generate hCD4+ T cells in the spleen that produce *Mtb* antigen-specific TNF-α responses.

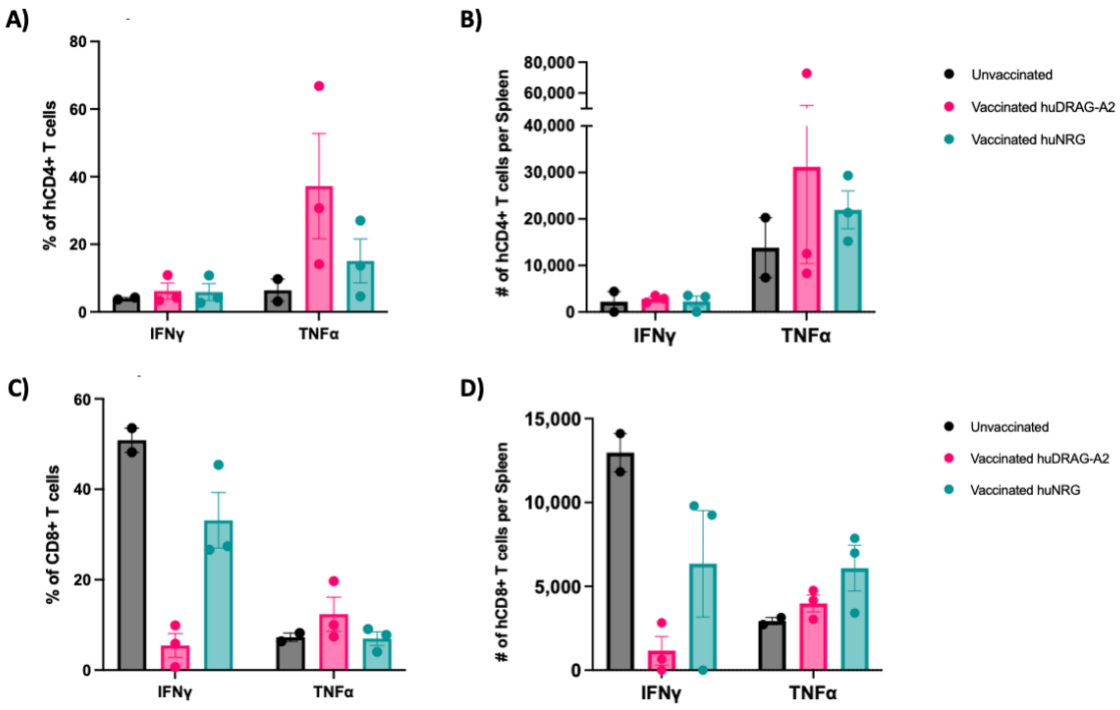

Figure 40. Antigen-specific spleen hCD4+ and hCD8+ T cell cytokine production after culture filtrate and crude BCG stimulation 4 weeks post-vaccination.
Percent of spleen **(A)** hCD4+ T cells and **(C)** hCD8+ T cells that produce pro-inflammatory cytokines after culture filtrate and crude BCG stimulation for 24 hours. Total number of cytokine producing **(B)** hCD4+ T cells and **(D)** hCD8+ T cells in whole spleen where the number of cells producing cytokines in the unstimulated condition were subtracted from CFCB stimulated cells (to remove non-specifically stimulated cells in each condition). Unvaccinated group (huNRG n=1, huDRAG-A2 n=1); vaccinated huDRAG-A2 group n=3; vaccinated huNRG group n=3. Data are expressed as mean +/- SEM. Note: percent of cytokine producing cells in unstimulated conditions were not subtracted from percent of cytokines produced by stimulated conditions.

In the literature, different clones of co-stimulatory antibodies (hCD28, hCD49d) were used to supplement stimulation conditions [104]. The co-stimulatory antibodies used in our lab are more cost-effective options than those used by Yao et al. 2017, but to determine if this may affect the ability of the cells to respond, the two different co-stimulatory antibodies supplementations were compared. CFCB stimulation conditions were supplemented with in-lab established hCD28 and hCD49d antibody clones and compared to CFCB supplemented with hCD28 and hCD49d antibody clones used by Yao et al. 2017 (hereafter termed Y-CFCB condition). Within spleen tissue, no notable differences were observed between CFCB and Y-CFCB in frequencies of cytokine producing hCD4+ and hCD8+ T cells (Figure 41A, C). No notable differences were observed between CFCB and Y-CFCB in total cell counts of TNF-α producing hCD4+ and hCD8+ T cells, as there may be one outlier skewing the mean (Figure 41B, D). However, there may be a difference in producing antigen-specific IFN-γ response in hCD8+ T cells, as CFCB stimulation appear to show a trend of more IFN-γ producing hCD8+ T cells in the unvaccinated group than Y-CFCB stimulation (Figure 41D). Overall, no significant differences can be concluded from the use of different co-stimulatory antibody clones in this study, but further comparisons with a large sample size may be required for confirmation.

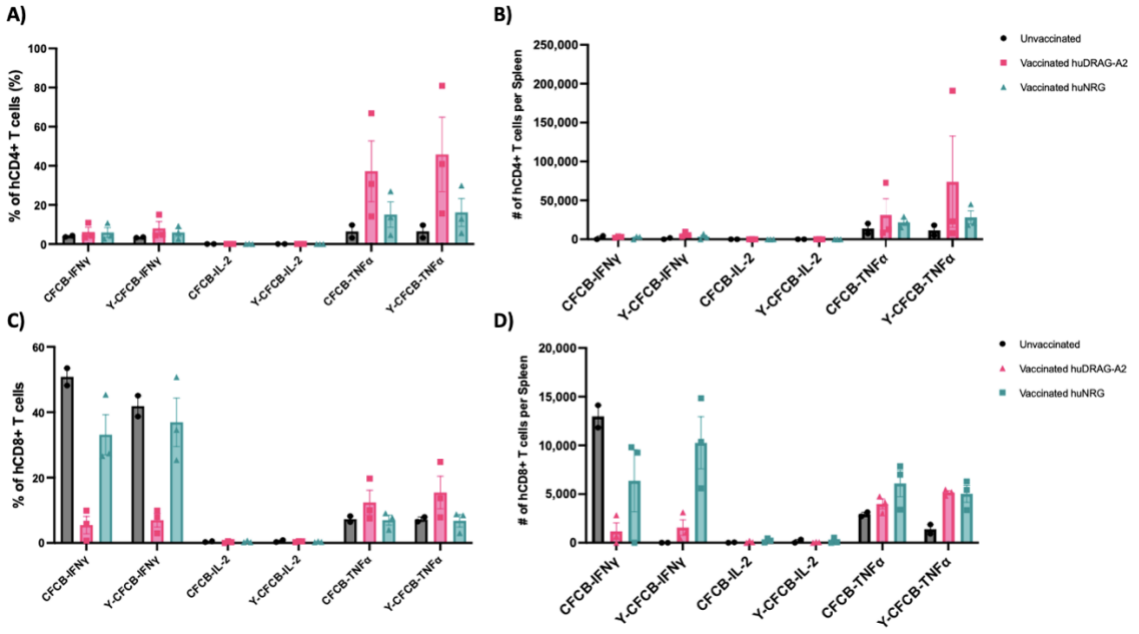

Figure 41. Comparison between the supplementation of in-lab co-stimulatory antibodies versus co-stimulatory antibodies used by Yao et al. 2017 in the culture filtrate and crude BCG stimulation condition.

Percent of spleen **(A)** hCD4+ T cells and **(C)** hCD8+ T cells that produce pro-inflammatory cytokines after culture filtrate and crude BCG stimulation supplemented with different co-stimulatory antibodies for 24 hours. Total number of cytokine producing **(B)** hCD4+ T cells and **(D)** hCD8+ T cells in whole spleen where the number of cells producing cytokines in the unstimulated condition were subtracted from CFCB/Y-CFCB stimulated cells (to remove non-specifically stimulated cells in each condition). CFCB = culture filtrate and crude BCG supplemented with in-lab costimulatory antibodies; Y-CFCB = culture filtrate and crude BCG supplemented with costimulatory antibodies used by Yushi Yao et al. 2017. Unvaccinated group (huNRG n=1, huDRAG-A2 n=1); vaccinated huDRAG-A2 group n=3; vaccinated huNRG group n=3. Data are expressed as mean +/- SEM. Note: percent of cytokine producing cells in unstimulated conditions were not subtracted from percent of cytokines produced by stimulated conditions.

Chapter 4. DISCUSSION

Chapter 4.1. Develop and compare current- and next-generation humanized mouse models with human immune cells capable of sustaining both HIV and TB infections.

HLA-typing of HSC samples yielded approximately 15.5% to be HLA-DRB1*04:01 positive and 47.8% to be HLA-A*02:01 positive (Table 1). This frequency is as expected within the European Caucasian population as the HLA allele database (http://www.allelefrequencies.net/hla.asp) reports allele phenotype/population frequencies of approximately 16.8% and 47.5%, respectively. Given these proportions, around 8% of double positives are expected, and based on results, 7% was double positive. Although these results align well with what is reported within the HLA databases, it is important to note that our UCB samples were (and continue to be) obtained from the McMaster University Children's Hospital based in Hamilton Ontario. The population of those donating UCB samples in Hamilton is unlikely to all be European Caucasian; since demographics data were not collected from UCB donors, the rate of positive samples in future testing can be expected to vary. Due to the COVID-19 pandemic, samples received by the McMaster Children's Hospital labor and delivery ward became limited. This meant it was necessary to maximize every double HLA-positive sample to engraft as many DRAG-A2 mice as possible. Multiple breeding pairs of DRAG-A2 mice were set up around similar times and litters would be weaned and kept until between 6-8 weeks of age to engraft with double-positive HSCs. This ensures that each thawed sample would have a larger number of mice to engraft. Although more DRAG-A2 mice can be engrafted using

the tail vein injection method as adults, each mouse would consequently receive fewer HSCs. This is likely contributing to the decreased number of successfully engrafted mice when compared to humanizing mice as newborns (Supplementary Table 1). An average litter usually yields 7-12 newborns to engraft, and around 20 mice were pooled for engraftment as adults. The main advantage of engrafting mice as adults is the ability to choose the sex of mice to engraft, and having a larger age range of engraftment window that allow for increased numbers of mice engrafted per sample. For instance, female mice are preferred as we perform intravaginal infections for most of our HIV and HIV/*Mtb* co-infection studies. As a result, this method may still yield higher numbers of female hu-mice despite having fewer successfully engrafted mice in total. Even though we found that we can successfully engraft DRAG-A2 mice using the adult tail vein engraftment method, it was evident that sample size and number of HSCs to engraft are still critical factors to ensure high success rate.

As a part of this project, the current-generation huNRG model and next-generation huDRAG-A2 models were established and compared. HuDRAG-A2 mice developed significantly higher levels of hCD14+ monocytes and hCD3+ T cells (in particular, hCD4+ T cells) in peripheral blood upon intrahepatic engraftment of HSCs as newborns (Lepard and Yang, 2022; *Viruses* - in review). Higher engraftment of hCD4+ T cells was expected as previous studies using a similar model termed huDRAGA had observed similar findings [270]. However, hCD14+ monocytes were not previously compared, and may be an additional reconstitution improvement of the huDRAG-A2 model. The capability of the

huDRAG-A2 mice to develop more robust levels of both T cells and monocytes illustrated their potential in studying HIV and TB, where both aforementioned human immune cells are heavily involved in host-pathogen responses. As part of our initial characterization of our models, we were also able to show that hCD4+ T cells from huDRAG-A2 mice could differentiate into the Th17 subset and produce hIL-17 (Figure 8). This can be an important subset for HIV mucosal immunity investigations and thus further illustrates the suitability of huDRAGA2 mice for studies involving HIV and elucidating the role of Th17 in the context of HIV-infection [331].

Human NK cells are largely absent in many humanized mouse models, and yet are important to innate immune responses to many pathogens as well as the functionality of therapeutics such as monoclonal antibodies. Therefore, we characterized a newly available (The Jackson Laboratory) transgenic strain of NSG mice that express human IL-15 (NSG-hIL15), a cytokine necessary for NK cell differentiation, expansion and function [268,328,332,333]. Although NSG-hIL15 background mice are commercially available and do not require further breeding to generate allele homozygosity of the IL-15 transgene, a genotyping protocol was established to confirm the expression of the transgene prior to HSC engraftment. Either the NSG or NRG background can be a good negative control for the genotyping qPCR as they do not express any transgenes. However, other different strains of immunocompromised mice expressing transgenes (NRG-A2 and DRAG) were also tested as negative controls to see if human transgene expression would affect genotyping results. The genotyping protocol developed was efficacious at identifying the

correct mouse transgene (Figures 9 & 10). To humanize and characterize these mice, HSCs were engrafted via intrahepatic injection in newborn NRG and NSG-hIL15 mice. While huNRG mice are not the ideal engraftment control for an NSG transgenic strain, they were still used as we did not have access to huNSG mice at the time. However, huNRG mice are still valid control as they show very similar immune reconstitution profiles as huNSG mice [261]. Both huNRG and huNSG-hIL15 mice developed human T cell populations (Figure 11). However, huNSG-hIL15 mice developed significantly higher percentage and absolute counts of hCD56+CD3- NK cells at 16 weeks post-engraftment whereas in huNRG mice, this population was nearly absent (Figure 12). HuNSG-hIL15 mice developed an average of approximately $2.5x10^4$ NK cells per mL of blood which is a substantial population even when compared to humans [334]. Next steps would be to investigate the functionality of the human NK cells produced by the model, but this data still illustrates the potential for huNSG-hIL15 mice to be used in NK cell-related studies.

Chapter 4.2. Characterizing HIV/*Mtb* co-infection immune responses and pathology within huNRG mice and huDRAG-A2 mice

4.2.1. HIV/*Mtb* co-infection immune responses and pathology within huNRG mice

There are 2 likely clinical scenarios in the context of HIV/*Mtb* co-infections where an individual can either be infected first by HIV followed by a co-infection with *Mtb*, or establish a primary *Mtb* infection followed by HIV. This project focused on the first scenario involving primary HIV infection in humanized mice followed by subsequent *Mtb*

infection. This case would model scenarios such as HIV-positive newborns or individuals that have established HIV infections prior to TB infection. Prior to developing models of HIV/*Mtb* co-infection in huNRG and huDRAG-A2 mice, both hu-mice models were first demonstrated to well-recapitulate HIV-1 and *Mtb* infections alone (Lepard and Yang, 2022; *Viruses* - in review).

In huNRG mice, the *Mtb* infection-only group (n=3) and HIV/*Mtb* co-infected group (n=4) were compared (Figure 4). As the first co-infection experiment conducted in the lab, we aimed to establish primary HIV-1 infection by vaginal mucosal infection, which is one of the most common methods of transmission. 3 of 4 huNRG mice sustained substantial plasma viral loads by 2 weeks post-infection, while 1 of 4 huNRG had viral load that was near the detection threshold (~10,000 RNA copies/mL) and thus successful HIV infection could not be confirmed prior to *Mtb* infection (Table 2). This indicates that the animal may be harbouring very low levels of HIV in the plasma, or that HIV-1 has mostly become pro-viral and are residing within cells, or they may not be successfully infected with HIV. Nevertheless, all the mice were co-infected with *Mtb* at 3.5 weeks post-HIV infection as we wanted to model established but not chronic HIV-1 infection in our initial co-infection studies. Plasma samples taken at later timepoints (post-*Mtb* infection) will be used to determine if the unconfirmed huNRG mouse was indeed HIV-infected. However, containment level 3 protocols are still pending to perform RNA extractions for RT-qPCR. If the huNRG is later confirmed to be uninfected, it will be removed from all analyses as it would not fit either the *Mtb*-only or co-infected group. Both the TB-only and co-infection

groups were infected with low-dose $1x10^3$ CFU/mouse (actual dose = $2.3x10^3$ CFU) of H37Rv *Mtb* intranasally. We predicted that lower doses of H37Rv are likely necessary in a co-infection model as primary HIV infection may exacerbate disease and progress to endpoint earlier. An even lower intranasal dose of H37Rv ($2.5x10^2$ CFU/mouse) demonstrated successful infection using the NSG-BLT model [320], and thus we estimated that $1x10^3$ CFU/mouse is likely neither too high to induce rapid disease progression upon co-infection nor too low that *Mtb* fails to establish a productive infection in the lower respiratory tract.

Starting at 4 weeks post-*Mtb* infection, huNRG mice in both groups (especially the HIV/*Mtb* co-infected group began losing weight rapidly (Supplemental Figure 1), and thus sacrifice and experimental endpoint was planned to be 4.5 weeks post-*Mtb* infection. With 1 mouse failing to reach endpoint in the TB-only group, there are n=2 remaining in the group at experimental endpoint. CFU counts revealed that both the TB-only and co-infection group sustained very high bacterial loads (between 8 to 9 log CFU) within the lungs and high levels of *Mtb* dissemination to spleen and liver tissue with no statistically significant differences between the two groups (Figure 15). It was expected that primary HIV infection exacerbate TB pathology within the lungs and as a result increases bacterial load/burden [320]. However, we speculate that there may be two main reasons for not observing significant differences between the groups. First, both groups may have already progressed to severe pathology at experimental endpoint, and any difference in the rapidness of progression may have been missed. Another reason for the unexpected

development of substantial bacterial load despite receiving a low infection inoculum may be due to the pre-treatment of DMPA prior to HIV-1 infection. Upon post-hoc literature review, we found that studies have demonstrated a measurable negative effect of medroxyprogesterone acetate (MPA), also known as DMPA, on immune cell responses to *Mtb* containment [335,336]. DMPA can increase Treg cell activity while downregulating cytotoxic T cell activities [335]. Therefore, despite the low dose of *Mtb*, the TB-only group may have exacerbated disease progression due to the potential confounding factor of the administration of DMPA resulting in higher *Mtb* load in the lungs comparable to the co-infected group. This finding prompted us to avoid the use of DMPA in the later co-infection experiment with hu-DRAG-A2 mice by administering HIV-1 infection via intraperitoneal injection.

Tissue histology and immunohistochemistry offered more insight to disease pathology within the lung and spleen. Despite showing similar bacterial load within the lungs, H&E Staining revealed that co-infected granulomas may develop more central caseating necrosis compared to the TB-only lung granulomas (Figure 16). The co-infected granulomas displayed more features of "necrotic granulomas" where the central necrotic core (light pink and fluid-like) and *Mtb* bacilli that appeared to be uncontained by the immune cell aggregates surrounding the structure (Figure 17). Immunohistochemistry staining showed that while the granulomas of TB-only huNRGs were surrounded by a ring of hCD4+ T cells accompanied with hCD68+ macrophages scattered throughout the granuloma, both hCD4+ T cells and hCD68+ macrophages were almost completely absent throughout the lungs of

co-infected huNRG mice (Figure 18). This may be due to HIV directly depleting the T cells and macrophages, which are both target cells of HIV. Although, the depletion of hCD4+ T cells is expected as HIV infection can kill hCD4+ T cell by pyroptosis or apoptosis [337], macrophages do not typically undergo cell death as readily since they act as viral reservoirs with altered functionality [338]. For instance, functionality such as phagocytosis of alveolar macrophages can be impaired during HIV infection [339], but mechanisms that lead to either cell depletion or downregulation of hCD4 and hCD68 cell markers require further investigation. Furthermore, it is notable that hCD4+ T cell depletion within the lungs was more prominent than that in the spleen (Figure 18B & 20B). This may offer additional evidence that hCD4+ T cells are preferentially depleted within the lungs, as a recent study demonstrated rapid loss of lung interstitial CD4+ T cells in the first weeks post-HIV infection [217]. This has great implications in subsequent pulmonary opportunistic infections such as potential increased susceptibility to *Mtb* infections.

Co-infected HuNRG mice also presented with granuloma pathology consistent with humans. Granulomatous lesions showed large sections of severe karyorrhexis (the destructive fragmentation of nuclei), foamy macrophages around granulomatous tissue that harbour *Mtb* bacilli, and airway foamy macrophages that were present around the airways of severe granuloma lesions (Figure 22 & 23). Interestingly, the foamy macrophages in the airway/alveoli were not infected with *Mtb* (Figure 23B). The observation of foamy macrophages within the airways was characterized within rats [340] and other hu-mice as foamy alveolar macrophages [321]. Similar to our observations, the foamy alveolar

macrophages within the hu-mice also did not harbour *Mtb* bacilli [321]. We hypothesize that based on the fact that they were not infected with *Mtb*, they could not have migrated from the lung parenchyma or phagocytosed *Mtb* in the parenchyma and/or the airway. Therefore, these foamy alveolar macrophages may originate from alveolar macrophages that were initially uninfected but continue to reside within the airway. Upon development of severe pathology within the lungs, lipid bodies may be released into the airways which these uninfected alveolar macrophages uptake and subsequently develop more lipid vacuoles and eventually develop the foamy macrophage morphology [41,341]. Overall, these features display huNRG mice as a good hu-mouse model to recapitulate and investigate human TB and granuloma pathology.

4.2.2. HIV/*Mtb* co-infection immune responses and pathology within huDRAG-A2 mice

To investigate HIV/*Mtb* co-infection in huDRAG-A2 mice, primary HIV infection was established using intraperitoneal injection of HIV-1 to avoid the use of DMPA (Figure 5). It was evident based on the huNRG co-infection study and the literature that DMPA is likely a factor that can exacerbate *Mtb* disease progression and pathogenesis [335,336], resulting in minor differences in lung bacterial load between the co-infected and TB-only groups. Similar to the huNRG co-infection study, productive HIV infection was confirmed at 2 and 3 weeks post-HIV infection where 1 mouse in the co-infected group had low plasma HIV viral load and thus successful infection could not be confirmed. Upon low-dose $1x10^3$ CFU/mouse (actual dose = $2.3x10^3$ CFU/mouse) intranasal H37Rv *Mtb* infection, respiration was stopped in 1 of 4 huDRAG-A2 mice from the TB-only group and

the animal did not wake up from the intranasal administration. Normal protocols for intranasal infection were followed in the CL3 facility, but we have noted the sensitivity of humanized mice to anesthetics as previous problems with intranasal fluid intake and animal recovery post-isoflurane anesthesia was observed. Based on experience and observations, hu-mice appear to have weaker respiration (lower respiratory force) when compared to their non-humanized counterparts. For instance, huNRG mice would not inhale fluid boluses on the nares as well as NRG mice. During intranasal administration, liquids/fluids applied on the nares of hu-mice appear to pool as respiration slows/stops and would require adjustments to open the mouth and reintroduce respiration. BALB/c mice and non-humanized mice in our experience were capable of intaking larger volumes of fluid and respiration rarely stops when fluid is applied to the nares. We hypothesize that this may be caused by the irradiation during the humanizing process leading to damage to lung structure or cells responsible for maintaining lung surface tension resulting in weaker inspiration [342–344].

Flow cytometry analysis at 2.5 weeks post-*Mtb* infection (6 weeks post-HIV infection) showed that co-infected huDRAG-A2 mice had significantly lower frequencies of hCD4+ T cells in peripheral blood compared to the TB-only infected group (Figure 30). Since hCD4+ T cells are directly targeted and killed by HIV-1, this depletion is likely HIV-mediated and is consistent to observations in HIV/*Mtb* co-infected humans where hCD4+ T cell counts are significantly reduced compared to TB patients [202]. At the same time, co-infected huDRAG-A2 mice also had significantly higher frequencies of hCD8+ T cells

in the peripheral blood (Figure 30A). The increase in hCD8+ T cell frequency could partly be due to lower hCD4+ T cell counts leading to a higher ratio of hCD8+ T cells since the frequencies are calculated as percentages of hCD3+ T cells. However, not only are hCD4+ T cells heavily involved in the containment of TB granulomas and dissemination, hCD8+ T cells can also play an important role in disease control, especially in more chronic stages of disease [345,346]. Therefore, another explanation for a higher proportion of hCD8+ T cells may be increased involvement and recruitment to help with containment of the infection and eliminate infected cells [346]. Since hCD8+ T cells also play an important role in controlling HIV disease progression, functionality of CD8+ T cell may be another direction for future investigations in the context of both HIV and TB [347].

At 4 weeks post-*Mtb* infection (7.5 weeks post-HIV infection), both flow cytometry and immunohistochemistry of lungs also revealed significant depletion of hCD4+ T cells in co-infected hu-DRAG-A2 mice when compared to the single-TB infection group (Figure 28 & 32). This finding is consistent with another recent co-infection study using SIV/*Mtb* co-infection in rhesus macaques where co-infected animals showed rapid depletion of granuloma CD4+ T cells [348]. Although no significant differences in immune cell counts in peripheral blood were observed, it appears that the co-infected (HIV low) huDRAG-A2 mouse could be an outlier where cell counts were substantially higher than other co-infected huDRAG-A2 mice for every immune cell type. A trend of fewer total immune cells in the co-infected group may be observed if this animal (represented as a blue point) was excluded from the analysis (Figure 31). Upon approval of Containment Level 3 protocols, we will

be confirming HIV infection at later timepoints (post-*Mtb* infection) in this mouse, and quantify the HIV plasma viral load in all mice within the experiment to determine if co-infection affects levels of HIV-1 in the plasma. It is also notable that the co-infected (HIV low) huDRAG-A2 mouse reconstituted with extremely high human immune cell counts pre-experiment (Supplementary Table 3).

In addition to hCD4+ T cell depletion within the lungs and blood, co-infected huDRAG-A2 mice also developed significantly higher lung bacterial burden and extrapulmonary dissemination into spleen and liver (Figure 25); a potential trend of more granulomatous tissue with more caseating necrosis in the lungs was also observed when compared to the TB-only group (Figure 26). Additionally, granulomas in co-infected mice harbour an abundance of foamy macrophages that were infected with *Mtb* bacilli, while only the largest granuloma found within TB-only mice contained foamy macrophages (Figure 27, & 34). Interestingly, co-infected granulomas in huDRAG-A2 mice also formed small cavities within necrotic regions with severe karyorrhexis and around foamy macrophages (Figure 33). We hypothesize that the necrotic foamy macrophages release extensive amounts of lipid bodies and create a pocket/space of lipids, and upon the dissolution of these lipid pockets, the small cavities remain [349,350]. This is based on the observations in Figure 33 that foamy macrophages have a distinct nucleus and lipid filled vacuoles, while some of the pockets do not have a nucleus with just lipid vacuoles/bubbles, and other pockets only contains a dark nucleus [41,351–353]. Furthermore, we hypothesize that as TB disease progresses, many more of these small pocket cavities will develop and eventually

contribute to the formation of large cavitation within the granulomas [354]. This can contribute to bacterial dissemination and release of *Mtb* bacilli into the airspace and subsequent transmission of *Mtb* to other individuals [62,352]. It is also notable that these foamy macrophages harbour a high concentration of *Mtb* bacilli when observed at a lower magnification Figure 34. This indicates foamy macrophages may be a large pool of *Mtb* reservoir especially during chronic infection [341]. Finally, bronchial occlusion was also observed within the lungs of a HIV/*Mtb* co-infected huDRAG-A2 mouse at 4 weeks post-*Mtb* infection (Supplementary figure 3). This is consistent with the bronchial occlusion/obstruction observed in a huNSG-BLT model at 5 weeks post-*Mtb* infection in co-infected huNSG-BLT mice [320], and approximately 7 weeks post-infection in *Mtb*-only infected huNSG-BLT mice [316]. Since bronchial occlusion can be considered more severe/advanced lung pathology as it is only observed at 7 weeks post-infection in *Mtb*-only infected hu-mice [316], the observation of bronchial occlusion in our co-infected hu-mice 4 weeks post-*Mtb* infection may also demonstrate more rapidly exacerbated lung pathology. Overall, these features illustrates the ability for both the huNRG and huDRAG-A2 models to recapitulate advanced TB pathology.

HuDRAG-A2 mice developed heterogenous granulomas upon *Mtb* infection and may provide some additional insight specifically into granuloma formation and development. These observations were made in Figure 35 where potential stages of granuloma formations were illustrated and hypothesized. These images were all obtained from the *Mtb*-only group of huDRAG-A2 mice. 4 week after low dose *Mtb*-infection, innate (or early stage)

granulomas can be seen where an initial aggregation of immune cells, in particular hCD68+ macrophages and some hCD4+ T cells infiltrate the local region to contain the infection. Macrophages were concentrated at the very center of the granuloma structure while hCD4+ T cells are more frequent in the granuloma periphery (Figure 35G & J). In this early stage granuloma, *Mtb* bacilli appear to be very well contained within the structure. The next stage of granuloma observed may be considered and termed the "immune" granuloma due to the prolific recruitment of adaptive immune cells [45]. Notable differences include the significant hCD4+ T cell recruitment to the granuloma structure and the formation of an organized halo/ring around the granuloma (Figure 35H). In this particular granuloma, hCD68+ macrophages appear to be less involved in the containment of *Mtb* as they are more scattered in the granuloma periphery (Figure 35K). This may indicate that further cell differentiation has already occurred due to *Mtb* infection, or that the hCD68 markers were downregulated in the granuloma specifically, since hCD68+ macrophages were still present and scattered throughout the rest of the lung. With a depletion of classical hCD68+ macrophages, this may mark the beginning of more severely pathological granulomas developing. In the late-stage granuloma (or termed here: the disseminated granuloma), development of foamy macrophages occurs and the structure fails to contain *Mtb* bacilli, as *Mtb* can be identified outside of the poorly-formed granuloma structure (Figure 35C). Interestingly, foamy alveolar macrophages can also be identified in the airway near the periphery of the granuloma structure. This further supports the aforementioned hypothesis that alveolar macrophages may be phagocytosing lipid body secretions that are released into the airway from granuloma lesions and eventually become foamy alveolar

macrophages. In the late-stage granuloma the organization of hCD4+ T cells surrounding the granuloma was also lost, and hCD68+ macrophages are no longer concentrated within the granuloma (Figure 35I & L) [348]. Furthermore, neither the foamy macrophages within the granulomas nor the foamy alveolar macrophages within the airway express hCD68 (Figure 35L). This illustrates that hCD68 is not the ideal marker to identify foamy macrophages, and other markers such as CD36 (scavenger receptor), CD163 (scavenger and M2-activation marker), or CD205 (DC-associated marker), may be better surface markers to help with identification and quantification of these highly differentiated cells [355–357]. In particular, CD205 may be useful for identifying *Mtb*-infected foamy macrophages, while alternatively-activated CD163+ macrophages may be induced/polarized by HIV-1 [357,358]. Therefore, identification of these marker may also provide more insight on HIV and *Mtb* host-pathogen interactions *in vivo*. A limitation to the data thus far is the fact that the potential contributions of any remaining poorly-functioning mouse macrophages along with other human cell subtypes have not been characterized. In future investigations, we will be using the Multiplexed Ion Beam Imager (MIBI) Scope to identify and better characterize the cells involved in granuloma formation.

Chapter 4.3. Elucidating the immunogenicity of adeno-vectored TB vaccines in huNRG and huDRAG-A2 mice.

Currently, the only approved vaccine against TB is the BCG vaccine. However, the efficacy of BCG vaccination has been demonstrated mostly for early childhood protection where older children and adults are still largely unprotected and it is rarely used in PLWH [359]. HIV/*Mtb* co-infection further complicates matters in studying efficacy and in elucidating immune responses to TB vaccination. In the clinical setting, PLWH may require different vaccination strategies that are both safe and effective given their immunocompromised status, and yet they are usually not included in TB vaccine clinical trials even though they are one of the most vulnerable groups to this disease [360]. The development of vaccines from basic science and through the clinical phase trials requires extensive funding, time, and resources. Therefore, establishing a pre-clinical *in vivo* model to investigate human immune cell responses to TB vaccines in those with and without HIV is a critical step to advancing the development of effective vaccines for TB infection, especially for PLWH. The Xing lab at McMaster University (Hamilton, ON) has made considerable progress in the development of adenoviral-vectored TB vaccines. A successful phase one clinical trial of the human type 5 adenovirus expressing Ag85A (an immune dominant *Mtb* antigen) (AdHu5Ag85A) demonstrated safety and immunogenicity as primary and booster vaccinations against *Mtb* infection [102,103]. AdHu5Ag85A was also administered in humanized mice showing protection against TB and improved pathogen-specific T cell responses [104]. Moreover, the development of a novel chimpanzee based AdCh68Ag85A expressing the same antigen showed enhanced immunogenicity and efficacy, especially following respiratory mucosal (intranasal) administration when compared to their human adeno-vector counterpart [105,106]. These findings illustrate the potential of using

humanized mice to further elucidate the generation of antigen-specific T cell responses *in vivo* for the more immunogenic chimpanzee-based AdCh68Ag85A vaccine (unpublished data, Dr. Zhou Xing Lab).

In this project, we demonstrated that the AdCh68Ag85A vaccine may be capable of generating T cell IL-2 responses to *Mtb*-antigens in huNRG mice upon stimulation with live BCG (Figure 37). Lung and spleen cells stimulated for 24 hours non-specifically by PMA/Ionomycin also showed that the human CD4+ and CD8+ T cells in huNRG mice were polyfunctional and able to produce human pro-inflammatory cytokines such as IFN-γ, IL-2, and TNF-α (Figure 36). This also served as a positive control for the methods/protocol of our T cell stimulation experiment, and indicated that the protocol was functional. Therefore, our observation that the Ag85A peptide pool (1-57) stimulation condition did not generate antigen-specific responses is likely due to factors other than errors within the stimulation protocol. For instance, 24 hour stimulation may be an insufficient amount of time for the antigen presenting cells (APCs) to process and present antigens from the specific Ag85A peptide pool (1-57) to activate enough T cells to observe differences. Additionally, we observed from this experiment that the 24-hour stimulation with PMA/Ionomycin caused extensive cell death, and the stimulation timepoint may be further optimized for future experiments if non-specific responses are an outcome for the study. A later optimization experiment showed that 6 hours of PMA/Ionomycin stimulation is able to reduce cell death and increase T cell frequencies while still maintaining high levels of cytokine production (Supplementary figure 5). Therefore, it can be concluded that

time points between 6 to 24 hours can be used for PMA/Ionomycin stimulation, but timepoints closer to 6 hours can improve cell viability if desired, especially when direct comparisons are to be made with the PMA/Ionomycin stimulation condition. Although larger samples sizes will be required to make further conclusions from the AdCh68Ag85A pilot study, this study has still greatly informed the methods and protocols for one of the main aims of this project; to investigate immunogenicity of an even more novel adenoviral-vector based trivalent vaccine AdCh68MV.

The AdCh68MV vaccine (also known as AdCh68Ag85A:rpfB:TB10.4) is another chimpanzee adenovirus 68-vectored TB vaccine constructed to express three different *Mtb* antigens (Ag85A, rpfB, and TB10.4). This vaccine was designed by the Xing Lab (McMaster University, Hamilton, ON) and takes into consideration many of the ideal features within a vaccine platform (as discussed in Chapter 1.1.6.). RpfB is a protein involved in resuscitating *Mtb* from dormancy associated with chronic infection, while TB10.4 is a *Mtb* virulence factor mostly associated with early/acute infection [318,361,362]. These additional antigens are added with the goal of targeting the different life-stages that *Mtb* can undergo *in vivo*, and thus provide a more comprehensive repertoire of targets when immune cells are primed [363]. As a result, this strategy may be the key to inducing longer-lasting immune memory after vaccination.

To investigate the immunogenicity of AdCh68MV, both huNRG (n=3) and huDRAG-A2 (n=3) mice were vaccinated with $1x10^7$ PFU via intranasal administration. 4 weeks post-

infection, lung and spleen cells were processed and stimulated with 5 different conditions (Unstimulated, whole protein pool, BCG, cell filtrate/crude BCG, and PMA/Ionomycin) (Figure 7). Multiple antigen-stimulation conditions were tested to determine what the best condition would be to induce human immune cell responses from a humanized mouse model. Based on the results in Figure 38, culture filtrate in combination with crude BCG (CFCB) was the only condition that consistently produced appreciable antigen-specific cytokine responses within both the lung and spleen. Therefore, cytokine responses were further examined in samples stimulated by CFCB, and this condition should be considered for use in future *in vitro* stimulation experiments. Upon CFCB antigen-stimulation, hCD4+ T cells in both lung and spleen of vaccinated huNRG and huDRAG-A2 mice demonstrated trends of higher frequencies and total numbers of cells with the ability to produce *Mtb* antigen-specific TNF-α responses (Figure 39 & 40). Albeit responses produced by hCD8+ T cells demonstrated similar trends within both the lung and spleen of vaccinated huNRG and huDRAG-A2 mice, there are fewer total numbers of cytokine producing hCD8+ T cells in both tissues (Figure 39B, D & Figure 40B, D). This is expected as similar results were seen after mucosal administration of the AdHu5Ag85A in huNRG mice showed higher number of responding hCD4+ T cells [104]. In both lung and spleen, antigen-specific IFN-γ responses appear to be inconsistent as hCD8+ T cells in unvaccinated hu-mice also produced substantial levels of IFN-γ upon antigen-stimulation (Figure 40C, D). On the other hand, little to no IFN-γ responses were generate by hCD4+ T cells in both vaccinated and unvaccinated groups within the spleen (Figure 40A, B). A limitation to our humanized mouse model may be the relatively low human myeloid populations which are largely

APCs within huNRG and huDRAG-A2 [364,365]. Given low numbers of APCs to process and present *Mtb* antigens to the T cells of interest, both number of cells and amount of time for antigen presentation may be insufficient to generate T cell responses to show significant differences between groups in different conditions. Finally, it is notable that despite relatively lower antigen-specific responses, hCD4+ and huCD8+ T cells in the lungs of both huNRG and huDRAG-A2 mice were polyfunctional upon non-specific PMA/ionomycin stimulation as high levels of at least 2 of IFN-γ, IL-2, and TNF-α were produced (Supplementary figure 6).

All stimulation conditions were supplemented with human CD28 and CD49d co-stimulatory antibodies which assists in the activation of T cells in this model due to the low numbers of APCs [104]. However, the antibodies used in our experiments were different clones than those used by Yao et al. 2017 and may yield differences in co-stimulation. This was tested in the spleen within the CFCB condition supplemented with the in-lab antibodies compared to CFCB supplemented by antibodies used by Yao et al. 2017 (termed Y-CFCB condition). No notable differences were observed other than in the total counts of IFN-γ producing hCD8+ T cells where non-specific stimulation may have been reduced in the Y-CFCB condition (as unvaccinated mice did not produce significant cytokine responses) (Figure 41D). Overall, no significant concluded could be made from this test as larger sample sizes will be required for confirmation of any differences that may warrant the change in the use of Y-CFCB rather than CFCB supplemented with in-lab co-stimulatory antibodies.

Chapter 5. CONCLUSIONS & FUTURE DIRECTIONS

In this project, we have established the huNRG, huNSG-hIL15, and huDRAG-A2 models that are capable of producing substantial numbers of human immune cell populations for infectious diseases research. The next generation huNSG-hIL15 mice developed significantly higher levels of human CD56+CD3- NK cells at 16 week post-engraftment compared to the current generation huNRG mice. While the next-generation huDRAGA2 mice reconstituted with higher total numbers of hCD4+ T cells, hCD19+ B cells, and monocytes at 12 weeks post-engraftment compared to the current generation huNRG mice. Additionally, the huDRAGA2 mice were also capable of producing functional Th17 cells upon stimulation. In future experiments, huNSG-hIL15 mice will be compared to better controls (huNSG mice rather than huNRG mice) where further NK cell functionality testing would also be investigated using cytotoxicity assays.

After successfully establishing HIV and *Mtb* infections alone, it was evident that both huNRG and huDRAGA2 mice were able to recapitulate hallmark pathological feature of HIV and TB disease and thus allowed for the models to be used for HIV/*Mtb* co-infection studies. In huNRG mice, both co-infected and *Mtb*-only infected mice showed severe TB pathology and high bacterial burden in the lungs along with high bacterial dissemination into spleen and liver at 4.5 weeks post-*Mtb* infection. Although co-infected huNRG mice may show trends of higher lung pathology and spleen bacterial load, the negative effects of

DMPA on immune cell control of *Mtb* may have exacerbated disease progression in both groups confounding any differences observed between the groups. However, immunohistochemistry showed notable depletion of hCD4+ T cells within co-infected huNRG lungs, likely due to HIV killing the cells and/or downregulating hCD4 markers and function. Co-infected huNRG mice also presented various human-like pathology characteristics such as the development of necrotic cores with severe karyorrhexis and *Mtb*-infected foamy macrophages in granulomatous tissue, as well as multinucleated giant cells within the spleen. After generating more huNRG mice, a future co-infection experiment in huNRG mice could be repeated where primary HIV-1 infection is established with intraperitoneal infection (rather than intravaginal infection) to avoid the use of DMPA.

HIV/*Mtb* co-infection in huDRAG-A2 mice resulted in significantly higher bacterial burden within the lungs and increased extrapulmonary dissemination into spleen and liver when compared to *Mtb*-only infected huDRAG-A2 mice. HIV/*Mtb* co-infection also led to a trend of greater total areas of granulomatous lesions within the lungs along with significantly depleted frequencies of hCD4+ T cells at the 4 week experimental endpoint post-*Mtb* infection. Frequencies of hCD4+ T cells in peripheral blood was already significantly lower in the co-infected group at 2.5 weeks post-*Mtb* infection likely due to HIV-1 depletion, while hCD8+ T cell frequencies were significantly higher. Co-infected huDRAG-A2 mice also recapitulated many aspects of human-like pathology within the lungs such as displaying severe necrosis with foamy macrophages undergoing lipid dissolution. These foamy macrophages were highly concentrated with *Mtb* bacilli and may

be large source of *Mtb* bacterial reservoir during later stages of infection. Moreover, low dose intranasal *Mtb* infection was able to generate heterogenous granulomas in both *Mtb*-only and co-infected huDRAG-A2 mice. These observations have led to our hypotheses of possible appearances, structures, and pathologies within granulomas at different stages of granuloma development illustrated by histology and immunohistochemistry images. Finally, other human-like features of pathology such as bronchial obstruction and foamy alveolar macrophages within the airway was also observed within the lungs of both co-infected huNRG and huDRAG-A2 mice.

Results from our vaccine immunogenicity studies showed that both huNRG and huDRAG-A2 mice are capable of producing polyfunctional hCD4+ and hCD8+ T cells. Mice immunized mucosally with the trivalent AdCh68MV vaccine showed trends of higher *Mtb* antigen-specific hCD4+ T cell responses in the lungs and spleen, where culture filtrate with crude BCG appeared to be the best stimulation condition. Some trends of increased antigen-specific hCD8+ T cell responses were also observed in immunized mice, but require larger sample sizes to confirm these trends.

One main step beyond this project will be staining and scanning tissues from both the huNRG and huDRAG-A2 co-infection studies using the Multiplexed Ion Beam Imager Scope (MIBIScope) to better visualize characterize lung pathology, granuloma structure, and immune cell composition within granulomas. Since the MIBI scope technology is capable of multicolor viewing of over 40 different markers simultaneously, a much more

detailed visualization of whole lung sections and granuloma lesions is possible. Changes associated with HIV co-infection such as phenotypic expression, cell types/differentiation, and cellular interactions can be observed. For instance, despite the lack of two major cell types (hCD4+ T cells and hCD68+ macrophages) that form classical granulomas in the co-infected huNRG and huDRAG-A2 mice, the granuloma structures were still present. The clearer imaging would provide insight on other cell types (alveolar and interstitial macrophages, giant cells, dendritic cells, NK cells, neutrophils, etc.) that may be contributing to the structure formation/maintenance and potentially also leftover non-functional mouse immune cells such as macrophages.

Upon validation of containment level 3 protocols and procedures, plasma HIV-1 viral load in co-infected huNRG and huDRAG-A2 mice will be quantified using RT-qPCR and correlated with *Mtb* bacterial load and disease severity. Cytokine analysis can be performed on plasma samples collected at the same time points for further insight on systemic immune responses during co-infection compared to *Mtb*-single infection. Once more hu-mice are generated, additional groups for the co-infection study can be supplemented such as a group infected with HIV-only collecting samples at identical timepoints to be compared to the co-infected group.

The immunogenicity of the trivalent AdCh68MV vaccine in huNRG and huDRAG-A2 mice show potential in the vaccine inducting protection against *Mtb* infection. A vaccine protection study immunizing huNRG mice with AdCh68MV has been completed and is

currently awaiting results. This data would not only provide insight on the efficacy of AdCh68MV in *Mtb* protection, but also further illustrate hu-mice as potential strong candidates for pre-clinical testing of vaccines and therapeutics.

Long term future directions from this project include investigations in granuloma microenvironments during HIV/*Mtb* co-infection. Transcriptomic analyses of heavily involved immune cells such as T cells and macrophages may help with fully elucidating specific mechanisms and pathways of immune responses during co-infection. Furthermore other models may be developed using our current and next-generation hu-mice such as modelling ART-controlled HIV-infection (common clinical presentations of PLWH) prior to TB immunization to determine safety and efficacy of a vaccine within a more clinically representative scenario *in vivo*. Finally, the scenario in HIV/*Mtb* co-infection where the host is initially infected with *Mtb* and is subsequently exposed to HIV is also a viable future step for investigation following similar experimental techniques and methodologies as described in this project. Overall, the utility of both huNRG and huDRAG-A2 mice can extend beyond the *in vivo* investigation of HIV and/or TB, as these models may also be suitable for widespread use in other infectious disease, cancer, and other long term/chronic human disease studies.

Chapter 6. SUPPLEMENTAL MATERIALS:

Supplementary Table 1.
Cord blood samples used for humanizing NRG and DRAG-A2 mice, and success rate of humanization given intrahepatic newborn and intravenous adult HSC-engraftment methods.

Cord blood sample #	1	7	9	2	3	4	5	6	8
HLA type	DR4+A2+	DR4+A2+	DR4+A2+	DR4–A2–	DR4–A2–	DR4–A2–	DR4–A2–	DR4–A2–	DR4–A2–
Mouse strain engrafted	DRAG-A2	DRAG-A2	DRAG-A2	NRG	NRG	NRG	NRG	NRG	NRG
Engraftment Method	IH, newborn	IV, adult	IV, adult	IH, newborn	IH, newborn	IH, newborn	IH, newborn	IH, newborn	IH, newborn
Success rate	6/6 (100%)	10/21 (47.6%)	9/18 (50%)	9/9 (100%)	4/8 (50%)	9/9 (100%)	3/7 (42.8%)	6/7 (85.7%)	11/12 (91.7%)

Supplementary Table 2.
Pre-experiment engraftment for huNRG used in the HIV/*Mtb* co-infection experiment. *Co-infected (HIV low). All huNRG mice used were female.

Baseline (Pre-Experiment)													
	Mouse ID	%hCD45	#hCD45 /mL	%hCD3	#hCD3 /mL	%hCD4	#hCD4 /mL	%hCD8	#hCD8 /mL	%hCD19	#hCD19 /mL	%hCD14	#hCD14 /mL
Mtb only N=2	TB-N1	2.73	11,040	98.20	10,841	60.50	6,559	31.40	3,404	2.50	280	0.00	-
	TB-N2	48.03	122,720	53.70	65,901	43.30	28,535	44.30	29,194	40.80	50,070	2.97	3,645
	Average	**25.38**	**66,880**	**75.95**	**38,371**	**51.90**	**17,547**	**37.85**	**16,299**	**21.65**	**25,175**	**1.49**	**1,823**
HIV/*Mtb* Co-infected N=4	HTB-N1	16.88	32,800	68.00	22,304	67.90	15,144	23.30	5,197	25.20	8,266	4.27	1,401
	HTB-N2*	63.49	151,560	52.10	78,963	66.80	52,747	25.00	19,741	45.00	68,202	1.29	1,955
	HTB-N3	18.14	16,480	95.90	15,804	72.20	11,411	22.30	3,524	1.20	199	0.00	-
	HTB-N4	8.22	23,240	79.90	18,569	49.80	9,247	43.80	8,133	14.30	3,323	0.52	121
	Average	**26.68**	**56,020**	**73.98**	**33,910**	**64.18**	**22,137**	**28.60**	**9,149**	**21.43**	**19,998**	**1.52**	**869**

Supplementary Table 3.
Pre-experiment engraftment for huDRAG-A2 used in the HIV/*Mtb* co-infection experiment. *Co-infected (HIV low). All huDRAG-A2 mice used were female.

Baseline (Pre-Experiment)													
	Mouse ID	%hCD45	#hCD45 /mL	%hCD3	#hCD3 /mL	%hCD4	#hCD4 /mL	%hCD8	#hCD8 /mL	%hCD19	#hCD19 /mL	%hCD14	#hCD14 /mL
Mtb only N=3	TB-D1	3.03	42,640	31.50	13,440	60.10	8,080	28.00	3,760	6.38	2,720	66.40	28,320
	TB-D2	46.00	380,000	57.60	218,800	82.50	180,600	4.62	10,100	0.26	1,000	10.50	39,800
	TB-D4	10.00	34,900	26.60	9,300	60.20	5,600	26.90	2,500	3.72	1,300	69.60	24,300
	Average	**19.68**	**152,513**	**38.57**	**80,513**	**67.60**	**64,760**	**19.84**	**5,453**	**3.45**	**1,673**	**48.83**	**30,807**
HIV/*Mtb* Co-infected N=3	HTB-D1*	8.14	49,360	25.00	12,320	60.40	7,440	27.30	3,360	6.00	2,960	77.10	38,080
	HTB-D2	13.70	56,160	17.20	9,680	57.00	5,520	26.40	2,560	4.84	2,720	76.20	42,800
	HTB-D3	14.40	60,600	64.70	39,200	56.60	22,200	36.20	14,200	3.96	2,400	48.50	29,400
	Average	**12.08**	**55,373**	**35.63**	**20,400**	**58.00**	**11,720**	**29.97**	**6,707**	**4.93**	**2,693**	**67.27**	**36,760**

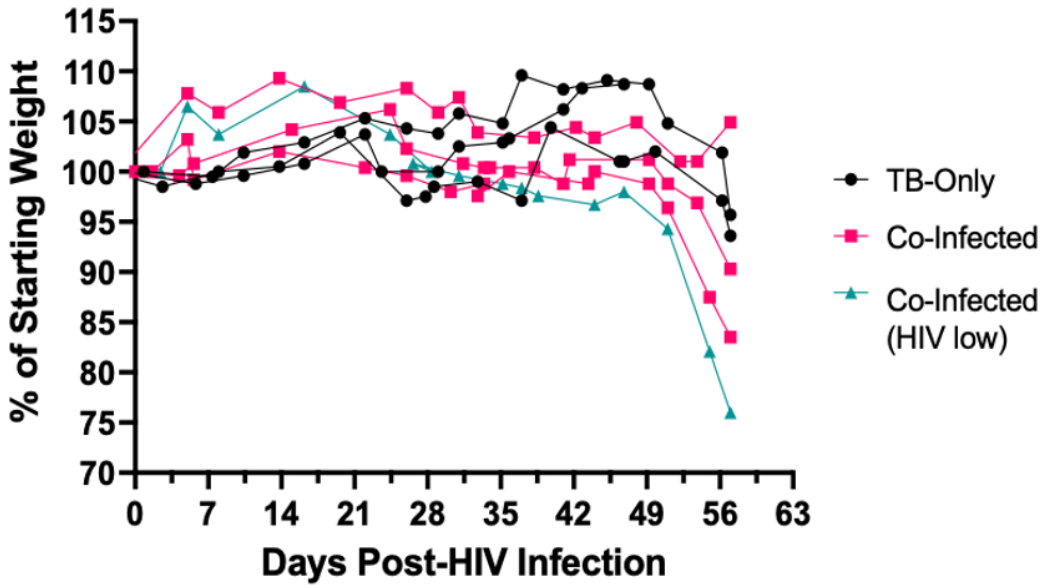

Supplementary Figure 1. Weight loss in huNRG mice infected with *Mtb*-only and co-infected with HIV and *Mtb*.

Individual weights of huNRG mice are plotted as percent of initial starting weight (on the day of HIV-1 infection).

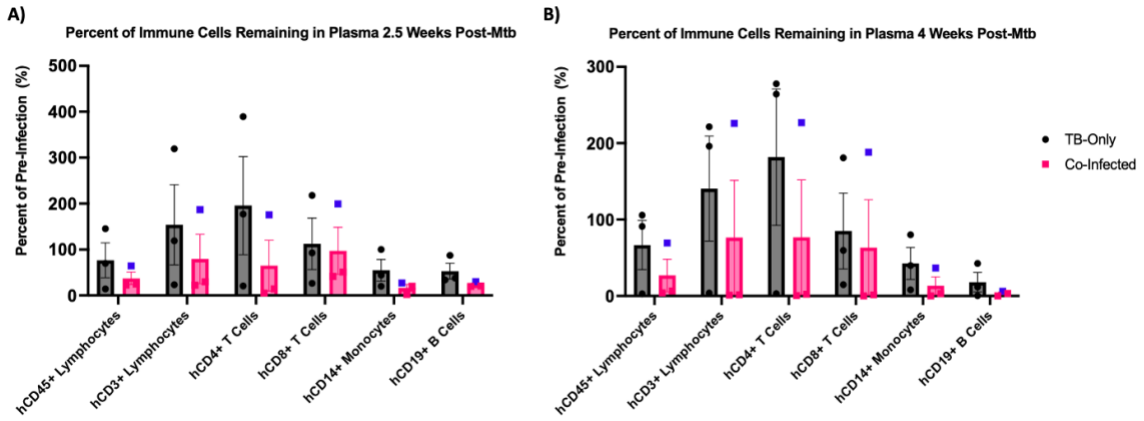

Supplementary Figure 2. Human immune cells remaining in *Mtb*-only and co-infected huDRAG-A2 mice at 2.5 weeks and 4 weeks post-*Mtb* infection.

Percent of human immune cells remaining within peripheral blood at **(A)** 2.5 weeks post-*Mtb* infection and **(B)** 4 weeks post-*Mtb* infection (experimental endpoint). Percentage calculated by dividing total numbers of cells/mL of peripheral blood at 2.5 or 4 weeks post-*Mtb* infection by total numbers of cells/mL pre-experiment. TB-Only (n=3) and Co-infected (n=3). Blue data points represent co-infected huDRAGA2 mouse with low HIV viral load pre-*Mtb* infection. Data are expressed as mean +/- SEM.

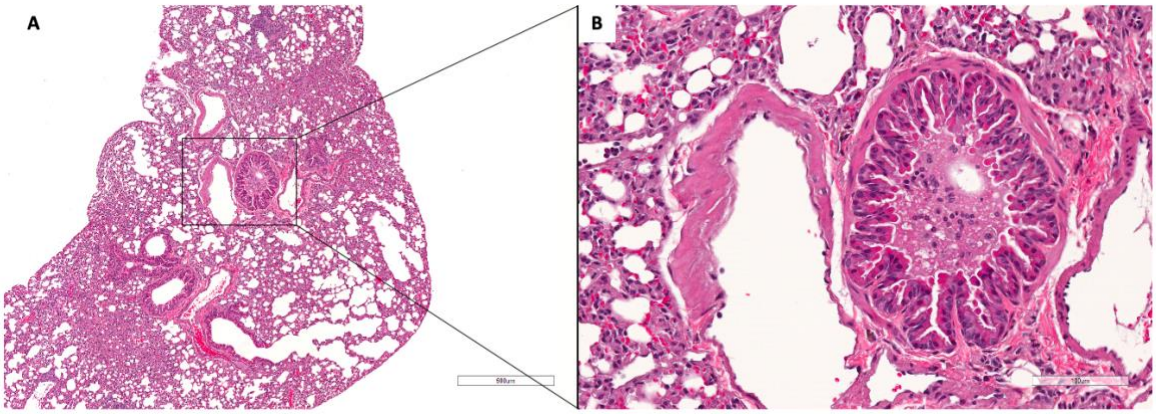

Supplementary Figure 3. Bronchial occlusion in the lungs of co-infected huDRAG-A2 mouse at 4 weeks post-*Mtb* infection.

(A) H&E stain visualizing bronchial occlusion in co-infected huDRAG-A2 lung at 4x magnification, and **(B)** at 20x magnification (n=1).

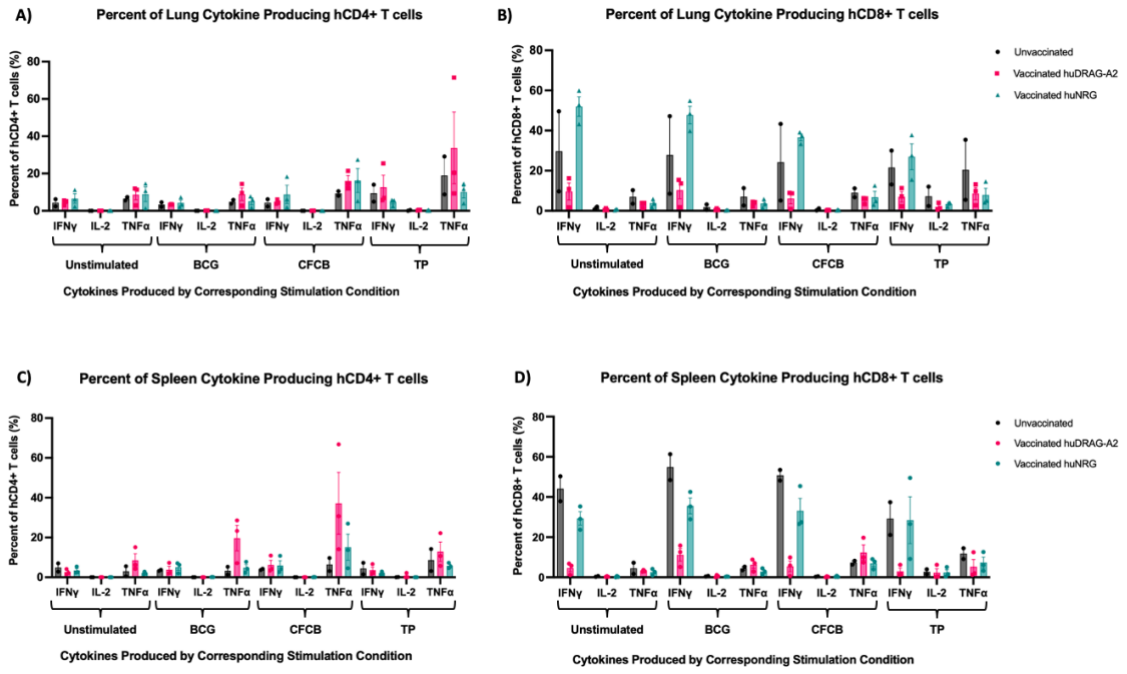

Supplementary Figure 4. Percent of hCD4+ and hCD8+ T cell cytokine production under different stimulations conditions.

Percent of cytokine producing hCD4+ T cells after stimulation in **(A)** lung and **(C)** spleen for 24 hours. Percent of cytokine producing hCD8+ T cells in **(B)** lung and **(D)** spleen. Unstimulated = Unstimulated control condition; BCG = Bacillus Calmette–Guérin; CFCB = Culture filtrate and crude BCG; TP = Trivalent Protein Pool (Ag85A, rpfB, and TB10.4 whole protein). Unvaccinated group (huNRG n=1, huDRAG-A2 n=1); vaccinated huDRAG-A2 group n=3; vaccinated huNRG group n=3. Data are expressed as mean +/- SEM. Note: percent of cytokine producing cells in unstimulated conditions were not subtracted from percent of cytokines produced by stimulated conditions.

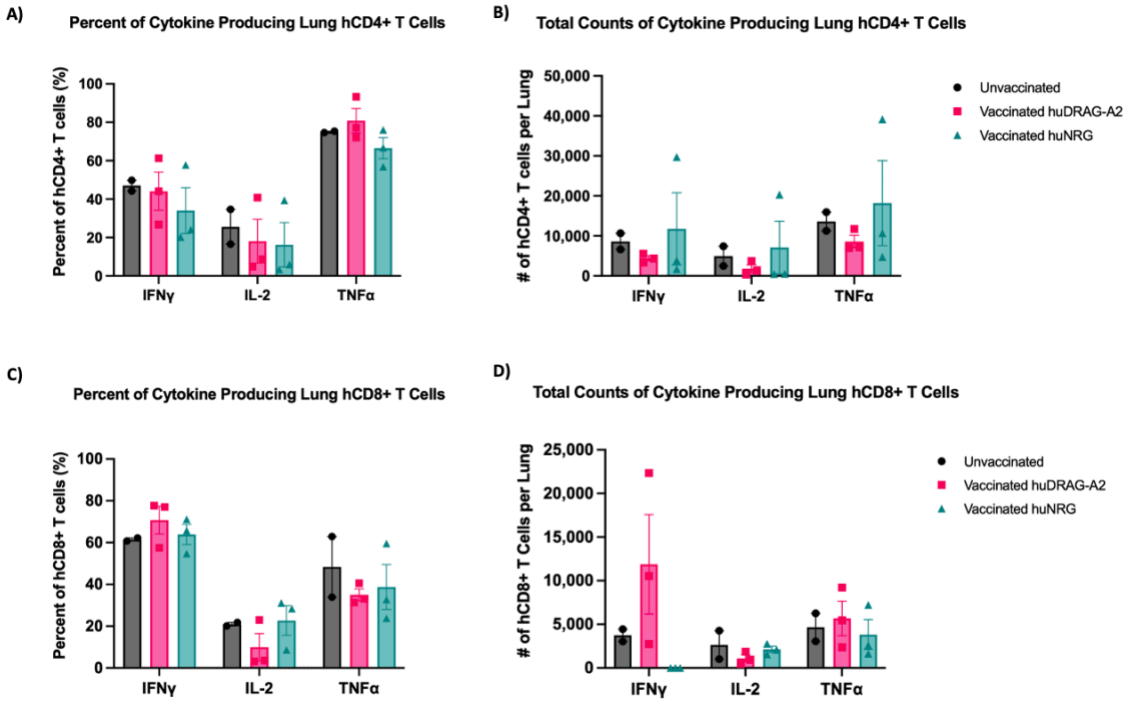

Supplementary Figure 5. Human CD4+ and CD8+ T cells are polyfunctional upon 6-hour PMA/Ionomycin stimulation.

Percent of lung **(A)** hCD4+ T cells and **(C)** hCD8+ T cells that produce pro-inflammatory cytokines after PMA/Ionomycin stimulation for 6 hours. Total number of cytokine producing **(B)** hCD4+ T cells and **(D)** hCD8+ T cells in whole lung where the number of cells producing cytokines in the unstimulated condition were subtracted from PMA/Ionomycin stimulated cells (to remove non-specifically stimulated cells in each condition). Unvaccinated group (huNRG n=1, huDRAG-A2 n=1); vaccinated huDRAG-A2 group n=3; vaccinated huNRG group n=3. Data are expressed as mean +/- SEM. Note: percent of cytokine producing cells in unstimulated conditions were not subtracted from percent of cytokines produced by stimulated conditions.

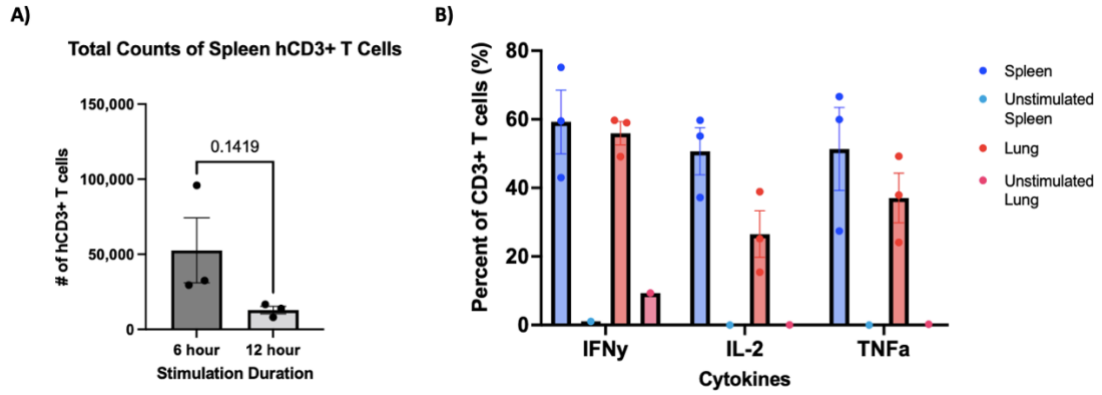

Supplementary Figure 6. Comparing *in vitro* stimulation of PMA/Ionomycin for 6 hours versus 12 hours.

(A) PMA/Ionomycin stimulation for 6 hours show a trend of higher hCD3+ T cell viability in spleen than stimulation for 12 hours in huNRG mice (n=3). **(B)** High percentages of T cells still produce pro-inflammatory cytokines after stimulation with PMA/Ionomycin for 6 hours within huNRG lung and spleen. Data are expressed as mean +/- SEM.

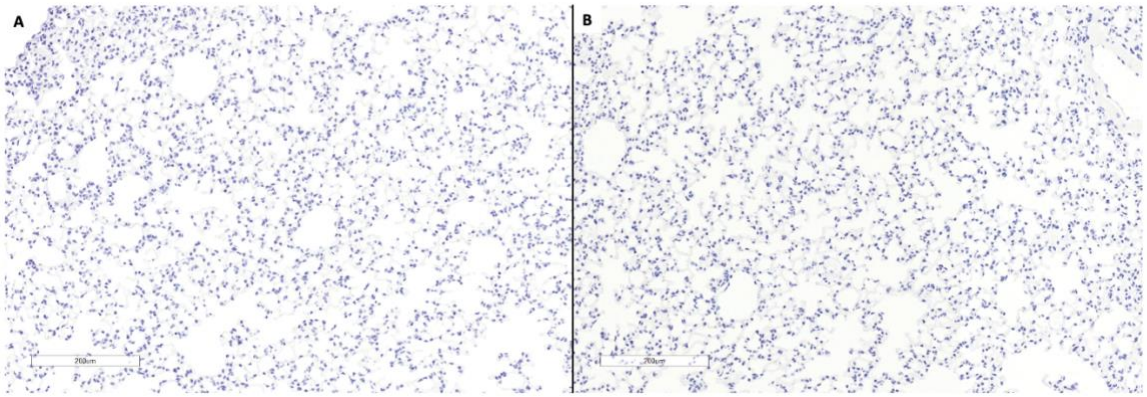

Supplementary Figure 7. Immunohistochemistry of non-humanized mouse negative control.

Non-humanized NRG mouse lung **(A)** hCD4+ and **(B)** hCD68+ IHC negative controls at 10x magnification; both hCD4 and hCD68 are stained brown.

Chapter 7. REFERENCES

1. Houben, R.M.G.J.; Dodd, P.J. The Global Burden of Latent Tuberculosis Infection: A Re-Estimation Using Mathematical Modelling. *PLOS Med.* **2016**, *13*, e1002152, doi:10.1371/journal.pmed.1002152.
2. World Health Organization (Global Tuberculosis Programme) *Global Tuberculosis Report 2020*; 2020;
3. Barter, D.M.; Agboola, S.O.; Murray, M.B.; Bärnighausen, T. Tuberculosis and Poverty: The Contribution of Patient Costs in Sub-Saharan Africa - A Systematic Review. *BMC Public Health* **2012**, *12*, 1–21, doi:10.1186/1471-2458-12-980/TABLES/8.
4. Chen, X.; Wang, W.; Wang, X.; Chai, C.; Liu, K.; Peng, Y.; Wang, F.; Chen, B.; Jiang, J. Public Awareness of Tuberculosis in Southeast China: A Population-Based Study. *Int. J. Environ. Res. Public Health* **2019**, *16*, doi:10.3390/IJERPH16214290.
5. Zhang, R.; Li, Y.; Yu, H.; Wei, Y.; Hu, Y.; Zhao, D.; Li, J.; He, L. An Analysis of Public Awareness of Core Information on Tuberculosis in Guizhou Province. *Ann. Palliat. Med.* **2021**, *10*, 33339–33339, doi:10.21037/APM-20-2473.
6. Naidoo, P.; Simbayi, L.; Labadarios, D.; Ntsepe, Y.; Bikitsha, N.; Khan, G.; Sewpaul, R.; Moyo, S.; Rehle, T. Predictors of Knowledge about Tuberculosis: Results from SANHANES I, a National, Cross-Sectional Household Survey in South Africa. *BMC Public Health* **2016**, *16*, 1–12, doi:10.1186/S12889-016-2951-Y/TABLES/4.
7. Seung, K.J.; Keshavjee, S.; Rich, M.L. Multidrug-Resistant Tuberculosis and Extensively Drug-Resistant Tuberculosis. *Cold Spring Harb. Perspect. Med.* **2015**, *5*, doi:10.1101/CSHPERSPECT.A017863.
8. Soeroto, A.Y.; Pratiwi, C.; Santoso, P.; Lestari, B.W. Factors Affecting Outcome of Longer Regimen Multidrug-Resistant Tuberculosis Treatment in West Java Indonesia: A Retrospective Cohort Study. *PLoS One* **2021**, *16*, doi:10.1371/JOURNAL.PONE.0246284.
9. WHO Tuberculosis Fact Sheet Available online: https://www.who.int/news-room/fact-sheets/detail/tuberculosis (accessed on 23 April 2022).
10. Vynnycky, E.; Fine, P.E.M. Lifetime Risks, Incubation Period, and Serial Interval of Tuberculosis. *Am. J. Epidemiol.* **2000**, *152*, 247–263, doi:10.1093/AJE/152.3.247.
11. Behr, M.A.; Kaufmann, E.; Duffin, J.; Edelstein, P.H.; Ramakrishnan, L. Latent Tuberculosis: Two Centuries of Confusion. *Am. J. Respir. Crit. Care Med.* **2021**, *204*, 142–148, doi:10.1164/RCCM.202011-

4239PP/SUPPL_FILE/DISCLOSURES.PDF.

12. Emery, J.C.; Richards, A.S.; Dale, K.D.; McQuaid, C.F.; White, R.G.; Denholm, J.T.; Houben, R.M.G.J. Self-Clearance of Mycobacterium Tuberculosis Infection: Implications for Lifetime Risk and Population at-Risk of Tuberculosis Disease. *Proc. R. Soc. B Biol. Sci.* **2021**, *288*, doi:10.1098/RSPB.2020.1635.
13. Behr, M.A.; Edelstein, P.H.; Ramakrishnan, L. Is Mycobacterium Tuberculosis Infection Life Long? *BMJ* **2019**, *367*, doi:10.1136/BMJ.L5770.
14. Pai, M.; Behr, M.A.; Dowdy, D.; Dheda, K.; Divangahi, M.; Boehme, C.C.; Ginsberg, A.; Swaminathan, S.; Spigelman, M.; Getahun, H.; et al. Tuberculosis. *Nat. Rev. Dis. Prim.* 2016, *2*, 1–23.
15. Lienhardt, C. From Exposure to Disease: The Role of Environmental Factors in Susceptibility to and Development of Tuberculosis. **2001**, *23*.
16. Beggs, C.B.; Noakes, C.J.; Sleigh, P.A.; Fletcher, L.A.; Siddiqi, K. The Transmission of Tuberculosis in Confined Spaces: An Analytical Review of Alternative Epidemiological Models. *INT J TUBERC LUNG DIS* **2003**, *7*, 1015–1026.
17. Fennelly, K.P.; Jones-López, E.C. Quantity and Quality of Inhaled Dose Predicts Immunopathology in Tuberculosis. *Front. Immunol.* **2015**, *6*, 313, doi:10.3389/FIMMU.2015.00313/BIBTEX.
18. Queval, C.J.; Brosch, R.; Simeone, R. The Macrophage: A Disputed Fortress in the Battle against Mycobacterium Tuberculosis. *Front. Microbiol.* **2017**, *0*, 2284, doi:10.3389/FMICB.2017.02284.
19. Pethe, K.; Swenson, D.L.; Alonso, S.; Anderson, J.; Wang, C.; Russell, D.G. Isolation of Mycobacterium Tuberculosis Mutants Defective in the Arrest of Phagosome Maturation. *Proc. Natl. Acad. Sci. U. S. A.* **2004**, *101*, 13642, doi:10.1073/PNAS.0401657101.
20. Flynn, J.A.L.; Chan, J. Immune Evasion by Mycobacterium Tuberculosis: Living with the Enemy. *Curr. Opin. Immunol.* **2003**, *15*, 450–455, doi:10.1016/S0952-7915(03)00075-X.
21. Behar, S.M.; Divangahi, M.; Remold, H.G. Evasion of Innate Immunity by Mycobacterium Tuberculosis: Is Death an Exit Strategy? *Nat. Rev. Microbiol.* **2010**, *8*, 668, doi:10.1038/NRMICRO2387.
22. Brightbill, H.D.; Libraty, D.H.; Krutzik, S.R.; Yang, R.B.; Belisle, J.T.; Bleharski, J.R.; Maitland, M.; Norgard, M. V.; Plevy, S.E.; Smale, S.T.; et al. Host Defense Mechanisms Triggered by Microbial Lipoproteins through Toll-like Receptors. *Science* **1999**, *285*, 732–736, doi:10.1126/SCIENCE.285.5428.732.
23. Eum, S.Y.; Kong, J.H.; Hong, M.S.; Lee, Y.J.; Kim, J.H.; Hwang, S.H.; Cho, S.N.; Via, L.E.; Barry, C.E. Neutrophils Are the Predominant Infected Phagocytic Cells

in the Airways of Patients With Active Pulmonary TB. *Chest* **2010**, *137*, 122–128, doi:10.1378/CHEST.09-0903.

24. Korb, V.C.; Chuturgoon, A.A.; Moodley, D. Mycobacterium Tuberculosis: Manipulator of Protective Immunity. *Int. J. Mol. Sci.* **2016**, *17*, doi:10.3390/IJMS17030131.
25. Liu, C.H.; Liu, H.; Ge, B. Innate Immunity in Tuberculosis: Host Defense vs Pathogen Evasion. *Cell. Mol. Immunol.* 2017, *14*, 963–975.
26. Prezzemolo, T.; Guggino, G.; La Manna, M.P.; Di Liberto, D. Di; Dieli, F.; Caccamo, N. Functional Signatures of Human CD4 and CD8 T Cell Responses to Mycobacterium Tuberculosis. *Front. Immunol.* **2014**, *5*, 180, doi:10.3389/FIMMU.2014.00180/BIBTEX.
27. Lin, P.L.; Flynn, J.A.L. CD8 T Cells and Mycobacterium Tuberculosis Infection. *Semin. Immunopathol.* **2015**, *37*, 239, doi:10.1007/S00281-015-0490-8.
28. Lyadova, I. V.; Panteleev, A. V. Th1 and Th17 Cells in Tuberculosis: Protection, Pathology, and Biomarkers. *Mediators Inflamm.* **2015**, *2015*, doi:10.1155/2015/854507.
29. Woodworth, J.S.M.; Behar, S.M. Mycobacterium Tuberculosis Specific CD8+ T Cells and Their Role in Immunity. *Crit. Rev. Immunol.* **2006**, *26*, 317, doi:10.1615/CRITREVIMMUNOL.V26.I4.30.
30. Wolf, A.J.; Desvignes, L.; Linas, B.; Banaiee, N.; Tamura, T.; Takatsu, K.; Ernst, J.D. Initiation of the Adaptive Immune Response to Mycobacterium Tuberculosis Depends on Antigen Production in the Local Lymph Node, Not the Lungs. *J. Exp. Med.* **2008**, *205*, 105, doi:10.1084/JEM.20071367.
31. Shafiani, S.; Tucker-Heard, G.; Kariyone, A.; Takatsu, K.; Urdahl, K.B. Pathogen-Specific Regulatory T Cells Delay the Arrival of Effector T Cells in the Lung during Early Tuberculosis. *J. Exp. Med.* **2010**, *207*, 1409, doi:10.1084/JEM.20091885.
32. Paige, C.; Bishai, W.R. Penitentiary or Penthouse Condo: The Tuberculous Granuloma from the Microbe's Point of View. *Cell. Microbiol.* **2010**, *12*, 301–309, doi:10.1111/J.1462-5822.2009.01424.X.
33. Cavalcanti, Y.V.N.; Brelaz, M.C.A.; Neves, J.K.D.A.L.; Ferraz, J.C.; Pereira, V.R.A. Role of TNF-Alpha, IFN-Gamma, and IL-10 in the Development of Pulmonary Tuberculosis. *Pulm. Med.* **2012**, *2012*, doi:10.1155/2012/745483.
34. Hmama, Z.; Gabathuler, R.; Jefferies, W.A.; de Jong, G.; Reiner, N.E. Attenuation of HLA-DR Expression by Mononuclear Phagocytes Infected with Mycobacterium Tuberculosis Is Related to Intracellular Sequestration of Immature Class II Heterodimers. *J. Immunol.* **1998**, *161*.
35. O'Garra, A.; Redford, P.S.; McNab, F.W.; Bloom, C.I.; Wilkinson, R.J.; Berry,

M.P.R. The Immune Response in Tuberculosis. *http://dx.doi.org.libaccess.lib.mcmaster.ca/10.1146/annurev-immunol-032712-095939* **2013**, *31*, 475–527, doi:10.1146/ANNUREV-IMMUNOL-032712-095939.

36. Kumar, P. IFNγ-Producing CD4+ T Lymphocytes: The Double-Edged Swords in Tuberculosis. *Clin. Transl. Med. 2017 61* **2017**, *6*, 1–7, doi:10.1186/S40169-017-0151-8.
37. Lin, P.L.; Ford, C.B.; Coleman, M.T.; Myers, A.J.; Gawande, R.; Ioerger, T.; Sacchettini, J.; Fortune, S.M.; Flynn, J.L. Sterilization of Granulomas Is Common in Both Active and Latent Tuberculosis despite Extensive Within-Host Variability in Bacterial Killing. *Nat. Med.* **2014**, *20*, 75, doi:10.1038/NM.3412.
38. Ramakrishnan, L. Revisiting the Role of the Granuloma in Tuberculosis. *Nat. Rev. Immunol.* 2012, *12*, 352–366.
39. Flynn, J.L.; Chan, J.; Lin, P.L. Macrophages and Control of Granulomatous Inflammation in Tuberculosis. *Mucosal Immunol. 2011 43* **2011**, *4*, 271–278, doi:10.1038/mi.2011.14.
40. Silva Miranda, M.; Breiman, A.; Allain, S.; Deknuydt, F.; Altare, F. The Tuberculous Granuloma: An Unsuccessful Host Defence Mechanism Providing a Safety Shelter for the Bacteria? *Clin. Dev. Immunol.* **2012**, *2012*, 14, doi:10.1155/2012/139127.
41. Russell, D.G.; Cardona, P.J.; Kim, M.J.; Allain, S.; Altare, F. Foamy Macrophages and the Progression of the Human TB Granuloma. *Nat. Immunol.* **2009**, *10*, 943, doi:10.1038/NI.1781.
42. Kim, M.J.; Wainwright, H.C.; Locketz, M.; Bekker, L.G.; Walther, G.B.; Dittrich, C.; Visser, A.; Wang, W.; Hsu, F.F.; Wiehart, U.; et al. Caseation of Human Tuberculosis Granulomas Correlates with Elevated Host Lipid Metabolism. *EMBO Mol. Med.* **2010**, *2*, 258, doi:10.1002/EMMM.201000079.
43. Cáceres, N.; Tapia, G.; Ojanguren, I.; Altare, F.; Gil, O.; Pinto, S.; Vilaplana, C.; Cardona, P.J. Evolution of Foamy Macrophages in the Pulmonary Granulomas of Experimental Tuberculosis Models. *Tuberculosis* **2009**, *89*, 175–182, doi:10.1016/J.TUBE.2008.11.001.
44. Cadena, A.M.; Fortune, S.M.; Flynn, J.L. Heterogeneity in Tuberculosis. *Nat. Rev. Immunol.* **2017**, *17*, 691, doi:10.1038/NRI.2017.69.
45. Shaler, C.R.; Horvath, C.N.; Jeyanathan, M.; Xing, Z. Within the Enemy's Camp: Contribution of the Granuloma to the Dissemination, Persistence and Transmission of Mycobacterium Tuberculosis. *Front. Immunol.* 2013, *4*.
46. Harris, J.; Keane, J. How Tumour Necrosis Factor Blockers Interfere with Tuberculosis Immunity. *Clin. Exp. Immunol.* **2010**, *161*, 1, doi:10.1111/J.1365-2249.2010.04146.X.

47. Solovic, I.; Sester, M.; Gomez-Reino, J.J.; Rieder, H.L.; Ehlers, S.; Milburn, H.J.; Kampmann, B.; Hellmich, B.; Groves, R.; Schreiber, S.; et al. The Risk of Tuberculosis Related to Tumour Necrosis Factor Antagonist Therapies: A TBNET Consensus Statement. *Eur. Respir. J.* **2010**, *36*, 1185–1206, doi:10.1183/09031936.00028510.
48. Diedrich, C.R.; O'Hern, J.; Wilkinson, R.J. HIV-1 and the Mycobacterium Tuberculosis Granuloma: A Systematic Review and Meta-Analysis. *Tuberculosis* **2016**, *98*, 62–76, doi:10.1016/J.TUBE.2016.02.010.
49. Ernst, J.D. The Immunological Life Cycle of Tuberculosis. *Nat. Rev. Immunol.* 2012, *12*, 581–591.
50. Pai, M.; Zwerling, A.; Menzies, D. Systematic Review: T-Cell–Based Assays for the Diagnosis of Latent Tuberculosis Infection: An Update. *Ann. Intern. Med.* **2008**, *149*, 177, doi:10.7326/0003-4819-149-3-200808050-00241.
51. Starke, J.R.; Byington, C.L.; Maldonado, Y.A.; Barnett, E.D.; Davies, H.D.; Edwards, K.M.; Jackson, M.A.; Murray, D.L.; Rathore, M.H.; Sawyer, M.H.; et al. Interferon-γ Release Assays for Diagnosis of Tuberculosis Infection and Disease in Children. *Pediatrics* **2014**, *134*, e1763–e1773, doi:10.1542/PEDS.2014-2983.
52. Sun, L.; Xiao, J.; Miao, Q.; Feng, W.X.; Wu, X.R.; Yin, Q.Q.; Jiao, W.W.; Shen, C.; Liu, F.; Shen, D.; et al. Interferon Gamma Release Assay in Diagnosis of Pediatric Tuberculosis: A Meta-Analysis. *FEMS Immunol. Med. Microbiol.* **2011**, *63*, 165–173, doi:10.1111/J.1574-695X.2011.00838.X.
53. Steingart, K.R.; Henry, M.; Ng, V.; Hopewell, P.C.; Ramsay, A.; Cunningham, J.; Urbanczik, R.; Perkins, M.; Aziz, M.A.; Pai, M. Fluorescence versus Conventional Sputum Smear Microscopy for Tuberculosis: A Systematic Review. *Lancet. Infect. Dis.* **2006**, *6*, 570–581, doi:10.1016/S1473-3099(06)70578-3.
54. Cruciani, M.; Scarparo, C.; Malena, M.; Bosco, O.; Serpelloni, G.; Mengoli, C. Meta-Analysis of BACTEC MGIT 960 and BACTEC 460 TB, with or without Solid Media, for Detection of Mycobacteria. *J. Clin. Microbiol.* **2004**, *42*, 2321, doi:10.1128/JCM.42.5.2321-2325.2004.
55. Ling, D.I.; Zwerling, A.A.; Pai, M. GenoType *MTB*DR Assays for the Diagnosis of Multidrug-Resistant Tuberculosis: A Meta-Analysis. *Eur. Respir. J.* **2008**, *32*, 1165–1174, doi:10.1183/09031936.00061808.
56. Kay, A.W.; González Fernández, L.; Takwoingi, Y.; Eisenhut, M.; Detjen, A.K.; Steingart, K.R.; Mandalakas, A.M. Xpert *MTB*/RIF and Xpert *MTB*/RIF Ultra Assays for Active Tuberculosis and Rifampicin Resistance in Children. *Cochrane Database Syst. Rev.* **2020**, *2020*, doi:10.1002/14651858.CD013359.PUB2.
57. Zifodya, J.S.; Kreniske, J.S.; Schiller, I.; Kohli, M.; Dendukuri, N.; Schumacher, S.G.; Ochodo, E.A.; Haraka, F.; Zwerling, A.A.; Pai, M.; et al. Xpert Ultra versus

Xpert *MTB*/RIF for Pulmonary Tuberculosis and Rifampicin Resistance in Adults with Presumptive Pulmonary Tuberculosis. *Cochrane Database Syst. Rev.* **2021**, *2021*, doi:10.1002/14651858.CD009593.PUB5/MEDIA/CDSR/CD009593/IMAGE_N/NCD009593-TST-023.PNG.

58. Muyoyeta, M.; Maduskar, P.; Moyo, M.; Kasese, N.; Milimo, D.; Spooner, R.; Kapata, N.; Hogeweg, L.; Van Ginneken, B.; Ayles, H. The Sensitivity and Specificity of Using a Computer Aided Diagnosis Program for Automatically Scoring Chest X-Rays of Presumptive TB Patients Compared with Xpert *MTB*/RIF in Lusaka Zambia. *PLoS One* **2014**, *9*, e93757, doi:10.1371/JOURNAL.PONE.0093757.
59. Lawn, S.D.; Zumla, A.I. Tuberculosis. *Lancet* **2011**, *378*, 57–72, doi:10.1016/S0140-6736(10)62173-3.
60. Hunter, R.L.; Jagannath, C.; Actor, J.K. Pathology of Postprimary Tuberculosis in Humans and Mice: Contradiction of Long-Held Beliefs. *Tuberculosis (Edinb).* **2007**, *87*, 267–278, doi:10.1016/J.TUBE.2006.11.003.
61. Hunter, R.L. The Pathogenesis of Tuberculosis: The Early Infiltrate of Post-Primary (Adult Pulmonary) Tuberculosis: A Distinct Disease Entity. *Front. Immunol.* **2018**, *9*, 2108, doi:10.3389/FIMMU.2018.02108/BIBTEX.
62. Basaraba, R.J.; Hunter, R.L. Pathology of Tuberculosis: How the Pathology of Human Tuberculosis Informs and Directs Animal Models. *Tuberc. Tuber. Bacillus Second Ed.* **2017**, 117–129, doi:10.1128/9781555819569.ch5.
63. Ordonez, A.A.; Tucker, E.W.; Anderson, C.J.; Carter, C.L.; Ganatra, S.; Kaushal, D.; Kramnik, I.; Lin, P.L.; Madigan, C.A.; Mendez, S.; et al. Visualizing the Dynamics of Tuberculosis Pathology Using Molecular Imaging. *J. Clin. Invest.* **2021**, *131*, doi:10.1172/JCI145107.
64. Lenaerts, A.; Barry, C.E.; Dartois, V. Heterogeneity in Tuberculosis Pathology, Microenvironments and Therapeutic Responses. *Immunol. Rev.* **2015**, *264*, 288–307, doi:10.1111/IMR.12252.
65. McCaffrey, E.F.; Donato, M.; Keren, L.; Chen, Z.; Delmastro, A.; Fitzpatrick, M.B.; Gupta, S.; Greenwald, N.F.; Baranski, A.; Graf, W.; et al. The Immunoregulatory Landscape of Human Tuberculosis Granulomas. *Nat. Immunol. 2022 232* **2022**, *23*, 318–329, doi:10.1038/s41590-021-01121-x.
66. Abengozar-Muela, M.; Esparza, M.V.; Garcia-Ros, D.; Vásquez, C.E.; Echeveste, J.I.; Idoate, M.A.; Lozano, M.D.; Melero, I.; de Andrea, C.E. Diverse Immune Environments in Human Lung Tuberculosis Granulomas Assessed by Quantitative Multiplexed Immunofluorescence. *Mod. Pathol. 2020 3312* **2020**, *33*, 2507–2519, doi:10.1038/s41379-020-0600-6.

67. Jarnicki, A.G.; Lysaght, J.; Todryk, S.; Mills, K.H.G. Suppression of Antitumor Immunity by IL-10 and TGF-β-Producing T Cells Infiltrating the Growing Tumor: Influence of Tumor Environment on the Induction of CD4+ and CD8+ Regulatory T Cells. *J. Immunol.* **2006**, *177*, 896–904, doi:10.4049/JIMMUNOL.177.2.896.
68. Ehlers, S.; Schaible, U.E. The Granuloma in Tuberculosis: Dynamics of a Host–Pathogen Collusion. *Front. Immunol.* **2012**, *3*, doi:10.3389/FIMMU.2012.00411.
69. Wong, E.A.; Joslyn, L.; Grant, N.L.; Klein, E.; Lin, P.L.; Kirschner, D.E.; Flynn, J.A.L. Low Levels of T Cell Exhaustion in Tuberculous Lung Granulomas. *Infect. Immun.* **2018**, *86*, doi:10.1128/IAI.00426-18.
70. Singh, A.K.; Gupta, U.D. Animal Models of Tuberculosis: Lesson Learnt. *Indian J. Med. Res.* **2018**, *147*, 456, doi:10.4103/IJMR.IJMR_554_18.
71. Takaki, K.; Davis, J.M.; Winglee, K.; Ramakrishnan, L. Evaluation of the Pathogenesis and Treatment of Mycobacterium Marinum Infection in Zebrafish. *Nat. Protoc. 2013 86* **2013**, *8*, 1114–1124, doi:10.1038/NPROT.2013.068.
72. Swaim, L.E.; Connolly, L.E.; Volkman, H.E.; Humbert, O.; Born, D.E.; Ramakrishnan, L. Mycobacterium Marinum Infection of Adult Zebrafish Causes Caseating Granulomatous Tuberculosis and Is Moderated by Adaptive Immunity. *Infect. Immun.* **2006**, *74*, 6108, doi:10.1128/IAI.00887-06.
73. Ramakrishnan, L. Looking within the Zebrafish to Understand the Tuberculous Granuloma. *Adv. Exp. Med. Biol.* **2013**, *783*, 251–266, doi:10.1007/978-1-4614-6111-1_13.
74. Yang, C.T.; Cambier, C.J.; Davis, J.M.; Hall, C.J.; Crosier, P.S.; Ramakrishnan, L. Neutrophils Exert Protection in the Early Tuberculous Granuloma by Oxidative Killing of Mycobacteria Phagocytosed from Infected Macrophages. *Cell Host Microbe* **2012**, *12*, 301–312, doi:10.1016/J.CHOM.2012.07.009.
75. Cooper, A.M. Mouse Model of Tuberculosis. *Cold Spring Harb. Perspect. Med.* **2015**, *5*, doi:10.1101/CSHPERSPECT.A018556.
76. Orme, I.M. The Mouse as a Useful Model of Tuberculosis. In Proceedings of the Tuberculosis; Churchill Livingstone, February 1 2003; Vol. 83, pp. 112–115.
77. Driver, E.R.; Ryan, G.J.; Hoff, D.R.; Irwin, S.M.; Basaraba, R.J.; Kramnik, I.; Lenaerts, A.J. Evaluation of a Mouse Model of Necrotic Granuloma Formation Using C3HeB/FeJ Mice for Testing of Drugs against Mycobacterium Tuberculosis. *Antimicrob. Agents Chemother.* **2012**, *56*, 3181, doi:10.1128/AAC.00217-12.
78. Cooper, A.M.; Dalton, D.K.; Stewart, T.A.; Griffin, J.P.; Russell, D.G.; Orme, I.M. Disseminated Tuberculosis in Interferon Gamma Gene-Disrupted Mice. *J. Exp. Med.* **1993**, *178*, 2243–2247, doi:10.1084/JEM.178.6.2243.
79. Flynn, J.A.L.; Goldstein, M.M.; Chan, J.; Triebold, K.J.; Pfeffer, K.; Lowenstein, C.J.; Schrelber, R.; Mak, T.W.; Bloom, B.R. Tumor Necrosis Factor-α Is Required

in the Protective Immune Response against Mycobacterium Tuberculosis in Mice. *Immunity* **1995**, *2*, 561–572, doi:10.1016/1074-7613(95)90001-2.

80. Saunders, B.M.; Frank, A.A.; Orme, I.M.; Cooper, A.M. CD4 Is Required for the Development of a Protective Granulomatous Response to Pulmonary Tuberculosis. *Cell. Immunol.* **2002**, *216*, 65–72, doi:10.1016/S0008-8749(02)00510-5.
81. Lenaerts, A.J.; Hoff, D.; Aly, S.; Ehlers, S.; Andries, K.; Cantarero, L.; Orme, I.M.; Basaraba, R.J. Location of Persisting Mycobacteria in a Guinea Pig Model of Tuberculosis Revealed by R207910. *Antimicrob. Agents Chemother.* **2007**, *51*, 3338, doi:10.1128/AAC.00276-07.
82. Palanisamy, G.S.; Smith, E.E.; Shanley, C.A.; Ordway, D.J.; Orme, I.M.; Basaraba, R.J. Disseminated Disease Severity as a Measure of Virulence of Mycobacterium Tuberculosis in the Guinea Pig Model. *Tuberculosis (Edinb).* **2008**, *88*, 295, doi:10.1016/J.TUBE.2007.12.003.
83. Manabe, Y.C.; Kesavan, A.K.; Lopez-Molina, J.; Hatem, C.L.; Brooks, M.; Fujiwara, R.; Hochstein, K.; Pitt, M.L.M.; Tufariello, J.A.; Chan, J.; et al. The Aerosol Rabbit Model of TB Latency, Reactivation and Immune Reconstitution Inflammatory Syndrome. *Tuberculosis (Edinb).* **2008**, *88*, 187, doi:10.1016/J.TUBE.2007.10.006.
84. Manabe, Y.C.; Dannenberg, A.M.; Tyagi, S.K.; Hatem, C.L.; Yoder, M.; Woolwine, S.C.; Zook, B.C.; Pitt, M.L.M.; Bishai, W.R. Different Strains of Mycobacterium Tuberculosis Cause Various Spectrums of Disease in the Rabbit Model of Tuberculosis. *Infect. Immun.* **2003**, *71*, 6004–6011, doi:10.1128/IAI.71.10.6004-6011.2003.
85. Kaushal, D.; Mehra, S.; Didier, P.J.; Lackner, A.A. The Non-Human Primate Model of Tuberculosis. *J. Med. Primatol.* **2012**, *41*, 191–201, doi:10.1111/j.1600-0684.2012.00536.x.
86. Peña, J.C.; Ho, W.-Z. Non-Human Primate Models of Tuberculosis. *Microbiol. Spectr.* **2016**, *4*, doi:10.1128/MICROBIOLSPEC.TBTB2-0007-2016/ASSET/EDD895E2-EC35-4E0A-9D50-03E93443FDF8/ASSETS/GRAPHIC/TBTB2-0007-2016-FIG2.GIF.
87. Flynn, J.L.; Gideon, H.P.; Mattila, J.T.; Lin, P.L. Immunology Studies in Non-Human Primate Models of Tuberculosis. *Immunol. Rev.* **2015**, *264*, 60–73, doi:10.1111/imr.12258.
88. Furin, J.; Cox, H.; Pai, M. Seminar Tuberculosis. *www.thelancet.com* **2019**, *393*, doi:10.1016/S0140-6736(19)30308-3.
89. Nahid, P.; Dorman, S.E.; Alipanah, N.; Barry, P.M.; Brozek, J.L.; Cattamanchi, A.; Chaisson, L.H.; Chaisson, R.E.; Daley, C.L.; Grzemska, M.; et al. Executive Summary: Official American Thoracic Society/Centers for Disease Control and

Prevention/Infectious Diseases Society of America Clinical Practice Guidelines: Treatment of Drug-Susceptible Tuberculosis. *Clin. Infect. Dis.* **2016**, *63*, 853–867, doi:10.1093/CID/CIW566.

90. Pillay, S.; Steingart, K.R.; Davies, G.R.; Chaplin, M.; Vos, M. De; Schumacher, S.G.; Warren, R.; Theron, G. Xpert *MTB*/XDR for Detection of Pulmonary Tuberculosis and Resistance to Isoniazid, Fluoroquinolones, Ethionamide, and Amikacin. *Cochrane Database Syst. Rev.* **2022**, *2022*, doi:10.1002/14651858.CD014841.PUB2.
91. Dorman, S.E.; Schumacher, S.G.; Alland, D.; Nabeta, P.; Armstrong, D.T.; King, B.; Hall, S.L.; Chakravorty, S.; Cirillo, D.M.; Tukvadze, N.; et al. Xpert *MTB*/RIF Ultra for Detection of Mycobacterium Tuberculosis and Rifampicin Resistance: A Prospective Multicentre Diagnostic Accuracy Study. *Lancet. Infect. Dis.* **2018**, *18*, 76, doi:10.1016/S1473-3099(17)30691-6.
92. Tornheim, J.A.; Dooley, K.E. The Global Landscape of Tuberculosis Therapeutics. *https://doi-org.libaccess.lib.mcmaster.ca/10.1146/annurev-med-040717-051150* **2019**, *70*, 105–120, doi:10.1146/ANNUREV-MED-040717-051150.
93. Colditz, G.A.; Brewer, T.F.; Berkey, C.S.; Wilson, M.E.; Burdick, E.; Fineberg, H. V.; Mosteller, F. Efficacy of BCG Vaccine in the Prevention of Tuberculosis: Meta-Analysis of the Published Literature. *JAMA* **1994**, *271*, 698–702, doi:10.1001/JAMA.1994.03510330076038.
94. Hawn, T.R.; Day, T.A.; Scriba, T.J.; Hatherill, M.; Hanekom, W.A.; Evans, T.G.; Churchyard, G.J.; Kublin, J.G.; Bekker, L.-G.; Self, S.G. Tuberculosis Vaccines and Prevention of Infection. *Microbiol. Mol. Biol. Rev.* **2014**, *78*, 650, doi:10.1128/MMBR.00021-14.
95. Grode, L.; Seiler, P.; Baumann, S.; Hess, J.; Brinkmann, V.; Eddine, A.N.; Mann, P.; Goosmann, C.; Bandermann, S.; Smith, D.; et al. Increased Vaccine Efficacy against Tuberculosis of Recombinant Mycobacterium Bovis Bacille Calmette-Guérin Mutants That Secrete Listeriolysin. *J. Clin. Invest.* **2005**, *115*, 2472–2479, doi:10.1172/JCI24617.
96. Loxton, A.G.; Knaul, J.K.; Grode, L.; Gutschmidt, A.; Meller, C.; Eisele, B.; Johnstone, H.; Van Der Spuy, G.; Maertzdorf, J.; Kaufmann, S.H.E.; et al. Safety and Immunogenicity of the Recombinant Mycobacterium Bovis BCG Vaccine VPM1002 in HIV-Unexposed Newborn Infants in South Africa. *Clin. Vaccine Immunol.* **2017**, *24*, doi:10.1128/CVI.00439-16/ASSET/DA1308F0-2412-4008-9E4D-D27C3B6CE914/ASSETS/GRAPHIC/ZCD9990954460006.JPEG.
97. Nieuwenhuizen, N.E.; Kulkarni, P.S.; Shaligram, U.; Cotton, M.F.; Rentsch, C.A.; Eisele, B.; Grode, L.; Kaufmann, S.H.E. The Recombinant Bacille Calmette-Guérin Vaccine VPM1002: Ready for Clinical Efficacy Testing. *Front. Immunol.*

2017, *8*, 1147, doi:10.3389/FIMMU.2017.01147/BIBTEX.

98. Van Der Meeren, O.; Hatherill, M.; Nduba, V.; Wilkinson, R.J.; Muyoyeta, M.; Van Brakel, E.; Ayles, H.M.; Henostroza, G.; Thienemann, F.; Scriba, T.J.; et al. Phase 2b Controlled Trial of M72/AS01 E Vaccine to Prevent Tuberculosis . *N. Engl. J. Med.* **2018**, *379*, 1621–1634, doi:10.1056/NEJMOA1803484/SUPPL_FILE/NEJMOA1803484_DISCLOSURES.PDF.
99. Kumarasamy, N.; Poongulali, S.; Beulah, F.E.; Akite, E.J.; Ayuk, L.N.; Bollaerts, A.; Demoitié, M.A.; Jongert, E.; Ofori-Anyinam, O.; Van Der Meeren, O. Long-Term Safety and Immunogenicity of the M72/AS01E Candidate Tuberculosis Vaccine in HIV-Positive and -Negative Indian Adults Results from a Phase II Randomized Controlled Trial. *Med. (United States)* **2018**, *97*, doi:10.1097/MD.0000000000013120.
100. Kumarasamy, N.; Poongulali, S.; Bollaerts, A.; Moris, P.; Beulah, F.E.; Ayuk, L.N.; Demoitie, M.A.; Jongert, E.; Ofori-Anyinam, O. A Randomized, Controlled Safety, and Immunogenicity Trial of the M72/AS01 Candidate Tuberculosis Vaccine in HIV-Positive Indian Adults. *Med. (United States)* **2016**, *95*, doi:10.1097/MD.0000000000002459.
101. Tameris, M.D.; Hatherill, M.; Landry, B.S.; Scriba, T.J.; Snowden, M.A.; Lockhart, S.; Shea, J.E.; McClain, J.B.; Hussey, G.D.; Hanekom, W.A.; et al. Safety and Efficacy of MVA85A, a New Tuberculosis Vaccine, in Infants Previously Vaccinated with BCG: A Randomised, Placebo-Controlled Phase 2b Trial. *Lancet* **2013**, *381*, 1021–1028, doi:10.1016/S0140-6736(13)60177-4/ATTACHMENT/476E8FE3-F266-48CA-A661-A562F7B1E701/MMC1.PDF.
102. Smaill, F.; Jeyanathan, M.; Smieja, M.; Medina, M.F.; Thanthrige-Don, N.; Zganiacz, A.; Yin, C.; Heriazon, A.; Damjanovic, D.; Puri, L.; et al. A Human Type 5 Adenovirus-Based Tuberculosis Vaccine Induces Robust T Cell Responses in Humans despite Preexisting Anti-Adenovirus Immunity. *Sci. Transl. Med.* **2013**, *5*, doi:10.1126/SCITRANSLMED.3006843/SUPPL_FILE/5-205RA134_SM.PDF.
103. Wiker, H.G.; Harboe, M. The Antigen 85 Complex: A Major Secretion Product of Mycobacterium Tuberculosis. *Microbiol. Rev.* **1992**, *56*, 648–661, doi:10.1128/MR.56.4.648-661.1992.
104. Yao, Y.; Lai, R.; Afkhami, S.; Haddadi, S.; Zganiacz, A.; Vahedi, F.; Ashkar, A.A.; Kaushic, C.; Jeyanathan, M.; Xing, Z. Enhancement of Antituberculosis Immunity in a Humanized Model System by a Novel Virus-Vectored Respiratory Mucosal Vaccine. *J. Infect. Dis.* **2017**, *216*, 135–145, doi:10.1093/infdis/jix252.
105. Afkhami, S.; Lai, R.; D'Agostino, M.R.; Vaseghi-Shanjani, M.; Zganiacz, A.; Yao, Y.; Jeyanathan, M.; Xing, Z. Single-Dose Mucosal Immunotherapy with

Chimpanzee Adenovirus-Based Vaccine Accelerates Tuberculosis Disease Control and Limits Its Rebound after Antibiotic Cessation. *J. Infect. Dis.* **2019**, *220*, 1355–1366, doi:10.1093/infdis/jiz306.

106. Jeyanathan, M.; Thanthrige-Don, N.; Afkhami, S.; Lai, R.; Damjanovic, D.; Zganiacz, A.; Feng, X.; Yao, X.D.; Rosenthal, K.L.; Fe Medina, M.; et al. Novel Chimpanzee Adenovirus-Vectored Respiratory Mucosal Tuberculosis Vaccine: Overcoming Local Anti-Human Adenovirus Immunity for Potent TB Protection. *Mucosal Immunol.* **2015**, *8*, 1373–1387, doi:10.1038/mi.2015.29.
107. Jeyanathan, M.; Afkhami, S.; Khera, A.; Mandur, T.; Damjanovic, D.; Yao, Y.; Lai, R.; Haddadi, S.; Dvorkin-Gheva, A.; Jordana, M.; et al. CXCR3 Signaling Is Required for Restricted Homing of Parenteral Tuberculosis Vaccine-Induced T Cells to Both the Lung Parenchyma and Airway. *J. Immunol.* **2017**, *199*, 2555–2569, doi:10.4049/JIMMUNOL.1700382.
108. Lai, R.; Afkhami, S.; Haddadi, S.; Jeyanathan, M.; Xing, Z. Mucosal Immunity and Novel Tuberculosis Vaccine Strategies: Route of Immunisationdetermined T-Cell Homing to Restricted Lung Mucosal Compartments. *Eur. Respir. Rev.* **2015**, *24*, 356–360, doi:10.1183/16000617.00002515.
109. Price, D.N.; Kusewitt, D.F.; Lino, C.A.; McBride, A.A.; Muttil, P. Oral Tolerance to Environmental Mycobacteria Interferes with Intradermal, but Not Pulmonary, Immunization against Tuberculosis. *PLOS Pathog.* **2016**, *12*, e1005614, doi:10.1371/JOURNAL.PPAT.1005614.
110. Zaiss, A.K.; Machado, H.B.; Herschman, H.R. The Influence of Innate and Pre-Existing Immunity on Adenovirus Therapy. *J. Cell. Biochem.* **2009**, *108*, 778–790, doi:10.1002/JCB.22328.
111. Bertholet, S.; Ireton, G.C.; Kahn, M.; Guderian, J.; Mohamath, R.; Stride, N.; Laughlin, E.M.; Baldwin, S.L.; Vedvick, T.S.; Coler, R.N.; et al. Identification of Human T Cell Antigens for the Development of Vaccines Against Mycobacterium Tuberculosis. *J. Immunol.* **2008**, *181*, 7948, doi:10.4049/JIMMUNOL.181.11.7948.
112. Zvi, A.; Ariel, N.; Fulkerson, J.; Sadoff, J.C.; Shafferman, A. Whole Genome Identification of Mycobacterium Tuberculosisvaccine Candidates by Comprehensive Data Mining and Bioinformatic Analyses. *BMC Med. Genomics 2008 11* **2008**, *1*, 1–25, doi:10.1186/1755-8794-1-18.
113. Rogerson, B.J.; Jung, Y.J.; LaCourse, R.; Ryan, L.; Enright, N.; North, R.J. Expression Levels of Mycobacterium Tuberculosis Antigen-Encoding Genes versus Production Levels of Antigen-Specific T Cells during Stationary Level Lung Infection in Mice. *Immunology* **2006**, *118*, 195, doi:10.1111/J.1365-2567.2006.02355.X.

114. Cayabyab, M.J.; Qin, L.; Kashino, S.S.; Izzo, A.; Campos-Neto, A. An Unbiased Peptide-Wide Discovery Approach to Select Mycobacterium Tuberculosis Antigens That Target CD8+ T Cell Response During Infection. *Vaccine* **2013**, *31*, 4834, doi:10.1016/J.VACCINE.2013.07.077.
115. UNAIDS Global HIV & AIDS Statistics — Fact Sheet | UNAIDS Available online: https://www.unaids.org/en/resources/fact-sheet (accessed on 23 May 2022).
116. The Gap Report Available online: https://www.refworld.org/docid/53f1e1604.html (accessed on 24 May 2022).
117. Johnson, M.; Samarina, A.; Xi, H.; Valdez Ramalho Madruga, J.; Hocqueloux, L.; Loutfy, M.; Fournelle, M.J.; Norton, M.; Van Wyk, J.; Zachry, W.; et al. Barriers to Access to Care Reported by Women Living with HIV across 27 Countries. *AIDS Care* **2015**, *27*, 1220, doi:10.1080/09540121.2015.1046416.
118. Gandhi, M.; Bacchetti, P.; Miotti, P.; Quinn, T.C.; Veronese, F.; Greenblatt, R.M. Does Patient Sex Affect Human Immunodeficiency Virus Levels? **2002**, *35*, 313–322.
119. Chang, J.J.; Woods, M.; Lindsay, R.J.; Doyle, E.H.; Griesbeck, M.; Chan, E.S.; Robbins, G.K.; Bosch, R.J.; Altfeld, M. Higher Expression of Several Interferon-Stimulated Genes in HIV-1-Infected Females after Adjusting for the Level of Viral Replication. *J. Infect. Dis.* **2013**, *208*, 830–838, doi:10.1093/INFDIS/JIT262.
120. Gregson, S.; Adamson, S.; Papaya, S.; Mundondo, J.; Nyamukapa, C.A.; Mason, P.R.; Garnett, G.P.; Chandiwana, S.K.; Foster, G.; Anderson, R.M. Impact and Process Evaluation of Integrated Community and Clinic-Based HIV-1 Control: A Cluster-Randomised Trial in Eastern Zimbabwe. *PLoS Med.* **2007**, *4*, 545–555, doi:10.1371/JOURNAL.PMED.0040102.
121. Galvin, S.R.; Cohen, M.S. The Role of Sexually Transmitted Diseases in HIV Transmission. *Nat. Rev. Microbiol. 2004 21* **2004**, *2*, 33–42, doi:10.1038/NRMICRO794.
122. Cohen, M.S.; Chen, Y.Q.; McCauley, M.; Gamble, T.; Hosseinipour, M.C.; Kumarasamy, N.; Hakim, J.G.; Kumwenda, J.; Grinsztejn, B.; Pilotto, J.H.S.; et al. Antiretroviral Therapy for the Prevention of HIV-1 Transmission. *N. Engl. J. Med.* **2016**, *375*, 830, doi:10.1056/NEJMOA1600693.
123. Yu, Y.; Luo, D.; Chen, X.; Huang, Z.; Wang, M.; Xiao, S. Medication Adherence to Antiretroviral Therapy among Newly Treated People Living with HIV. *BMC Public Health* **2018**, *18*, 1–8, doi:10.1186/S12889-018-5731-Z/TABLES/1.
124. Bruchfeld, J.; Correia-Neves, M.; Kallenius, G. Tuberculosis and HIV Coinfection. *Cold Spring Harb. Perspect. Med.* **2015**, *5*, doi:10.1101/CSHPERSPECT.A017871.
125. Ssentongo, P.; Heilbrunn, E.S.; Ssentongo, A.E.; Advani, S.; Chinchilli, V.M.;

Nunez, J.J.; Du, P. Epidemiology and Outcomes of COVID-19 in HIV-Infected Individuals: A Systematic Review and Meta-Analysis. *Sci. Rep.* **2021**, *11*, 6283, doi:10.1038/S41598-021-85359-3.

126. German Advisory Committee Blood (Arbeitskreis Blut), S. 'Assessment of P.T. by B. Human Immunodeficiency Virus (HIV). *Transfus. Med. Hemotherapy* **2016**, *43*, 203–222, doi:10.1159/000445852.
127. Maartens, G.; Celum, C.; Lewin, S.R. HIV Infection: Epidemiology, Pathogenesis, Treatment, and Prevention. *Lancet* **2014**, *384*, 258–271, doi:10.1016/S0140-6736(14)60164-1.
128. Quinn, T.C.; Wawer, M.J.; Sewankambo, N.; Serwadda, D.; Li, C.; Wabwire-Mangen, F.; Meehan, M.O.; Lutalo, T.; Gray, R.H. Viral Load and Heterosexual Transmission of Human Immunodeficiency Virus Type 1. *https://doi.org/10.1056/NEJM200003303421303* **2000**, *342*, 921–929, doi:10.1056/NEJM200003303421303.
129. Polis, C.B.; Curtis, K.M. Use of Hormonal Contraceptives and HIV Acquisition in Women: A Systematic Review of the Epidemiological Evidence. *Lancet Infect. Dis.* **2013**, *13*, 797–808, doi:10.1016/S1473-3099(13)70155-5.
130. Wessels, J.M.; Lajoie, J.; Hay Cooper, M.I.J.; Omollo, K.; Felker, A.M.; Vitali, D.; Dupont, H.A.; Nguyen, P. V.; Mueller, K.; Vahedi, F.; et al. Medroxyprogesterone Acetate Alters the Vaginal Microbiota and Microenvironment in Women and Increases Susceptibility to HIV-1 in Humanized Mice. *DMM Dis. Model. Mech.* 2019, *12*.
131. Wessels, J.M.; Nguyen, P. V.; Vitali, D.; Mueller, K.; Vahedi, F.; Felker, A.M.; Dupont, H.A.; Bagri, P.; Verschoor, C.P.; Deshiere, A.; et al. Depot Medroxyprogesterone Acetate (DMPA) Enhances Susceptibility and Increases the Window of Vulnerability to HIV-1 in Humanized Mice. *Sci. Rep.* **2021**, *11*, 3894, doi:10.1038/S41598-021-83242-9.
132. Haase, A.T. Targeting Early Infection to Prevent HIV-1 Mucosal Transmission. *Nature* 2010, *464*, 217–223.
133. Connor, R.I.; Sheridan, K.E.; Ceradini, D.; Choe, S.; Landau, N.R. Change in Coreceptor Use Correlates with Disease Progression in HIV-1- Infected Individuals. *J. Exp. Med.* **1997**, *185*, 621–628, doi:10.1084/jem.185.4.621.
134. Keele, B.F.; Giorgi, E.E.; Salazar-Gonzalez, J.F.; Decker, J.M.; Pham, K.T.; Salazar, M.G.; Sun, C.; Grayson, T.; Wang, S.; Li, H.; et al. Identification and Characterization of Transmitted and Early Founder Virus Envelopes in Primary HIV-1 Infection. *Proc. Natl. Acad. Sci. U. S. A.* **2008**, *105*, 7552, doi:10.1073/PNAS.0802203105.
135. Deeks, S.G.; Overbaugh, J.; Phillips, A.; Buchbinder, S. HIV Infection. *Nat. Rev.*

Dis. Prim. 2015 11 **2015**, *1*, 1–22, doi:10.1038/nrdp.2015.35.

136. Zhang, C.; Hu, W.; Jin, J.H.; Zhou, M.J.; Song, J.W.; Deng, J.N.; Huang, L.; Wang, S.Y.; Wang, F.S. The Role of CD8 T Cells in Controlling HIV beyond the Antigen-Specific Face. *HIV Med.* **2020**, *21*, 692–700, doi:10.1111/HIV.13021.
137. Reynolds, M.R.; Rakasz, E.; Skinner, P.J.; White, C.; Abel, K.; Ma, Z.-M.; Compton, L.; Napoé, G.; Wilson, N.; Miller, C.J.; et al. CD8+ T-Lymphocyte Response to Major Immunodominant Epitopes after Vaginal Exposure to Simian Immunodeficiency Virus: Too Late and Too Little. *J. Virol.* **2005**, *79*, 9228, doi:10.1128/JVI.79.14.9228-9235.2005.
138. Trautmann, L.; Janbazian, L.; Chomont, N.; Said, E.A.; Gimmig, S.; Bessette, B.; Boulassel, M.R.; Delwart, E.; Sepulveda, H.; Balderas, R.S.; et al. Upregulation of PD-1 Expression on HIV-Specific CD8+ T Cells Leads to Reversible Immune Dysfunction. *Nat. Med. 2006 1210* **2006**, *12*, 1198–1202, doi:10.1038/NM1482.
139. Day, C.L.; Kaufmann, D.E.; Kiepiela, P.; Brown, J.A.; Moodley, E.S.; Reddy, S.; Mackey, E.W.; Miller, J.D.; Leslie, A.J.; DePierres, C.; et al. PD-1 Expression on HIV-Specific T Cells Is Associated with T-Cell Exhaustion and Disease Progression. *Nat. 2006 4437109* **2006**, *443*, 350–354, doi:10.1038/nature05115.
140. Chun, T.W.; Engel, D.; Mizell, S.B.; Ehler, L.A.; Fauci, A.S. Induction of HIV-1 Replication in Latently Infected CD4+ T Cells Using a Combination of Cytokines. *J. Exp. Med.* **1998**, *188*, 83–91, doi:10.1084/jem.188.1.83.
141. Alexaki, A.; Liu, Y.; Wigdahl, B. Cellular Reservoirs of HIV-1 and Their Role in Viral Persistence. *Curr. HIV Res.* **2008**, *6*, 388, doi:10.2174/157016208785861195.
142. Whitney, J.B.; Hill, A.L.; Sanisetty, S.; Penaloza-Macmaster, P.; Liu, J.; Shetty, M.; Parenteau, L.; Cabral, C.; Shields, J.; Blackmore, S.; et al. Rapid Seeding of the Viral Reservoir Prior to SIV Viraemia in Rhesus Monkeys. *Nature* **2014**, *512*, 74–77, doi:10.1038/NATURE13594.
143. Colby, D.J.; Trautmann, L.; Pinyakorn, S.; Leyre, L.; Pagliuzza, A.; Kroon, E.; Rolland, M.; Takata, H.; Buranapraditkun, S.; Intasan, J.; et al. Rapid HIV RNA Rebound after Antiretroviral Treatment Interruption in Persons Durably Suppressed in Fiebig I Acute HIV Infection. *Nat. Med. 2018 247* **2018**, *24*, 923–926, doi:10.1038/s41591-018-0026-6.
144. Rothenberger, M.K.; Keele, B.F.; Wietgrefe, S.W.; Fletcher, C. V.; Beilman, G.J.; Chipman, J.G.; Khoruts, A.; Estes, J.D.; Anderson, J.; Callisto, S.P.; et al. Large Number of Rebounding/Founder HIV Variants Emerge from Multifocal Infection in Lymphatic Tissues after Treatment Interruption. *Proc. Natl. Acad. Sci. U. S. A.* **2015**, *112*, E1126–E1134, doi:10.1073/PNAS.1414926112.
145. Gökengin, D.; Geretti, A.M.; Begovac, J.; Palfreeman, A.; Stevanovic, M.; Tarasenko, O.; Radcliffe, K. 2014 European Guideline on HIV Testing. *Int. J. STD*

AIDS **2014**, *25*, 695–704, doi:10.1177/0956462414531244.

146. Armstrong-Mensah, E.; Tetteh, A.K.; Choi, S. Utilization of Rapid Diagnostic Testing in Sub-Saharan Africa: Challenges and Effects on HIV Prevention. *Int. J. Matern. Child Heal. AIDS* **2021**, *10*, 1, doi:10.21106/IJMA.423.
147. Fraser, C.; Hollingsworth, T.D.; Chapman, R.; De Wolf, F.; Hanage, W.P. From the Cover: Variation in HIV-1 Set-Point Viral Load: Epidemiological Analysis and an Evolutionary Hypothesis. *Proc. Natl. Acad. Sci. U. S. A.* **2007**, *104*, 17441, doi:10.1073/PNAS.0708559104.
148. Richardson, B.A.; Mbori-Ngacha, D.; Lavreys, L.; John-Stewart, G.C.; Nduati, R.; Panteleeff, D.D.; Emery, S.; Kreiss, J.K.; Overbaugh, J. Comparison of Human Immunodeficiency Virus Type 1 Viral Loads in Kenyan Women, Men, and Infants during Primary and Early Infection. *J. Virol.* **2003**, *77*, 7120, doi:10.1128/JVI.77.12.7120-7123.2003.
149. Mellors, J.W.; Muñoz, A.; Giorgi, J. V.; Margolick, J.B.; Tassoni, C.J.; Gupta, P.; Kingsley, L.A.; Todd, J.A.; Saah, A.J.; Detels, R.; et al. Plasma Viral Load and CD4+ Lymphocytes as Prognostic Markers of HIV-1 Infection. *Ann. Intern. Med.* **1997**, *126*, 946–954, doi:10.7326/0003-4819-126-12-199706150-00003.
150. Mellors, J.W.; Rinaldo, C.R.; Gupta, P.; White, R.M.; Todd, J.A.; Kingsley, L.A. Prognosis in HIV-1 Infection Predicted by the Quantity of Virus in Plasma. *Science* **1996**, *272*, 1167–1170, doi:10.1126/SCIENCE.272.5265.1167.
151. Broder, S. The Development of Antiretroviral Therapy and Its Impact on the HIV-1/AIDS Pandemic. *Antiviral Res.* **2010**, *85*, 1, doi:10.1016/J.ANTIVIRAL.2009.10.002.
152. Department of Health and Human Services What to Start: Initial Combination Regimens for the Antiretroviral-Naive Patient | NIH Available online: https://clinicalinfo.hiv.gov/en/guidelines/adult-and-adolescent-arv/what-start-initial-combination-regimens-antiretroviral-naive (accessed on 24 May 2022).
153. Chun, T.W.; Stuyver, L.; Mizell, S.B.; Ehler, L.A.; Mican, J.A.M.; Baseler, M.; Lloyd, A.L.; Nowak, M.A.; Fauci, A.S. Presence of an Inducible HIV-1 Latent Reservoir during Highly Active Antiretroviral Therapy. *Proc. Natl. Acad. Sci. U. S. A.* **1997**, *94*, 13193–13197, doi:10.1073/PNAS.94.24.13193.
154. Baeten, J.M.; Donnell, D.; Ndase, P.; Mugo, N.R.; Campbell, J.D.; Wangisi, J.; Tappero, J.W.; Bukusi, E.A.; Cohen, C.R.; Katabira, E.; et al. Antiretroviral Prophylaxis for HIV-1 Prevention among Heterosexual Men and Women. *N. Engl. J. Med.* **2012**, *367*, 399, doi:10.1056/NEJMOA1108524.
155. Young, T.N.; Arens, F.J.; Kennedy, G.E.; Laurie, J.W.; Rutherford, G.W. Antiretroviral Post-exposure Prophylaxis (PEP) for Occupational HIV Exposure. *Cochrane Database Syst. Rev.* **2007**, *2007*,

doi:10.1002/14651858.CD002835.PUB3.

156. Morrow, W.J.; Wharton, M.; Lau, D.; Levy, J.A. Small Animals Are Not Susceptible to Human Immunodeficiency Virus Infection. *J. Gen. Virol.* **1987**, *68 (Pt 8)*, 2253–2257, doi:10.1099/0022-1317-68-8-2253.
157. Browning, J.; Horner, J.W.; Pettoello-Mantovani, M.; Raker, C.; Yurasov, S.; Depinho, R.A.; Goldstein, H. Mice Transgenic for Human CD4 and CCR5 Are Susceptible to HIV Infection. *Proc. Natl. Acad. Sci. U. S. A.* **1997**, *94*, 14637, doi:10.1073/PNAS.94.26.14637.
158. Keppler, O.T.; Welte, F.J.; Ngo, T.A.; Chin, P.S.; Patton, K.S.; Tsou, C.L.; Abbey, N.W.; Sharkey, M.E.; Grant, R.M.; You, Y.; et al. Progress Toward a Human CD4/CCR5 Transgenic Rat Model for De Novo Infection by Human Immunodeficiency Virus Type 1. *J. Exp. Med.* **2002**, *195*, 719, doi:10.1084/JEM.20011549.
159. Baroncelli, S.; Negri, D.R.M.; Michelini, Z.; Cara, A. Macaca Mulatta, Fascicularis and Nemestrina in AIDS Vaccine Development. *Expert Rev. Vaccines* **2008**, *7*, 1419–1435, doi:10.1586/14760584.7.9.1419.
160. Sharp, P.M.; Hahn, B.H. Origins of HIV and the AIDS Pandemic. *Cold Spring Harb. Perspect. Med.* **2011**, *1*, doi:10.1101/CSHPERSPECT.A006841.
161. Keele, B.F.; Li, H.; Learn, G.H.; Hraber, P.; Giorgi, E.E.; Grayson, T.; Sun, C.; Chen, Y.; Yeh, W.W.; Letvin, N.L.; et al. Low-Dose Rectal Inoculation of Rhesus Macaques by SIVsmE660 or SIVmac251 Recapitulates Human Mucosal Infection by HIV-1. *J. Exp. Med.* **2009**, *206*, 1117, doi:10.1084/JEM.20082831.
162. Stone, M.; Keele, B.F.; Ma, Z.-M.; Bailes, E.; Dutra, J.; Hahn, B.H.; Shaw, G.M.; Miller, C.J. A Limited Number of Simian Immunodeficiency Virus (SIV) Env Variants Are Transmitted to Rhesus Macaques Vaginally Inoculated with SIVmac251. *J. Virol.* **2010**, *84*, 7083, doi:10.1128/JVI.00481-10.
163. Veazey, R.S.; Shattock, R.J.; Klasse, P.J.; Moore, J.P. Animal Models for Microbicide Studies. *Curr. HIV Res.* **2012**, *10*, 79, doi:10.2174/157016212799304715.
164. Paiardini, M.; Cervasi, B.; Reyes-Aviles, E.; Micci, L.; Ortiz, A.M.; Chahroudi, A.; Vinton, C.; Gordon, S.N.; Bosinger, S.E.; Francella, N.; et al. Low Levels of SIV Infection in Sooty Mangabey Central-Memory CD4+ T-Cells Is Associated with Limited CCR5 Expression. *Nat. Med.* **2011**, *17*, 830, doi:10.1038/NM.2395.
165. Brenchley, J.M.; Vinton, C.; Tabb, B.; Hao, X.P.; Connick, E.; Paiardini, M.; Lifson, J.D.; Silvestri, G.; Estes, J.D. Differential Infection Patterns of CD4+ T Cells and Lymphoid Tissue Viral Burden Distinguish Progressive and Nonprogressive Lentiviral Infections. *Blood* **2012**, *120*, 4172, doi:10.1182/BLOOD-2012-06-437608.

166. Klatt, N.R.; Canary, L.A.; Sun, X.; Vinton, C.L.; Funderburg, N.T.; Morcock, D.R.; Quiñones, M.; Deming, C.B.; Perkins, M.; Hazuda, D.J.; et al. Probiotic/Prebiotic Supplementation of Antiretrovirals Improves Gastrointestinal Immunity in SIV-Infected Macaques. *J. Clin. Invest.* **2013**, *123*, 903, doi:10.1172/JCI66227.
167. Shytaj, I.L.; Norelli, S.; Chirullo, B.; Della Corte, A.; Collins, M.; Yalley-Ogunro, J.; Greenhouse, J.; Iraci, N.; Acosta, E.P.; Barreca, M.L.; et al. A Highly Intensified ART Regimen Induces Long-Term Viral Suppression and Restriction of the Viral Reservoir in a Simian AIDS Model. *PLoS Pathog.* **2012**, *8*, 1002774, doi:10.1371/JOURNAL.PPAT.1002774.
168. Dinoso, J.B.; Rabi, S.A.; Blankson, J.N.; Gama, L.; Mankowski, J.L.; Siliciano, R.F.; Zink, M.C.; Clements, J.E. A Simian Immunodeficiency Virus-Infected Macaque Model To Study Viral Reservoirs That Persist during Highly Active Antiretroviral Therapy. *J. Virol.* **2009**, *83*, 9247, doi:10.1128/JVI.00840-09.
169. Basmaciogullari, S.; Pizzato, M. The Activity of Nef on HIV-1 Infectivity. *Front. Microbiol.* **2014**, *5*, 232, doi:10.3389/FMICB.2014.00232/BIBTEX.
170. Daniel, M.D.; Kirchhoff, F.; Czajak, S.C.; Sehgal, P.K.; Desrosiers, R.C. Protective Effects of a Live Attenuated SIV Vaccine with a Deletion in the Nef Gene. *Science* **1992**, *258*, 1938–1941, doi:10.1126/SCIENCE.1470917.
171. Fukazawa, Y.; Park, H.; Cameron, M.J.; Lefebvre, F.; Lum, R.; Coombes, N.; Mahyari, E.; Hagen, S.I.; Bae, J.Y.; Reyes, M.D.; et al. Lymph Node T Cell Responses Predict the Efficacy of Live Attenuated SIV Vaccines. *Nat. Med.* **2012**, *18*, 1673, doi:10.1038/NM.2934.
172. Shaw, G.M.; Hunter, E. HIV Transmission. *Cold Spring Harb. Perspect. Med.* **2012**, *2*, doi:10.1101/cshperspect.a006965.
173. Getahun, H.; Gunneberg, C.; Granich, R.; Nunn, P. HIV Infection-Associated Tuberculosis: The Epidemiology and the Response. **2010**, *50*, 201–207, doi:10.1086/651492.
174. Gupta, A.; Wood, R.; Kaplan, R.; Bekker, L.G.; Lawn, S.D. Tuberculosis Incidence Rates during 8 Years of Follow-Up of an Antiretroviral Treatment Cohort in South Africa: Comparison with Rates in the Community. *PLoS One* **2012**, *7*, doi:10.1371/JOURNAL.PONE.0034156.
175. Gatechompol, S.; Sophonphan, J.; Ubolyam, S.; Avihingsanon, A.; van Leth, F.; Cobelens, F.; Kerr, S.J. Incidence and Factors Associated with Active Tuberculosis among People Living with HIV after Long-Term Antiretroviral Therapy in Thailand: A Competing Risk Model. *BMC Infect. Dis.* **2022**, *22*, 1–8, doi:10.1186/S12879-022-07332-3/TABLES/4.
176. World Health Organization *Global Tuberculosis Report 2021. Geneva: World*

Health Organization; 2021.; Geneva, 2021;
177. World Health Organization *Global Tuberculosis Report 2017*; Geneva, 2017;
178. Craig, G.M.; Daftary, A.; Engel, N.; O'Driscoll, S.; Ioannaki, A. Tuberculosis Stigma as a Social Determinant of Health: A Systematic Mapping Review of Research in Low Incidence Countries. *Int. J. Infect. Dis.* **2017**, *56*, 90–100, doi:10.1016/J.IJID.2016.10.011.
179. Rueda, S.; Mitra, S.; Chen, S.; Gogolishvili, D.; Globerman, J.; Chambers, L.; Wilson, M.; Logie, C.H.; Shi, Q.; Morassaei, S.; et al. Examining the Associations between HIV-Related Stigma and Health Outcomes in People Living with HIV/AIDS: A Series of Meta-Analyses. *BMJ Open* **2016**, *6*, e011453, doi:10.1136/BMJOPEN-2016-011453.
180. Pawlowski, A.; Jansson, M.; Sköld, M.; Rottenberg, M.E.; Källenius, G. Tuberculosis and HIV Co-Infection. *PLoS Pathog.* 2012, *8*, e1002464.
181. Günthard, H.F.; Saag, M.S.; Benson, C.A.; Del Rio, C.; Eron, J.J.; Gallant, J.E.; Hoy, J.F.; Mugavero, M.J.; Sax, P.E.; Thompson, M.A.; et al. Antiretroviral Drugs for Treatment and Prevention of HIV Infection in Adults: 2016 Recommendations of the International Antiviral Society–USA Panel. *JAMA* **2016**, *316*, 191–210, doi:10.1001/JAMA.2016.8900.
182. World Health Organization *WHO Consolidated Guidelines on Tuberculosis. Module 4, Treatment : Drug-Resistant Tuberculosis Treatment.*; 2020;
183. Organization, W.H. *Consolidated Guidelines on the Use of Antiretroviral Drugs for Treating and Preventing HIV Infection: Recommendations for a Public Health Approach*; 2nd ed.; World Health Organization, 2016;
184. Mesfin, Y.M.; Hailemariam, D.; Biadglign, S.; Kibret, K.T. Association between HIV/AIDS and Multi-Drug Resistance Tuberculosis: A Systematic Review and Meta-Analysis. *PLoS One* **2014**, *9*, doi:10.1371/journal.pone.0082235.
185. Chung-Delgado, K.; Guillen-Bravo, S.; Revilla-Montag, A.; Bernabe-Ortiz, A. Mortality among MDR-TB Cases: Comparison with Drug-Susceptible Tuberculosis and Associated Factors. *PLoS One* **2015**, *10*, e0119332, doi:10.1371/JOURNAL.PONE.0119332.
186. Bell, L.C.K.; Breen, R.; Miller, R.F.; Noursadeghi, M.; Lipman, M. Paradoxical Reactions and Immune Reconstitution Inflammatory Syndrome in Tuberculosis. *Int. J. Infect. Dis.* 2015, *32*, 39–45.
187. Lin, C.H.; Lin, C.J.; Kuo, Y.W.; Wang, J.Y.; Hsu, C.L.; Chen, J.M.; Cheng, W.C.; Lee, L.N. Tuberculosis Mortality: Patient Characteristics and Causes. *BMC Infect. Dis.* **2014**, *14*, 5, doi:10.1186/1471-2334-14-5.
188. Aabye, M.G.; Ravn, P.; PrayGod, G.; Jeremiah, K.; Mugomela, A.; Jepsen, M.; Faurholt, D.; Range, N.; Friis, H.; Changalucha, J.; et al. The Impact of HIV

Infection and CD4 Cell Count on the Performance of an Interferon Gamma Release Assay in Patients with Pulmonary Tuberculosis. *PLoS One* **2009**, *4*, e4220, doi:10.1371/JOURNAL.PONE.0004220.

189. Ma, Y.; Xu, Y.; Cao, X.; Chen, X.; Zhong, Y. Diagnostic Value of Interferon-γ Release Assay in HIV-Infected Individuals Complicated with Active Tuberculosis: A Systematic Review and Meta-Analysis. *Epidemiol. Infect.* **2021**, *149*, doi:10.1017/S0950268821001953.
190. Xue, M.; Xie, R.; Pang, Y.; Yan, S.; Du, Y.; Guan, C.; Chen, B. Prevalence and Risk Factors of Paradoxical Tuberculosis Associated Immune Reconstitution Inflammatory Syndrome among HIV-Infected Patients in Beijing, China. *BMC Infect. Dis.* **2020**, *20*, 554, doi:10.1186/s12879-020-05225-x.
191. Cevaal, P.M.; Bekker, L.G.; Hermans, S. TB-IRIS Pathogenesis and New Strategies for Intervention: Insights from Related Inflammatory Disorders. *Tuberculosis* 2019, *118*, 101863.
192. Lanzafame, M.; Vento, S. Tuberculosis-Immune Reconstitution Inflammatory Syndrome. *J. Clin. Tuberc. Other Mycobact. Dis.* 2016, *3*, 6–9.
193. Lanzafame, M.; Vento, S. Tuberculosis-Immune Reconstitution Inflammatory Syndrome. *J. Clin. Tuberc. Other Mycobact. Dis.* **2016**, *3*, 6–9, doi:10.1016/J.JCTUBE.2016.03.002.
194. Pawlowski, A.; Jansson, M.; Sköld, M.; Rottenberg, M.E.; Källenius, G. Tuberculosis and HIV Co-Infection. *PLoS Pathog.* 2012, *8*.
195. Bell, L.C.K.; Noursadeghi, M. Pathogenesis of HIV-1 and Mycobacterium Tuberculosis Co-Infection. *Nat. Rev. Microbiol.* **2018**, *16*, 80–90, doi:10.1038/nrmicro.2017.128.
196. Brune, K.A.; Ferreira, F.; Mandke, P.; Chau, E.; Aggarwal, N.R.; D'alessio, F.R.; Lambert, A.A.; Kirk, G.; Blankson, J.; Drummond, M.B.; et al. HIV Impairs Lung Epithelial Integrity and Enters the Epithelium to Promote Chronic Lung Inflammation. *PLoS One* **2016**, *11*, e0149679, doi:10.1371/JOURNAL.PONE.0149679.
197. Patel, N.R.; Swan, K.; Li, X.; Tachado, S.D.; Koziel, H. Impaired M. Tuberculosis-Mediated Apoptosis in Alveolar Macrophages from HIV+ Persons: Potential Role of IL-10 and BCL-3. *J. Leukoc. Biol.* **2009**, *86*, 53, doi:10.1189/JLB.0908574.
198. Patel, N.R.; Zhu, J.; Tachado, S.D.; Zhang, J.; Wan, Z.; Saukkonen, J.; Koziel, H. HIV Impairs TNF-α Mediated Macrophage Apoptotic Response to Mycobacterium Tuberculosis. *J. Immunol.* **2007**, *179*, 6973–6980, doi:10.4049/JIMMUNOL.179.10.6973.
199. Juffermans, N.P.; Speelman, P.; Verbon, A.; Veenstra, J.; Jie, C.; Van Deventer, S.J.H.; Van der Poll, T. Patients with Active Tuberculosis Have Increased

Expression of HIV Coreceptors CXCR4 and CCR5 on CD4(+) T Cells. *Clin. Infect. Dis.* **2001**, *32*, 650–652, doi:10.1086/318701.

200. Hoshino, Y.; Nakata, K.; Hoshino, S.; Honda, Y.; Tse, D.B.; Shioda, T.; Rom, W.N.; Weiden, M. Maximal HIV-1 Replication in Alveolar Macrophages during Tuberculosis Requires Both Lymphocyte Contact and Cytokines. *J. Exp. Med.* **2002**, *195*, 495–505, doi:10.1084/JEM.20011614.
201. Nakata, K.; Rom, W.N.; Honda, Y.; Condos, R.; Kanegasaki, S.; Cao, Y.; Weiden, M. Mycobacterium Tuberculosis Enhances Human Immunodeficiency Virus-1 Replication in the Lung. *Am. J. Respir. Crit. Care Med.* **1997**, *155*, 996–1003, doi:10.1164/AJRCCM.155.3.9117038.
202. Amelio, P.; Portevin, D.; Hella, J.; Reither, K.; Kamwela, L.; Lweno, O.; Tumbo, A.; Geoffrey, L.; Ohmiti, K.; Ding, S.; et al. HIV Infection Functionally Impairs Mycobacterium Tuberculosis-Specific CD4 and CD8 T-Cell Responses. *J. Virol.* **2019**, *93*, doi:10.1128/JVI.01728-18/ASSET/4E426FDC-5563-41FE-8743-D369A429E57A/ASSETS/GRAPHIC/JVI.01728-18-F0008.JPEG.
203. Day, C.L.; Mkhwanazi, N.; Reddy, S.; Mncube, Z.; Van Der Stok, M.; Klenerman, P.; Walker, B.D. Detection of Polyfunctional Mycobacterium Tubercubsis-Specific T Cells and Association with Viral Load in HIV-1-Infected Persons. *J. Infect. Dis.* **2008**, *197*, 990, doi:10.1086/529048.
204. Kalsdorf, B.; Scriba, T.J.; Wood, K.; Day, C.L.; Dheda, K.; Dawson, R.; Hanekom, W.A.; Lange, C.; Wilkinson, R.J. HIV-1 Infection Impairs the Bronchoalveolar T-Cell Response to Mycobacteria. *Am. J. Respir. Crit. Care Med.* **2009**, *180*, 1262, doi:10.1164/RCCM.200907-1011OC.
205. Cooper, A.M.; Torrado, E. Protection versus Pathology in Tuberculosis: Recent Insights. *Curr. Opin. Immunol.* **2012**, *24*, 431, doi:10.1016/J.COI.2012.04.008.
206. Huynh, K.K.; Joshi, S.A.; Brown, E.J. A Delicate Dance: Host Response to Mycobacteria. *Curr. Opin. Immunol.* **2011**, *23*, 464–472, doi:10.1016/J.COI.2011.06.002.
207. Donovan, M.L.; Schultz, T.E.; Duke, T.J.; Blumenthal, A. Type I Interferons in the Pathogenesis of Tuberculosis: Molecular Drivers and Immunological Consequences. *Front. Immunol.* **2017**, *8*, 1633, doi:10.3389/FIMMU.2017.01633.
208. Heyderman, R.S.; Makunike, R.; Muza, T.; Odwee, M.; Kadzirange, G.; Manyemba, J.; Muchedzi, C.; Ndemera, B.; Gomo, Z.A.R.; Gwanzura, L.K.Z.; et al. Pleural Tuberculosis in Harare, Zimbabwe: The Relationship between Human Immunodeficiency Virus, CD4 Lymphocyte Count, Granuloma Formation and Disseminated Disease. *Trop. Med. Int. Heal.* **1998**, *3*, 14–20, doi:10.1046/J.1365-3156.1998.00167.X.
209. Yone, E.W.P.; Kuaban, C.; Simo, L. [Tuberculous Pleural Effusion in Yaounde,

Cameroon: The Influence of HIV Infection]. *Rev. Mal. Respir.* **2011**, *28*, 1138–1145, doi:10.1016/J.RMR.2011.05.008.

210. Shen, J.-Y.; Barnest, P.F.; Rea, T.H.; Meyerj, P.R. Immunohistology of Tuberculous Adenitis in Symptomatic HIV Infection. *Clin. Exp. Immunol.* **1988**, *72*, 186.
211. Müller, H.; Krüger, S. Immunohistochemical Analysis of Cell Composition and in Situ Cytokine Expression in HIV- and Non-HIV-Associated Tuberculous Lymphadenitis. *Immunobiology* **1994**, *191*, 354–368, doi:10.1016/S0171-2985(11)80441-9.
212. Bezuidenhout, J.; Roberts, T.; Muller, L.; van Helden, P.; Walzl, G. Pleural Tuberculosis in Patients with Early HIV Infection Is Associated with Increased TNF-Alpha Expression and Necrosis in Granulomas. *PLoS One* **2009**, *4*, e4228, doi:10.1371/JOURNAL.PONE.0004228.
213. Van Der Ende, M.E.; Schutten, M.; Raschdorff, B.; Großschupff, G.; Racz, P.; Osterhaus, A.D.M.E.; Tenner-Racz, K. CD4 T Cells Remain the Major Source of HIV-1 during End Stage Disease. *AIDS* **1999**, *13*, 1015–1019, doi:10.1097/00002030-199906180-00002.
214. Shen, Y.; Zhou, D.; Chalifoux, L.; Shen, L.; Simon, M.; Zeng, X.; Lai, X.; Li, Y.; Sehgal, P.; Letvin, N.L.; et al. Induction of an AIDS Virus-Related Tuberculosis-like Disease in Macaques: A Model of Simian Immunodeficiency Virus-Mycobacterium Coinfection. *Infect. Immun.* **2002**, *70*, 869–877, doi:10.1128/IAI.70.2.869-877.2002/ASSET/733B60F0-84CF-421E-BD72-F02EA0989E4A/ASSETS/GRAPHIC/II0220774006.JPEG.
215. Foreman, T.W.; Mehra, S.; LoBato, D.N.; Malek, A.; Alvarez, X.; Golden, N.A.; Bucşan, A.N.; Didier, P.J.; Doyle-Meyers, L.A.; Russell-Lodrigue, K.E.; et al. CD4+ T-Cell-Independent Mechanisms Suppress Reactivation of Latent Tuberculosis in a Macaque Model of HIV Coinfection. *Proc. Natl. Acad. Sci. U. S. A.* **2016**, *113*, E5636–E5644, doi:10.1073/PNAS.1611987113/-/DCSUPPLEMENTAL.
216. Shen, Y.; Shen, L.; Sehgal, P.; Huang, D.; Qiu, L.; Du, G.; Letvin, N.L.; Chen, Z.W. Clinical Latency and Reactivation of AIDS-Related Mycobacterial Infections. *J. Virol.* **2004**, *78*, 14023–14032, doi:10.1128/JVI.78.24.14023-14032.2004/ASSET/3D30D429-4B5B-41E2-9442-522F43C601D9/ASSETS/GRAPHIC/ZJV0240455170005.JPEG.
217. Corleis, B.; Bucsan, A.N.; Deruaz, M.; Vrbanac, V.D.; Lisanti-Park, A.C.; Gates, S.J.; Linder, A.H.; Paer, J.M.; Olson, G.S.; Bowman, B.A.; et al. HIV-1 and SIV Infection Are Associated with Early Loss of Lung Interstitial CD4+ T Cells and Dissemination of Pulmonary Tuberculosis. *Cell Rep.* **2019**, *26*, 1409-1418.e5,

doi:10.1016/j.celrep.2019.01.021.

218. Mehra, S.; Golden, N.A.; Dutta, N.K.; Midkiff, C.C.; Alvarez, X.; Doyle, L.A.; Asher, M.; Russell-Lodrigue, K.; Monjure, C.; Roy, C.J.; et al. Reactivation of Latent Tuberculosis in Rhesus Macaques by Co-Infection with Simian Immunodeficiency Virus. *J. Med. Primatol.* **2011**, *40*, 233, doi:10.1111/J.1600-0684.2011.00485.X.
219. Diedrich, C.R.; Mattila, J.T.; Klein, E.; Janssen, C.; Phuah, J.; Sturgeon, T.J.; Montelaro, R.C.; Lin, P.L.; Flynn, J.A.L. Reactivation of Latent Tuberculosis in Cynomolgus Macaques Infected with SIV Is Associated with Early Peripheral T Cell Depletion and Not Virus Load. *PLoS One* **2010**, *5*, doi:10.1371/JOURNAL.PONE.0009611.
220. Bucşan, A.N.; Chatterjee, A.; Singh, D.K.; Foreman, T.W.; Lee, T.H.; Threeton, B.; Kirkpatrick, M.G.; Ahmed, M.; Golden, N.; Alvarez, X.; et al. Mechanisms of Reactivation of Latent Tuberculosis Infection Due to SIV Coinfection. *J. Clin. Invest.* **2019**, *129*, 5254, doi:10.1172/JCI125810.
221. Ganatra, S.R.; Bucşan, A.N.; Alvarez, X.; Kumar, S.; Chatterjee, A.; Quezada, M.; Fish, A.; Singh, D.K.; Singh, B.; Sharan, R.; et al. Antiretroviral Therapy Does Not Reduce Tuberculosis Reactivation in a Tuberculosis-HIV Coinfection Model. *J. Clin. Invest.* **2020**, *130*, 5171–5179, doi:10.1172/JCI136502.
222. Sharan, R.; Ganatra, S.R.; Bucsan, A.N.; Cole, J.; Singh, D.K.; Alvarez, X.; Gough, M.; Alvarez, C.; Blakley, A.; Ferdin, J.; et al. Antiretroviral Therapy Timing Impacts Latent Tuberculosis Infection Reactivation in a Mycobacterium Tuberculosis/SIV Coinfection Model. *J. Clin. Invest.* **2022**, *132*, doi:10.1172/JCI153090.
223. Rangaka, M.X.; Wilkinson, R.J.; Boulle, A.; Glynn, J.R.; Fielding, K.; Van Cutsem, G.; Wilkinson, K.A.; Goliath, R.; Mathee, S.; Goemaere, E.; et al. Isoniazid plus Antiretroviral Therapy to Prevent Tuberculosis: A Randomised Double-Blind Placebo-Controlled Trial. *Lancet* **2014**, *384*, 682, doi:10.1016/S0140-6736(14)60162-8.
224. Depincé-Berger, A.E.; Vergnon-Miszczycha, D.; Girard, A.; Frésard, A.; Botelho-Nevers, E.; Lambert, C.; Tedesco, E.; Genin, C.; Pozzetto, B.; Lucht, F.; et al. Major Influence of CD4 Count at the Initiation of CART on Viral and Immunological Reservoir Constitution in HIV-1 Infected Patients. *Retrovirology* **2016**, *13*, 44, doi:10.1186/S12977-016-0278-5.
225. Potash, M.J.; Chao, W.; Bentsman, G.; Paris, N.; Saini, M.; Nitkiewicz, J.; Belem, P.; Sharer, L.; Brooks, A.I.; Volsky, D.J. A Mouse Model for Study of Systemic HIV-1 Infection, Antiviral Immune Responses, and Neuroinvasiveness. *Proc. Natl. Acad. Sci. U. S. A.* **2005**, *102*, 3760, doi:10.1073/PNAS.0500649102.

226. Hadas, E.; Borjabad, A.; Chao, W.; Saini, M.; Ichiyama, K.; Potash, M.J.; Volsky, D.J. Testing Antiretroviral Drug Efficacy in Conventional Mice Infected with Chimeric HIV-1. *AIDS* **2007**, *21*, 905–909, doi:10.1097/QAD.0B013E3281574549.
227. Evans, D.T.; Silvestri, G. Nonhuman Primate Models in AIDS Research. *Curr. Opin. HIV AIDS* 2013, *8*, 255–261.
228. Shultz, L.D.; Brehm, M.A.; Victor Garcia-Martinez, J.; Greiner, D.L. Humanized Mice for Immune System Investigation: Progress, Promise and Challenges. *Nat. Rev. Immunol.* 2012, *12*, 786–798.
229. Shultz, L.D.; Brehm, M.A.; Bavari, S.; Greiner, D.L. Humanized Mice as a Preclinical Tool for Infectious Disease and Biomedical Research., doi:10.1111/j.1749-6632.2011.06310.x.
230. Skelton, J.K.; Ortega-Prieto, A.M.; Dorner, M. A Hitchhiker's Guide to Humanized Mice: New Pathways to Studying Viral Infections. *Immunology* **2018**, *154*, 50–61, doi:10.1111/imm.12906.
231. Gillgrass, A.; Wessels, J.M.; Yang, J.X.; Kaushic, C. Advances in Humanized Mouse Models to Improve Understanding of HIV-1 Pathogenesis and Immune Responses. *Front. Immunol.* **2021**, *11*, 1, doi:10.3389/fimmu.2020.617516.
232. Walsh, N.C.; Kenney, L.L.; Jangalwe, S.; Aryee, K.-E.; Greiner, D.L.; Brehm, M.A.; Shultz, L.D. Humanized Mouse Models of Clinical Disease. *Annu. Rev. Pathol. Mech. Dis.* **2017**, *12*, 187–215, doi:10.1146/annurev-pathol-052016-100332.
233. Yong, K.S.M.; Her, Z.; Chen, Q. Humanized Mice as Unique Tools for Human-Specific Studies. *Arch. Immunol. Ther. Exp. (Warsz).* 2018, *66*, 245–266.
234. McCune, J.M.; Namikawa, R.; Kaneshima, H.; Shultz, L.D.; Lieberman, M.; Weissman, I.L. The SCID-Hu Mouse: Murine Model for the Analysis of Human Hematolymphoid Differentiation and Function. *Science (80-.).* **1988**, *241*, 1632–1639, doi:10.1126/science.2971269.
235. PRKDC Protein Kinase, DNA-Activated, Catalytic Subunit [Homo Sapiens (Human)] - Gene - NCBI Available online: https://www.ncbi.nlm.nih.gov/gene?Db=gene&Cmd=ShowDetailView&TermToSearch=5591 (accessed on 23 December 2019).
236. Moore, J.K.; Haber, J.E. Cell Cycle and Genetic Requirements of Two Pathways of Nonhomologous End-Joining Repair of Double-Strand Breaks in Saccharomyces Cerevisiae. *Mol. Cell. Biol.* **1996**, *16*, 2164–2173, doi:10.1128/mcb.16.5.2164.
237. Bosma, M.J.; Carroll, A.M. The Scid Mouse Mutant: Definition, Characterization, and Potential Uses. *Annu. Rev. Immunol.* 1991, *9*, 323–350.
238. Hoffmann-Fezer, G.; Gall, C.; Zengerle, U.; Kranz, B.; Thierfelder, S.

Immunohistology and Immunocytology of Human T-Cell Chimerism and Graft-versus-Host Disease in SCID Mice. *Blood* **1993**, *81*, 3440–3448, doi:10.1182/blood.V81.12.3440.3440.

239. Takenaka, K.; Prasolava, T.K.; Wang, J.C.Y.; Mortin-Toth, S.M.; Khalouei, S.; Gan, O.I.; Dick, J.E.; Danska, J.S. Polymorphism in Sirpa Modulates Engraftment of Human Hematopoietic Stem Cells. **2007**, doi:10.1038/ni1527.
240. Kwong, L.S.; Brown, M.H.; Barclay, A.N.; Hatherley, D. Signal-Regulatory Protein α from the NOD Mouse Binds Human CD47 with an Exceptionally High Affinity - Implications for Engraftment of Human Cells. *Immunology* **2014**, *143*, 61–67, doi:10.1111/imm.12290.
241. Tang, Q.; Adams, J.Y.; Penaranda, C.; Melli, K.; Piaggio, E.; Sgouroudis, E.; Piccirillo, C.A.; Salomon, B.L.; Bluestone, J.A. Central Role of Defective Interleukin-2 Production in the Triggering of Islet Autoimmune Destruction. *Immunity* **2008**, *28*, 687–697, doi:10.1016/j.immuni.2008.03.016.
242. Sugamura, K.; Asao, H.; Kondo, M.; Tanaka, N.; Ishii, N.; Ohbo, K.; Nakamura, M.; Takeshita, T. *THE INTERLEUKIN-2 RECEPTOR γ CHAIN: Its Role in the Multiple Cytokine Receptor Complexes and T Cell Development in XSCID*; 1996; Vol. 14;.
243. Cao, X.; Shores, E.W.; Hu-LI, J.; Ft Anver, M.; Kelsall, B.L.; R, S.M.; Drago, J.; Masayuki Noguchi, O.; Grinberg, A.; Eda Bloom, O.T.; et al. *Defective Lymphoid Development in Mice Lacking Expression of the Common Cytokine Receptor y Chain*; 1995; Vol. 2;.
244. Shultz, L.D.; Lyons, B.L.; Burzenski, L.M.; Gott, B.; Chen, X.; Chaleff, S.; Kotb, M.; Gillies, S.D.; King, M.; Mangada, J.; et al. Human Lymphoid and Myeloid Cell Development in NOD/LtSz- Scid IL2R γ Null Mice Engrafted with Mobilized Human Hemopoietic Stem Cells . *J. Immunol.* **2005**, *174*, 6477–6489, doi:10.4049/jimmunol.174.10.6477.
245. McDermott, S.P.; Eppert, K.; Lechman, E.R.; Doedens, M.; Dick, J.E. Comparison of Human Cord Blood Engraftment between Immunocompromised Mouse Strains. *Blood* **2010**, *116*, 193–200, doi:10.1182/blood-2010-02-271841.
246. Watanabe, Y.; Takahashi, T.; Okajima, A.; Shiokawa, M.; Ishii, N.; Katano, I.; Ito, R.; Ito, M.; Minegishi, M.; Minegishi, N.; et al. The Analysis of the Functions of Human B and T Cells in Humanized NOD/Shi-Scid/Γcnull (NOG) Mice (Hu-HSC NOG Mice). *Int. Immunol.* **2009**, *21*, 843–858, doi:10.1093/intimm/dxp050.
247. Goldman, J.P.; Blundell, M.P.; Lopes, L.; Kinnon, C.; DI Santo, J.P.; Thrasher, A.J. Enhanced Human Cell Engraftment in Mice Deficient in RAG2 and the Common Cytokine Receptor Gamma Chain. *Br. J. Haematol.* **1998**, *103*, 335–342, doi:10.1046/j.1365-2141.1998.00980.x.

248. Pearson, T.; Shultz, L.D.; Miller, D.; King, M.; Laning, J.; Fodor, W.; Cuthbert, A.; Burzenski, L.; Gott, B.; Lyons, B.; et al. Non-Obese Diabetic-Recombination Activating Gene-1 (NOD-Rag1 Null) Interleukin (IL)-2 Receptor Common Gamma Chain (IL2rg Null) Null Mice: A Radioresistant Model for Human Lymphohaematopoietic Engraftment. **2008**, doi:10.1111/j.1365-2249.2008.03753.x.
249. Pearson, T.; Greiner, D.L.; Shultz, L.D. Creation of "Humanized" Mice to Study Human Immunity. *Curr. Protoc. Immunol.* **2008**, *81*, 15.21.1-15.21.21, doi:10.1002/0471142735.im1521s81.
250. Karpel, M.E.; Boutwell, C.L.; Allen, T.M. BLT Humanized Mice as a Small Animal Model of HIV Infection. *Curr. Opin. Virol.* **2015**, *13*, 75–80, doi:10.1016/j.coviro.2015.05.002.
251. Brainard, D.M.; Seung, E.; Frahm, N.; Cariappa, A.; Bailey, C.C.; Hart, W.K.; Shin, H.-S.; Brooks, S.F.; Knight, H.L.; Eichbaum, Q.; et al. Induction of Robust Cellular and Humoral Virus-Specific Adaptive Immune Responses in Human Immunodeficiency Virus-Infected Humanized BLT Mice. *J. Virol.* **2009**, *83*, 7305–7321, doi:10.1128/jvi.02207-08.
252. Lan, P.; Tonomura, N.; Shimizu, A.; Wang, S.; Yang, Y.G. Reconstitution of a Functional Human Immune System in Immunodeficient Mice through Combined Human Fetal Thymus/Liver and CD34+ Cell Transplantation. *Blood* **2006**, *108*, 487–492, doi:10.1182/blood-2005-11-4388.
253. Cheng, L.; Ma, J.; Li, G.; Su, L. Humanized Mice Engrafted with Human HSC Only or HSC and Thymus Support Comparable HIV-1 Replication, Immunopathology, and Responses to ART and Immune Therapy. *Front. Immunol.* **2018**, *9*, doi:10.3389/fimmu.2018.00817.
254. Denton, P.W.; Nochi, T.; Lim, A.; Krisko, J.F.; Martinez-Torres, F.; Choudhary, S.K.; Wahl, A.; Olesen, R.; Zou, W.; Di Santo, J.P.; et al. IL-2 Receptor γ-Chain Molecule Is Critical for Intestinal T-Cell Reconstitution in Humanized Mice. *Mucosal Immunol.* **2012**, *5*, 555–566, doi:10.1038/mi.2012.31.
255. Nochi, T.; Denton, P.W.; Wahl, A.; Garcia, J.V. Cryptopatches Are Essential for the Development of Human GALT. *Cell Rep.* **2013**, *3*, 1874–1884, doi:10.1016/j.celrep.2013.05.037.
256. Brehm, M.A.; Wiles, M. V.; Greiner, D.L.; Shultz, L.D. Generation of Improved Humanized Mouse Models for Human Infectious Diseases. *J. Immunol. Methods* **2014**, *410*, 3–17, doi:10.1016/J.JIM.2014.02.011.
257. Allen, T.M.; Brehm, M.A.; Bridges, S.; Ferguson, S.; Kumar, P.; Mirochnitchenko, O.; Palucka, K.; Pelanda, R.; Sanders-Beer, B.; Shultz, L.D.; et al. *Humanized Immune System Mouse Models: Progress, Challenges and Opportunities the*

National Institute of Allergy and Infectious Diseases Convened a Workshop Entitled 'Recent Advances and Opportunities in the Development and Use of Humanized Immune System Mo; 2018;

258. Shultz, L.D.; Brehm, M.A.; Victor Garcia-Martinez, J.; Greiner, D.L. Humanized Mice for Immune System Investigation: Progress, Promise and Challenges. *Nat. Rev. Immunol.* **2012**, *12*, 786, doi:10.1038/NRI3311.
259. Brehm, M.A.; Cuthbert, A.; Yang, C.; Miller, D.M.; DiIorio, P.; Laning, J.; Burzenski, L.; Gott, B.; Foreman, O.; Kavirayani, A.; et al. Parameters for Establishing Humanized Mouse Models to Study Human Immunity: Analysis of Human Hematopoietic Stem Cell Engraftment in Three Immunodeficient Strains of Mice Bearing the IL2rγnull Mutation. *Clin. Immunol.* **2010**, *135*, 84–98, doi:10.1016/j.clim.2009.12.008.
260. Ohbo, K.; Suda, T.; Hashiyama, M.; Mantani, A.; Ikebe, M.; Miyakawa, K.; Moriyama, M.; Nakamura, M.; Katsuki, M.; Takahashi, K.; et al. Modulation of Hematopoiesis in Mice with a Truncated Mutant of the Interleukin-2 Receptor γ Chain. *Blood* **1996**, *87*, 956–967, doi:10.1182/blood.v87.3.956.bloodjournal873956.
261. Pearson, T.; Shultz, L.D.; Miller, D.; King, M.; Laning, J.; Fodor, W.; Cuthbert, A.; Burzenski, L.; Gott, B.; Lyons, B.; et al. Non-Obese Diabetic-Recombination Activating Gene-1 (NOD-Rag1 Null) Interleukin (IL)-2 Receptor Common Gamma Chain (IL2rγnull) Null Mice: A Radioresistant Model for Human Lymphohaematopoietic Engraftment. *Clin. Exp. Immunol.* **2008**, *154*, 270–284, doi:10.1111/j.1365-2249.2008.03753.x.
262. Fulop, G.M.; Phillips, R.A. The Scid Mutation in Mice Causes a General Defect in DNA Repair. *Nature* **1990**, *347*, 479–482, doi:10.1038/347479a0.
263. McCune, J.M.; Weissman, I.L. The Ban on US Government Funding Research Using Human Fetal Tissues: How Does This Fit with the NIH Mission to Advance Medical Science for the Benefit of the Citizenry? *Stem Cell Reports* 2019, *13*, 777–786.
264. Lavender, K.J.; Pang, W.W.; Messer, R.J.; Duley, A.K.; Race, B.; Phillips, K.; Scott, D.; Peterson, K.E.; Chan, C.K.; Dittmer, U.; et al. BLT-Humanized C57BL/6 Rag2-/-Γc-/-CD47-/- Mice Are Resistant to GVHD and Develop B- and T-Cell Immunity to HIV Infection. *Blood* **2013**, *122*, 4013–4020, doi:10.1182/blood-2013-06-506949.
265. Masemann, D.; Ludwig, S.; Boergeling, Y. Advances in Transgenic Mouse Models to Study Infections by Human Pathogenic Viruses. *Int. J. Mol. Sci.* **2020**, *21*, 1–20, doi:10.3390/IJMS21239289.
266. Dash, P.K.; Gorantla, S.; Poluektova, L.; Hasan, M.; Waight, E.; Zhang, C.;

Markovic, M.; Edagwa, B.; Machhi, J.; Olson, K.E.; et al. Humanized Mice for Infectious and Neurodegenerative Disorders. *Retrovirology 2021 181* **2021**, *18*, 1–17, doi:10.1186/S12977-021-00557-1.

267. Li, Y.; Masse-Ranson, G.; Garcia, Z.; Bruel, T.; Kök, A.; Strick-Marchand, H.; Jouvion, G.; Serafini, N.; Lim, A.I.; Dusseaux, M.; et al. A Human Immune System Mouse Model with Robust Lymph Node Development. *Nat. Methods* **2018**, *15*, 623–630, doi:10.1038/s41592-018-0071-6.
268. Matsuda, M.; Ono, R.; Iyoda, T.; Endo, T.; Iwasaki, M.; Tomizawa-Murasawa, M.; Saito, Y.; Kaneko, A.; Shimizu, K.; Yamada, D.; et al. Human NK Cell Development in HIL-7 and HIL-15 Knockin NOD/SCID/IL2rgKO Mice. *Life Sci. Alliance* **2019**, *2*, e201800195, doi:10.26508/lsa.201800195.
269. Herndler-Brandstetter, D.; Shan, L.; Yao, Y.; Stecher, C.; Plajer, V.; Lietzenmayer, M.; Strowig, T.; De Zoete, M.R.; Palm, N.W.; Chen, J.; et al. Humanized Mouse Model Supports Development, Function, and Tissue Residency of Human Natural Killer Cells. *Proc. Natl. Acad. Sci. U. S. A.* **2017**, *114*, E9626–E9634, doi:10.1073/pnas.1705301114.
270. Majji, S.; Wijayalath, W.; Shashikumar, S.; Pow-Sang, L.; Villasante, E.; Brumeanu, T.D.; Casares, S. Differential Effect of HLA Class-I versus Class-II Transgenes on Human T and B Cell Reconstitution and Function in NRG Mice. *Sci. Rep.* **2016**, *6*, 1–13, doi:10.1038/srep28093.
271. Allam, A.; Majji, S.; Peachman, K.; Jagodzinski, L.; Kim, J.; Ratto-Kim, S.; Wijayalath, W.; Merbah, M.; Kim, J.H.; Michael, N.L.; et al. TFH Cells Accumulate in Mucosal Tissues of Humanized-DRAG Mice and Are Highly Permissive to HIV-1. *Sci. Rep.* **2015**, *5*, 10443–16, doi:10.1038/srep10443.
272. Kim, J.; Peachman, K.K.; Jobe, O.; Morrison, E.B.; Allam, A.; Jagodzinski, L.; Casares, S.A.; Rao, M. Tracking Human Immunodeficiency Virus-1 Infection in the Humanized DRAG Mouse Model. *Front. Immunol.* **2017**, *8*, doi:10.3389/fimmu.2017.01405.
273. Jaiswal, S.; Pearson, T.; Friberg, H.; Shultz, L.D.; Greiner, D.L.; Rothman, A.L.; Mathew, A. Dengue Virus Infection and Virus-Specific HLA-A2 Restricted Immune Responses in Humanized NOD-Scid IL2rγnull Mice. *PLoS One* **2009**, *4*, doi:10.1371/journal.pone.0007251.
274. Shultz, L.D.; Saito, Y.; Najima, Y.; Tanaka, S.; Ochi, T.; Tomizawa, M.; Doi, T.; Sone, A.; Suzuki, N.; Fujiwara, H.; et al. Generation of Functional Human T-Cell Subsets with HLA-Restricted Immune Responses in HLA Class I Expressing NOD/SCID/IL2rγnull Humanized Mice. *Proc. Natl. Acad. Sci. U. S. A.* **2010**, *107*, 13022–13027, doi:10.1073/pnas.1000475107.
275. Danner, R.; Chaudhari, S.N.; Rosenberger, J.; Surls, J.; Richie, T.L.; Brumeanu,

T.D.; Casares, S. Expression of HLA Class II Molecules in Humanized NOD.Rag1KO.IL2RgcKO Mice Is Critical for Development and Function of Human T and B Cells. *PLoS One* **2011**, *6*, e19826, doi:10.1371/journal.pone.0019826.

276. Cauvin, A.J.; Peters, C.; Brennan, F. Advantages and Limitations of Commonly Used Nonhuman Primate Species in Research and Development of Biopharmaceuticals. *Nonhum. Primate Nonclinical Drug Dev. Saf. Assess.* **2015**, 379, doi:10.1016/B978-0-12-417144-2.00019-6.
277. Abeynaike, S.; Paust, S. Humanized Mice for the Evaluation of Novel HIV-1 Therapies. *Front. Immunol.* **2021**, *12*, 776, doi:10.3389/FIMMU.2021.636775/BIBTEX.
278. Tager, A.M.; Pensiero, M.; Allen, T.M. Recent Advances in Humanized Mice: Accelerating the Development of an HIV Vaccine. *J. Infect. Dis.* **2013**, *208*, S121, doi:10.1093/INFDIS/JIT451.
279. Berges, B.K.; Akkina, S.R.; Folkvord, J.M.; Connick, E.; Akkina, R. Mucosal Transmission of R5 and X4 Tropic HIV-1 via Vaginal and Rectal Routes in Humanized Rag2-/-Γc-/- (RAG-Hu) Mice. *Virology* **2008**, *373*, 342–351, doi:10.1016/j.virol.2007.11.020.
280. Sun, Z.; Denton, P.W.; Estes, J.D.; Othieno, F.A.; Wei, B.L.; Wege, A.K.; Melkus, M.W.; Padgett-Thomas, A.; Zupancic, M.; Haase, A.T.; et al. Intrarectal Transmission, Systemic Infection, and CD4+ T Cell Depletion in Humanized Mice Infected with HIV-1. *J. Exp. Med.* **2007**, *204*, 705–714, doi:10.1084/jem.20062411.
281. Dudek, T.E.; No, D.C.; Seung, E.; Vrbanac, V.D.; Fadda, L.; Bhoumik, P.; Boutwell, C.L.; Power, K.A.; Gladden, A.D.; Battis, L.; et al. Rapid Evolution of HIV-1 to Functional CD8+ T Cell Responses in Humanized BLT Mice. *Sci. Transl. Med.* **2012**, *4*, doi:10.1126/scitranslmed.3003984.
282. Denton, P.W.; Estes, J.D.; Sun, Z.; Othieno, F.A.; Wei, B.L.; Wege, A.K.; Powell, D.A.; Payne, D.; Haase, A.T.; Garcia, J.V. Antiretroviral Pre-Exposure Prophylaxis Prevents Vaginal Transmission of HIV-1 in Humanized BLT Mice. *PLoS Med.* **2008**, *5*, e16, doi:10.1371/journal.pmed.0050016.
283. Watanabe, S.; Terashima, K.; Ohta, S.; Horibata, S.; Yajima, M.; Shiozawa, Y.; Zahidunnabi Dewan, M.; Yu, Z.; Ito, M.; Morio, T.; et al. Hematopoietic Stem Cell-Engrafted NOD/SCID/IL2Rγnull Mice Develop Human Lymphoid Systems and Induce Long-Lasting HIV-1 Infection with Specific Humoral Immune Responses. *Blood* **2007**, *109*, 212–218, doi:10.1182/blood-2006-04-017681.
284. Sato, K.; Nie, C.; Misawa, N.; Tanaka, Y.; Ito, M.; Koyanagi, Y. Dynamics of Memory and Naïve CD8+ T Lymphocytes in Humanized NOD/SCID/IL-2Rγnull

Mice Infected with CCR5-Tropic HIV-1. *Vaccine* **2010**, *28*, B32–B37, doi:10.1016/j.vaccine.2009.10.154.

285. Nie, C.; Sato, K.; Misawa, N.; Kitayama, H.; Fujino, H.; Hiramatsu, H.; Heike, T.; Nakahata, T.; Tanaka, Y.; Ito, M.; et al. Selective Infection of CD4+ Effector Memory T Lymphocytes Leads to Preferential Depletion of Memory T Lymphocytes in R5 HIV-1-Infected Humanized NOD/SCID/IL-2Rγnull Mice. *Virology* **2009**, *394*, 64–72, doi:10.1016/j.virol.2009.08.011.
286. Berges, B.K.; Wheat, W.H.; Palmer, B.E.; Connick, E.; Akkina, R. HIV-1 Infection and CD4 T Cell Depletion in the Humanized Rag2-/-Γc-/- (RAG-Hu) Mouse Model. *Retrovirology* **2006**, *3*, doi:10.1186/1742-4690-3-76.
287. Dong, S.A.; Poon, B.; Fang, R.H.T.; Weijer, K.; Blom, B.; Spits, H.; Chen, I.S.Y.; Uittenbogaart, C.H. Use of a Novel Chimeric Mouse Model with a Functionally Active Human Immune System to Study Human Immunodeficiency Virus Type 1 Infection. *Clin. Vaccine Immunol.* **2007**, *14*, 391–396, doi:10.1128/CVI.00403-06.
288. Zhang, L.; Kovalev, G.I.; Su, L. HIV-1 Infection and Pathogenesis in a Novel Humanized Mouse Model. *Blood* **2007**, *109*, 2978–2981, doi:10.1182/blood-2006-07-033159.
289. Berges, B.K.; Akkina, S.R.; Remling, L.; Akkina, R. Humanized Rag2-/-Γc-/- (RAG-Hu) Mice Can Sustain Long-Term Chronic HIV-1 Infection Lasting More than a Year. *Virology* **2010**, *397*, 100–103, doi:10.1016/j.virol.2009.10.034.
290. Su, H.; Cheng, Y.; Sravanam, S.; Mathews, S.; Gorantla, S.; Poluektova, L.Y.; Dash, P.K.; Gendelman, H.E. Immune Activations and Viral Tissue Compartmentalization during Progressive HIV-1 Infection of Humanized Mice. *Front. Immunol.* **2019**, *10*, 340–17, doi:10.3389/fimmu.2019.00340.
291. Honeycutt, J.B.; Wahl, A.; Baker, C.; Spagnuolo, R.A.; Foster, J.; Zakharova, O.; Wietgrefe, S.; Caro-Vegas, C.; Madden, V.; Sharpe, G.; et al. Macrophages Sustain HIV Replication *in vivo* Independently of T Cells. *J. Clin. Invest.* **2016**, *126*, 1353–1366, doi:10.1172/JCI84456.
292. Islas-Ohlmayer, M.; Padgett-Thomas, A.; Domiati-Saad, R.; Melkus, M.W.; Cravens, P.D.; Martin, M. d. P.; Netto, G.; Garcia, J. V. Experimental Infection of NOD/SCID Mice Reconstituted with Human CD34+ Cells with Epstein-Barr Virus. *J. Virol.* **2004**, *78*, 13891–13900, doi:10.1128/jvi.78.24.13891-13900.2004.
293. Cravens, P.D.; Melkus, M.W.; Padgett-Thomas, A.; Islas-Ohlmayer, M.; del P. Martin, M.; Garcia, J.V. Development and Activation of Human Dendritic Cells *In vivo* in a Xenograft Model of Human Hematopoiesis. *Stem Cells* **2005**, *23*, 264–278, doi:10.1634/stemcells.2004-0116.
294. Choudhary, S.K.; Rezk, N.L.; Ince, W.L.; Cheema, M.; Zhang, L.; Su, L.; Swanstrom, R.; Kashuba, A.D.M.; Margolis, D.M. Suppression of Human

Immunodeficiency Virus Type 1 (HIV-1) Viremia with Reverse Transcriptase and Integrase Inhibitors, CD4+ T-Cell Recovery, and Viral Rebound upon Interruption of Therapy in a New Model for HIV Treatment in the Humanized Rag2-/- c-/- Mouse. *J. Virol.* **2009**, *83*, 8254–8258, doi:10.1128/jvi.00580-09.

295. Satheesan, S.; Li, H.; Burnett, J.C.; Takahashi, M.; Li, S.; Wu, S.X.; Synold, T.W.; Rossi, J.J.; Zhou, J. HIV Replication and Latency in a Humanized NSG Mouse Model during Suppressive Oral Combinational Antiretroviral Therapy. *J. Virol.* **2018**, *92*, e02118-17, doi:10.1128/jvi.02118-17.
296. Stoddart, C.A.; Galkina, S.A.; Joshi, P.; Kosikova, G.; Moreno, M.E.; Rivera, J.M.; Sloan, B.; Reeve, A.B.; Sarafianos, S.G.; Murphey-Corb, M.; et al. Oral Administration of the Nucleoside EFdA (4′-Ethynyl-2-Fluoro-2′-Deoxyadenosine) Provides Rapid Suppression of HIV Viremia in Humanized Mice and Favorable Pharmacokinetic Properties in Mice and the Rhesus Macaque. *Antimicrob. Agents Chemother.* **2015**, *59*, 4190–4198, doi:10.1128/AAC.05036-14.
297. Shanmugasundaram, U.; Kovarova, M.; Ho, P.T.; Schramm, N.; Wahl, A.; Parniak, M.A.; Garcia, J.V. Efficient Inhibition of HIV Replication in the Gastrointestinal and Female Reproductive Tracts of Humanized BLT Mice by EFdA. *PLoS One* **2016**, *11*, e0159517, doi:10.1371/journal.pone.0159517.
298. Sango, K.; Joseph, A.; Patel, M.; Osiecki, K.; Dutta, M.; Goldstein, H. Highly Active Antiretroviral Therapy Potently Suppresses HIV Infection in Humanized Rag2-/-Γc-/- Mice. *AIDS Res. Hum. Retroviruses* **2010**, *26*, 735–746, doi:10.1089/aid.2009.0136.
299. Kim, K.C.; Choi, B.S.; Kim, K.C.; Park, K.H.; Lee, H.J.; Cho, Y.K.; Kim, S. Il; Kim, S.S.; Oh, Y.K.; Kim, Y.B. A Simple Mouse Model for the Study of Human Immunodeficiency Virus. *AIDS Res. Hum. Retroviruses* **2016**, *32*, 194–202, doi:10.1089/aid.2015.0211.
300. Kovarova, M.; Rahima Benhabbour, S.; Massud, I.; Spagnuolo, R.A.; Skinner, B.; Baker, C.E.; Sykes, C.; Mollan, K.R.; Kashuba, A.D.M.; Gerardo García-Lerma, J.; et al. Ultra-Long-Acting Removable Drug Delivery System for HIV Treatment and Prevention., doi:10.1038/s41467-018-06490-w.
301. Kovarova, M.; Swanson, M.D.; Sanchez, R.I.; Baker, C.E.; Steve, J.; Spagnuolo, R.A.; Howell, B.J.; Hazuda, D.J.; Victor Garcia, J. A Long-Acting Formulation of the Integrase Inhibitor Raltegravir Protects Humanized BLT Mice from Repeated High-Dose Vaginal HIV Challenges. *J. Antimicrob. Chemother.* **2016**, *71*, 1586–1596, doi:10.1093/jac/dkw042.
302. Neff, C.P.; Kurisu, T.; Ndolo, T.; Fox, K.; Akkina, R. A Topical Microbicide Gel Formulation of CCR5 Antagonist Maraviroc Prevents HIV-1 Vaginal Transmission in Humanized RAG-Hu Mice. *PLoS One* **2011**, *6*, e20209,

doi:10.1371/journal.pone.0020209.

303. Denton, P.W.; Krisko, J.F.; Powell, D.A.; Mathias, M.; Kwak, Y.T.; Martinez-Torres, F.; Zou, W.; Payne, D.A.; Estes, J.D.; Garcia, J.V. Systemic Administration of Antiretrovirals Prior to Exposure Prevents Rectal and Intravenous HIV-1 Transmission in Humanized BLT Mice. *PLoS One* **2010**, *5*, e8829, doi:10.1371/journal.pone.0008829.
304. Veselinovic, M.; Yang, K.H.; Sykes, C.; Remling-Mulder, L.; Kashuba, A.D.M.; Akkina, R. Mucosal Tissue Pharmacokinetics of the Integrase Inhibitor Raltegravir in a Humanized Mouse Model: Implications for HIV Pre-Exposure Prophylaxis. *Virology* **2016**, *489*, 173–178, doi:10.1016/j.virol.2015.12.014.
305. Rochat, M.A.; Schlaepfer, E.; Kuster, S.P.; Li, D.; Audige, A.; Ivic, S.; Fahrny, A.; Speck, R.F. Monitoring HIV DNA and Cellular Activation Markers in HIV-Infected Humanized Mice under CART. *Virol. J.* **2018**, *15*, 191–198, doi:10.1186/s12985-018-1101-9.
306. Amet, T.; Nonaka, M.; Dewan, M.Z.; Saitoh, Y.; Qi, X.; Ichinose, S.; Yamamoto, N.; Yamaoka, S. Statin-Induced Inhibition of HIV-1 Release from Latently Infected U1 Cells Reveals a Critical Role for Protein Prenylation in HIV-1 Replication. *Microbes Infect.* **2008**, *10*, 471–480, doi:10.1016/j.micinf.2008.01.009.
307. Perez, E.E.; Wang, J.; Miller, J.C.; Jouvenot, Y.; Kim, K.A.; Liu, O.; Wang, N.; Lee, G.; Bartsevich, V. V.; Lee, Y.L.; et al. Establishment of HIV-1 Resistance in CD4+ T Cells by Genome Editing Using Zinc-Finger Nucleases. *Nat. Biotechnol.* **2008**, *26*, 808–816, doi:10.1038/nbt1410.
308. Klein, F.; Halper-Stromberg, A.; Horwitz, J.A.; Gruell, H.; Scheid, J.F.; Bournazos, S.; Mouquet, H.; Abadir, A.; Diskin, R.; Abadir, A.; et al. HIV Therapy by a Combination of Broadly Neutralizing Antibodies in Humanized Mice. *Nature* 2012, *492*, 118–122.
309. Klein, F.; Nogueira, L.; Nishimura, Y.; Phad, G.; West, A.P.; Halper-Stromberg, A.; Horwitz, J.A.; Gazumyan, A.; Liu, C.; Eisenreich, T.R.; et al. Enhanced HIV-1 Immunotherapy by Commonly Arising Antibodies That Target Virus Escape Variants. *J. Exp. Med.* **2014**, *211*, 2361–2372, doi:10.1084/jem.20141050.
310. Deruaz, M.; Moldt, B.; Le, K.M.; Power, K.A.; Vrbanac, V.D.; Tanno, S.; Ghebremichael, M.S.; Allen, T.M.; Tager, A.M.; Burton, D.R.; et al. Protection of Humanized Mice from Repeated Intravaginal HIV Challenge by Passive Immunization: A Model for Studying the Efficacy of Neutralizing Antibodies *in vivo*. *J. Infect. Dis.* **2016**, *214*, 612–616, doi:10.1093/infdis/jiw203.
311. Tsai, P.; Wu, G.; Baker, C.E.; Thayer, W.O.; Spagnuolo, R.A.; Sanchez, R.; Barrett, S.; Howell, B.; Margolis, D.; Hazuda, D.J.; et al. *In vivo* Analysis of the

Effect of Panobinostat on Cell-Associated HIV RNA and DNA Levels and Latent HIV Infection. *Retrovirology* **2016**, *13*, 36–12, doi:10.1186/s12977-016-0268-7.

312. Khamaikawin, W.; Shimizu, S.; Kamata, M.; Cortado, R.; Jung, Y.; Lam, J.; Wen, J.; Kim, P.; Xie, Y.; Kim, S.; et al. Modeling Anti-HIV-1 HSPC-Based Gene Therapy in Humanized Mice Previously Infected with HIV-1. *Mol. Ther. - Methods Clin. Dev.* **2018**, *9*, 23–32, doi:10.1016/j.omtm.2017.11.008.
313. Dash, P.K.; Kaminski, R.; Bella, R.; Su, H.; Mathews, S.; Ahooyi, T.M.; Chen, C.; Mancuso, P.; Sariyer, R.; Ferrante, P.; et al. Sequential LASER ART and CRISPR Treatments Eliminate HIV-1 in a Subset of Infected Humanized Mice. *Nat. Commun.* **2019**, *10*, 2753–20, doi:10.1038/s41467-019-10366-y.
314. Lee, J.; Brehm, M.A.; Greiner, D.; Shultz, L.D.; Kornfeld, H. Engrafted Human Cells Generate Adaptive Immune Responses to Mycobacterium Bovis BCG Infection in Humanized Mice. *BMC Immunol.* **2013**, *14*, doi:10.1186/1471-2172-14-53.
315. Heuts, F.; Gavier-Widén, D.; Carow, B.; Juarez, J.; Wigzell, H.; Rottenberg, M.E. CD4+ Cell-Dependent Granuloma Formation in Humanized Mice Infected with Mycobacteria. *Proc. Natl. Acad. Sci. U. S. A.* **2013**, *110*, 6482–6487, doi:10.1073/pnas.1219985110.
316. Calderon, V.E.; Valbuena, G.; Goez, Y.; Judy, B.M.; Huante, M.B.; Sutjita, P.; Johnston, R.K.; Estes, D.M.; Hunter, R.L.; Actor, J.K.; et al. A Humanized Mouse Model of Tuberculosis. *PLoS One* **2013**, *8*, 63331, doi:10.1371/journal.pone.0063331.
317. Arrey, F.; Löwe, D.; Kuhlmann, S.; Kaiser, P.; Moura-Alves, P.; Krishnamoorthy, G.; Lozza, L.; Maertzdorf, J.; Skrahina, T.; Skrahina, A.; et al. Humanized Mouse Model Mimicking Pathology of Human Tuberculosis for *in vivo* Evaluation of Drug Regimens. *Front. Immunol.* **2019**, *10*, 89, doi:10.3389/fimmu.2019.00089.
318. Gong, W.; Liang, Y.; Mi, J.; Jia, Z.; Xue, Y.; Wang, J.; Wang, L.; Zhou, Y.; Sun, S.; Wu, X. Peptides-Based Vaccine MP3RT Induced Protective Immunity Against Mycobacterium Tuberculosis Infection in a Humanized Mouse Model. *Front. Immunol.* **2021**, *12*, 666290, doi:10.3389/FIMMU.2021.666290/FULL.
319. Smart, M.; Behrens, M.; David, L.; Conway, C.; Taneja, V. Immune Response to Immunodominant Mycobacterium Tuberculosis Antigen ESAT-6 Derived Peptide Is HLA-Haplotype Dependent. *Jacobs J. allergy Immunol.* **2014**, *1*, 002.
320. Nusbaum, R.J.; Calderon, V.E.; Huante, M.B.; Sutjita, P.; Vijayakumar, S.; Lancaster, K.L.; Hunter, R.L.; Actor, J.K.; Cirillo, J.D.; Aronson, J.; et al. Pulmonary Tuberculosis in Humanized Mice Infected with HIV-1. *Sci. Rep.* **2016**, *6*, doi:10.1038/srep21522.
321. Huante, M.B.; Saito, T.B.; Nusbaum, R.J.; Naqvi, K.F.; Chauhan, S.; Hunter, R.L.;

Actor, J.K.; Rudra, J.S.; Endsley, M.A.; Lisinicchia, J.G.; et al. Small Animal Model of Post-Chemotherapy Tuberculosis Relapse in the Setting of HIV Co-Infection. *Front. Cell. Infect. Microbiol.* **2020**, *10*, 150, doi:10.3389/fcimb.2020.00150.

322. Kwant-Mitchell, A.; Ashkar, A.A.; Rosenthal, K.L. Mucosal Innate and Adaptive Immune Responses against Herpes Simplex Virus Type 2 in a Humanized Mouse Model. *J. Virol.* **2009**, *83*, 10664–10676, doi:10.1128/jvi.02584-08.
323. Kwant-Mitchell, A.; Pek, E.A.; Rosenthal, K.L.; Ashkar, A.A. Development of Functional Human NK Cells in an Immunodeficient Mouse Model with the Ability to Provide Protection against Tumor Challenge. *PLoS One* **2009**, *4*, doi:10.1371/journal.pone.0008379.
324. Majji, S.; Wijayalath, W.; Shashikumar, S.; Pow-Sang, L.; Villasante, E.; Brumeanu, T.D.; Casares, S. Differential Effect of HLA Class-I versus Class-II Transgenes on Human T and B Cell Reconstitution and Function in NRG Mice OPEN. **2016**, doi:10.1038/srep28093.
325. Mack, S.J.; Cano, P.; Hollenbach, J.A.; He, J.; Hurley, C.K.; Middleton, D.; Moraes, M.E.; Pereira, S.E.; Kempenich, J.H.; Reed, E.F.; et al. Common and Well-Documented HLA Alleles: 2012 Update to the CWD Catalogue. *Tissue Antigens* **2013**, *81*, 194–203, doi:10.1111/tan.12093.
326. Gonzalez-Galarza, F.F.; Christmas, S.; Middleton, D.; Jones, A.R. Allele Frequency Net: A Database and Online Repository for Immune Gene Frequencies in Worldwide Populations., doi:10.1093/nar/gkq1128.
327. Yao, Y.; Lai, R.; Afkhami, S.; Haddadi, S.; Zganiacz, A.; Vahedi, F.; Ashkar, A.A.; Kaushic, C.; Jeyanathan, M.; Xing, Z. Enhancement of Antituberculosis Immunity in a Humanized Model System by a Novel Virus-Vectored Respiratory Mucosal Vaccine. *J. Infect. Dis.* **2017**, *216*, 135–145, doi:10.1093/infdis/jix252.
328. Huntington, N.D.; Legrand, N.; Alves, N.L.; Jaron, B.; Weijer, K.; Plet, A.; Corcuff, E.; Mortier, E.; Jacques, Y.; Spits, H.; et al. IL-15 Trans-Presentation Promotes Human NK Cell Development and Differentiation *in vivo*. *J. Exp. Med.* **2009**, *206*, 25–34, doi:10.1084/jem.20082013.
329. Crawford, T.Q.; Jalbert, E.; Ndhlovu, L.C.; Barbour, J.D. Concomitant Evaluation of PMA+ionomycin-Induced Kinase Phosphorylation and Cytokine Production in T Cell Subsets by Flow Cytometry. *Cytom. Part A* **2014**, *85*, 268–276, doi:10.1002/cyto.a.22444.
330. Ai, W.; Li, H.; Song, N.; Li, L.; Chen, H. Optimal Method to Stimulate Cytokine Production and Its Use in Immunotoxicity Assessment. *Int. J. Environ. Res. Public Health* **2013**, *10*, 3834–3842, doi:10.3390/ijerph10093834.
331. Zhao, L.; Chou, Y.; Jiang, Y.; Jiang, Z.; Chu, C.Q. Analysis of IL-17 Production

by Flow Cytometry and ELISPOT Assays. *Methods Mol. Biol.* **2014**, *1172*, 243–256, doi:10.1007/978-1-4939-0928-5_22/FIGURES/4.

332. Wu, Y.; Tian, Z.; Wei, H. Developmental and Functional Control of Natural Killer Cells by Cytokines. *Front. Immunol.* **2017**, *8*, 930, doi:10.3389/FIMMU.2017.00930/BIBTEX.
333. Ranson, T.; Vosshenrich, C.A.J.; Corcuff, E.; Richard, O.; Müller, W.; Di Santo, J.P. IL-15 Is an Essential Mediator of Peripheral NK-Cell Homeostasis. *Blood* **2003**, *101*, 4887–4893, doi:10.1182/BLOOD-2002-11-3392.
334. Kokuina, E.; Breff-Fonseca, M.C.; Villegas-Valverde, C.A.; Mora-Díaz, I. Normal Values of T, B and NK Lymphocyte Subpopulations in Peripheral Blood of Healthy Cuban Adults. *MEDICC Rev.* **2019**, *21*, 16–21, doi:10.37757/MR2019.V21.N2-3.5.
335. Tomasicchio, M.; Davids, M.; Pooran, A.; Theron, G.; Smith, L.; Semple, L.; Meldau, R.; Hapgood, J.P.; Dheda, K. The Injectable Contraceptive Medroxyprogesterone Acetate Attenuates Mycobacterium Tuberculosis–Specific Host Immunity Through the Glucocorticoid Receptor. *J. Infect. Dis.* **2019**, *219*, 1329, doi:10.1093/INFDIS/JIY657.
336. Kleynhans, L.; Du Plessis, N.; Allie, N.; Jacobs, M.; Kidd, M.; van Helden, P.D.; Walzl, G.; Ronachera, K. The Contraceptive Depot Medroxyprogesterone Acetate Impairs Mycobacterial Control and Inhibits Cytokine Secretion in Mice Infected with Mycobacterium Tuberculosis. *Infect. Immun.* **2013**, *81*, 1234–1244, doi:10.1128/IAI.01189-12/ASSET/86BE05DD-7FAB-4511-B25E-8D8B651C1921/ASSETS/GRAPHIC/ZII9990900660010.JPEG.
337. Doitsh, G.; Galloway, N.L.K.; Geng, X.; Yang, Z.; Monroe, K.M.; Zepeda, O.; Hunt, P.W.; Hatano, H.; Sowinski, S.; Muñoz-Arias, I.; et al. Cell Death by Pyroptosis Drives CD4 T-Cell Depletion in HIV-1 Infection. *Nat. 2014 5057484* **2013**, *505*, 509–514, doi:10.1038/nature12940.
338. Hendricks, C.M.; Cordeiro, T.; Gomes, A.P.; Stevenson, M. The Interplay of HIV-1 and Macrophages in Viral Persistence. *Front. Microbiol.* **2021**, *12*, 728, doi:10.3389/FMICB.2021.646447/BIBTEX.
339. Jambo, K.C.; Banda, D.H.; Kankwatira, A.M.; Sukumar, N.; Allain, T.J.; Heyderman, R.S.; Russell, D.G.; Mwandumba, H.C. Small Alveolar Macrophages Are Infected Preferentially by HIV and Exhibit Impaired Phagocytic Function. *Mucosal Immunol.* **2014**, *7*, 1116, doi:10.1038/MI.2013.127.
340. Lewis, D.J.; Williams, T.C.; Beck, S.L. Foamy Macrophage Responses in the Rat Lung Following Exposure to Inhaled Pharmaceuticals: A Simple, Pragmatic Approach for Inhaled Drug Development. *J. Appl. Toxicol.* **2014**, *34*, 319–331, doi:10.1002/JAT.2950.

341. Peyron, P.; Vaubourgeix, J.; Poquet, Y.; Levillain, F.; Botanch, C.; Bardou, F.; Daffé, M.; Emile, J.F.; Marchou, B.; Cardona, P.J.; et al. Foamy Macrophages from Tuberculous Patients' Granulomas Constitute a Nutrient-Rich Reservoir for M. Tuberculosis Persistence. *PLOS Pathog.* **2008**, *4*, e1000204, doi:10.1371/JOURNAL.PPAT.1000204.
342. Penney, D.P.; Rubin, P. Specific Early Fine Structural Changes in the Lung Following Irradiation. *Int. J. Radiat. Oncol.* **1977**, *2*, 1123–1132, doi:10.1016/0360-3016(77)90119-5.
343. Saito, S.; Murase, K. Detection and Early Phase Assessment of Radiation-Induced Lung Injury in Mice Using Micro-CT. *PLoS One* **2012**, *7*, e45960, doi:10.1371/JOURNAL.PONE.0045960.
344. Giuranno, L.; Ient, J.; De Ruysscher, D.; Vooijs, M.A. Radiation-Induced Lung Injury (RILI). *Front. Oncol.* **2019**, *9*, 877, doi:10.3389/FONC.2019.00877/BIBTEX.
345. Scanga, C.A.; Mohan, V.P.; Yu, K.; Joseph, H.; Tanaka, K.; Chan, J.; Flynn, J.A.L. Depletion of CD4+ T Cells Causes Reactivation of Murine Persistent Tuberculosis despite Continued Expression of Interferon γ and Nitric Oxide Synthase 2. *J. Exp. Med.* **2000**, *192*, 347–358, doi:10.1084/jem.192.3.347.
346. Lewinsohn, D.A.; Heinzel, A.S.; Gardner, J.M.; Zhu, L.; Alderson, M.R.; Lewinsohn, D.M. Mycobacterium Tuberculosis-Specific CD8+ T Cells Preferentially Recognize Heavily Infected Cells. *Am. J. Respir. Crit. Care Med.* **2003**, *168*, 1346–1352, doi:10.1164/RCCM.200306-837OC.
347. McBrien, J.B.; Kumar, N.A.; Silvestri, G. Mechanisms of CD8+ T Cell-Mediated Suppression of HIV/SIV Replication. *Eur. J. Immunol.* **2018**, *48*, 898, doi:10.1002/EJI.201747172.
348. Foreman, T.W.; Nelson, C.E.; Kauffman, K.D.; Lora, N.E.; Vinhaes, C.L.; Dorosky, D.E.; Sakai, S.; Gomez, F.; Fleegle, J.D.; Parham, M.; et al. CD4 T Cells Are Rapidly Depleted from Tuberculosis Granulomas Following Acute SIV Co-Infection. *Cell Rep.* **2022**, *39*, 110896, doi:10.1016/J.CELREP.2022.110896.
349. Agarwal, P.; Gordon, S.; Martinez, F.O. Foam Cell Macrophages in Tuberculosis. *Front. Immunol.* **2021**, *12*, 5395, doi:10.3389/FIMMU.2021.775326/BIBTEX.
350. Genoula, M.; Franco, J.L.M.; Dupont, M.; Kviatcovsky, D.; Milillo, A.; Schierloh, P.; Moraña, E.J.; Poggi, S.; Palmero, D.; Mata-Espinosa, D.; et al. Formation of Foamy Macrophages by Tuberculous Pleural Effusions Is Triggered by the Interleukin-10/Signal Transducer and Activator of Transcription 3 Axis through ACAT Upregulation. *Front. Immunol.* **2018**, *9*, 459, doi:10.3389/FIMMU.2018.00459/BIBTEX.
351. Santucci, P.; Bouzid, F.; Smichi, N.; Poncin, I.; Kremer, L.; De Chastellier, C.;

Drancourt, M.; Canaan, S. Experimental Models of Foamy Macrophages and Approaches for Dissecting the Mechanisms of Lipid Accumulation and Consumption during Dormancy and Reactivation of Tuberculosis. *Front. Cell. Infect. Microbiol.* **2016**, *6*, 122, doi:10.3389/FCIMB.2016.00122.

352. Hunter, R.L. Tuberculosis as a Three-Act Play: A New Paradigm for the Pathogenesis of Pulmonary Tuberculosis. *Tuberculosis* **2016**, *97*, 8–17, doi:10.1016/J.TUBE.2015.11.010.
353. Shim, D.; Kim, H.; Shin, S.J. Mycobacterium Tuberculosis Infection-Driven Foamy Macrophages and Their Implications in Tuberculosis Control as Targets for Host-Directed Therapy. *Front. Immunol.* **2020**, *11*, 910, doi:10.3389/FIMMU.2020.00910/BIBTEX.
354. Urbanowski, M.E.; Ordonez, A.A.; Ruiz-Bedoya, C.A.; Jain, S.K.; Bishai, W.R. Cavitary Tuberculosis: The Gateway of Disease Transmission. *Lancet. Infect. Dis.* **2020**, *20*, e117, doi:10.1016/S1473-3099(20)30148-1.
355. Kunjathoor, V. V.; Febbraio, M.; Podrez, E.A.; Moore, K.J.; Andersson, L.; Koehn, S.; Rhee, J.S.; Silverstein, R.; Hoff, H.F.; Freeman, M.W. Scavenger Receptors Class A-I/II and CD36 Are the Principal Receptors Responsible for the Uptake of Modified Low Density Lipoprotein Leading to Lipid Loading in Macrophages *. *J. Biol. Chem.* **2002**, *277*, 49982–49988, doi:10.1074/JBC.M209649200.
356. Mattila, J.T.; Ojo, O.O.; Kepka-Lenhart, D.; Marino, S.; Kim, J.H.; Eum, S.Y.; Via, L.E.; Barry, C.E.; Klein, E.; Kirschner, D.E.; et al. Microenvironments in Tuberculous Granulomas Are Delineated by Distinct Populations of Macrophage Subsets and Expression of Nitric Oxide Synthase and Arginase Isoforms. *J. Immunol.* **2013**, *191*, 773–784, doi:10.4049/JIMMUNOL.1300113.
357. Ordway, D.; Henao-Tamayo, M.; Orme, I.M.; Gonzalez-Juarrero, M. Foamy Macrophages within Lung Granulomas of Mice Infected with Mycobacterium Tuberculosis Express Molecules Characteristic of Dendritic Cells and Antiapoptotic Markers of the TNF Receptor-Associated Factor Family. *J. Immunol.* **2005**, *175*, 3873–3881, doi:10.4049/JIMMUNOL.175.6.3873.
358. Cassol, E.; Cassetta, L.; Alfano, M.; Poli, G. Macrophage Polarization and HIV-1 Infection. *J. Leukoc. Biol.* **2010**, *87*, 599–608, doi:10.1189/JLB.1009673.
359. Sharan, R.; Kaushal, D. Vaccine Strategies for the *Mtb*/HIV Copandemic. *npj Vaccines 2020 51* **2020**, *5*, 1–10, doi:10.1038/s41541-020-00245-9.
360. Gupta, A.; Hughes, M.D.; Garcia-Prats, A.J.; McIntire, K.; Hesseling, A.C. Inclusion of Key Populations in Clinical Trials of New Antituberculosis Treatments: Current Barriers and Recommendations for Pregnant and Lactating Women, Children, and HIV-Infected Persons. *PLoS Med.* **2019**, *16*,

doi:10.1371/JOURNAL.PMED.1002882.

361. Schrager, L.K.; Harris, R.C.; Vekemans, J. Research and Development of New Tuberculosis Vaccines: A Review. *F1000Research* 2019, *7*.
362. Schrager, L.K.; Vekemens, J.; Drager, N.; Lewinsohn, D.M.; Olesen, O.F. The Status of Tuberculosis Vaccine Development. *Lancet Infect. Dis.* 2020, *20*, e28–e37.
363. Coppola, M.; Ottenhoff, T.H. Genome Wide Approaches Discover Novel Mycobacterium Tuberculosis Antigens as Correlates of Infection, Disease, Immunity and Targets for Vaccination. *Semin. Immunol.* **2018**, *39*, 88–101, doi:10.1016/J.SMIM.2018.07.001.
364. Danner, R.; Chaudhari, S.N.; Rosenberger, J.; Surls, J.; Richie, T.L.; Brumeanu, T.D.; Casares, S. Expression of HLA Class II Molecules in Humanized NOD.Rag1KO.IL2RgcKO Mice Is Critical for Development and Function of Human T and B Cells. *PLoS One* **2011**, *6*, doi:10.1371/journal.pone.0019826.
365. Brehm, M.A.; Shultz, L.D.; Luban, J.; Greiner, D.L. Overcoming Current Limitations in Humanized Mouse Research. *J. Infect. Dis.* **2013**, *208*, S125–S130, doi:10.1093/infdis/jit319.